

**PICES Scientific Report No. 12
1999**

**PROCEEDINGS OF THE SECOND PICES WORKSHOP
ON THE OKHOTSK SEA AND ADJACENT AREAS**

Edited by

Drs. Vyacheslav B. Lobanov, Yutaka Nagata and Stephen C. Riser

September 1999

Secretariat / Publisher

North Pacific Marine Science Organization (PICES)

c/o Institute of Ocean Sciences, P.O. Box 6000, Sidney, B.C., Canada. V8L 4B2

E-mail: pices@ios.bc.ca Home Page: <http://pices.ios.bc.ca>

TABLE OF CONTENTS

	Page
Preface	v
Masaaki Aota. Long-term tendencies of sea ice concentration and air temperature in the Okhotsk Sea coast of Hokkaido	1
Hajime Ito & Miki Yoshioka. Geography of the seasonally ice covered seas	3
George V. Shevchenko & Victor F. Putov. On wind and tide induced sea-ice drift on the northeastern shelf of Sakhalin Island (analysis of radar data).....	11
Boris S. Dyakov, A.A. Nikitin, L. S. Muktepavel & T.A. Shatilina. Variability of the Japan and Okhotsk Seas ice cover depending on geopotential field H500 over the Far-Eastern region	19
Aleksandr G. Petrov & Nikolay A. Rykov. Intermediate cold layer and ice cover in the Sea of Okhotsk	25
Vladimir Ponomarev, Olga Trusenkova, Elena Ustinova & Dmitry Kaplunenko. Interannual variations of oceanographic and meteorological characteristics in the Sea of Okhotsk	31
George V. Shevchenko & Akie Kato. Seasonal and interannual changes of atmospheric pressure, air and water temperature in the area of the Kuril Ridge.....	41
George V. Shevchenko & Vladimir Yu. Saveliev. Spatial variability of the wind field in the area of the Kuril Islands	49
Alexander L. Figurkin & Igor A. Zhigalov. Seasonal variability and specificity of the oceanological conditions in the northern Okhotsk Sea in 1997	55
Igor A. Zhabin. Ventilation of the upper portion of the intermediate water in the Okhotsk Sea.....	61
Vladimir A. Luchin & Alexander L. Figurkin. Oceanographic conditions over the Kashevarov Bank	69
Toshiyuki Awaji, Tomohiro Nakamura, Takaki Hatayama, Kazunori Akimoto & Takatoshi Takizawa. Tidal exchange through the Kuril Straits.....	77
Tomohiro Nakamura, Toshiyuki Awaji, Takaki Hatayama, Kazunori Akimoto, Takatoshi Takizawa & Masao Fukasawa. Vertical mixing induced by tidally generated internal waves in the Kuril Straits	83
Katsuro Katsumata & Ichiro Yasuda. Water exchange between the Okhotsk Sea and the North Pacific Ocean estimated by simple models	89
Konstantin A. Rogachev. Oyashio west path culmination as the consequence of a rapid thermohaline transition in the Pacific Subarctic.....	95
Yasuhiro Kawasaki. On the year-to-year change in subarctic water characteristics around the Kuril Islands	101
Alexander L. Figurkin & Evgeniy E. Ovsyannikov. Influence of oceanological conditions of the West Kamchatka shelf waters on spawning grounds and on pollock egg distribution	107
Igor E. Kochergin & Alexander A. Bogdanovsky. Transport and turbulence characteristics for the northeastern Sakhalin shelf conditions.....	115
Igor E. Kochergin, Alexander A. Bogdanovsky, Valentina D. Budaeva, Vyacheslav G. Makarov, Vasily F. Mishukov, S.N. Ovsienko, Victor F. Putov, L.A. Reitsema, J.W. Sciallabba, O.O. Sergucheva & P.V. Yarosh. Modeling of oil spills for the shelf conditions of northeastern Sakhalin	123

Valentina D. Budaeva & Vyacheslav G. Makarov. A peculiar water regime of currents in the area of eastern Sakhalin shelf	131
Nikolay A. Rykov. The oceanographic databases on the Sakhalin shelf	139
Akifumi Nakata, Iori Tanaka, Hiroki Yagi, Tomomi Watanabe, Gennady A. Kantakov & Andrew D. Samatov. Formation of high-density water (over 26.8 sigma-t) near the La Perouse Strait (the Soya Strait)	145
Minoru Odomaki & Kouji Iwamoto. Currents and tidal observations by Hydrographic Department of Maritime Safety Agency, off the Okhotsk coast of Hokkaido	149
Yasushi Fukamachi, Genta Mizuta, Kay I. Ohshima, Motoyo Itoh, Masaaki Wakatsuchi & Masaaki Aota. Mooring measurements off Shiretoko Peninsula, Hokkaido in 1997-1998.....	153
Mikhail A. Danchenkov, David Aubrey & Stephen C. Riser. Oceanographic features of the La Perouse Strait	159
Iori Tanaka & Akifumi Nakata. Results of direct current measurements in the La Perouse Strait (the Soya Strait), 1995-1998.....	173
Gennady A. Kantakov & George V. Shevchenko. <i>In situ</i> observations of Tsushima and West-Sakhalin currents near La Perouse (Soya) Strait.....	177
Irina Y. Bragina. Geographical and biological characteristics of the net zooplankton in the southwestern part of the Sea of Okhotsk during 1987-1996.....	187
List of corresponding authors	201

PREFACE

The Second PICES Workshop on the Okhotsk Sea and Adjacent Areas was held in Nemuro, Japan, November 9-12, 1998. The workshop was coordinated by the Physical Oceanography and Climate Committee (POC) of PICES, and co-convened by Drs. Yutaka Nagata, Vyacheslav B. Lobanov and Lynne D. Talley (absent at the meeting). POC recognized the importance of the Okhotsk Sea, where sea ice is formed at the lowest latitudes in the world, and also as the formation area of North Pacific Intermediate Water (NPIW). POC previously formed PICES Working Group 1 on the Okhotsk Sea, and published a review volume "The Okhotsk Sea and Oyashio Region" in 1995 (*PICES Scientific Report No. 2*). Following this, PICES held the first Workshop on the Okhotsk Sea and Adjacent Areas in Vladivostok, Russia, in June 1995, the proceedings of which were published as *PICES Scientific Report No. 6* in 1996. In addition, POC published the "Multilingual Nomenclature of Place and Oceanographic Names in the Region of the Okhotsk Sea" as *PICES Scientific Report No. 8* in 1998. There has been a great deal of recent research activities in the Okhotsk Sea and adjacent areas, and many new findings and new knowledge have been generated since the first workshop in Vladivostok. The purpose of this Second Workshop is to exchange new findings and recent research results, and to review on-going and in-planning international and domestic projects in order to improve cooperative research.

The workshop was opened by the Mayor of Nemuro City, Mr. Hiroshi Fujiwara, and Dr. Vyacheslav B. Lobanov explained the aims and the expected products of the workshop. The workshop discussion focussed mainly on physical oceanography, and talks covered a wide range of research: sea-ice characteristics and its movements; the relation between ice-cover and atmospheric conditions; sea-ice and dense water (NPIW) formation; ventilation and modification of water masses; tides and their effects on water mixing and on water exchanges through straits; meso-scale eddies, yearly to decadal temporal variations, oceanographic databases and atlases; and the relation of the oceanic state to spawning grounds and to the nutrient and chlorophyll-*a* distributions. Relations of these to local environments such as the northern Okhotsk Sea Shelf, on the Sakhalin and west Kamchatka shelves, in the Kuril Islands region, and in the Soya (La Peoruse) Strait and northern coast of Hokkaido, were discussed. There were 42 participants and 38 presentations including 10 posters (22 papers and 10 posters by Russian scientists, 15 papers by Japanese scientists, and 1 paper by a US scientist).

Most of the on-going and in-planning international programs were discussed: such as the Soya/La Perouse program conducted by Sakhalin Research Institute of Fisheries and Oceanography (SakhNIRO) and the Hokkaido Central Fisheries Experimental Station, the Joint Japanese-Russian-US Study of the Sea of Okhotsk, and the joint studies between Pacific Research Institute of Fisheries and Oceanography (TINRO) and the Hokkaido National Fisheries Research Institute. Several research activities in Japan and Russia, for example, the Japanese Hydrographic Department, the Hokkaido University group, the Pacific Oceanological Institute (POI), TINRO, the Far Eastern Regional Hydrometeorological Research Institute (FERHRI), were also introduced. Additional information was presented on the future activities relating to these projects during the plenary session by participating institutes and scientists. The participants of the workshop appreciated these efforts, and were impressed by the recent progress of the many Okhotsk Sea studies. However, there are still many problems to be solved, and many logistic and other kinds of difficulties in expanding our research activities and in organizing further international cooperative studies on the Okhotsk Sea area.

The workshop recommends that PICES endorse and support the international cooperative projects mentioned above and that are to be developed in the near future. The activities should be extended not

only to the Okhotsk Sea, but also to the Kuril Islands region and the Western Subarctic Gyre. PICES member countries bordering the Okhotsk Sea should facilitate access to investigators to cooperate on scientific research in the region. The workshop participants greatly appreciate the publication of the proceedings of this workshop in the PICES Scientific Report Series, and agreed that Drs. Vyacheslav B. Lobanov, Stephen C. Riser and Yutaka Nagata will serve as co-editors of the publication. The workshop also recommends that POC/PICES continue to overview and support the Okhotsk Sea research activities, and consider holding another workshop in the near future, if warranted. Although the subjects of workshop talks were focussed on physical oceanography, many of the projects introduced are carried out in cooperation with other disciplines. The workshop recommends that the PICES Implementation Panel on Climate Change and Carrying Capacity takes the initiative to organize a GLOBEC-like study for the Okhotsk Sea area.

The workshop was closed following farewell addresses by the Vice-Chairman of the Nemuro Workshop Supporting Committee, Mr. Nobuyuki Fukui (Chairman of the Nemuro Junior Chamber) and the former PICES Science Board Chairman, Dr. Makoto Kashiwai. As mentioned by the PICES Executive Secretary, Dr. W. Doug McKone, at the Welcome Reception held by Nemuro City on the evening of November 10, this workshop is already the fifth PICES meeting in Nemuro. All of the participants thanked the people of Nemuro for the support and hard work in providing facilities for PICES meetings, and expressed their thanks for the financial support given by Nemuro City, Hokkaido University and other institutions. Without this support the outcome of the workshop would be substantially limited.

The proceedings of the Second PICES Workshop on the Okhotsk Sea and Adjacent Areas are published according to a POC/Science Board recommendation at the Seventh Annual Meeting in Fairbanks, Alaska. I would like to thank the PICES Secretariat for its support in various phases of editing.

Yutaka Nagata

Long-term tendencies of sea ice concentration and air temperature in the Okhotsk Sea coast of Hokkaido

Masaaki AOTA

Sea Ice Research Laboratory, Hokkaido University, Mombetsu, Japan

The Okhotsk Sea Coast of Hokkaido is located between 43°50'N and 45°30'N, and is covered with sea ice in winter season. These latitudes are the lowest among seas which are frozen in winter, except the very shallow Bohai Sea filled with much fresher water. The period when the coastal region is ice covered has been decreasing during recent years.

Long-term observations of sea ice coverage are rare, but along the Okhotsk Coast of Hokkaido, the Abashiri Weather Station of Hokkaido started sea ice observation in 1892. The Abashiri District Meteorological Observatory took over this observation later, and it is still continuing. This is one of the longest records of sea ice observation. Using these data, we discuss the long-term trend of the sea ice coverage of the Okhotsk Sea Coast of Hokkaido and its relation to the yearly mean air temperature.

Data and definition of accumulated ice concentration

The visual sea ice observations have been made from top of a coastal hill (approximately 40 m high). The observable radius is about 20 km. In the early period from 1892 to 1929, only the day of first appearance of sea ice and that of the last day are available. We call this the period from the day of the first appearance to the last day the sea ice period. Daily data on sea ice concentration are available after 1930. The first appearance of sea ice along the Okhotsk Coast of Hokkaido is in late January or in February. The ice disappears usually in late March, but it may stay until May in some years. The sea ice

concentration is defined as the area of ice cover within the range of observation, in percent.

Characteristics of the sea ice are represented both by the sea ice extent or the sea ice concentration and by the duration of ice stay. For the years after 1930, the daily value of sea ice concentration (%) is summed for the period of ice cover in each year, and this accumulated sea ice concentration (%-days) is used as a measure of annual sea ice strength. The correlation between the obtained accumulated concentration and the sea ice period were examined for the period after 1930, and we found a good correlation with a coefficient of about 0.8 ($n=68$). For the period before 1929, we estimated the accumulated concentration from the observed sea ice period, by using the regression line of the correlation plots, and used this result in our analysis.

Interannual variation of the accumulated sea ice concentration and the mean air temperature

The mean air temperature averaged over the period from April in the preceding year to March are calculated for each year, and its temporal variation is shown (Fig. 1a) for the period from 1892 to 1998. The corresponding temporal variation of the accumulated sea ice concentration is also shown (Fig. 1b). Though relatively short-period fluctuations are dominant in both curves, the linear trends of the variation can be recognized in both curves. The mean air temperature tends to increase for the analyzed period, while the accumulated sea ice concentration to decrease.

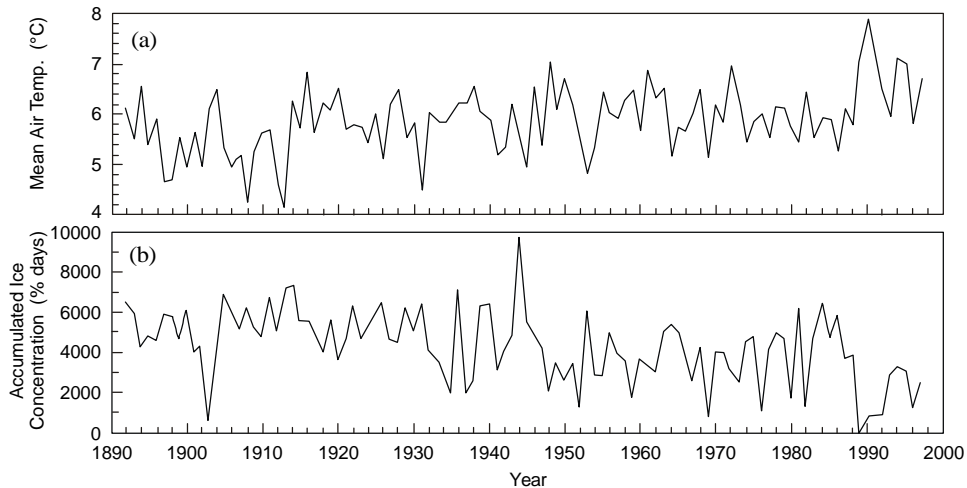


Fig. 1 Variations of the yearly mean air temperature (a: upper panel) and the accumulated sea ice concentration (b: lower panel) at Abashiri, Hokkaido.

Long-term tendencies of accumulated sea ice concentration and mean air temperature

Thirty year running averages of the yearly values of the accumulated sea ice concentration were calculated, and the obtained smoothed temporal variations are shown (Fig. 2). The smoothed air temperature (black circles in Fig. 2) exhibits a clear increasing tendency, and the amount of temperature increase during the past 106 years is about 0.6°C. On the other hand, the smoothed accumulated sea ice concentration (black squares in Fig. 2) tends to decrease during the analyzed period, and the sea ice

concentration in 1980 is only 60% of that in 1920s.

Conclusion

The clear decreasing tendency of the sea ice amount along the Okhotsk Coast of Hokkaido during the past 106 years can be shown from the ice concentration record taken at Abashiri, Hokkaido. The long-term variation of the sea ice concentration is well correlated with that of the yearly mean air temperature, which exhibits the clear increasing tendency during the same period. This would be one of the symptoms of the global warming, and is a warning to human beings!

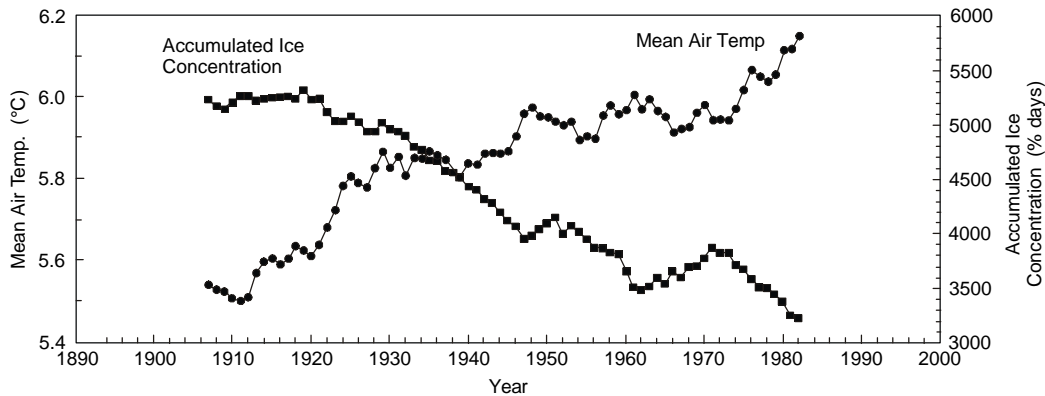


Fig. 2 Thirty year running averages of the yearly mean air temperature (●) and accumulated ice concentration (■) at Abashiri, Hokkaido.

Geography of the seasonally ice covered seas

Hajime ITO and Miki Yoshioka

National Institute of Polar Research, Tokyo, Japan

Abstract

The Okhotsk Sea and the Barents Sea are known to be ice covered during a part of the year and ice free in the rest of the year. The conditions surrounding both seas constitute their environment and contribute to the creation and maintenance of this particular state, which are investigated in geographic terms in this article. The common features of the two seas as well as the contrasting ones are elucidated. The results serves the investigation of a seasonally ice covered sea generally.

Introduction

Among the seas which are ice covered in winter and ice free during the summer months, the Barents Sea and the Okhotsk Sea are located at the northernmost and the southernmost extremes in the northern hemisphere, respectively. This article compares the seas in terms of geography, on which many, if not all, studies are based. There can be some similarities in geographic elements, since both seas belong to an identical type, i.e. the seasonally ice covered sea. The problem can be, however, formulated differently for each sea: why is the sea at that high/low latitude open in summer or frozen in winter, respectively. Hence contrasting elements are also expected. Through the comparative study, not only the characteristics of the two seas but that of a seasonally ice covered sea in general may be elucidated.

Scope

The Barents Sea and the Okhotsk Sea are shown in Figure 1. The surface area of each is defined to be the area inside of the curves drawn on the plane of the sea surface for the purpose of discussion: coast line of the continent, that of islands, linear lines connecting pairs of peninsulas facing to each other. Each sea is then defined to be the water body underneath the area. The Barents Sea and the Okhotsk Sea thus defined have particular shape and extent, and are placed at a particular location relative to the earth. The seas are described in this aspect in the next chapter.

The boundary of the seas consists of three different materials: rock, air and water. The water body in question is thus surrounded by the seabed, by the overlying atmosphere and by the adjacent sea, and interact with them. The attaching neighbors are described in separate chapters in this order.

The Barents Sea and the Okhotsk Sea obtain certain characteristics and present a particular state at a given time under the influence of these geographic elements. The detailed investigation of the seas themselves are certainly the most interesting and important topic, but are beyond the scope of the current article. The state of the sea is in fact merely regarded as the results of the geographical conditions. Nevertheless, a brief sketch of the present state of both seas is given in the succeeding chapter to get some idea to make the comparison possible. In the last section the similarity and difference of the Barents Sea and the Okhotsk Sea are discussed.

Geometry

The Okhotsk Sea is bounded by land, i.e. a continent or large islands at northeast, north, west and south. Two straits cut the land boundary, which connect the Okhotsk Sea to the

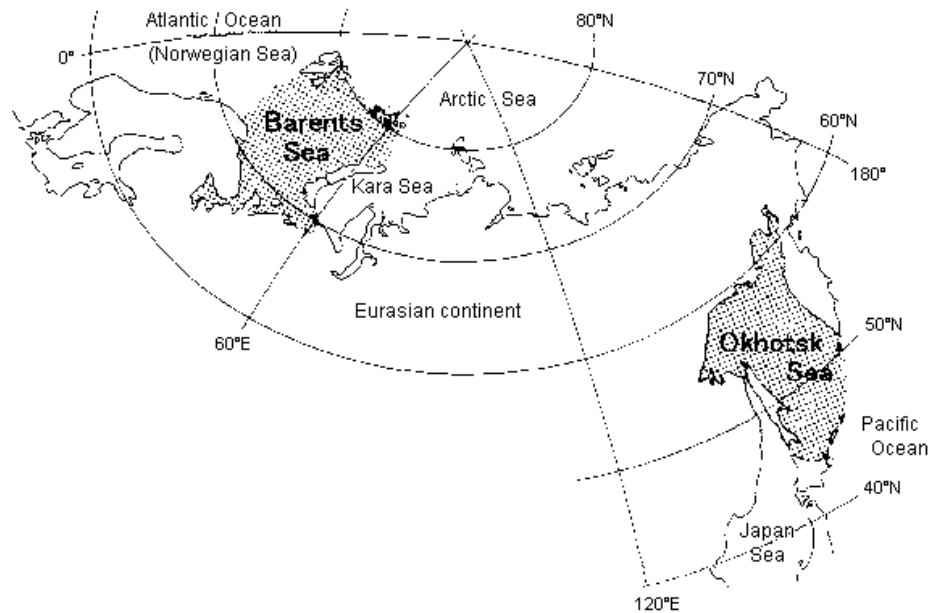


Fig. 1 Two seasonally ice covered seas.

neighboring Japan Sea. An island chain, Kuril Islands, draws the southeastern boundary, where the water body has direct contact to the Pacific Ocean.

The Okhotsk Sea covers an area of $1.5 \times 10^6 \text{ km}^2$. The mean depth is $0.8 \times 10^3 \text{ m}$, and the total volume is $1.2 \times 10^6 \text{ km}^3$ (National Astronomical Observatory, 1995). The total length of the boundary is 10043 km (6787 km), of which 9483 km (6227 km) is the coast line and 560 km is the boundary running on water. The contact with the Pacific prevails with the length of 513 km, whilst that to the Japan Sea is 47 km, through 7 km of Tatar Strait and 40 km of Soya Strait. These measurements were made from maps (Energy, Mines and Resources Canada, 1990; Nomura, 1997) where no reference is given.

The coast line length can be increased arbitrarily by using a large scale map, especially where the coast line is complicated in the shape, e.g. fjord. The comparison in the length with the boundary on the water, which is a linear line according to the definition, would be difficult. The coast line was smoothed for this purpose only, by cutting off the small bays with an entrance width of 100

km or less. The boundary length of this smoothed sea is given in the parenthesis. The Okhotsk Sea is a water body surrounded in the first place by a land mass, 92 % of the boundary length, with some opening to adjacent seas, 8 %.

The Barents Sea covers an area of $1.4 \times 10^6 \text{ km}^2$ including the White Sea. Mean depth is $0.2 \times 10^3 \text{ m}$ (Dzhenyuk and Zykova, 1992), and the volume is $0.3 \times 10^6 \text{ km}^3$. The southern side is bordered by a continent and the eastern and northwestern sides by large islands. Three straits cut through the land boundary to the east: Malygina Strait of 8 km wide, Karskiye Vorota Strait of 61 km wide, Matochkin Shar Strait of 4 km wide which connects the Barents Sea with the Kara Sea (Dzhenyuk and Zykova, 1992). Scattered small islands, Zemlya Frantsa Iosifa, are located on the northeastern boundary, through which the Barents Sea has contact with the Arctic Sea and Kara Sea. The western boundary has a single small island, Bear Island, and is practically open to an ocean, the Norwegian Sea.

The total boundary length is 9955 km (5639 km), of which the coastline is 8399 km (4083 km). The length of the border to other sea is 1556 km,

of which 640 km is the boundary to the Norwegian Sea (75% of the border is land). The contact length to the Norwegian Sea occupies 41% of the total water boundary.

The Okhotsk Sea is located at the latitude of 45°N to 60°N and the Barents Sea is at 68°N to 80°N. The latitudes of the centers are assumed to be 53°N and 74°N, respectively. Latitude has a direct influence on the potential solar radiation. The cosine is considered to its index and is calculated for both latitudes, and for different position of the sun. In summer, they are 0.870 for the Okhotsk Sea and 0.636 for the Barents Sea and do not differ from each other so much as the latitude difference would indicate. In the fall and spring, they are 0.602 and 0.276. The Okhotsk Sea receives double the amount of solar radiation in comparison to the Barents Sea. The difference becomes more clear in winter, they are 0.233 and 0, the cosine value being negative in Barents Sea.

Geology

Both seas with the given geometry are placed on the surface of the earth, where the distribution of the land has been established. They are placed at rather contrasting locations in relation to the land mass. The Barents Sea is attached to a northern coast at the west of the Eurasia Continent, and Okhotsk Sea is located on the southern coast at the east of the same continent.

The northern coast of Asia is attached to the widest continental shelf in the world. The Barents Sea is located entirely on the shelf. Caledonian and Uralian trends dominate in the old platform probably originating in the Archaean. The basement is covered by several layers of sediment (Embleton, 1984). This continental shelf is suspected to have been completely covered by an ice sheet in the last glacier age, hence the Barents Sea became filled quite recently. The sea bottom is not completely flat, but retains the landscape created underneath the ice sheet. Two wide submerged valleys run toward southwest and north respectively. The Barents Sea itself is shallow with the depth range of 100 m to 400 m, but to the north the shelf drops to the Nansen Basin with

the depth exceeding 3000 m and to the west to the Norwegian Basin with depth exceeding 2000 m.

The northern half of the Okhotsk Sea is also on the continental shelf. Forty percent of the area has the depth 200m (Wadachi, 1987). The Kuril Island chain was created as an island arc while the Pacific Plate submerges underneath the continent. A trench was made on the ocean side of the arc, and a basin on the other side, in the Okhotsk Sea. Thus the southeastern part of the Okhotsk Sea is quite deep. The area with a depth > 3000 m is 1.6×10^5 km², 10% of the entire sea (Wakatsuchi and Martin, 1990). The age of the basement of Kuril Basin is estimated to be 120 to 140 million years, the Cretaceous. The thickness of the sedimentary cover in the Okhotsk Sea exceeds 6 km in some place. Buried and submarine volcanic structures are found in the Kuril Basin (Shilo et al., 1982). The land surrounding the Okhotsk Sea is mountainous and volcanically active.

The total annual discharge of freshwater into the Okhotsk Sea is estimated to be 590 km³ (Groves and Nunt, 1980), of which the continental runoff is 463 km³/year (Zuenko and Yurasov, 1997). The majority of the freshwater is supplied by the Amur River, 315 km³ /year (Zuenko and Yurasov, 1997). The drainage area of the Okhotsk Sea is 2.6×10^6 km² (4.1×10^6 km², including the sea surface), of which the drainage basin of Amur is 1.8×10^6 km².

The Dvina and the Pechora are major rivers flowing into the Barents Sea. The drainage area of the Barents Sea is 1.3×10^6 km² (2.7×10^6 km², including sea surface), of which the Dvina is 0.3×10^6 km² and the Pechora is 0.2×10^6 km². The discharge into the Barents Sea is concentrated in the short summer season. (Cattle, 1985).

Zemlya Frantsa Iosifa, located at the northern margin of the Barents Sea, consists of many ice capped islands and the archipelago has 2600 km of tidewater ice cliffs. The archipelago supplies 1.5 km³/year of fresh water to the Barents Sea in the form of icebergs. (Løset and Carstens, 1996).

Climate

In winter, the Siberian high pressure develops on the continent adjacent to the Okhotsk Sea and the westerly wind blows onto the sea. The cold continental air meets the warm sea water and causes a considerable amount of precipitation. The large part of the Okhotsk Sea is classified as "Dfc" in Köppen climate classification, meaning that the monthly mean temperature of the coldest month is below -3°C , that of the warmest month is above 10°C but that of the fourth warmest month does not exceed 10°C , and that the region has rich precipitation all year through. The northwestern part is classified "Dwc", which describes the difference from Dfc, being dry in winter.

The systematic weather record for a certain time length is available on the coastal stations. For instance, at Abashiri, at the southernmost boundary, the annual mean air temperature is 6.0°C , the monthly mean temperature stays below 0°C for 4 months (National Astronomical Observatory, 1995). At the western boundary, at Chaivo Bay on Sakhalin Island, the air temperature ranges from 20°C to -30°C in a year (Shirasawa et al., 1996). Mean air temperature at Okhotsk Sea is estimated to be -6°C in winter and 18°C in summer (Groves and Nunt, 1980), using the data obtained on the sea and at the coastal stations. Extreme winter temperatures on the sea assumes the range from 0°C at the southern part in a warm year to -32°C at the northern part in a cold year (Wakatsuchi and Martin, 1990). The annual precipitation at Nemuro, at the southern boundary, is recorded to be 1370 mm, which is distributed in all the months of the year. At Okhotsk City, at the northern boundary, 467 mm of the precipitation is concentrated in summer. At Ust Khayryuzovo, at the eastern boundary, 766 mm of the annual precipitation is obtained and at Nikolaevskna-Amure, at the western boundary, 657 mm, mostly in summer and autumn at the both stations (Korzun et. al., 1974).

The precipitation over the Okhotsk Sea is estimated using these observations. At the southern Okhotsk Sea, annual precipitation is 1200 mm and in the northern part, 600 mm. It decreases

toward the center of the sea, where the minimum value of 400 mm is calculated. Annual evaporation is estimated to be 400 mm in the central part of the Okhotsk Sea. It increases to the south and southeast (Korzun et.al., 1974).

At the stations on the continental coast, along the northern boundary, the northerly wind prevails at the speed around 4.5 m/s in January (Fukutomi, 1952). The northwesterly wind prevails at Val, Sakhalin Island at an annual mean speed of 4 m/s. The wind speed is slightly higher during the winter (Shirasawa et al., 1996). At stations on the southern boundary, the monthly wind is reported: north or northwest at 4.6 m/s in February and March and south-southwest at 4.4 m/s in April (Fukutomi, 1952). At the Okhotsk Sea the wind seems to blow from the north, northeast, or northwest in winter (Parkinson and Gratz, 1983) and this northerly wind transports sea ice from the northwest continental shelf region to the southern area (Wakatsuchi and Martin, 1990).

The Barents Sea is in the Atlantic Arctic Frontal Zone, where the Arctic air mass and the polar air mass contact each other. The warm cyclones from the northern Atlantic and the cold anticyclones from the Arctic meet each other in the region (Groves and Nunt, 1980). Compared with other circum-Arctic seas, the Barents Sea has high air temperature and precipitation (Groves and Nunt, 1980). The Barents Sea area is classified as "E" in the Köppen climate classification, meaning that the mean monthly temperature of the warmest month does not exceed 10°C .

At Murmansk, on the southern boundary of Barents Sea, the annual mean air temperature is reported to be -0.1°C , and during six months of the year the monthly mean stays $<0^{\circ}\text{C}$ (National Astronomical Observatory, 1995). The annual mean air temperature decreases toward the east along the southern boundary, -2.9°C at North Kolguev, and -5.6°C at Varandey. At Varandey, the monthly mean air temperature of February is -18.3°C and the absolute recorded minimum is -48°C (Strass et al., 1997). The air temperature on the Barents Sea is estimated to fall as one moves from south to north and from west to east

within the area. The annual mean air temperature ranges from $<0^{\circ}\text{C}$ to 10°C (Strass et al., 1997).

At Vardo, at the southern boundary, the annual precipitation is recorded to be 1043 mm, most of which falls in winter. At Murmansk, also at the southern boundary but shifted a couple of hundreds of kilometers toward east, it is 589 mm, which is distributed throughout the year. At Bear Island, at the western boundary, it is 560 mm, where the summer precipitation is only half of that in winter. At Zemlya Frantsa Iosifa, at the northern boundary, it is 254 mm and at Mal. Karmakuly, at the eastern boundary, it is 413 mm. Most of the precipitation at the last two stations are recorded in summer and autumn. In the Barents Sea, the annual precipitation is estimated to be 1000 mm in the southwestern part, and decreases toward north and east to 300-400 mm. The seasonal change is considerably variable in pattern within the region.

The annual evaporation is estimated to be 800 mm in the southwestern part of the Barents Sea, and decreases toward north. In the northern part it reaches the minimum value of 100 mm (Korzun et al., 1974). At Kolguev Island, at the southern boundary, the southwesterly wind prevails at mean wind speed of 8.2 m/s in winter, but is scattered in all the directions in summer. The wind speed is higher in winter than in summer (Strass et al., 1997). At Hopen Island, at the western area, the monthly mean wind speed of 13-16 m/s is reported for November (Løset and Carstens, 1996). In the western part of the Barents Sea, the annual mean wind speed is estimated to exceed 9 m/s, with a maximum of 36 m/s. The wind speed decreases to the east and to the north. The wind speed is higher in winter, and is lowest in July (Strass et al., 1997). The wind direction is generally scattered in all directions. However, the strong wind has a particular direction, which is variable from a place to another; southwesterly wind in the western part and easterly wind in the northern and eastern parts.

Adjacent ocean

The cross section, through which the Okhotsk Sea and Pacific Ocean maintain the direct contact to each other, has an area of 200 km (Wadachi, 1987). The surface water temperature of the Pacific Ocean near the cross section is reported to be 1°C to 2°C in February, and around 10°C in August. The surface salinity is 33 psu in February (Wadachi, 1987).

At the surface, the Pacific Ocean water enters the Okhotsk Sea through the northern part of Kuril chain and the water flows out from the Okhotsk Sea into the Pacific Ocean through southern part of Kuril chain (Wadachi, 1987). At depth, the water flows out to the Pacific Ocean at the upper layer, e.g. through Bussol Straits at the southern Kuril chain, but the Pacific water flows in at the deep layer below 1500 m (Wadachi, 1987; Wakatsuchi and Martin, 1990). The Pacific water is warmer, more saline and poor in oxygen at all the depth compared with the water of Okhotsk Sea (Wakatsuchi and Martin, 1990). Hence the Pacific water is the source of the heat and salt but a sink for oxygen, when an exchange takes place across the cross section.

The Barents Sea has cross sections through which it has contact with adjacent seas: 160 km² to the Norwegian Sea, 53 km² to the Arctic Sea and 166 km² to the Kara Sea (Dzhenyuk and Zykova, 1992). A comparatively warm (4 to 12°C) and saline (> 35 psu) Atlantic water, a branch of the Gulf Stream, flows into the Barents Sea through the western boundary between North Cape and Bear Island (Groves and Nunt, 1980). The Atlantic water serves as the source of heat and salt. The surface current enters the Barents Sea with a speed of 0.75 to 0.8 m/s passing by Tromsøflaket from west. Cold Arctic water flows into the Barents Sea across its northern boundary through two routes, between Svalbard and Zemlya Frantsa Iosifa, and between Zemlya Frantsa Iosifa and Novaya Zemlya (Løset and Carstens, 1996). The Barents Sea contacts the ice sea at the northern boundary; the ice concentration in the area im-

mediately to the north of the Barents Sea is reported to have exceeded 80% in the summer of 1980 (Løset et al., 1997). Multi-year ice is dominant and the mean ice thickness exceeds 2.0 m. The Arctic Sea is thus a two-fold heat sink, i.e. cold water (sensible heat) and ice supplier (latent heat) to the Barents Sea, and is an additional source of the fresh water in the solid form.

State of the sea

At the Okhotsk Sea, the temperature of the surface water ranges from -1.8°C in winter to 18°C in summer (Groves and Nunt, 1980). The salinity of the surface water is reported to be 32 to 32.5 psu in summer (Wadachi, 1987). There is counterclockwise current on the surface in the Okhotsk Sea.

The sea ice is first formed in the northern part of the sea in the middle of November. The maximum development is reached in the middle of March; 80 % of the total area is covered by sea ice (Wadachi, 1987). There is no sea ice found in the summer months, from July to October. All sea ice is first year ice or younger in the Okhotsk Sea. The mean ice thickness in March is reported to be 1.0 m in the northern part, and 0.4 to 0.5 m in the southern part. (Wadachi, 1987; Aota and Uematsu, 1989).

At the Barents Sea, the temperature of the surface water ranges from -2°C in winter to 8°C in summer (Wadachi, 1987). The salinity of the surface water is around 34 psu in summer. The current is directed eastward in the southern part and westward and southward in the northern part (Løset and Carstens, 1996). The first sea ice appears in the northern and eastern area in October, and the maximum extension is reached in April. There is no sea ice in August and September. The southern quarter of the sea is ice free year round, except some bays and fjords (Groves and Nunt, 1980). The most common ice is first year ice. The ice thickness can be up to 2 m for first-year ice, and 3 to 5 m for multi-year ice. The mean ice thickness of the region is estimated to be 0.9 to 1.2 m (Løset et al., 1997). Icebergs are also found in the Barents Sea. Mean sail height is

estimated to be 15 m, and the mean diameter is 92 m (Løset and Carstens, 1996).

Comparison

The Okhotsk Sea and Barents Sea have several common features. The areal extent of the seas is quite similar, and the both are attached to the same continent and bounded by islands of various size, so that they have characteristics of a semi-mediterranean sea. A large part of the seas are shallow, but adjacent oceans are quite deep.

The air temperature, precipitation and evaporation have a similar range over the both seas. Hence, the climatic condition of the seas does not differ much in spite of the latitude difference. They are both generally windy seas and the wind speed is greater in winter. The strong wind is oriented in particular directions. Although the drainage area of the Barents Sea is half that of the Okhotsk Sea and the total precipitation is similar in both basins, a similar amount of total discharge is expected due to the difference in the terrestrial evaporation. Both seas have abundant fresh water supply in similar quantity.

The northern boundaries connect the seas to the coldest part of the continent and the coldest part of the ocean in the northern hemisphere respectively. Toward south both seas are connected to the water bodies, which are relatively warm and salty.

Differences are also found in the geographic elements of the Okhotsk Sea and that of the Barents Sea. The Okhotsk Sea has a geometry of a bay, where the current can make a round trip in the sea, whilst the Barents Sea is a wide channel, where two oppositely directed parallel currents can pass by each other within the region.

The Okhotsk Sea is strongly influenced by the climatic conditions of the continent, which invade the region. The maritime climate governs the Barents Sea, and it can be treated as a branch of the Atlantic Ocean. Although both seas are windy, there is a difference in the magnitude. The mean wind speed at the Barents Sea is esti-

mated to be almost twice as large as that at the Okhotsk Sea. The transport efficiency of pack ice is thus quite high in the former. The climate conditions of surrounding areas of the seas especially on the continent may differ from each other, even when they are similar on the seas. For instance, the latitude difference may lead different evaporation in river basins. The climate in enlarged area can thus influence the seas indirectly and possibly in different way. The Barents Sea has a supply of sea ice from the adjacent ocean, but no sea ice is produced in the sea around the Okhotsk Sea. Hence, the former has an additional fresh water supply in a solid form.

References

- Aota, M. and Uematsu, E. 1989. The study on the polar ocean and the sea of Okhotsk. *J. Geogr. (Chigaku-zasshi)*, 98(5), 70–82.
- Cattle, H. 1985. Diverting Soviet rivers: some possible repercussions for the Arctic Ocean. *Polar Record*, 22(140), 485–498.
- Dzhenyuk, S.L., Zykova, G.G. 1992. Hydro-meteorological studies of sea of the Northern Eurogean basin. *Proc. Arctic Antarctic Sci. Res. Inst.*, 426, 1–215. (in Russian).
- Embleton, C. (ed.) 1984. *Geomorphology of Europe*. Macmillan Press (Japanese translation by M. Ohya and K. Saka, 1997, Tai-meido Publishing Co., Tokyo, 703 pp.)
- Energy, Mines and Resources Canada. 1990. *The National Atlas of Canada, 5th edition*, North circumpolar region, 1:10000000.
- Fukutomi, T. 1952. Study of sea ice. (18th report). Drift of sea ice due to wind in the Sea of Okhotsk, especially in its southern part. *Low Temp. Sci.*, 9, 137–144.
- Groves, D.G. and Nunt, L.M. 1980. *The Ocean World Encyclopedia*. McGraw-Hill, New York, 443 pp.
- Korzun V. I. et.al. 1974. *Atlas of World Water Balance*. Chief administration of hydrometeorological service under the council of ministers of the USSR, Moscow, 65 sheets.
- Løset, S. and Carstens, T. 1996. Sea ice and iceberg observations in the western Barents Sea in 1987. *Cold Regions Sci. Tech.*, 24, 323–340.
- Løset, S., Shkhinek, K., Strass, P., Gudmestad, O.T., Michalenko, E.B. and Kärnä, T. 1997. Ice conditions in the Barents and Kara seas. pp. 173–181. In *OMAE and POAC, vol. IV*, H. Yamaguchi et al. (eds.), The American Society of Mechanical Engineers, New York.
- National Astronomical Observatory. 1995. *Rika nenpyo (Chronological Scientific Tables)*. Maruzen Co., Tokyo, 1043 pp.
- Nomura, S. (ed.) 1997. *The Atlas of the Modern World*. Shobunsha Publications, Tokyo, 214 pp.
- Parkinson, C.L. and Gratz, A.J. 1983. On the seasonal sea ice cover of the sea of Okhotsk. *J. Geophys. Res.*, 88(C5), 2793–2802.
- Shilo, N.A., Kosygin, Yu.A., Bersenev, I.I., Zhuravlyov, A.V., Kulinich, R.G., Sergeyev, K.F., Tuezov, I.K. and Khvedchuk, I.I. 1982. The structure and history of geological evolution of Earth's crust in the Japan and Okhotsk Sea regions. pp. 59–80. In *Geology of Japan Sea*. Hoshino, M. and Shibasaki, T. (eds.), Tokai University Press, Tokyo.
- Shirasawa, K. et al. 1996. Meteorological data report for the sea ice studies at Val, Chaivo and Kleye Strait, northern Sakhalin. *Low Temp. Sci., Ser. A, 55, Data Rep.*, 135–203.
- Strass, P., Løset, S., Shkhinek, K., Gudmestad, O.T., Kärnä, T. and Michalenko, E.B. 1997. Metocean parameters of the Barents and Kara seas – An overview. pp. 165–172. In *OMAE and POAC, vol. IV*, Yamaguchi, H. et al. (eds.), The American Society of Mechanical Engineers, New York.
- Wadachi, K. 1987. *Encyclopedia of Oceanography*. Tokyodo Publishing Co., Tokyo, 589 pp.
- Wakatsuchi, M. and Martin, S. 1990. Satellite observations of the ice cover of the Kuril basin region of the Okhotsk Sea and its relation to the regional oceanography. *J. Geophys. Res.*, 95(C8), 13,393–13,410.
- Zuenko, Y.I. and Yurasov, G.I. 1997. Structure of the coastal waters of the Sea of Okhotsk. *Russian Meteorol. Hydrol.*, 3, 32–37.

On wind and tide induced sea-ice drift on the northeastern shelf of Sakhalin Island (analysis of radar data)

George V. SHEVCHENKO¹ and Victor F. Putov²

¹Institute of Marine Geology and Geophysics, Russian Academy of Sciences, Yuzhno-Sakhalinsk, Russia

²Environmental Company of Sakhalin, Yuzhno-Sakhalinsk, Russia

Introduction: Radar measurements of sea ice drift

Severe ice conditions are typical for the northeastern shelf of Sakhalin Island. Sea-ice fields in this region are large, heavy and fast moving (Pokrasenko et al., 1987). Examination of these motions is interesting from the scientific point of view and has significant applied importance. In the present work we investigate the velocities of ice drift induced by tides and wind. The main purpose of the study is to estimate their nature, main parameters, and maximum values.

The properties of the Okhotsk Sea ice cover are determined by the sea circulation, winter winds, and tides (Martin et al., 1998). To examine the sea-ice drift in the region of oil and natural gas fields the Hydrometeorology Division of the Far Eastern Marine Engineering and Geology Expedition (now the Environmental Company of Sakhalin) installed three radar transceivers on the northeastern coast of Sakhalin Island. Temporary meteorological stations, measuring wind, atmospheric pressure, air temperature, precipitation, and visibility, were also established in the vicinity of these installations whose coordinates were as follows: 54.1°N, 142.9°E (Cape Levensterna, 1992–1995), 53.5°N, 143.1°E (Odoptu, 1985–1996), and 51.1°N, 143.6°E (Komrvo, 1991–1993). The location of these radar stations and current-meter recorders deployed on the shelf of Sakhalin Island are presented in Figure 1.

These radar stations recorded sea-ice drift at the distances of approximately 4, 8, 12 and 18 km (the latter only by the Odoptu radar). Hourly drift vectors were estimated by the differences in the ice field positions. The positions were fixed three times per hour: at 10 to the hour, at the hour and 10 min after the hour. We interpolated and averaged the data and get several hourly vector series for each installation. In this work we analyze only the drift series measured at the most distant points (12 and 18 km).

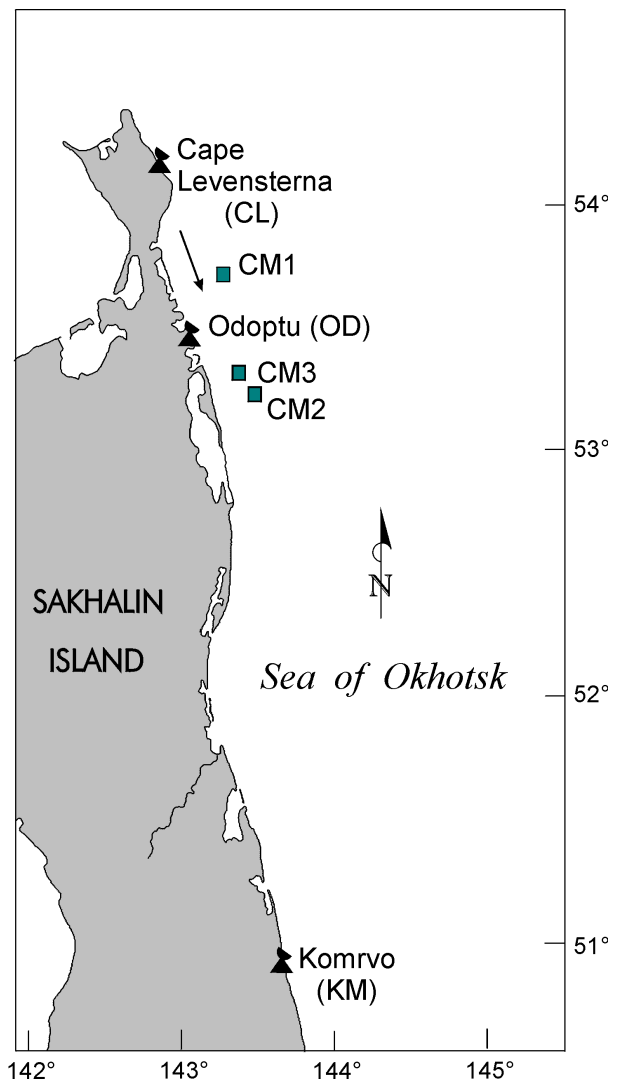


Fig. 1 Location of radar stations Cape Levensterna (CL), Odoptu (OD), and Komrvo (KM), meteorological station and tide gauge Nabil, and current meter stations CM1 (Hanhuzinsk area) and CM2, CM3 (Odoptinsk area) on the northeastern shelf of Sakhalin Island. The arrow indicates direction of propagation of tidal shelf waves.

Preliminary data analysis

The best quality data were obtained in 1993: 100-day series (March 1–June 8) at Cape Levensterna (CL), 73 days at Odoptu (OD), and 85 days at Komrvo (KM). We paid the most attention to the examination of just these series.

The velocity components of the ice drift were estimated in the eastward (u) and northward (v) directions, i.e. in the offshore and longshore directions relative to Sakhalin Island (Fig. 2). The offshore velocities were relatively small, of about 10–30 cm/s for all stations. In contrast, the longshore velocities were strong, approximately 100 cm/s. Preliminary analysis showed the dominant role of diurnal tides in the longshore drift motions (at least for the area of stations CL and OD).

The calculated spectra of u and v components for the radar stations CL, OD, and KM are presented in Figure 3. The northward components dominate at all frequencies, however, whereas for the low-frequency band the difference between the energy of two components is significant, for the high-frequency band it is relatively small. There are two noticeable low-frequency peaks at periods of about 12 and 5 days, apparently related to the

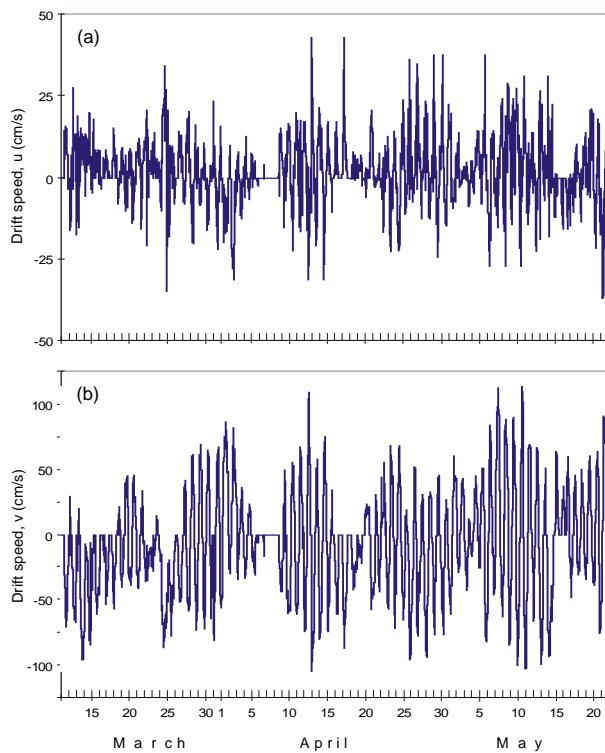


Fig. 2 Eastward (u) and northward (v) components of sea ice drift measured by radar at station OD in 1993.

atmospheric activity. The low-pass filtered data show also existence of the oscillations with a period of about 21 days. The corresponding peak is not seen in Figure 3, but we could detect it based on high-resolution spectral analysis. The same peaks were detected in wind spectra (not shown). Based on results of rotary spectral analysis (see Gonella, (1972)) we found that the angle between the wind and ice-drift vectors at the periods of the spectral peaks is about 20–30°.

The diurnal spectral peak is dominant at stations CL and OD, but is insignificant at station KM; the semidiurnal oscillations of the sea-ice are small at all stations (Fig. 3). These results are in agreement with the results of Rabinovich and Zhukov (1984) and Popudribko et al. (1998), who showed that semidiurnal tidal currents are negligible in this region, in comparison with diurnal currents.

Based on the results of the spectral analysis, we defined three “natural” frequency bands associated with different types of external forcing: The low frequency (LF) band, with frequencies less than 0.8 cpd; the tidal (TD), with frequencies between 0.8 and 2.2 cpd; and the high-frequency (HF), with frequencies greater than 2.2 cpd. In the text that follows, these three frequency bands are analyzed separately.

Low-frequency wind induced drift

The low-frequency ice motions, obtained by low-pass filtering of the residual (non-tidal) series with 25-h sliding window, were highly correlated with wind. Figure 4 presents the meridional (along-shore) components of the ice-drift and wind at station Odoptu (OD). We have not found any phase shift between the wind and ice drift. Estimation of the correlation function for all three stations showed that the sea-ice field responds to wind forcing almost immediately. These results are in contrast to the results of Pokrasenko et al. (1987) who pointed out that there is 8-h time shift between these processes.

The typical seasonal variations of longshore wind and low-frequency ice-drift motions are shown in Figure 4. Northerly and northwesterly winds with speeds of about 5–8 m/s normally prevail in January to March on the northeastern coast of Sakhalin Island. These winds are induced by a steady “winter monsoon” determining winter weather in this region (see Shevchenko and Saveliev in this

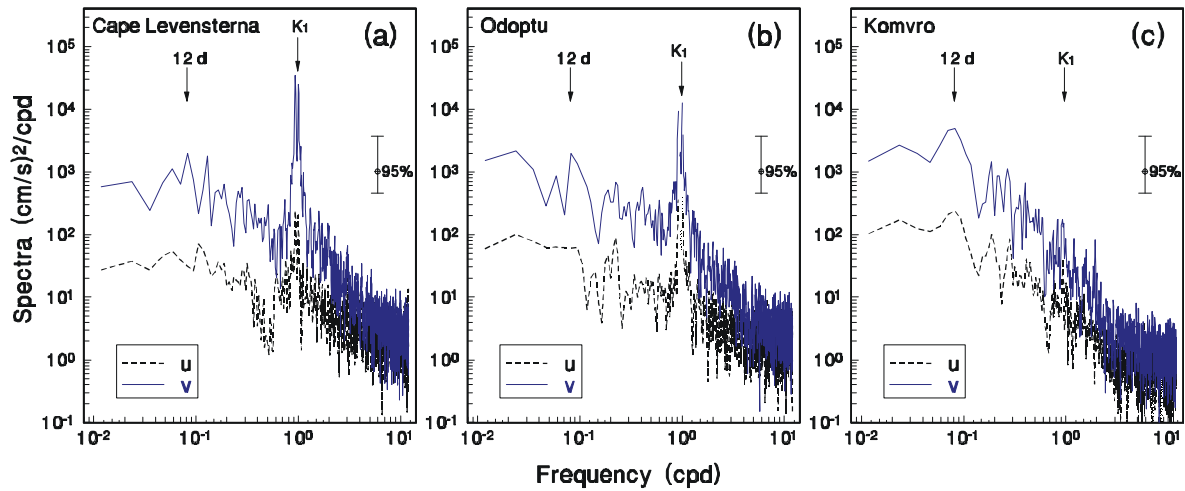


Fig. 3 Spectra of u and v components of sea ice drift at stations CL (a), OD (b), and KM (c). Spectra are computed for degree of freedom, DoF = 8.

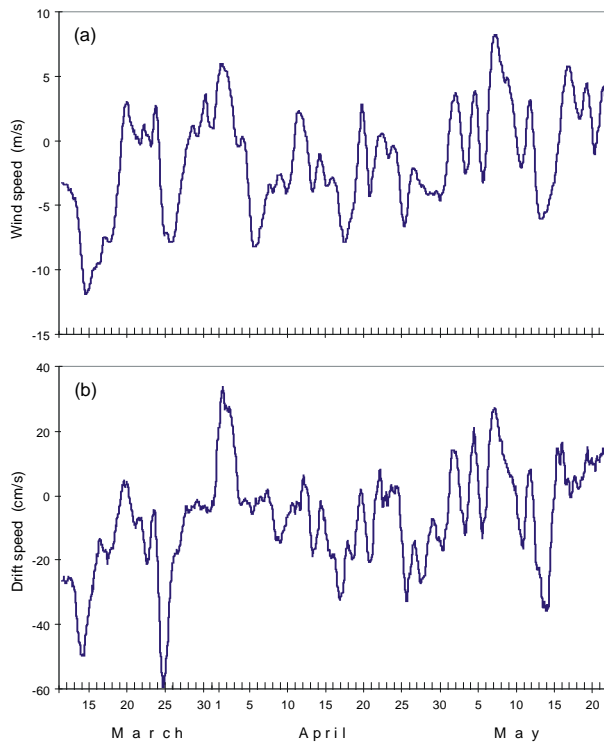


Fig. 4 Northward (longshore) components of (a) wind and (b) low-frequency ice drift at station OD, March 11 to May 23, 1993.

volume). Respectively, wind-induced ice-drift motions have southern and southeastern directions. The distribution of wind directions is less stable in April than in wintertime. In May southeasterly winds of about 3–5 m/s (‘summer monsoon’)

dominate in the area. The general southward propagation of sea ice in May and June is probably associated with the Eastern Sakhalin Current.

Strong winds with velocities of about 15–25 m/s are related to continental cyclones frequently occurring in this region during the ice-covered period. For cyclones crossing Sakhalin Island, wind directions change very fast and these winds do not produce significant currents and associated ice-drifts. In contrast, for cyclones staying in the Sea of Okhotsk, steady northerly and northwesterly winds are rather typical. Specifically, these winds produce maximum velocities of residual (non-tidal) ice-drift of about 1 m/s traveling in southern and southeastern directions.

The high correlation of low-frequency ice motions and wind is clearly seen in Figure 5. We used a linear regression model to estimate, R , the “wind coefficient of the ice-drift”. We made computations for longshore and cross-shore components independently and obtained the following values: $R_v = 4.0$ (cm/s)/(m/s) (Fig. 5), and $R_u = 2.0$ (cm/s)/(m/s), respectively. That means that a longshore wind of 10 m/s induces ice-drift moving with a speed of about 40 cm/s, and a cross-shore wind of the same speed produces ice-drift of about 20 cm/s. These regressional coefficients, R_v and R_u , can be used for short- and long-term forecasts of ice-drift on the northeastern shelf of Sakhalin Island.

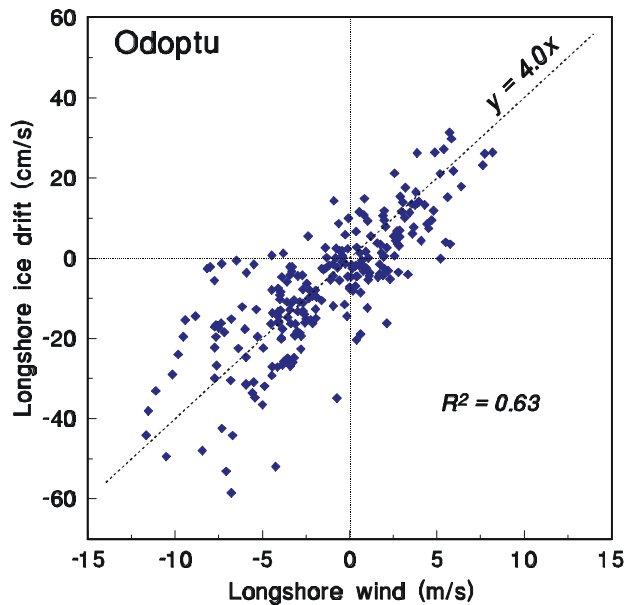


Fig. 5 Correlation (R^2) between longshore components of wind and low-frequency ice-drift. The solid straight line corresponds to “wind coefficient of ice drift” (cm/s)/(m/s) estimated using a linear regression model.

Tide-induced sea ice drift

The tide-induced drift motions of sea-ice were estimated using the least square method. The maximum values of the longshore tidal drift velocities were found to be of about 100–110 cm/s at CL, 90–100 cm/s at OD, and 15–25 cm/s at KM radar stations. These large tidal currents were related mainly to K_1 and O_1 diurnal tidal harmonics. As was shown first by Rabinovich and Zhukov (1984), and later by other authors (Suzuki and Kanari, 1986; Kowalik and Polyakov, 1998), strong diurnal currents on the northeastern shelf of Sakhalin Island are produced by tidally generated trapped shelf waves (a similar effect is well known for the Pacific coast of Vancouver Island (cf. Crawford and Thomson (1984); Foreman and Thomson (1997))).

Normally, for the areas with dominant diurnal tides, the extreme yearly tidal values have a prominent 19-year cycle. According to the computations made by Shevchenko et al. (1990), extreme tides for the northeastern shelf of Sakhalin Island were observed in 1968–1969, 1987–1988, etc. The year 1993 was the time when diurnal tides were approximately 20–30% weaker. So, the maximum tidal drift velocities can probably reach 120–140 cm/s.

It follows from the results of spectral analysis (Fig. 3), and from direct estimations of tidal currents by the least square method, that diurnal tides play a dominant role in the ice-drift motions at stations OD and CL, but are insignificant at KM. According to numerical modeling of tides on the northeastern shelf of Sakhalin Island (Suzuki and Kanari, 1986; Kowalik and Polyakov, 1998), diurnal tidal currents are very strong near the northern end of the island (the probable generation area of shelf waves), and then decrease in the southward direction. A similar picture of strong diurnal tidal currents decreasing with distance from the generation area of diurnal shelf waves (Juan de Fuca Strait) was described by Foreman and Thomson (1997) for the Pacific shelf of Vancouver Island. The main reason of this effect is dissipation of diurnal shelf waves (Rabinovich and Shevchenko, 1984). It is known that tidal shelf waves are normally accompanied by strong currents in near-shore zone (see the review article by Clarke (1991)), but bottom friction causes their fast dissipation. So, we may assume that weakening of diurnal currents and associated ice motions in the area of Komrvo is related to the decreasing (because of dissipation) of shelf waves propagating southward along the northeastern coast of Sakhalin Island. The other possibility is the presence of local amphidromic points for diurnal tides near to Sakhalin Island as was supposed by Rabinovich and Zhukov (1984). Existence of such local amphidromic points for diurnal tides near to the shore is also related to the influence of shelf waves (cf. Cartwright et al. (1980)).

We constructed ellipses of the tidal ice-drift for major diurnal constituents K_1 and O_1 . At stations CL and OD these ellipses are very similar: They have approximately the same magnitude, same direction of rotation (clockwise) and are strongly extended alongshore. The only significant difference between CL and OD ellipses is the phase shift. These ice-drift ellipses are in very good agreement with the respective ellipses of tidal currents measured at nearby current-meter stations CM1 and CM2 (Fig. 6), as well as with other measurements of tidal currents made on the northeastern shelf of Sakhalin Island (cf. Rabinovich and Zhukov (1984); Popudribko et al. (1998)). Maximum currents at these stations were about 40–50 cm/s for K_1 and 35–40 cm/s for O_1 .

So stable results and good agreement of ice-drift and current observations made at different years

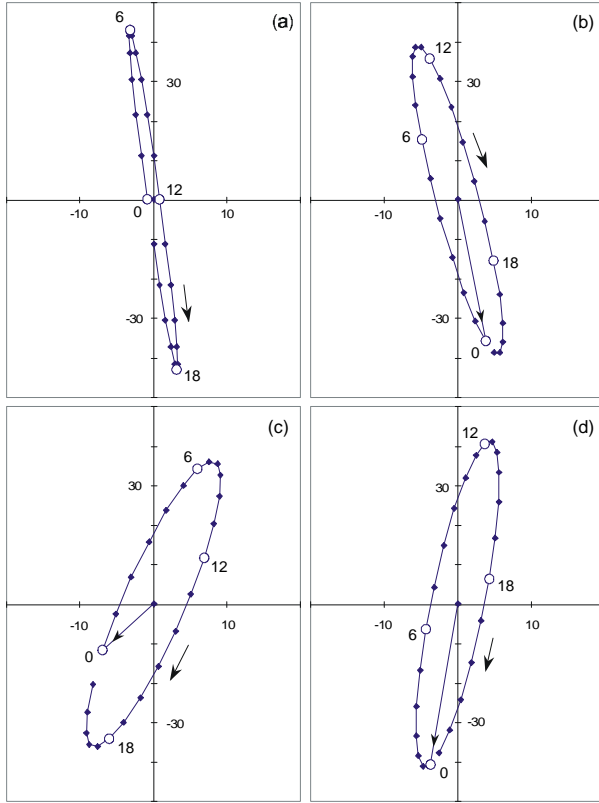


Fig. 6 Tidal ellipses for the main diurnal constituent K_1 for the ice drift measured by radar at stations (a) CL and (b) OD, and for the sea currents recorded at stations (c) CM1 and (d) CM2. Note that the scales of vertical (northward) and horizontal (eastward) axes are different.

and different seasons demonstrate that for the prediction of tidally induced sea-ice drift on the northeastern shelf of Sakhalin Island, we can apparently use the results of tidal analysis of currents formerly measured in this area. The other possibility is to use recent results of numerical modeling of tides and tidal currents in the Sea of Okhotsk (cf. Kowalik and Polyakov (1998)). Both approaches could be important for short- and long-term forecasts of sea ice drift in the vicinity of northeastern Sakhalin Island.

The phase shifts of tidal ellipses between CL and OD stations (both for K_1 and O_1 constituents), corresponding to time shifts of about 6–7 h, show that tidal waves propagate along the northeastern coast of Sakhalin Island from north to south (Fig. 1), i.e. in the direction coinciding with the theoretical direction of shelf waves (cf. Rabinovich and Zhukov (1984); Kowalik and Polyakov (1998)). If the

same tendency remains southward from Odoptu station (at the Piltun-Astokhsk, Chaivinsk or Arkutun-Daginsk oil and gas-bearing areas), then tidal sea-ice drifts in the vicinity of Cape Levensterna and at these areas have *opposite directions*. The southward tidal drift at CL station corresponds to the northward drift at the southern areas, and vice versa.

Following Rabinovich and Zhukov (1984), we estimated phase speeds of K_1 and O_1 diurnal tidal waves using the observed phases of longshore (v) component of ice-drift at stations CL and OD, and currents at stations CM1, CM2, and CM3 (Fig. 5). Least-square fit showed that the phases of diurnal waves increase southward per 1 degree of latitude on 117° (for K_1) and 101° (for O_1). The corresponding phase speeds are: $c = 14.3 \pm 1.6$ km/h (K_1) and $c = 15.8 \pm 1.8$ km/h (O_1). Evident dispersion of diurnal waves is interesting. This result as well as phase speed magnitudes themselves are in good agreement with theoretical estimates of phase speed of diurnal shelf waves made for this region by Rabinovich and Zhukov (1984): 13.9 km/h (for K_1) and 15.3 km/h (for O_1).

Results of tidal analysis show that the diurnal shelf waves play a key role in ice-drift motions on the northeastern shelf of Sakhalin Island. The main properties of shelf waves are well established (cf.

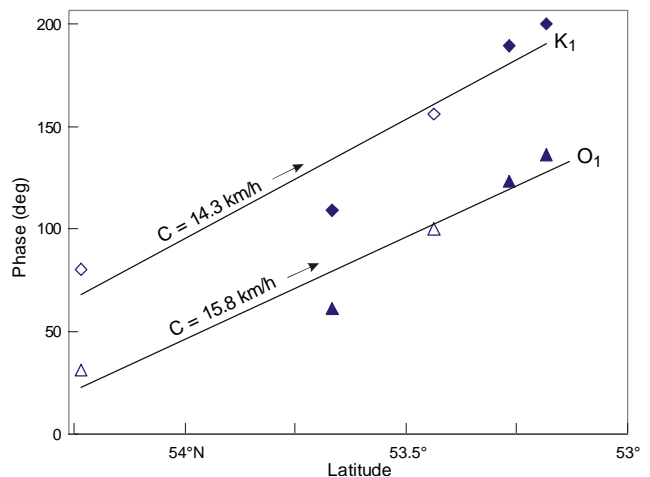


Fig. 7 The K_1 (diamonds) and O_1 (triangles) observed phases of the longshore component of sea ice drift (empty symbols) and sea currents (solid symbols) as functions of the latitude. The straight lines show phase speeds of diurnal shelf waves estimated by a linear regression model from the data.

LeBlond and Mysak (1978)). So, we can use these known properties to describe and predict essential features of ice motions in this area.

It is worthwhile to emphasize another aspect of the problem. A significant influence of shelf waves on various dynamical processes on the shelf is well known. In particular, they play an important role in sedimentation, meandering of boundary currents, coastal upwelling, shelf circulation, formation of storm surges, etc. (LeBlond and Mysak, 1978). However, this is one of the first demonstrations of direct influence of shelf waves on ice-drift. It is interesting to ask, is it a local phenomenon observed only in the northern part of the northeastern shelf of Sakhalin Island or it has a more general character and shelf waves affect the behavior of ice motions over the whole region of the Okhotsk Sea shelf of Sakhalin?. We plan to use the data from Piltun-Astokh, Arcutun-Daginsk, and Lunsk marine oil and natural gas-bearing areas to study this question in the future.

High-frequency drift

The difference between u and v components decreases at periods less than diurnal, and became negligible at periods of a few hours. There are no noticeable spectral peaks at high frequencies of ice-drift motions (Fig. 3). However, these high-frequency motions are quite significant (typical mean currents are of about 7–10 cm/s, maximum currents are 20–30 cm/s both for u and v components). Probably, the main source of these energetic motions is the turbulence induced by the bottom friction. Due to strong tidal currents in the shallow nearshore zone, there is a crucial effect of bottom friction on dynamical processes on the shelf of Sakhalin Island. Stronger high-frequency oscillations at CL and OD stations are associated with stronger tidal currents in this region, so we can assume that we see cascade transfer of tidal energy into high frequencies. As Figure 3 shows, in contrast to tidal and low-frequency bands, the difference between longshore and offshore components of ice-drift at high frequencies is very small, and they look like the spectra of the Gaussian stochastic process. A similar picture is observed for high frequency current oscillations, there is almost no difference between u and v components and between surface and near-bottom layers (Popudribko et al., 1998).

Conclusions

Coastal radar stations can be used effectively to measure sea ice drift over the shelf. Three radar stations established on the coast of Sakhalin Island recorded high quality data, which gave us the opportunity to examine ice motions on the northeastern shelf of the island in a wide frequency range.

Spectral analysis of ice-drift observations revealed three major types of ice motions: (1) Low-frequency, (2) diurnal, and (3) high-frequency. These three types of motions are related to three different generation sources: (1) Atmospheric activity, (2) tides, and (3) turbulence.

Low frequency drift motions are highly correlated with wind. A linear regression model showed that ‘wind coefficients of drift’ are 4.0 (cm/s)/(m/s) for longshore component and 2.0 (cm/s)/(m/s) for cross-shore component. Strong north winds in this region can induce ice motions with velocities more than 1 m/s. The computed ‘wind coefficients’ may be used for long-term and short term forecast of ice drift on the northeastern shelf of Sakhalin Island.

Diurnal tides play the major role in the sea-ice motions in the northern part of the northeastern shelf of Sakhalin. These diurnal tidal motions have velocities more than 1 m/s. Computed tidal ellipses of ice-drift are in good agreement with the respective ellipses of sea currents measured in this region. Computed tidal constituents of currents, as well as the results of numerical modeling of tidal motions, may be used for the prediction of ice-motions in the oil and gas-bearing areas of the Okhotsk Sea shelf of Sakhalin Island.

Strong diurnal tidal ice-motions on the northeastern shelf of Sakhalin Island are shown to be related to diurnal shelf waves. Phase shifts of K_1 and O_1 tidal ellipses estimated from ice-drift measurements and current-meter stations are in very good agreement with a theoretical model of diurnal shelf waves constructed by Rabinovich and Zhukov (1984) for this region. The observed phase speeds of K_1 and O_1 tidal harmonics are 14.3 and 15.8 km/h, in comparison with the theoretical values 13.9 and 15.3 km/h, respectively.

High frequency (0.1–0.5 cph) ice oscillations now and then exceed 20 cm/s in this area. In contrast to tidal and wind-induced motions, their spectra are

almost isotropic. It was found that strong high-frequency ice-motions are normally associated with strong tidal motions. The probable reason of these oscillations is cascade transfer of tidal energy into higher frequencies due to turbulence and bottom friction in a shallow nearshore zone.

Acknowledgments

We would like to thank Drs. Alexander Rabinovich of the Shirshov Institute of Oceanology, Moscow, Russia, and Howard Freeland of the Institute of Ocean Sciences, Sidney, Canada, for constructive comments and careful editing of the text.

References

- Cartwright, D.E., Huthnance, J.M., Spencer, R. and Vassie, J.M. 1980. On the St. Kilda tidal regime. *Deep-Sea Res.*, 27A, 61–70.
- Clarke, A.J. 1991. The dynamics of barotropic tides over the continental shelf and slope (Review). In *Tidal Hydrodynamics*, B.B. Parker (ed.), J. Wiley, New York, 79–108.
- Crawford, W.R. and Thomson, R.E. 1984. Diurnal-period continental shelf waves along Vancouver Island: A comparison of observations with theoretical models. *J. Phys. Oceanogr.*, 14, 1629–1646.
- Foreman, M.G.G., and Thomson, R.E. 1997. Three-dimensional model simulations of tides and buoyancy currents along the west coast of Vancouver Island. *J. Phys. Oceanogr.*, 27(7), 1300–1325.
- Gonella, J. 1972. A rotary-component method for analysing meteorological and oceanographic vector time series. *Deep-Sea Res.*, 19, 833–846.
- Kowalik, Z., and Polyakov, I. 1998. Tides in the Sea of Okhotsk. *J. Phys. Oceanogr.*, 28(7), 1389–1409.
- LeBlond, P.H. and Mysak, L.A. 1978. *Waves in the Ocean*. Elsevier, Amsterdam, 602 pp.
- Martin, S., Drucker, R. and Yamashita, K. 1998. The production of ice and dense shelf water in the Okhotsk Sea polynyas. *J. Geophys. Res.*, 103(C12), 27,771–27,782.
- Pokrasenko S.A., Truskov, P.A. and Yakunin, L.P. 1987. Investigation of sea ice drift on the shelf of Sakhalin Island using the radar methods. *Proc. (Trudy) Far Eastern Research Inst. (DVNII)*, 36, 49–52. (in Russian)
- Popudribko, K.K., Putov, V.F. and Shevchenko, G.V. 1998. Estimation of sea currents characteristics for the Piltun-Astokh oil and gas-bearing area (northeastern shelf of Sakhalin Island). *Meteorology and Hydrology*, 4, 82–95. (in Russian)
- Rabinovich, A.B. and Zhukov, A.E. 1984. Tidal oscillations on the shelf of Sakhalin Island. *Oceanology*, 24(2), 184–189.
- Rabinovich, A.B. and Shevchenko, G.V. 1984. Two-step mechanism for dissipation of tidal energy in the ocean. *Transact. (Doklady) USSR Acad. Sci., Earth Sci. Sec.*, 276, 228–231.
- Shevchenko, G.V. and Saveliev, V.Yu. 1999. Spatial variability of the wind field in the area of the Kuril Islands. pp. 49–53. In *Proc. of the Second Workshop on the Okhotsk Sea and Adjacent Areas, PICES Sci. Rep. No. 12*, Sidney, B.C. Canada.
- Shevchenko, G.V., Fine, A.V., Rabinovich, A.B. and Mansurov, R.N. 1990. Estimation of extreme sea level oscillations in the mouth of the Tym River. In *Natural Hazards in the Far-Eastern Region*, USSR Academy of Sciences, Vladivostok, 253–276. (in Russian)
- Suzuki, K. and Kanari, S. 1986. Tidal simulation of the Sea of Okhotsk. *Kaiyo Kagaku*, 18, 455–463. (in Japanese with English abstract)

Variability of the Japan and Okhotsk Seas ice cover depending on the geopotential field H500 average over the Far Eastern region

Boris S. DYAKOV, A.A. Nikitin, L.S. Muktepavel and T.A. Shatilina

Pacific Research Institute of Fisheries and Oceanography, Vladivostok, Russia

Introduction

Ice cover of the Japan and Okhotsk seas is one of the elements of the climatic system of the Far East and depends on a large number of the factors (Kryndin, 1964; Stolyarova, 1975; Biryulin, 1970; Yakunin, 1966; Plotnikov, 1996). Despite the extensive data on ice cover of the Far Eastern seas, the reasons for interannual and long-term variability are still vague.

The object of this work is to reveal the features in variability of the Japan and Okhotsk Seas' ice cover that depend on atmospheric large-scale processes above the Far East sector of the northern hemisphere.

Data

The following have been used:

1. Data on area of ice cover (%) of the Japan and Okhotsk Seas (1928–1960) published by Kryndin (1964) and obtained from the Far Eastern Regional Center of Data Reception and Processing (Khabarovsk) – 1961–1992. Data on ice cover of the Okhotsk Sea for 1993–1998 were received by satellite images (TV- and IK-images by “Meteor” and NOAA).
2. Data on water temperature at the Holmsk Hydrometeorological Station (1913–1996) were provided by the Sakhalin Hydrometeorological Administration.
3. Average monthly data on geopotential H500 (dam) at airological stations for January, 1950–1998 were given by the Primorskiy Hydrometeorological Service.

Results

The long-term variability of ice extent in the Tatar Strait (Japan Sea) and Okhotsk Sea is presented in Figure 1. Two periods of ice cover are found in

the Tatar Strait: one large (1930–1960), the other small (1962–1992). Extremal low ice cover was marked in 1957 and 1991, and high in 1951, 1954 and 1960. The curve of the course of the Okhotsk Sea ice cover differs significantly from a curve of ice cover in Tatar Strait. The period of high ice cover in winter is for 1966–1988 (22 years) in the Okhotsk Sea; within this large period 6–7 year cycles are observed. The cycle of warm winters began in 1989, with ice cover reaching a minimum in 1996.

During the almost 70-yr period for the Okhotsk Sea, there were observed two cycles of low ice cover winters: the first from 1952–1958 and the second from 1990–1997, with a minimum in 1996 (the duration of cycles is 6–7 years).

Ice cover changes have to be examined in the context of other elements of the climatic system of the Far Eastern sector (30°–60°N, 120°–160°E). From temperature data at GMS Holmsk for 1913–1996 (Fig. 2) the warming of coastal waters at western Sakhalin in the 1990s can be seen. The beginning of warming goes back to the 1960s and coincides with the ice cover change in the Japan Sea. The warming of waters in a surface layer in the southeast and northwest parts of the sea was noted also by satellite and hydrological data (Dyakov, 1996; Ponomarev et al., 1997; Shatilina et al., 1998).

Long-term variation of geopotential anomalies H500 for regions (I, II, III) are shown in Figure 3. The location of selected domains (regions) and airological observatory stations is shown in Figure 4. The amplitude of geopotential oscillations over the northern part of the Japan Sea is much higher than over the Okhotsk Sea. After 1970 in the northern areas (II) strong peaks prevailed there, which were especially characteristic for 1990s (Fig. 3b). The last decade is especially extremal, based on the number of large anomalies. They show changes which occurred in eastern Asia.

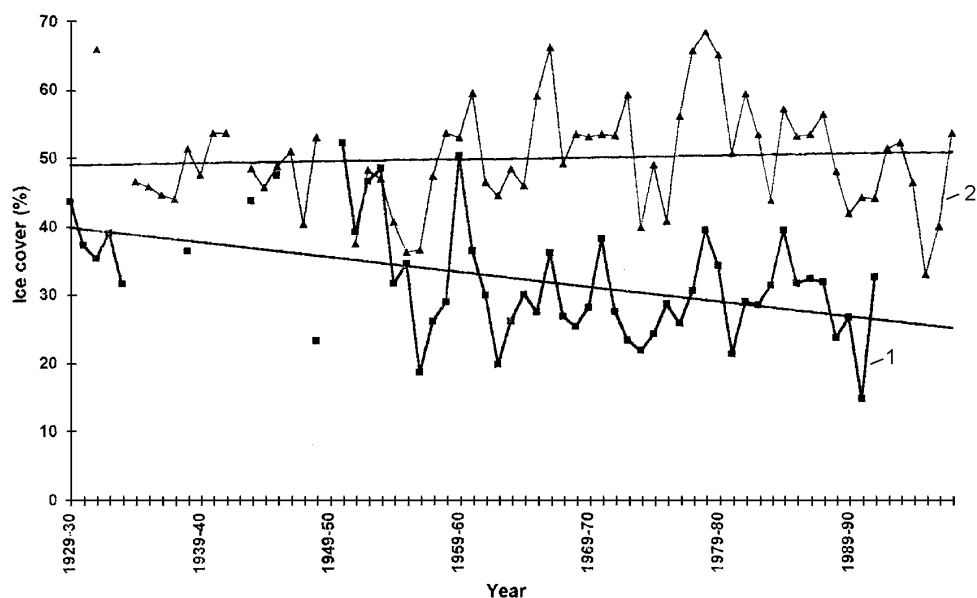


Fig. 1 Variability of ice extent in the Japan Sea (1) and Okhotsk Sea (2) 1930–1998.

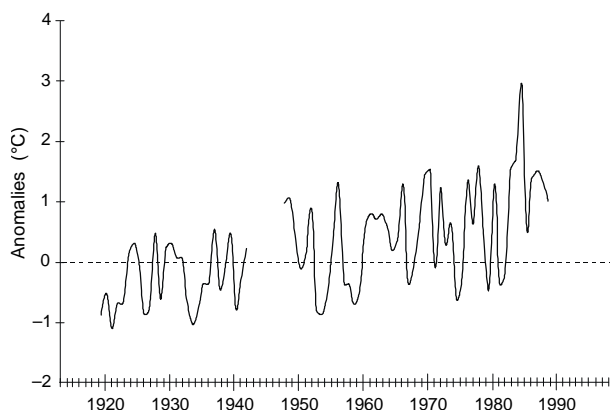


Fig. 2 Water temperature anomalies at Holmsk in January of 1913–1996.

Above the Okhotsk Sea are two periods (Fig. 3), distinguished by frequency of recurrence of strong peaks of pressure, 1950–1969 and 1970–1998. Great decreases of pressure were marked in 1966, 1967, 1978, 1979, 1988. Strong peaks occurred in 1963, 1974, 1991 and 1997. The general trend of pressure is increasing. It is traced more strongly in the second area.

The course of anomalies of geopotential H500 clearly testifies that a new period in variation of atmospheric circulation over the Far East has begun since 1989. These variations have started from a sharp growth of pressure in 1989. In con-

trast to the northern regions (II and III) after 1989 in the southern region (I) is a marked pressure drop (Fig. 3).

A completely contrasting picture in distribution of a field structure H500 in extremal ice cover in winter is observed in Figure 4. So during the extremal ice winters (1954) the Okhotsk minimum in the Tatar Strait is above the northwest part of the Okhotsk Sea (Fig 4a). The cold centers are located there. The Okhotsk minimum is extensive in extremal ice cover in winter (1979) in the Okhotsk Sea and the high-altitude ridge is not observed above western Kamchatka (Fig. 4). The cold centers are also located there.

In low ice cover winters the Okhotsk minimum in the Japan Sea is substituted for a field of high pressure. For example, in 1991 and 1996 in the Okhotsk Sea the Okhotsk minimum shifts to continental regions, and the Pacific ridge to the whole sea (Fig 4). The warm air masses are transferred to the northeastern part of the Okhotsk Sea, and a powerful center of warmth is located there. It is possible to assume that while a ridge of warmth stretches to the Okhotsk Sea, Pacific warm water inflow increases and it promotes an open water region to be larger.

The highest coefficient of correlation ($r = -0.59$) was obtained between the ice cover of the Tatar

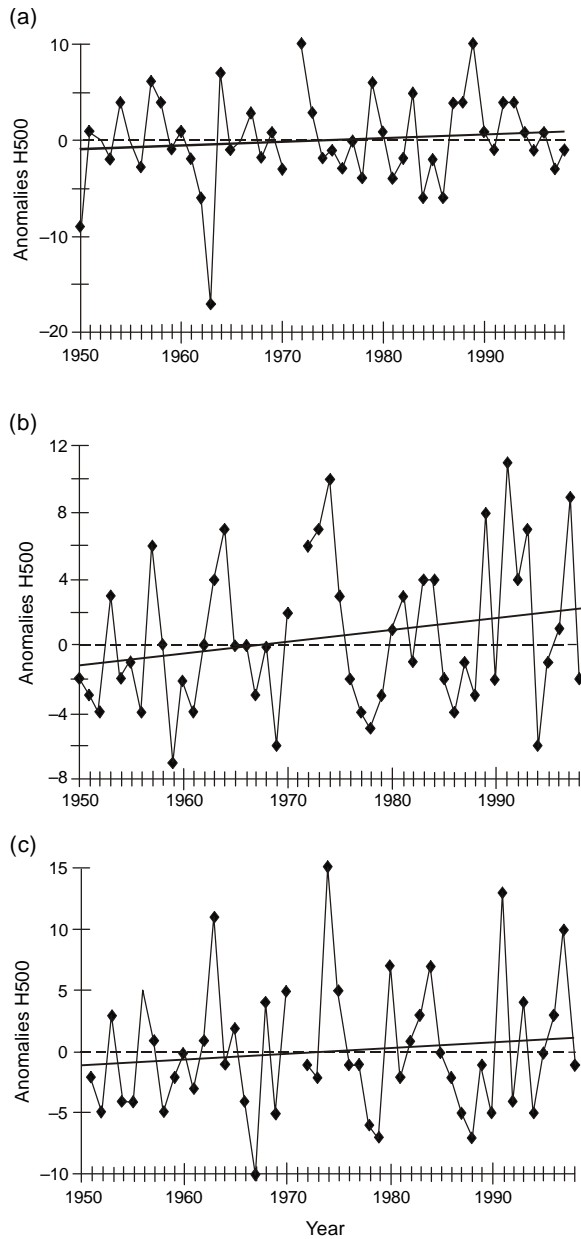


Fig. 3 Long-term variability of geopotential anomalies H500 (dam) over (a) the southern part and (b) the northern part of the Japan Sea and (c) the Okhotsk Sea in January of 1950–1998.

Strait and anomalies of geopotential H500 for Nikolaevsk-on-Amur. (Fig. 5a). The correlation between the ice cover of the Okhotsk Sea and anomalies of geopotential H500 for Nikolaevsk-on-Amur is equal ($r = -0.46$) (Fig. 5b).

In 1990s there was a displacement of the climatic center of low pressure above the Okhotsk Sea which testifies to the variation of circulation mechanisms above the Far Eastern region. In this connection, it is interesting to note that in the 1990s processes such as El Niño (1991, 1994–95) took place which have found a response in the Far Eastern sector of the northern hemisphere.

Conclusions

The comparison of ice cover changes in the Japan and Okhotsk Seas has shown a favourable correlation with changes of H500 structure. Ice cover of these seas is a result of circulation processes above the Far Eastern region. All low ice cover winters were observed when a high depression above the Okhotsk Sea was absent, which changed the transport of cold air masses to the Okhotsk Sea. Weak ice cover in winter was observed in Tatar Strait when there was a sharp increase in pressure over the northern part of the Japan Sea.

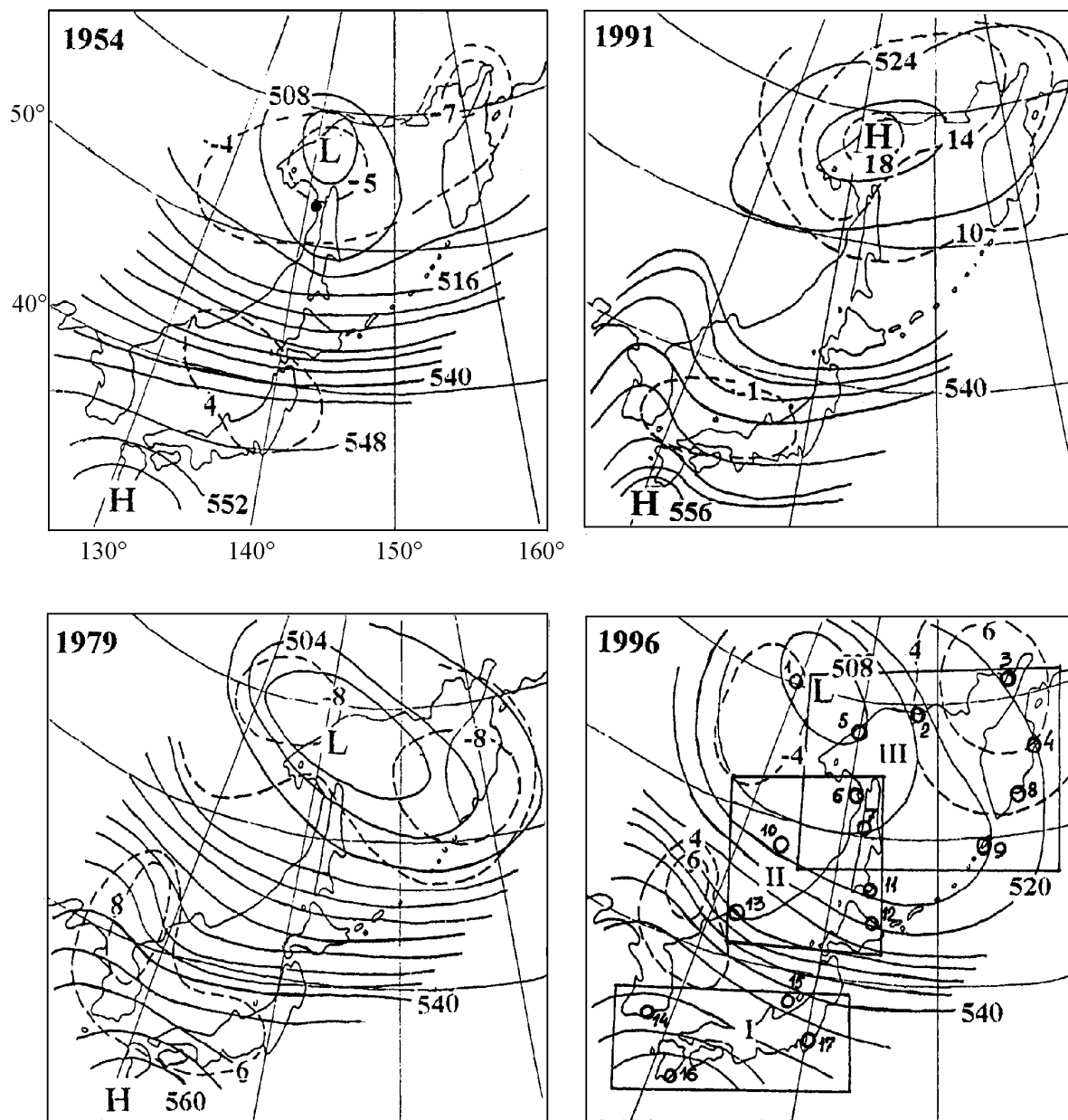


Fig. 4 Structure of geopotential field H500 in January of 1954, 1991, 1979 and 1996. Location of airological observatory stations and domains (I – southern part of the Japan Sea), II – northern part of the Japan Sea, III – Okhotsk Sea) are shown. Stations are: 1 Yakutsk, 2 Magadan, 3 Tayganos, 4 Ust-Kamchatsk, 5 Okhotsk, 6 Nikolaevsk-on-Amur, 7 Aleksandrovsk-Sakhalinsk, 8 Petropavlovsk-Kamchatskiy, 9 Vasilyevo, 10 Khabarovsk, 11 Yuzhno-Sakhalinsk, 12 Abashiri, 13 Vladivostok, 14 Pusan, 15 Aikawa, 16 Aburatsu, 17 Tokyo.

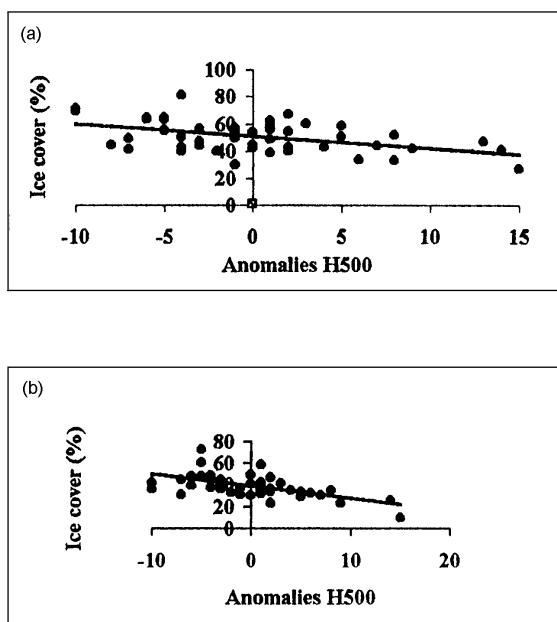


Fig. 5 Correlation between geopotential H500 for Nikolaevsk-on-Amur and ice cover of (a) the Tatar Strait and (b) Okhotsk Sea.

References

Biryulin, G.M. 1970. With a question about forecast of seas of Okhotsk and Bering ice cover. *Trudy DVNIGMI*, 30, 89–93.

Dyakov, B.S. 1996. The long-term variations of temperature and salinity in the south-eastern Japan Sea in winter. pp. 95–99. In *Proceed-*

ings of the Fourth CREAMS Workshop. R/V OKEAN, Vladivostok, 12–13 February, 1996.

Kryndin, A.N. 1964. Ice cover seasonal and inter-annual alteration and the edge of the ice position in the far eastern seas in connection with atmospheric circulation peculiarities. *Trudy GOIN*, 71, 5–83.

Plotnikov, V.V. 1996. The long-term forecast of Sea of Okhotsk ice cover according to the large-scale atmospheric processes. *Meteorol. Hydrol.*, 12, 93–100.

Ponomarev, V.I. and Salyuk, A.N. 1997. The climate regime shifts and heat accumulation in the Sea of Japan. pp. 157–161. In *Proceedings of the CREAMS'97 International Symposium (CREAMS)*, 28–30 January, 1997, Fukuoka, Japan.

Shatilina, T.A., Nikitin, A.A. and Dyakov, B.S. The anomaly development of the Tsushima Current in the northwestern part of the Japan Sea and variations of atmospheric circulation over the Far East. Abstract, pp. 547–550. In *PORSEC'98*, July 28–31 1998, Qungdao, China.

Stolyarova, G.A. 1975. On water mass advection influences on the Gulf of Tatory ice cover. *Trudy DVNIGMI*, 55, Hydromet, Leningrad, pp. 45–50.

Yakunin, L.P. 1966. On a matter of the Far Eastern ice cover fluctuations according to solar activity cyclic recurrence. *Zapiski PFGO USSR*, 25, 88–93, Vladivostok. (in Russian)

Intermediate cold layer and ice cover in the Sea of Okhotsk

Alekandr G. PETROV and Nikolay A. Rykov

Far Eastern Regional Hydrometeorological Research Institute, Vladivostok, Russia

Introduction

The ice cover of the seas is a product of the interaction of atmosphere and hydrosphere. The reason for the appearance of ice is a decrease of temperature of air. Air temperature is also the basic influence for the formation of ice cover in shallow seas. In deep-water seas (the Okhotsk Sea) the influence of hydrological conditions in a number of cases can prevail above meteorological ones. The experience of the FERHRI forecasts shows that the correspondence between ice cover of the Okhotsk Sea and air temperature data is observed only in 2/3 cases and success of the forecasts based only on meteorological factors does not exceed 70–80 %. This allows us to assume that ice cover is affected by other factors, in particular, hydrological conditions. This is confirmed by numerical experiments (Petrov and Frolov, 1980).

In the present paper we analyze the relationship between the characteristics of ice cover in the Sea of Okhotsk and meteorological and hydrological conditions.

Variations in the extent of ice cover by size and meteorological conditions

For the variability in the extent of ice cover, the diagram of the extent for 1962–1986 is constructed (Fig. 1). All range of variability is divided so that to the maximal size there corresponds to 100 (standardization on the maximal size in %), minimal to 0. Such division allows us to estimate better the conformity between size of ice cover of the sea and meteorological characteristics (Fig. 2).

For the effects of meteorological conditions we calculated the sums of average ten-day temperatures of air from November through March for the period from 1962 through 1986 for 18 meteorological stations located evenly along a perimeter of the Okhotsk Sea. The resulting values characterize a temperature background of the winter season. The analysis of the diagrams shows that the size of the ice cover and temperature background coincide

in general. The most interesting features are winters with extreme (minimal and maximal) values of the extent of ice cover and air temperature. Let us consider the diagrams more in detail. Here it is possible to classify the following winters according to Table 1.

There are however, the winters in which an essential discrepancy (20 and more %) between the size of an ice cover and meteorological conditions is found. The most significant of them are summarized at Tables 2 and 3 and presented in Figure 3.

Variations in winters and hydrological conditions

To relate winters and hydrological conditions data on the distribution of the characteristics of the cold intermediate layer (ICL) in the previous warm period of year were used. This layer of negative water temperatures in its core is the basic feature of the Okhotsk Sea. It is formed as a result of thermodynamic destruction of a winter homogeneous

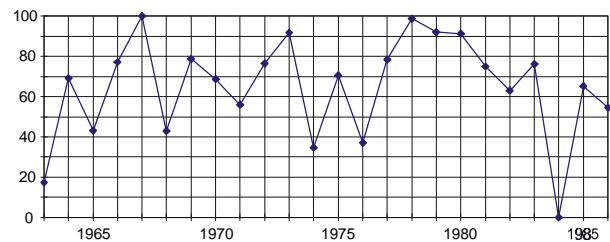


Fig. 1 Variability of an ice cover size (in %) in the Okhotsk Sea.

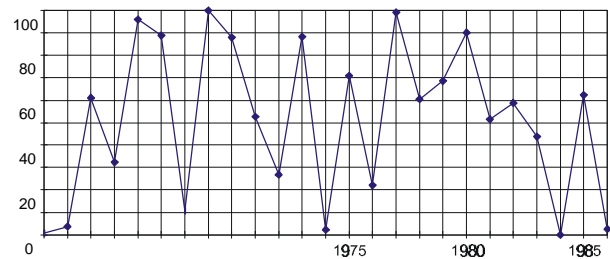


Fig. 2 Variability of air temperature (in %) over the Okhotsk Sea.

Table 1 Winters according to ice cover and air temperature.

with extremely small ice extent	with extremely large ice extent	with extremely low air temperature	with extremely high air temperature
1962–1963	1966–1967	1965–1966	1962–1963
(1973–1974)*	1972–1973	1966–1967	1967–1968
(1975–1976)	1977–1978	1968–1969	1973–1974
1983–1984	1978–1979	1969–1970	1983–1984
–	1979–1980	1972–1973	1985–1986
–	(1965–1966)	1976–1977	–
–	(1968–1969)	1979–1980	–
–	(1971–1972)	–	–
–	(1976–1977)	–	–
–	(1980–1981)	–	–
–	(1982–1983)	–	–

*The years in brackets are close to extreme.

Table 2 Size of an ice cover much below expected on meteorological conditions:

Year	1968–1969	1969–1970	1976–1977	1983–1984	1984–1985
%	+21	+20	+21	+32	+29

Table 3 Size of an ice cover much above expected on meteorological conditions:

Year	1967–1968	1967–1968	1973–1974	1977–1978	1978–1979	1980–1981	1982–1983	1985–1986
%	-32	-49	-32	-38	-23	-23	-32	-24

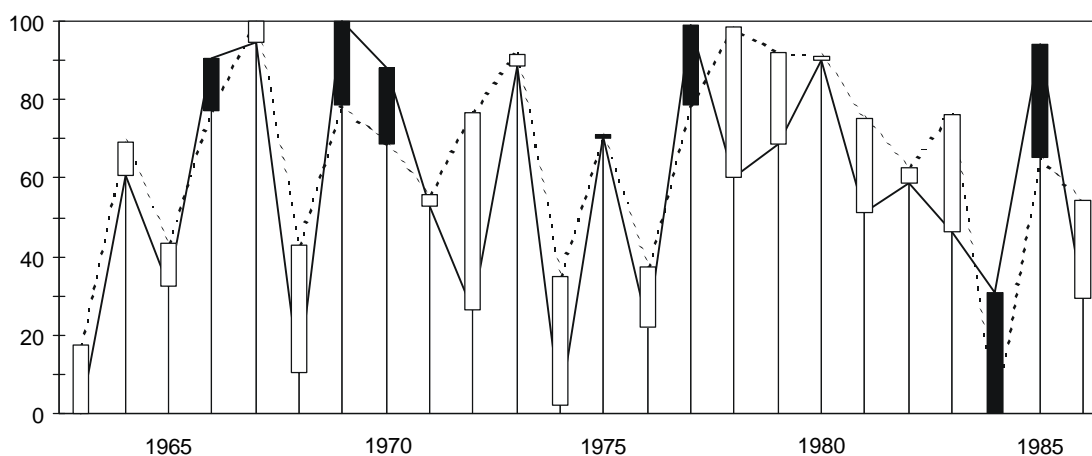


Fig. 3 Joint diagram of sea ice variability and meteorological conditions in the Okhotsk Sea (in %). Black bars refer to mean excess of real ice cover above the expected ice cover. White bars refer to the mean real ice cover below the expected on the meteorological conditions.

layer, which is formed as a result of winter convection. The more ice is formed in the sea, the thicker the water layers cooled down to negative temperatures and the more area it occupies.

ICL actively influences all thermodynamic processes in the sea. Among them it is possible to examine the influence of the ICL on an ice cover. The more extensive ICL is developed, the less the thermal content of the top active layer, and the more ice is formed with other conditions being equal. This given assumption used as a working hypothesis, which was confirmed by this work.

As the most significant influence of the hydrological conditions on the ice cover, we examined ICL parameters in the central part of the Okhotsk Sea to the east of Sakhalin Island.

First we constructed average long-term maps of the ICL characteristics based on all available historical data for months, which had being chosen as

an original definition of thermal conditions prior to each winter of the studied period. These are maps of the top and bottom borders of the layer with negative temperatures and its thickness. Maps for the period 1962–1986 were also constructed for July, August and September. From further analysis it was supposed that the hydrological conditions are characterized by the presence of the ICL, namely, when the ICL is increased strongly, the hydrological conditions are assumed to be extremely cold, and in the opposite case – extremely warm (Fig. 4).

Joint analysis of the characteristics of winters on the extent of ice cover, meteorological, and hydrological conditions

We carried out a joint analysis of the extent of an ice cover, meteorological and hydrological conditions. The results of the analysis are presented in Tables 4–6.

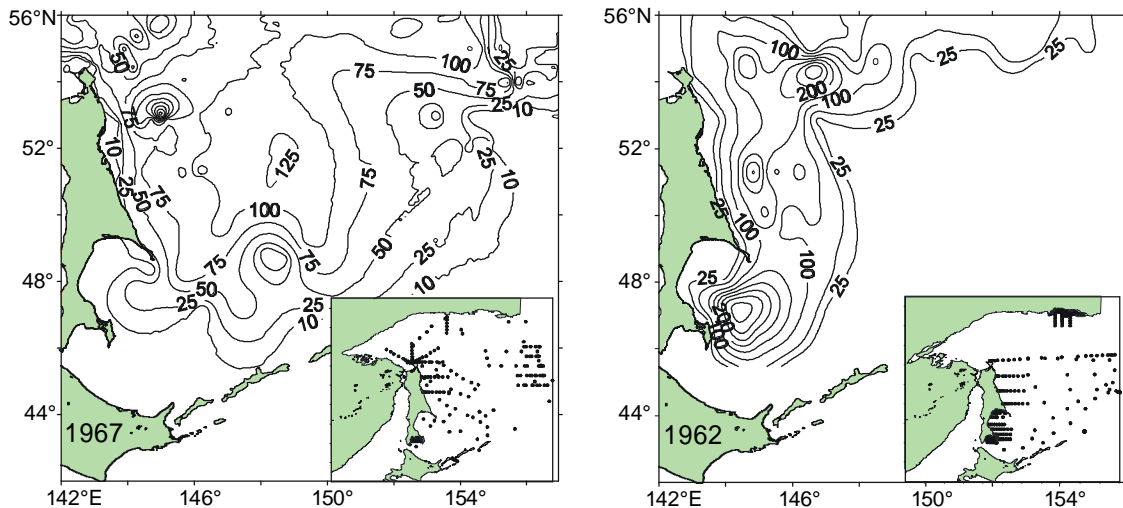


Fig. 4 Example of the classification of a cold (1967) and a warm (1962) year from hydrological conditions in summer. Contours of the thickness of the intermediate cold layer (ICL) are shown.

Table 4 The characteristic of winters with extreme values of an ice cover.

Winter with extremely small size of an ice cover		
Year	Meteorological conditions	Hydrological conditions
1962–1963	Extremely warm	Extremely warm
1983–1984	Extremely warm	Extremely warm
(1973–1974)	Extremely warm	Extremely cold

Table 4 Continued.

Winter with the extremely large sizes of an ice cover		
1966–1967	Extremely cold	Extremely cold
1972–1973	Extremely cold	Extremely cold
1977–1978	Warm	Warm
1978–1979	Warm	Extremely cold
1979–1980	Extremely cold	Extremely cold
(1976–1977)	Extremely cold	Warm

Table 5 The characteristic of winters with extreme values of air temperature.

Winters with extremely low temperatures of air		
Year	Size of an ice cover	Hydrological conditions
1965–1966	Close to the extremely high	No date
1968–1969	Close to the extremely high	No date
1969–1970	Is higher than the average	No date

Winters with extremely high temperature of air		
Year	Size of an ice cover	Hydrological conditions
1967–1968	Close to average	Cold
1985–1986	Average	Cold

Table 6 The characteristic of winters, in which the mutual discrepancy between an ice cover and air temperatures is observed.

Winters with size of an ice cover much below expected on meteorological conditions			
Year	Size ice ñover	Meteorological condition	Hydrological condition
1968–1969	Above the average	Extremely cold	No data
1969–1970	Above the average	Extremely cold	No data
1976–1977	Above the average	Extremely cold	Warm
1983–1984	Extremely small	Close to average	Extremely warm

Winter with size of an ice cover much above expected on to meteorological conditions			
Year	Size of an ice cover	Meteorological condition	Hydrological condition
1967–1968	Close to average	Extremely warm	Cold
1971–1972	Is higher average	Below average	Warm
1973–1974	Close to average	Extremely warm	Extremely cold
1977–1978	Extremely high	Warm	Warm
1978–1979	Extremely high	Close to average	Cold
1980–1981	Above average	Average	Warm
1982–1983	Above average	Below average	No data
1985–1986	Average	Extremely warm	Cold

Conclusions

It is necessary to note that the qualitative analysis of conditions of the cold intermediate layer (in view of the lack of reliable and representative initial data) does not allow us to characterize the thermal condition of an active layer of the sea objectively and fully enough. However, from the obtained results, in the absolute majority of cases the extent of an ice cover is completely defined only by appropriate combinations of meteorological and hydrological factors. At strongly advanced ICL, the ice cover of the next winter is frequently observed to be greater than that expected from meteorological conditions, and at a weaker state of the ICL, the ice extent is lower even under colder meteorological conditions. This conclusion is important for using the characteristics of the cold intermediate layer for forecasting, and for research

in connecting ice cover with meteorological parameters. Frequently, when using the data on only ice extent, one might calculate various periodicities caused by atmospheric circulation parameters (and by other factors) to try to explain their physical meaning. Taking into account hydrological factors can help researchers make more accurate statements regarding research problems, both for the ice cover studies directly and for other questions concerning atmospheric circulation, and the climate as a whole.

References

- Petrov, A.G. and Frolov, I.E. 1980. The numerical model of ice conditions during the pre-winter period. *Trudy DVNIGMI (Proc. FERHRI)*, 80, 3–12. (in Russian)

Interannual variations of oceanographic and meteorological characteristics in the Sea of Okhotsk

Vladimir PONOMAREV¹, Olga Trusenkova¹, Elena Ustinova², and Dmitry Kaplunenko¹

¹ Pacific Oceanological Institute, Russian Academy of Sciences, Vladivostok, Russia

² Pacific Research Institute of Fisheries and Oceanography, Vladivostok, Russia

This study is devoted to low-frequency variations of oceanographic and meteorological characteristics in the Sea of Okhotsk. Time series of sea ice extent, air temperature at the meteorological stations around the Sea, South Oscillation Index (SOI), North Pacific Index (NPI), and of frequency of occurrence for certain meteorological situations were subjected to correlation and spectral analyses. Monthly and seasonal (winter and summer) mean time series were considered for the periods of 40 years and more. Both 3-month (December–February and June–August) and 5-month (November–March and May–September) averaging was used to compose the seasonal time series. In a few cases, averaging was performed for April–June, July–September, October–December or January–March. A 95%-confidence level was chosen to test statistical significance of estimates obtained.

Characteristic time-scales of low-frequency air temperature variations were obtained from power spectra for winter mean time series for the 20th century, often for more than 100 years. We chose the 3 following intervals of interest in the time-scale: biennial (2–3 years), ENSO (3–7 years), and decadal (7–13 years) intervals. Every chosen time interval has, as a rule, the only maximum of 95%-significance level in spectra for monthly mean time series. Typical examples are shown in Table 1. There are biennial maximums for the most stations in the most months. ENSO-scale maximums occur usually in spring, rarer in summer or fall and almost never in winter. On the contrary, decadal-scale maximums are often present in winter, and, rarer, in fall.

The situation is different from that in the Sea of Japan where ENSO-scale maximums are present in air temperature spectra for all seasons of a year, although both ENSO and decadal peaks usually do not occur simultaneously for the spectrum of the same month or season (Ponomarev et al., 1999). The spectrum for the Nemuro station (Table 1)

which is actually located at the Hokkaido Pacific coast is close to those for the Japan Sea. The presence of well-pronounced ENSO and decadal scale variations in the subarctic area corresponds to findings based on analysis of North Pacific winter sea surface temperature (Nakamura 1997; Ponomarev et al., 1999) as well as of the Oyashio Intrusion and snow coverage over eastern Asia (Sekine, Yamada, 1996). Thus, the relationship between seasonal air temperature anomalies and ENSO should be analyzed.

Unlagged cross-correlation was estimated between winter mean time series of air temperature at the meteorological stations around the Sea of Okhotsk and SOI. Lagged cross-correlation was estimated between winter mean air temperature and SOI for the previous (lag of –6 months) or next (lag of +6 months) summer. A statistically significant positive unlagged cross-correlation was found for stations located at the Sakhalin, Siberian and Kamchatka coasts of the Okhotsk Sea. A statistically significant positive lagged cross-correlation, air temperature lagging behind SOI (SOI taken for a previous summer), was also found, although smaller in value compared to the unlagged correlation. Examples are shown in Table 2. A chart of winter air temperature at the Ust-Hairuzovo meteorological station located at the Kamchatka coast of the Okhotsk Sea superimposed with SOI and NPI is shown in Figure 1. It also has unlagged and lagged (SOI leading 6 months) cross-correlations with SOI (Table 3).

Air temperature at the northern Okhotsk Sea shelf has an unlagged cross-correlation with SOI in a transitional fall–winter period from October to December (Table 4). Moreover, it also has a lagged correlation with SOI averaged both for July–September and April–June.

Thus, air temperature over the Sea of Okhotsk tends to have negative (positive) anomaly during winter El Niño (La Niña) events. Likewise, air

temperature over the Sea tends to have positive anomaly in winters following summer La Niña events. This conclusion, however, is not valid for some southern coastal Okhotsk Sea stations. As seen in Table 2, the Nemuro and Abashiri stations situated at the northeast Hokkaido coast do not have a statistically significant correlation with SOI, or with the most northern coastal stations in the Okhotsk Sea (Okhotsk and Magadan).

Low-frequency thermal regime variations also manifest themselves in the Okhotsk Sea ice. Sea ice winter mean time series (1957–1989) were composed by averaging 10-day ice cover in winter and early spring (21–28 of February, 1–10, 11–20

and 21–30 of March, and 1–10 of April). Both its unlagged and lagged (ice 6 months lagging SOI) cross-correlation with SOI is statistically significant and negative (Table 3, Fig. 2). Thus, ice cover in the Okhotsk Sea tends to increase during winter El Niño events (when SOI reaches its highest negative values) and to decrease in winters following summer La Niña events (when SOI reaches its highest positive values).

As a whole, seasonal links between ENSO and oceanographic and meteorological characteristics suggest winter cooling in the Sea of Okhotsk during winter El Niño events and winter warming there after previous summer La Niña events.

Table 1 Characteristic time-scales of air temperature variations for the meteorological stations around the Sea of Okhotsk based on seasonal mean time series spectra. A 95% confidence level is accepted. Underlined are values corresponding to the middle of ENSO (3.0–6.9) or decadal (7.0–13.5) periods.

Month	Station	Periods (in years)			Station	Periods (in years)			
		2.0–2.9	3.0–6.9	7.0–13.5		2.0–2.9	3.0–6.9	7.0–13.5	
Winter	Okhotsk, 1926–1990	2.2	6.4	8.0	Icha, 1951–1990	<u>2.0</u>	<u>4.0</u>	<u>9.3</u>	
Spring		2.1	<u>4.9</u>			2.9			
Summer		2.0	3.0			<u>2.0</u>			
Fall		2.0	3.0			<u>2.0</u>			
Winter	Ajan, 1951–1990	2.9	3.7	8.0	Simushir, 1951–1990	<u>2.0</u>	<u>5.0</u>	8.0	
Spring		2.4				<u>5.6</u>			<u>2.0</u>
Summer						<u>2.4</u>			<u>2.0</u>
Fall						2.4			<u>2.4</u>
Winter	Vakkanai, 1951–1990	2.9	<u>4.4</u>	8.0	Nemuro, 1884–1990	2.1	<u>4.1</u>	8.2	
Spring						2.5			11.8
Summer						2.2			<u>5.6</u>
Fall						2.4			4.6
Winter	Yuzho- Sakhalinsk, 1951–1990	2.0	<u>5.0</u>	8.0	Abashiri 1951–1990	2.4	<u>5.0</u>	8.0	
Spring		2.0				3.1			
Summer		2.4				3.1			
Fall		2.4				13.3			13.3

Table 2 Cross-correlation of winter mean air temperature time series (1949–1990) at the coastal meteorological stations around the Sea of Okhotsk with each other and SOI averaged for the same winter, next summer (SOI, +6 months) and previous summer (SOI, –6 months). Linear trend is subtracted. A 95% confidence level is equal to 0.308, according to the Fisher test.

	Okhotsk	Ajan	Icha	Nikolaevsk	Alexndrvsk	Poronaysk	Abashiry	Nemuro	SOI	SOI, +6 mo	SOI, –6 mo
Magadan	0.93	0.53	0.79	0.42	0.43	0.52	none	none	0.54	none	0.43
Okhotsk		0.66	0.71	0.58	0.52	0.59	none	none	0.58	none	0.38
Ajan			0.48	0.68	0.78	0.69	0.4	0.47	0.41	none	none
Icha				0.46	0.57	0.59	0.46	0.47	0.51	none	0.42
Nikolaevsk					0.73	0.66	0.50	0.52	0.38	none	0.32
Alexndrvsk						0.84	0.71	0.75	0.42	none	0.28
Poronaysk							0.49	0.57	0.56	none	0.43
Abashiry								0.97	none	none	none
Nemuro									none	none	none

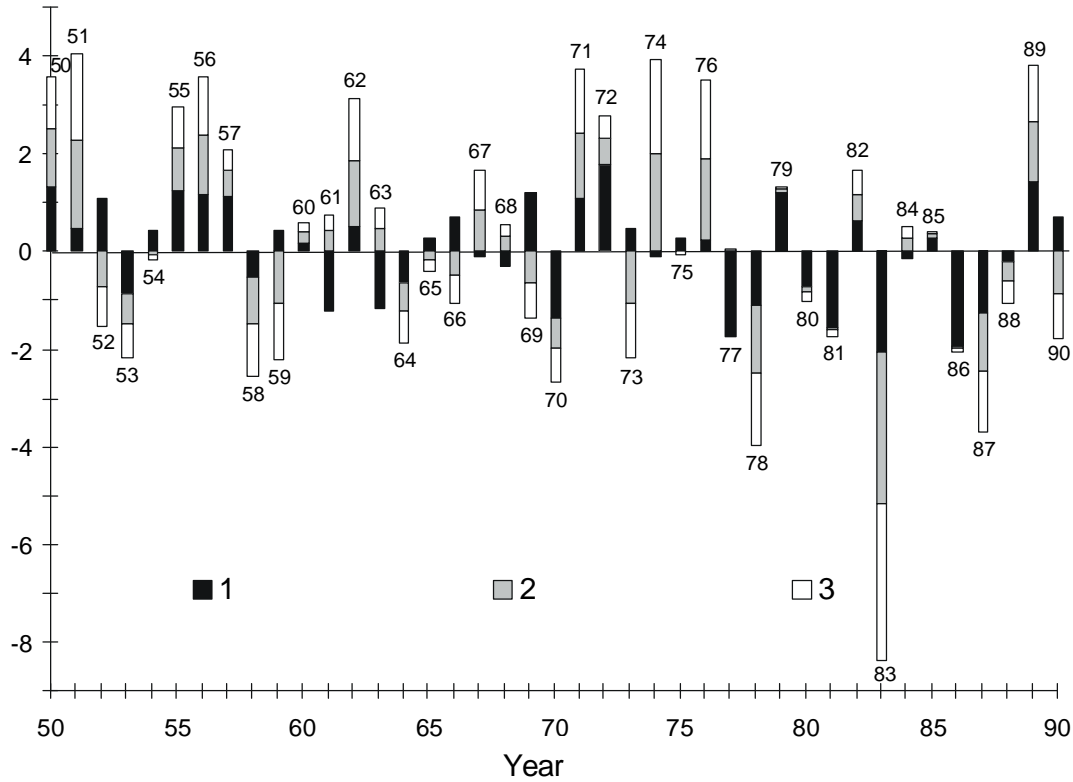


Fig. 1 Time series (1950–1990) of normalized winter anomalies of NPI (1), SOI (2), and air temperature at the Ust-Hairuzovo meteorological station (3). Positive anomalies of SOI correspond to La Niña events, negative anomalies correspond to El Niño events.

Table 3 Unlagged and lagged cross-correlation with SOI of some oceanographic and meteorological characteristics in the Sea of Okhotsk calculated for the winter mean time series. The 95% confidence levels are also shown, calculated based on the Fisher test.

Data	Unlagged SOI	SOI 6 months leading	95%-level
Ust-Hairuzovo air temperature, 1950–1990	0.55	0.34	0.312
Okhotsk sea ice, 1957–1990	-0.45	-0.46	0.349
North Pacific Index, 1940–1990	0.58	0.49	0.282

Table 4 Unlagged and lagged cross-correlation between air temperature at the coastal stations around the northern Okhotsk shelf averaged for October–December and SOI averaged for April–June (SOI, AMJ), July–September (SOI, JAS), October–December (SOI, OND) for the period from 1949 to 1990. A 95%-confidence level is equal to 0.308, according to the Fisher test.

	Ajan	Okhotsk	Magadan	Icha
SOI, AMJ	none	none	0.38	0.34
SOI, JAS	0.32	0.40	0.51	0.36
SOI, OND	none	0.47	0.56	none

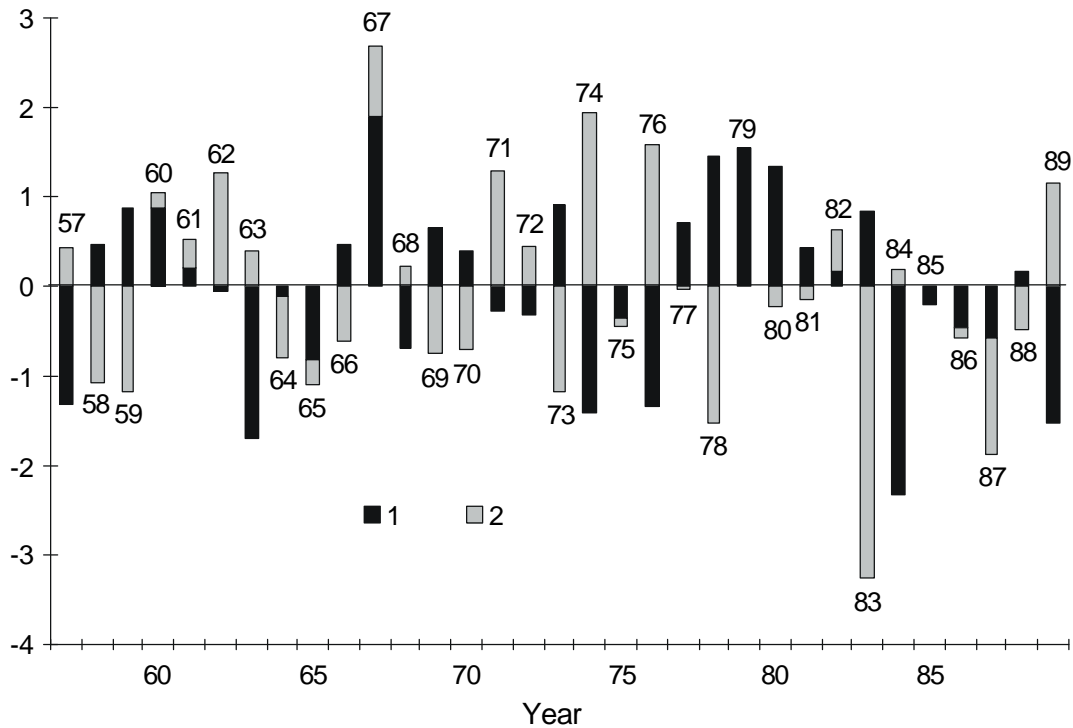


Fig. 2 Time series (1957–1989) of the Sea of Okhotsk ice extent normalized anomaly (1) and normalized winter anomaly of SOI (2). (Positive values of SOI correspond to La Niña events, negative values correspond to El Niño events.)

NPI measuring intensity of Aleutian Low also has statistically significant positive unlagged cross-correlation with SOI for winter. In winter, NPI also has positive lagged cross-correlation with SOI taken for a previous summer (Table 3). Figure 1 shows that NPI varies in phase with air temperature at the Ust-Hairuzovo meteorological station. At the same time, NPI spectra calculated for monthly mean time series in summer have a decadal spectral maximum, which is also present in the winter time series of air temperature over the Sea of Okhotsk. The Okhotsk Sea ice extent shows a decadal maximum in the spectrum as well (Plotnikov, 1997).

It was earlier shown that the ENSO cycle is accompanied by South Asian Monsoon anomalies (Webster and Yang, 1992; Sekine, 1996) and by a change in the jet stream and the associated storm tracks which, in turn, alters the heat and vorticity fluxes caused by the transient eddies over the Northern Hemisphere (Branstator, 1995). Therefore, it is reasonable to suggest that ENSO and decadal scale variations in the Sea of Okhotsk are connected via both annual–biennial oscillations of

the Asian monsoon system and ocean–atmosphere interaction in the western mid-latitude Pacific.

Palmer et al. (1992) and Molteni et al. (1993) argued that, despite very large natural variability of the extratropical atmosphere circulation, there exist certain preferred regimes with rather persistent flow patterns presumably associated with the land–sea distribution and climatological planetary waves. The effect of tropical sea surface temperature forcing associated with the ENSO cycle alters the frequency of occurrence and stability of certain pre-existing regimes (*Learning to Predict Climate Variations Associated with El Niño and Southern Oscillation. Accomplishments and Legacies of the TOGA Program*, 1996).

Polyakova (1997) suggested six typical synoptic patterns of atmospheric circulation over the North Pacific based on heuristic analysis of daily sea surface pressure fields with a special consideration of positions of cyclone tracks and of the Aleutian Low and Subtropical High pressure centers. Choice of original pressure fields rather than averaged, for example, monthly data, gave patterns which keep

information on synoptic processes. They were earlier described in detail (Ponomarev et al., 1999), and similarity were emphasized over the North Pacific with known atmospheric circulation patterns such as the Pacific–North American (PNA), East–West (EW), and Zonal Dipole (ZD) patterns (Wallace and Gutzler, 1981; Barnston and Livezey, 1987). The calendar developed by Polyakova (1997) for the period from 1949 to 1998 reflects alternation of these patterns in time and is hereafter used as a base for composing monthly time series of their frequency of occurrence in days per month.

Considering low-frequency variations of oceanographic and meteorological characteristics in the Sea of Okhotsk, two most frequent meteorological situations are of particular interest (Polyakova, 1997; Ponomarev et al., 1999). They are the Okhotsk–Aleutian and Cyclones Over North Pacific situations (Figs. 3 and 4). The Okhotsk–Aleutian (OA) situation (Fig. 3) represents the classical meridional dipoles with a high pressure ridge over the central Pacific from the Subtropics to the Subarctic and low pressure over the eastern and western Pacific. Northward tracks of southern cyclones dominate over the western and eastern Pacific Ocean. As for the western Pacific, cyclones come from the Philippine Sea through the Kuroshio–Oyashio area to the Kuril adjacent to the Pacific, Japan and Okhotsk Seas.

Figure 5 shows OA normalized annual frequency of occurrence. The biennial variations are clearly seen on the plot, and they are also typical for all six types. The estimated polynomial trend also shows interdecadal oscillations with the period of about 30 years.

To reveal ENSO-scale variations, a cross-correlation was estimated between OA and CN frequency of occurrence and SOI time series. As oscillations are present for different time-scales, correlation coefficients should not be high. In fact, we had to try various sub-samples of the 1949–1998 time series to obtain the best correlation with SOI. Some examples are shown in Table 5. Nevertheless, positive unlagged correlation was found between OA occurrence and SOI in June and November. This means that the OA situation occurs more often when SOI reaches its highest positive values during the La Niña event in June or in November.

Cross-correlation of the OA situation occurrence was estimated with monthly mean air temperature at the meteorological stations around the Sea of Okhotsk. Both unlagged and lagged, with air temperature lagging one month behind OA, correlation coefficients were calculated. As shown in Table 6, all coefficients are positive, that is, the OA situation is warm for the Sea in fall, winter and spring. So, the OA situation, meridional for

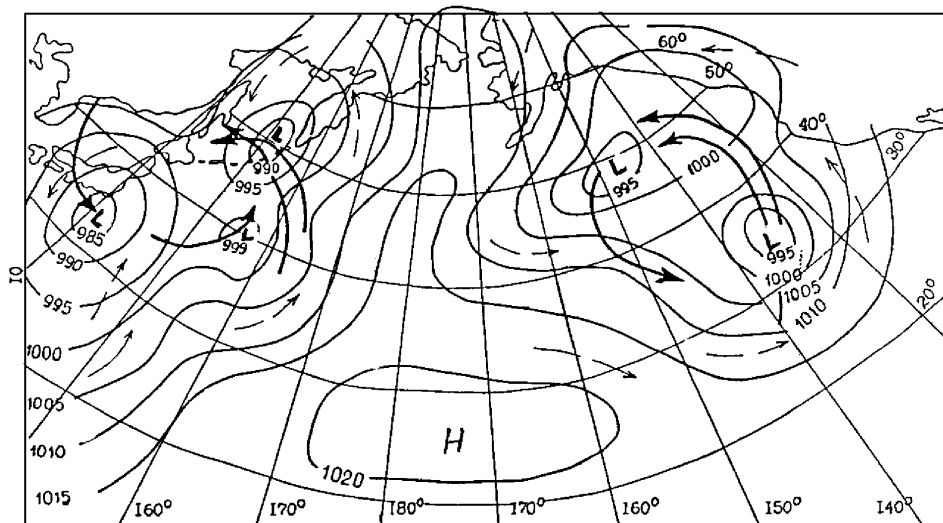


Fig. 3 Sea level pressure pattern corresponding to the Okhotsk–Aleutian synoptic situation. Air mass transport is shown by thin arrows, cyclone tracks are shown by thick arrows. (Reproduced from Polyakova (1997).)

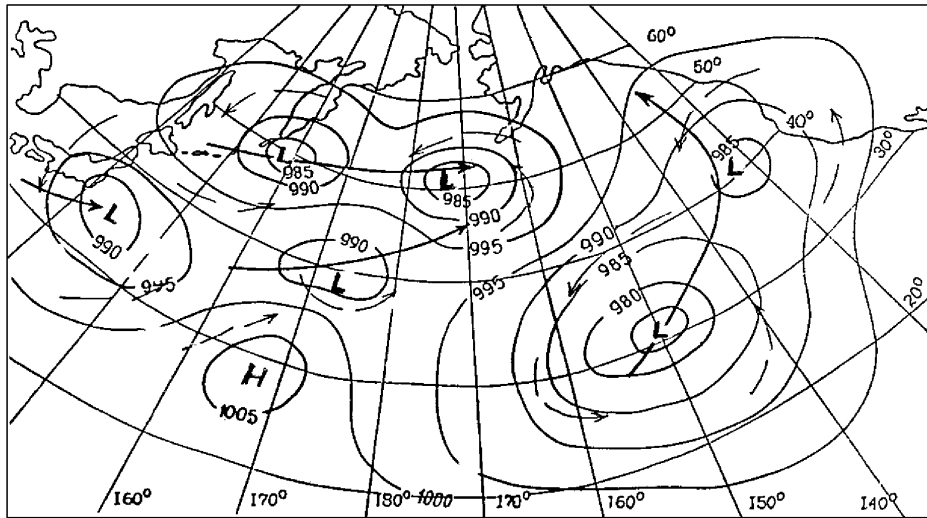


Fig. 4 Sea level pressure pattern corresponding to the Cyclones Over the North Pacific synoptic situation. Air mass transport is shown by thin arrows, cyclone tracks are shown by thick arrows. (Reproduced from Polyakova (1997).)

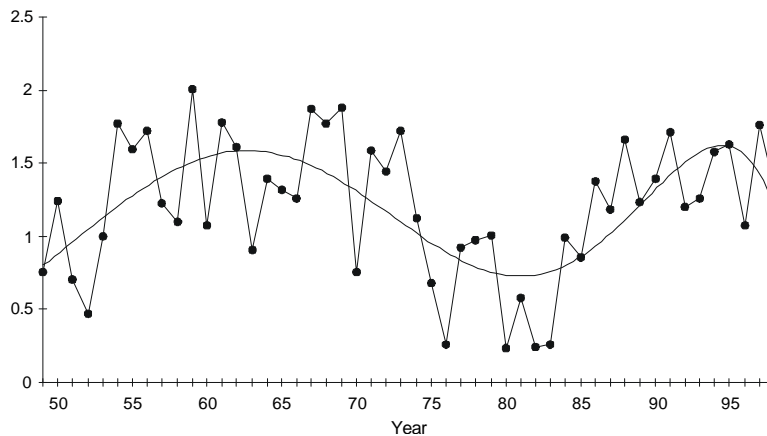


Fig. 5 Annual mean frequency of occurrence for the Okhotsk–Aleutian synoptic situation, normalized by root mean square difference. Polynomial trend of 6th order is also shown.

the whole North Pacific, corresponds to penetration of southern cyclones with characteristic weather patterns to the Northwest Pacific Margin and, in particular, over the Sea of Okhotsk. Positive correlation of OA occurrence with SOI means that decreased southern cyclones cool the Okhotsk Sea during El Niño events in fall or increased southern cyclones warm the Sea in fall after summer La Niña events.

The Cyclones Over the North Pacific (CN) synoptic situation (Fig. 4) is characterized by a meridional circulation pattern in the eastern Pacific with the western position of the Subtropic High Pressure, northward cyclone tracks over the Eastern Pacific, and eastward tracks over the Central and Western Pacific between latitudes of 40°–50°N. To the north of 50°N, cold air comes over the Okhotsk Sea from the Bering Sea and Siberia. The

CN occurrence has negative unlagged correlation with with SOI for March, April, May, October and November (Table 5). Therefore, it occurs more often in spring and fall during El Niño events. The CN situation is cold for the Sea of Okhotsk in winter and spring as estimated cross-correlation with air temperature around the Sea shows (Table 7). So, increased occurrence of the CN situation in spring during El Niño events tends to cool the Sea.

A plot of CN normalized annual mean frequency of occurrence (Fig. 6) shows typical biennial variations as well as multiannual peaks. Averaging intervals between corresponding maximums which took place in 1950, 1958, 1970, 1985, and 1992 gives a period of 10 years, that is, decadal oscillations.

Table 5 Unlagged cross-correlation of the Okhotsk–Aleutian and Cyclone Over the North Pacific synoptic atmosphere situations occurrence (days per month) with SOI based on monthly mean time series. The 95%-confidence levels are also shown, calculated according to the Fisher test.

Data	SOI	Sample size	95% level
Okhotsk-Aleutian, June, 1962–1992	0.415	31	0.360
Okhotsk-Aleutian, June, 1956–1992	0.35	37	0.329
Okhotsk-Aleutian, November, 1949–1996	0.38	48	0.290
Okhotsk-Aleutian, November, 1949–1998	0.35	50	0.282
Okhotsk-Aleutian, November, 1952–1993	0.36	42	0.308
Cyclone over the North Pacific, March, 1959–1997	–0.55	39	0.320
Cyclone over the North Pacific, April, 1959–1997	–0.33	39	0.320
Cyclone over the North Pacific, May, 1949–1994	–0.33	46	0.294
Cyclone over the North Pacific, October, 1966–1994	–0.47	29	0.373
Cyclone over the North Pacific, November, 1949–1994	–0.31	46	0.294

Table 6 Cross-correlation between the Okhotsk–Aleutian synoptic atmosphere situation frequency of occurrence and air temperature at the meteorological stations around the Okhotsk Sea, calculated for monthly mean time series and summarized by seasons of the year. Both unlagged and lagged with air temperature 1 month lagging behind the synoptic situation correlation coefficients are shown. A 95%-confidence level for monthly mean time series for the period 1949–1990 is estimated as 0.308 based on the Fisher test.

Stations	Winter		Spring		Summer		Fall	
	Zero lag	1 month lag	Zero lag	1 month lag	Zero lag	1 month lag	Zero lag	1 month lag
Icha	0.35, 0.49	–	0.31, 0.34	0.47	–	–	0.37	–
Magadan	–	0.36	–	0.35	–	–	–	–
Ajan	–	0.41	–	–	–	–	0.32	–
Nikolaevsk	–	–	0.38	0.37	0.41	–	–	–
Alexandrovsk	–	0.31	0.40	0.36	–	–	–	–
Poronaysk	–	0.33	0.41, 0.49	0.51	–	–	0.33	–
Abashiri	0.35	0.38	0.31, 0.34	0.39	–	–	–	–
Nemuro	0.35	0.42	0.32, 0.37	0.44	–	–	–	–

Table 7 Cross-correlation of the Cyclone Over the North Pacific synoptic atmosphere situation frequency of occurrence with air temperature at meteorological stations around the Okhotsk Sea, calculated for monthly mean time series and summarized by seasons of a year. (A) columns show unlagged correlation coefficients, (B) columns show lagged correlation with air temperature 1 month lagging behind the synoptic situation. A 95%-confidence level for monthly mean time series form 1949 to 1990 is estimated as 0.308 based on the Fisher test.

Stations	Winter		Spring	
	A	B	A	B
Icha	–	–	–0.47	–0.33
Magadan	–	–	–	–0.31
Okhotsk	–	–	–0.33	–0.4
Ajan	–	–0.40	–0.35	–
Nikolaevsk	–	–	–0.32	–
Alexandrovsk	–	–0.32	–0.31	–
Poronaysk	–	–0.42	–0.38	–0.31
Abashiri	–0.31	–	–	–
Nemuro	–0.33	–	–	–

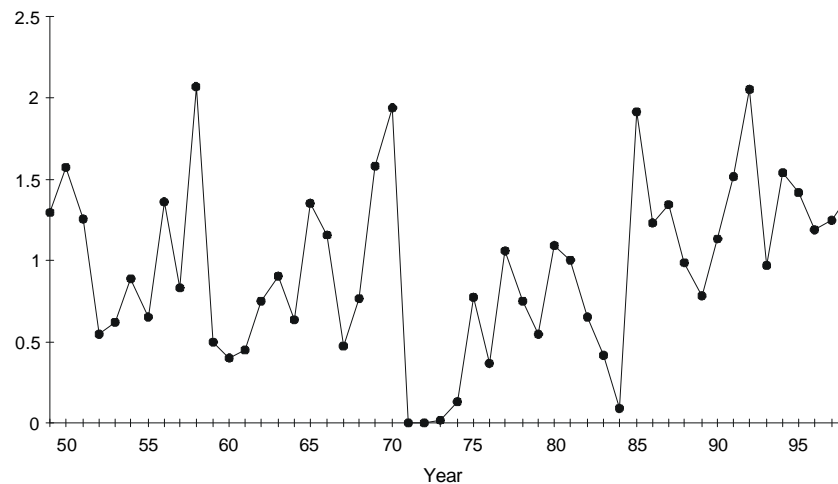


Fig. 6 Normalized annual mean frequency of occurrence for the Cyclones Over the North Pacific.

It is worth noting that the occurrence of the rare Southern-Zonal (SZ) situation seems to be related to the ENSO cycle. The SZ situation (Fig. 7) corresponds to a zonal dipole with high pressure over the Bering Sea and Alaska, extreme southern position of the subarctic low pressure system, eastward cyclone tracks in the subtropic Pacific area, and northeastward cyclone tracks over the subarctic eastern Pacific. The SZ situation may not occur at all during periods from few months to 2–3 years but, when it does occur, its duration (10–20 days) is comparable with the duration of frequent situations like the OA and CN ones (Fig. 8). The SZ situation shows increased occurrence between

typical ENSO cycles and huge occurrence in the 1–2 years before strong El-Niño events, particularly before winters of 1957–1958, 1972–1973, 1982–1983 and 1997–1998 (Fig. 8). As a whole, the highest SZ occurrence was observed in 1953, 1957, 1962–1963, 1968, 1971, 1972, 1974, 1977, 1979, 1981, 1985, 1989, 1993, and 1996–1997, which gives a mean period of 3.2 years consistent with the ENSO cycle. The SZ situation lasted 24 days in August 1996, its maximum occurrence during 1949–1998 (Fig. 8).

Thus, El Niño (La Niña)-accompanying processes in the Northwest Pacific result in cooling (warm-

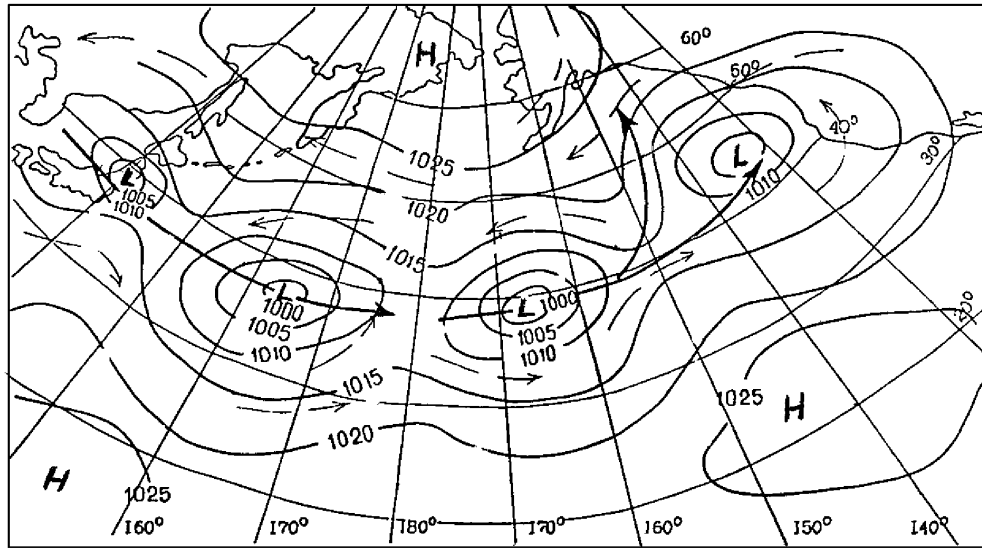


Fig. 7 Sea level pressure pattern corresponding to the Southern-Zonal synoptic situation. Air mass transport is shown by thin arrows, cyclone tracks are shown by thick arrows

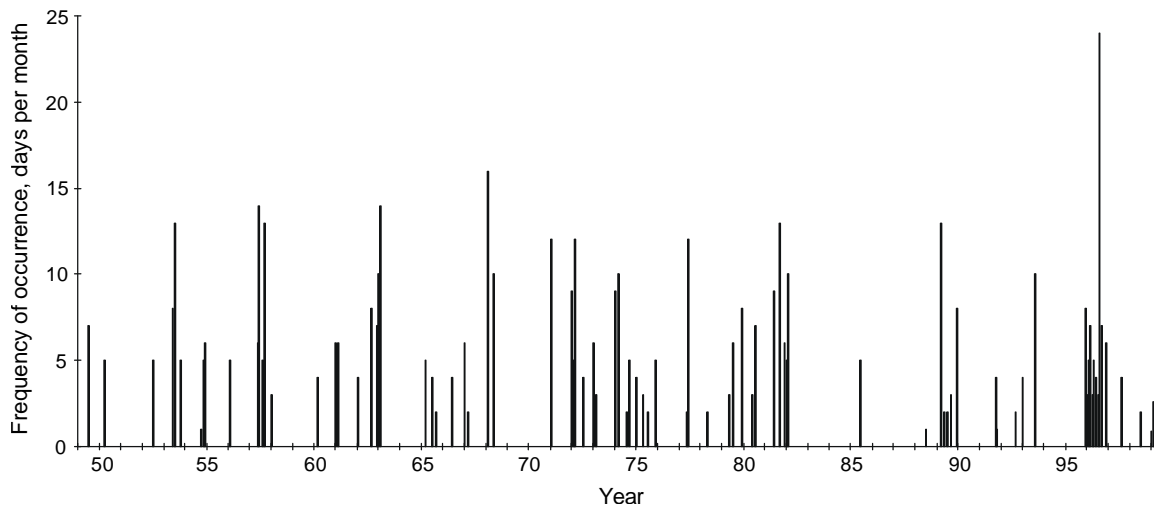


Fig. 8 Time series of monthly occurrence of Southern-Zonal synoptic situation for the period of 1949–1998 in days per month.

ing) the Sea of Okhotsk through changing occurrence of certain atmosphere circulation patterns. At the same time, correlation between air temperature around the Sea of Okhotsk and SOI with a lag of about half a year may be associated with the Northwest Pacific Ocean memory in a seasonal cycle.

References

- Barnston, A.G. and Livezey, R.E. 1987. Classification, seasonality and persistence of low-frequency atmospheric circulation patterns. *Mon. Weather Rev.*, 115, 1083–1125.
- Branstator, G.W. 1995. Organization of stormtrack

- anomalies by recurring low frequency circulation anomalies. *J. Atmos. Sci.*, 52, 207–226.
- Learning to Predict Climate Variations Associated with El Niño and Southern Oscillation. Accomplishments and Legacies of the TOGA Program.* 1996. National Academy Press, Washington, 235 pp.
- Molteni, F., Ferranti, L. Palmer, T.N. and Viterbo, P. 1993. A dynamical interpretation of the global response to equatorial Pacific sea surface temperature anomalies. *J. Climate*, 6, 777–795.
- Nakamura, H., Lin, G. and Yamagata, T. 1997. Decadal climate variability in the North Pacific during the recent decades. *Bull. Amer. Meteorol. Soc.*, 78(10), 2215–2225.
- Palmer, T.N., Brankovic, C., Viterbo, P. and Miller, M.J. 1992. Modeling interannual variations of summer monsoons. *J. Climate*, 5, 399–417.
- Plotnikov, V.V. 1997. Space–time relations between ice conditions in the Far Eastern Seas. *Meteorol. Gidrol.*, 3, 77–85. (in Russian)
- Polyakova, A.M. 1997. Types of atmospheric circulation over the North Pacific and climate variations in the North Pacific. pp. 98–105. In *Pacific Oceanol. Inst. Proc. of Annual Session, 1994.* Dalnauka, Vladivostok, Russia. (in Russian)
- Ponomarev, V.I., Trusenkova, O.O., Trousenkov, S.T., Kaplunenko, D.D., Ustinova, E.I. and Polyakova, A.M. 1999. The ENSO Signal in the Northwest Pacific. pp. 9–32. In *Proc. of the 1998 Science Board Symposium on the Impacts of the 1997/98 El Niño Event on the North Pacific Ocean and its Marginal Seas, PICES Sci. Rep. No. 10,* Sidney, B.C., Canada.
- Sekine, Y. 1996. Anomalous Oyashio intrusion and its teleconnection with Subarctic North Pacific circulation, sea ice of the Okhotsk Sea and air temperature of the northern Asian continent. pp. 177–187. In *Proc. of the Workshop on the Okhotsk Sea and Adjacent Areas, PICES Rep. No. 6,* Sidney, B.C. Canada.
- Sekine, Y. and F. Yamada, Y. 1996. Atmosphere and ocean global teleconnection around the Okhotsk Sea. pp. 148–150. In *The Eleventh Intl. Symp. on Okhotsk Sea and Sea Ice, Abstracts,* 25–28 February 1996, Mombetsu, Hokkaido, Japan.
- Wallace, J.M. and Gutzler, D.S. 1981. Teleconnections in the geopotential height field during the Northern Hemisphere winter. *Mon. Weather Rev.*, 109, 784–812.
- Webster, P.J. and Yang, S. 1992. Monsoon and ENSO: Selectively interactive systems. *Quart. J. Roy. Meteorol. Soc.*, 118, 877–926.

Seasonal and interannual changes of atmospheric pressure, air and water temperatures in the area of the Kuril Ridge

George V. SHEVCHENKO¹ and Akie Kato²

¹ Institute of Marine Geology and Geophysics, Russian Academy of Sciences, Yuzhno-Sakhalinsk, Russia

² Sakhalin Regional Hydrometeorological Agency, Yuzhno-Sakhalinsk, Russia

Introduction

Poezzhalova and Shevchenko (1997a, b) found significant seasonal and interannual sea level changes in the area of the Kuril Ridge. They also detected strong sea level trends probably associated with vertical ground motions. The purpose of the present paper is to verify these findings and to investigate long-term variations of some other meteorological parameters which probably influence sea level changes. It was also interesting to estimate possible effect of the 1997 El Niño on the northwestern part of the Pacific Ocean. The series of monthly means of atmospheric pressure, air and water temperatures from 4 meteorological stations were analyzed to estimate various statistical characteristics (mean and extreme values, standard errors, etc.) for every month and for all stations. The stations were located in the area of Kuril Ridge: Shumshu (Shumshu Island), Simushir (Simushir Island), Kurilsk (Iturup Island), and Yuzhno-Kurilsk (Kunashir Island) (Fig. 1).

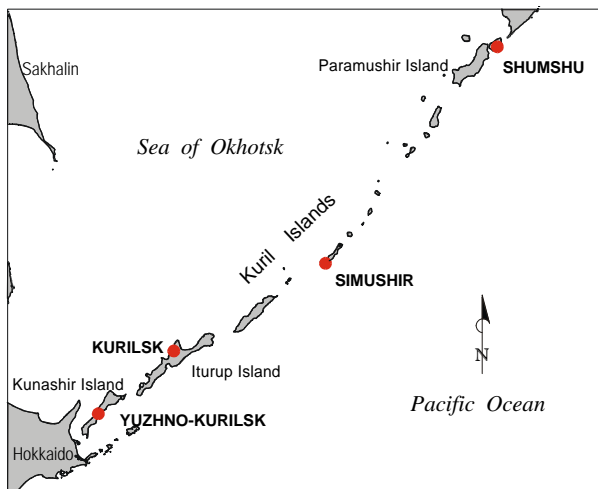


Fig. 1 Location of the meteorological stations in the area of the Kuril Islands.

Seasonal oscillations

The seasonal variations of oceanographic and meteorological parameters may be described as

$$y(t) = A_1 \cos(\omega t - \mathbf{j}_1) + A_2 \cos(2\omega t - \mathbf{j}_2) + \mathbf{e}(t),$$

where $\omega = 2\pi/12$ is the annual frequency, t is the time (in months), A_1 and A_2 are the amplitudes of annual (Sa) and semiannual (Ssa) harmonics, \mathbf{j}_1 and \mathbf{j}_2 are their phases ($\mathbf{j}_1 = 0$ corresponds to January 15), \mathbf{e} are the residual background oscillations. We used the least square method to calculate the amplitudes and phases of these harmonics. The results of this analysis are presented in Table 1.

The amplitudes of the annual oscillations of the atmospheric pressure are rather small in the area of the South Kuril Islands but quite significant in the area of the North Kuril Islands. These results are in good agreement with the results of sea level analysis made by Poezzhalova and Shevchenko (1997a, b): The sea level amplitudes of the Sa harmonic for the former region were considerably smaller than for the latter (5 and 10 cm, respectively).

Seasonal sea level and atmospheric pressure oscillations are approximately in antiphase, maximum sea level heights correspond to minimum atmospheric pressure, and vice versa. Normally, these maximum sea levels and minimum pressure are observed in December or January and are associated with influence of the Aleutian Low. However, these seasonal variations of sea level cannot be described by the simple “inverted barometer law”. The Sa sea level amplitudes are approximately twice as large as those of the atmospheric pressure. We may assume that there are some additional oceanic and atmospheric factors influencing seasonal sea level variations.

The Sa (annual) harmonic strongly dominates in

the variations of air and sea surface temperatures (95–98% of the total variance). Maximum amplitudes of this harmonic, both for air (AT) and sea surface (SST) temperatures, occur near Kunashir Island (southern part of the Kuril Ridge) and minimum amplitudes are observed in the vicinity of Simushir Island (central part of the Kuril Ridge). In general, the seasonal changes of SST are relatively small, apparently due to the sup-

pressing influence of the Pacific Ocean water masses. The annual changes of SST and sea level are in antiphase. Probably, rather strong seasonal sea level oscillations in the area of the Kuril Ridge are determined by the changes in ocean circulation in the Northwest Pacific induced by the large-scale atmospheric fluctuations (such effect is well known for the Northeast Pacific (cf. Emery and Hamilton, (1985))).

Table 1 Parameters (amplitude and phase) of annual and semiannual harmonics and their contribution to the total variance. The multiyear mean values are presented in brackets.

I. Atmospheric pressure

Period (month)	Amplitude (mBar)	Phase (deg)	Relative contribution (%)
<i>Yuzhno-Kurilsk</i> (1006.8 mBar)			
12	0.9	274.1	17.0
6	1.8	177.1	73.1
<i>Kurilsk</i> (1007.2 mBar)			
12	1.0	231.7	19.9
6	2.0	175.6	71.1
<i>Simushir</i> (1007.2 mBar)			
12	3.1	201.6	65.9
6	2.1	179.9	31.0
<i>Shumshu</i> (1004.8 mBar)			
12	4.8	185.1	83.3
6	2.0	178.3	14.9

II. Air temperature

Period (month)	Amplitude (°C)	Phase (deg)	Relative contribution (%)
<i>Yuzhno-Kurilsk</i> (4.8°C)			
12	10.2	208.2	98.0
6	1.4	144.0	1.6
<i>Kurilsk</i> (4.5°C)			
12	10.3	204.4	99.1
6	0.5	149.6	0.7
<i>Simushir</i> (2.8°C)			
12	7.4	207.8	97.8
6	1.0	148.1	1.7
<i>Shumshu</i> (1.7°C)			
12	8.1	205.9	98.8
6	0.8	92.6	1.0

III. Sea surface temperature (SST)

Period (month)	Amplitude (°C)	Phase (deg)	Relative contribution (%)
<i>Yuzhno-Kurilsk (6.7°C)</i>			
12	8.7	223.0	98.1
6	1.1	125.6	1.8
<i>Kurilsk (5.6°C)</i>			
12	7.0	226.9	97.5
6	1.1	117.2	2.2
<i>Simushir (2.3°C)</i>			
12	2.0	225.7	99.1
6	0.2	171.6	0.6
<i>Shumshu (3.4°C)</i>			
12	5.7	210.9	98.3
6	0.7	81.5	1.6

Interannual changes

The mean annual values of meteorological parameters were used to estimate respective multiyear averaged values and linear trends. The coefficients of the linear trends were calculated by the least square method. These coefficients for the atmospheric pressure are -0.030 and 0.022 mbar/yr at stations Yuzhno-Kurilsk and Kurilsk, and negligibly small at Shumshu and Simushir (Fig. 2). This means that the interannual changes of the atmospheric pressure cannot induce sea level drift with coefficients of about 0.4 – 0.6 cm/yr observed in the area of the Kuril Islands (Yakushko et al., 1982; Poezzhalova and Shevchenko, 1997b).

The air temperature increased slowly with time (except Shumshu), the regression coefficients ranged from $0.0055^{\circ}\text{C}/\text{yr}$ (Yuzhno-Kurilsk) to $0.019^{\circ}\text{C}/\text{yr}$ (Kurilsk). The multiyear mean values were from 1.8°C (Shumshu) to 4.8°C (Yuzhno-Kurilsk) (Fig. 3.).

The sea surface temperature had the opposite tendency, the linear trend coefficients ranged from $-0.001^{\circ}\text{C}/\text{yr}$ (Simushir) to $-0.0078^{\circ}\text{C}/\text{yr}$ (Yuzhno-

Kurilsk); the mean values at these stations were 2.3 and 6.7°C , respectively. The coldest month weather was observed in 1967, the warmest in 1990–1991. The direct effects of the 1982 or 1997 El Niño are not evident in the area of the Kuril Islands.

We calculated also the coefficients of the linear trends for different seasons using seasonal (3-month) averaged values of air temperature (Table 2). In this way we got more interesting results. Thus, the air temperature for all stations (also, except Shumshu) relatively fast increased for winter seasons with the coefficients of about 0.02 – $0.034^{\circ}\text{C}/\text{yr}$ and somewhat weaker for fall seasons (0.015 – $0.02^{\circ}\text{C}/\text{yr}$). Probably, this effect is the result of the global climate warming. In contrast, sea surface temperature for some stations noticeably decreased from year to year: at Yuzhno-Kurilsk for summer seasons (for about 1.5°C during the period of observations), and at Kurilsk for fall seasons (Fig. 4). Unfortunately, we could not calculate SST linear trends at Simushir and Shumshu because the corresponding data had too many gaps.

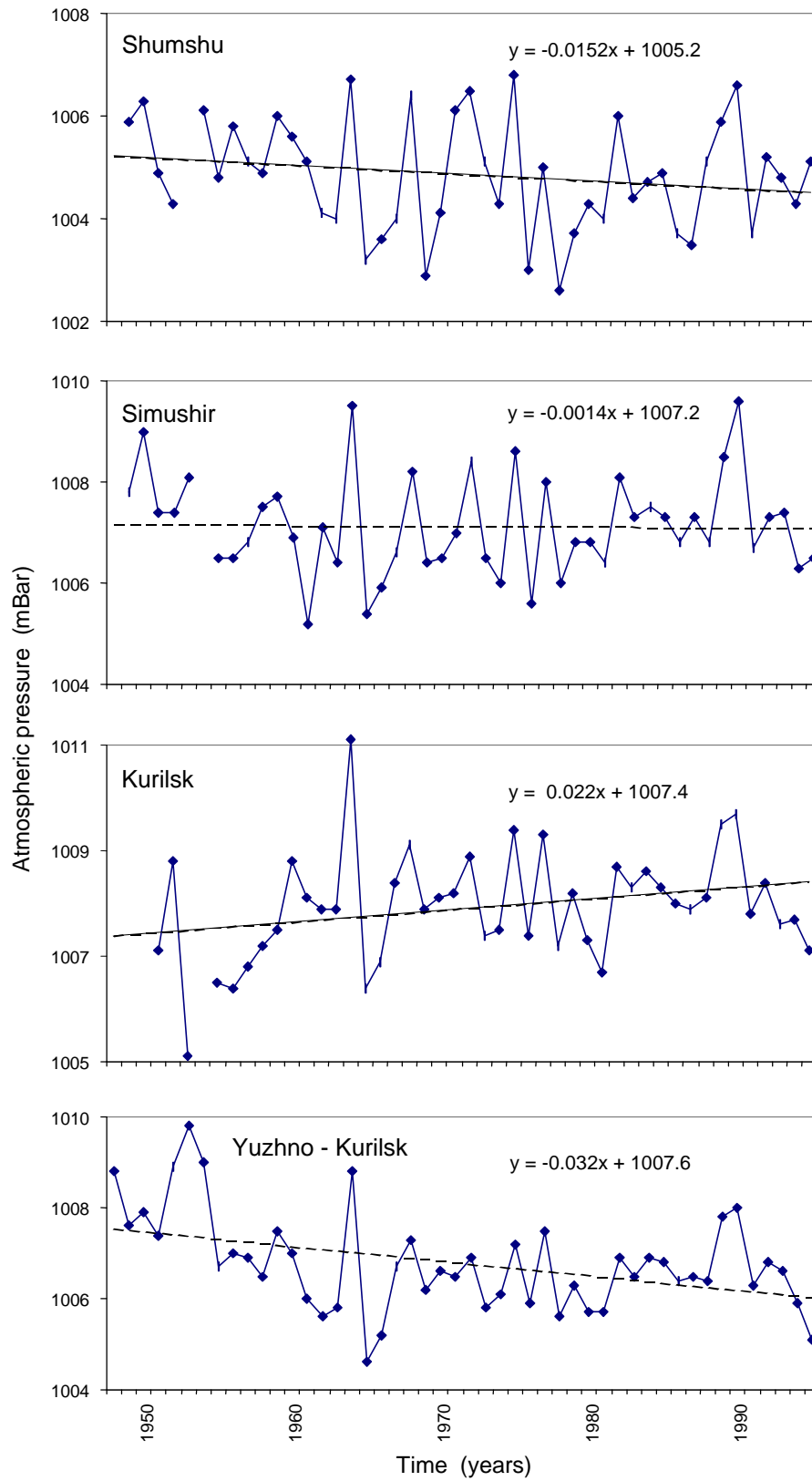


Fig. 2 Mean annual values of atmospheric pressure (solid lines) and linear trends (dashed lines) calculated by the least square method for various stations of the Kuril Islands.

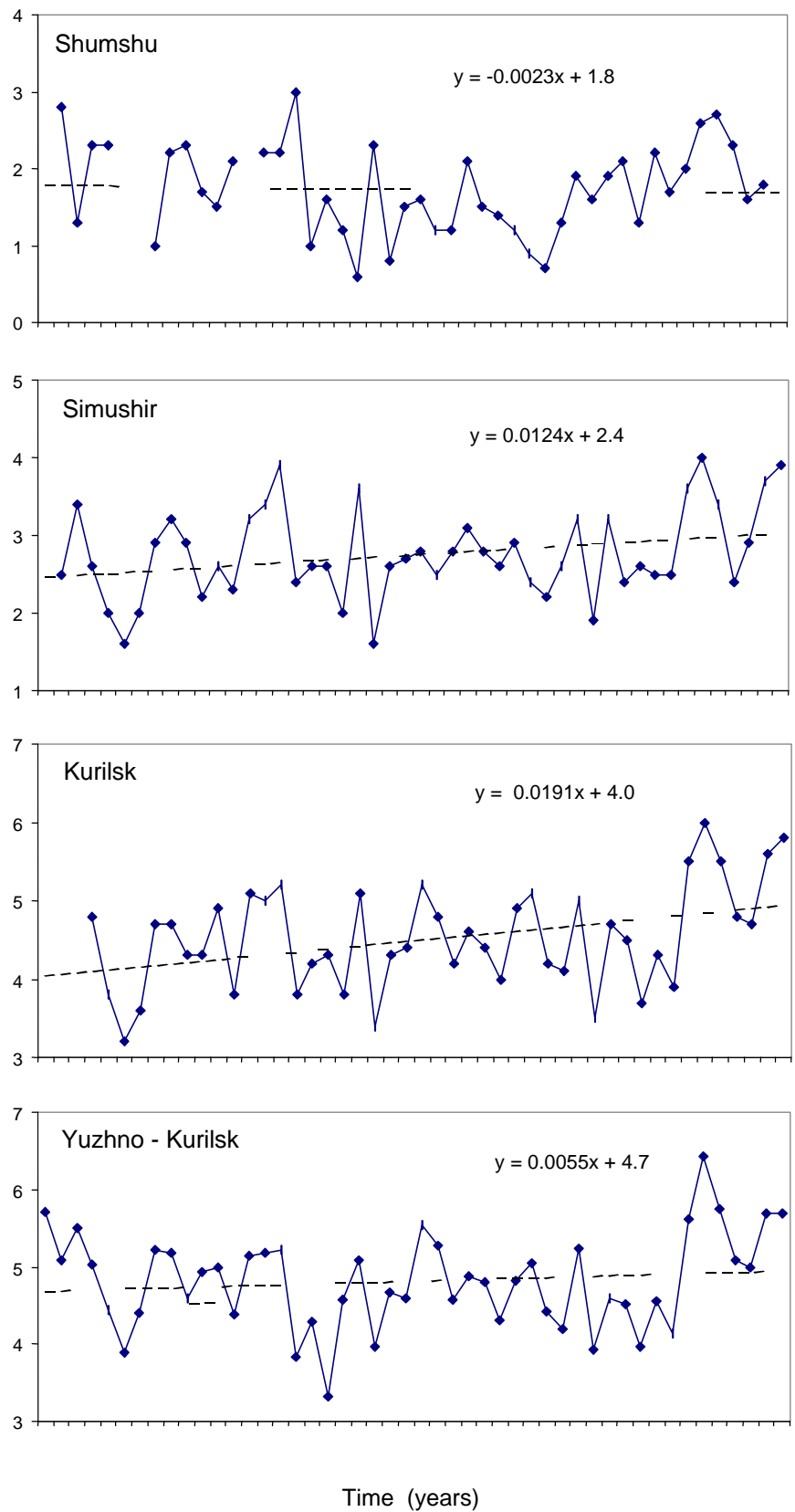


Fig. 3 Mean annual values of air temperature (solid line) and linear trend (dashed line) for various stations.

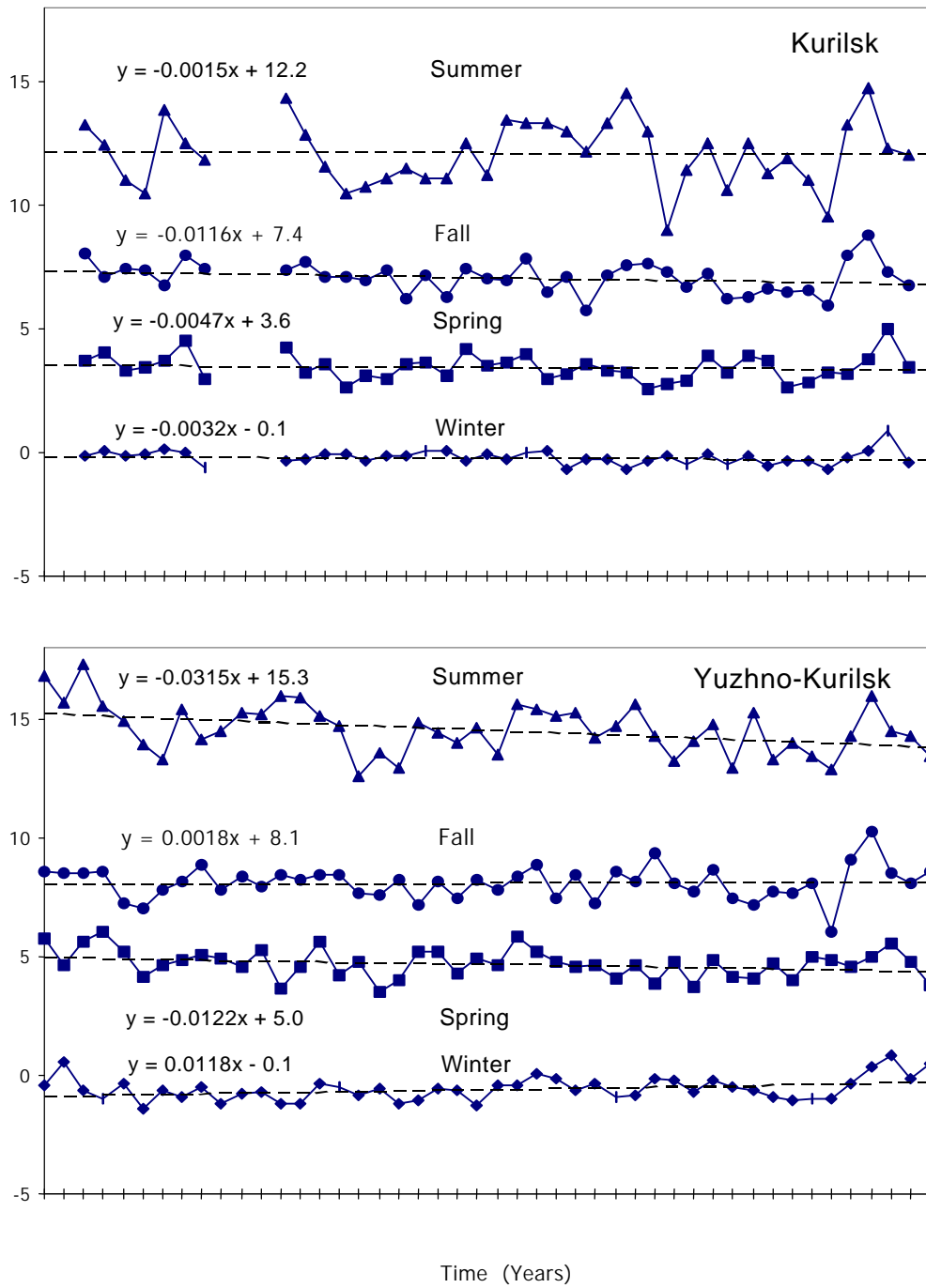


Fig. 4 Seasonally (3-month) averaged values of sea surface temperature and parameters of linear trend for different seasons at Kurilsk and Yuzhno-Kurilsk.

Table 2 The coefficients of linear trend (°C/yr) based on 3-month averaged values of air temperature for different seasons at various Kuril stations.

Station	Winter	Spring	Summer	Fall
Shumshu	0.0029	0.0068	-0.0075	0.0001
Simushir	0.0256	0.0089	0.0021	0.0157
Kurilsk	0.0338	0.0088	0.0124	0.0173
Y-Kurilsk	0.0196	-0.0035	-0.0111	0.0203

Acknowledgments

We wish to thank Dr. Alexander Rabinovich of the Shirshov Institute of Oceanology, Moscow for his constructive criticism and valuable comments, and to Willie Rapatz for help with English.

References

Emery, W.J. and Hamilton, K. 1985. Atmospheric forcing of interannual variability in the North-east Pacific Ocean: Connections with El Niño, *J. Geophys. Res.*, 90(C1), 857–868.

Poezzhalova, O.S. and Shevchenko, G.V. 1997a. Seasonal oscillations of sea level in the Sea of Okhotsk, *Twelfth Intl. Symp. on Okhotsk Sea and Sea Ice, Abstracts*, Mombetsu, Japan.

Poezzhalova, O.S. and Shevchenko, G.V. 1997b. The Okhotsk Sea mean level variations. pp. 131–144. In *Tsunami and Accompanying Phenomena*, Institute of Marine Geology and Geophysics, Yuzhno-Sakhalinsk. (in Russian)

Yakushko, G.G., Nikonov, A.A. and Yurkevich, N.E. 1982. Modern vertical motions of the Kuril Islands. *Trans. (Doklady) USSR Acad. Sci.*, 265(2), 444–449. (in Russian)

Spatial variability of the wind field in the area of the Kuril Islands

George V. SHEVCHENKO and Vladimir Yu. Saveliev

Institute of Marine Geology and Geophysics, Russian Academy of Sciences, Yuzhno-Sakhalinsk, Russia

Introduction

Examination of time and spatial variability of wind field is important for various applied problems. In particular, the problem of evaluation and development of wind power stations recently became crucial for the region of the Kuril Islands. Climatic characteristics of wind presented in generally used manuals (Climate Guide, 1969; Koshinsky, 1978; Pacific Ocean, 1966) are mainly based on wind data obtained by weather vanes. Since the end of the 1970s more precise instruments have begun to be used to measure wind at meteorological stations of the former USSR. Preliminary analysis of old and modern data showed significant difference of the corresponding estimates. The purpose of the present work is to examine the spatial structure and to obtain some climatic characteristics of the wind field in the vicinity of the Kuril Islands based on the modern wind data.

Observational data

For analysis we used 10-min averaged wind data from stations Shumshu, Matua, Simushir and Shikotan, located on the corresponding islands, and from station Kurilsk, located on Iturup Island, for the period 1966–1984, prepared at the World Data Center at Obninsk, Russia. The location of the meteorological stations is shown in Figure 1. We chose stations Shumshu and Shikotan rather than the nearby stations Severo-Kurilsk on Paramushir Island and Yuzhno-Kurilsk on Kunashir Island, for the reason that the former pair is less influenced by the local orography than the latter. The analysis of the data has revealed their essential heterogeneity, much of the information before 1980 pertaining to measurements executed by weather vanes. For a more detailed examination we used a series for 1980–1984, since these data had no gaps and were obtained by the same type of instrument, an anemorumbometer M-63M.

We used for analysis 10-min averaged wind data from the stations Shumshu, Matua, Simushir, Shikotan (located at the corresponding islands)

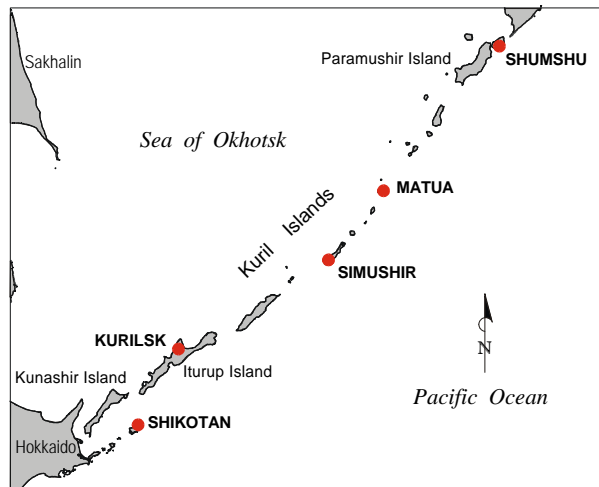


Fig. 1 Location of the meteorological stations in the area of the Kuril Islands.

and Kurilsk (Iturup Island) for the period 1966–1984 prepared at the World Data Center (Obninsk, Russia). The location of the meteorological stations is shown in Figure 1. We chose stations Shumshu and Shikotan rather than the nearby stations Severo-Kurilsk (Paramushir Island) and Yuzhno-Kurilsk (Kunashir Island) since the wind at the former pair is less influenced by the local orography than at the latter. The analysis of the data has revealed their essential heterogeneity, much of the information before 1980 pertaining to measurements executed by weather vanes. So, for more detailed examination we used series for 1980–1984 since all these data were made by the same type of the instrument (anemorumbometer M-63M) and had no gaps.

Recurrence of the wind by directions and speed gradations

Figure 2 presents diagrams illustrating the wind distribution by directions and speed gradations. There are two maxima in the distribution of the wind speed: the main maximum corresponding to the typical wind speed of 2–4 m/s (3–5 m/s at Shumshu), and a secondary maximum at 10–12 m/s. Such character of speed distribution remains

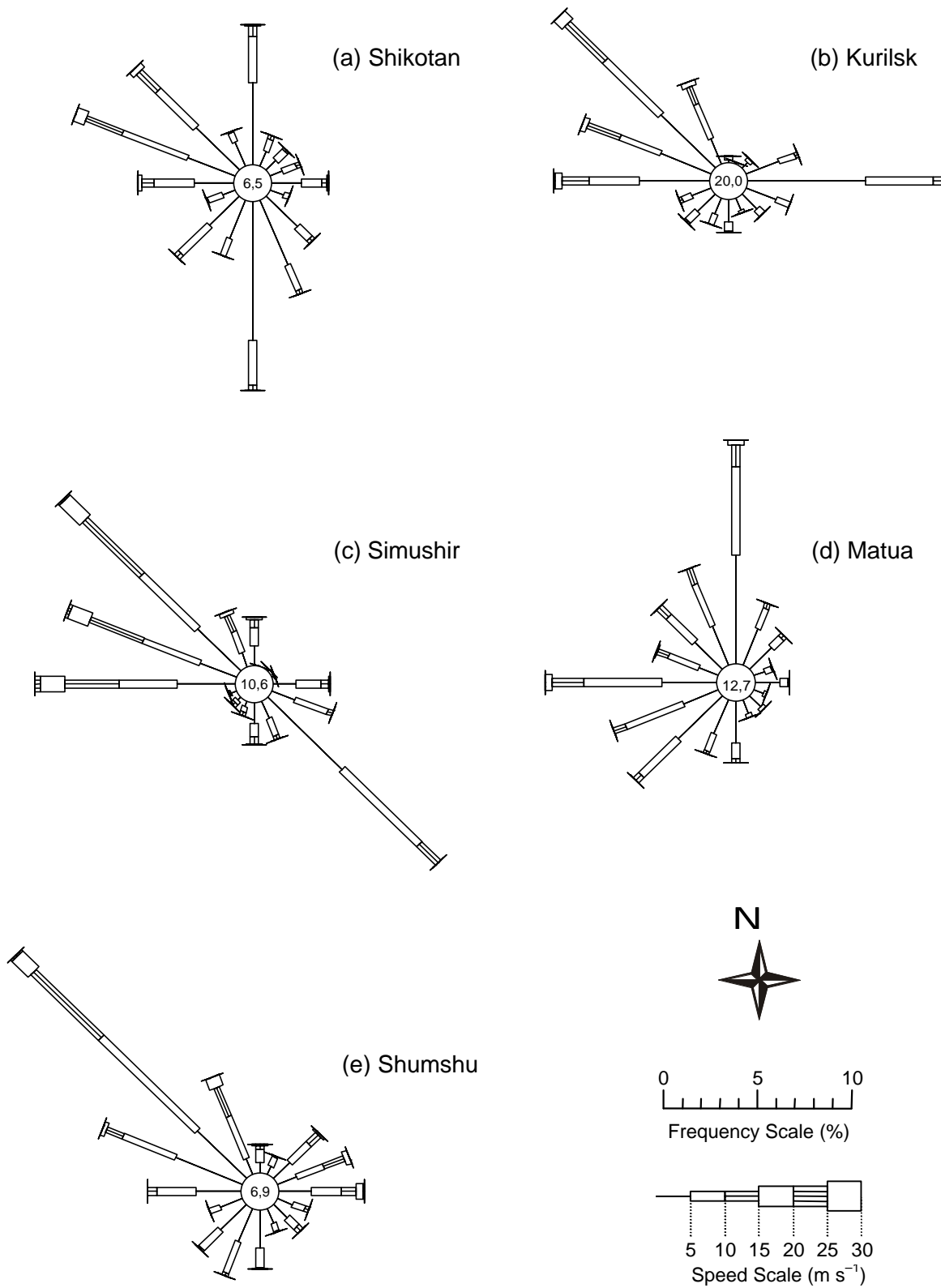


Fig. 2 Diagrams of the direction distribution by the 5-yr averaged wind velocities for various Kuril meteorological stations. Contribution of calm weather (winds weaker than 1 m/s) is presented in the centers of the diagrams (in %).

basically the same for all stations and all seasons. However, in winter, when winds are normally stronger, the second maximum intensifies and the main maximum becomes weaker; the opposite tendency is observed in summer.

The “wind roses” (Fig. 2) demonstrate noticeable spatial variability of wind directions. Northwest-erly winds prevail at all stations, however the other features are different for different stations. Thus, in the vicinity of Shumshu Island winds from directions other than northwest are weak and infrequent. In contrast, near Matua Island north-erly winds are observed frequently, for Kurilsk easterly winds are rather frequent, for Simushir southeasterly, and for the area of Shikotan Island southerly winds occur quite often.

The dominant northwesterly winds are a typical autumn-winter feature for the whole area of the Sea of Okhotsk (so-called “winter monsoon”, related to the influence of the Aleutian Low). The corresponding spatial distribution of the sea surface atmospheric pressure in the area of Okhotsk Sea is shown in the Figure 3a. In the spring-summer period the air streams near the Kuril Islands are apparently not so stable, resulting in the variety of the winds from the other directions observed in this period. (Figure 3b presents a typical

distribution of atmospheric pressure in summer.) That means that the wind field in this area cannot be satisfactorily described by a simple layout: The winter monsoon with northwesterly winds is replaced by the summer monsoon with southeasterly winds (Pacific Ocean, 1966).

It is interesting to note that the wind velocities near the Kuril Islands are found to be weaker than is usually assumed: according to Climate Guide (1969) extreme wind velocities in this region are up to 50 m/s. Results of the present examination of wind data for the period 1970–1984 showed that none of the five analyzing stations recorded wind velocities exceeding 30 m/s. The total amount of the cases with wind exceeding 20 m/s is rather insignificant, from 0.4% at Matua up to 2.5% at Simushir. These extreme winds with speed up to 28–30 m/s are mainly observed in March or in October and November (Fig. 4a). The strongest winds have northwesterly direction for the southern and central parts of the Kuril Islands, southwesterly at Matua, and northeasterly at Shumshu. These months correspond to the time of the major cyclonic activity in this area. The distribution of the extreme wind shows that the corresponding cyclones cross the chain of the Kuril Islands just in the center, near Matua Island.

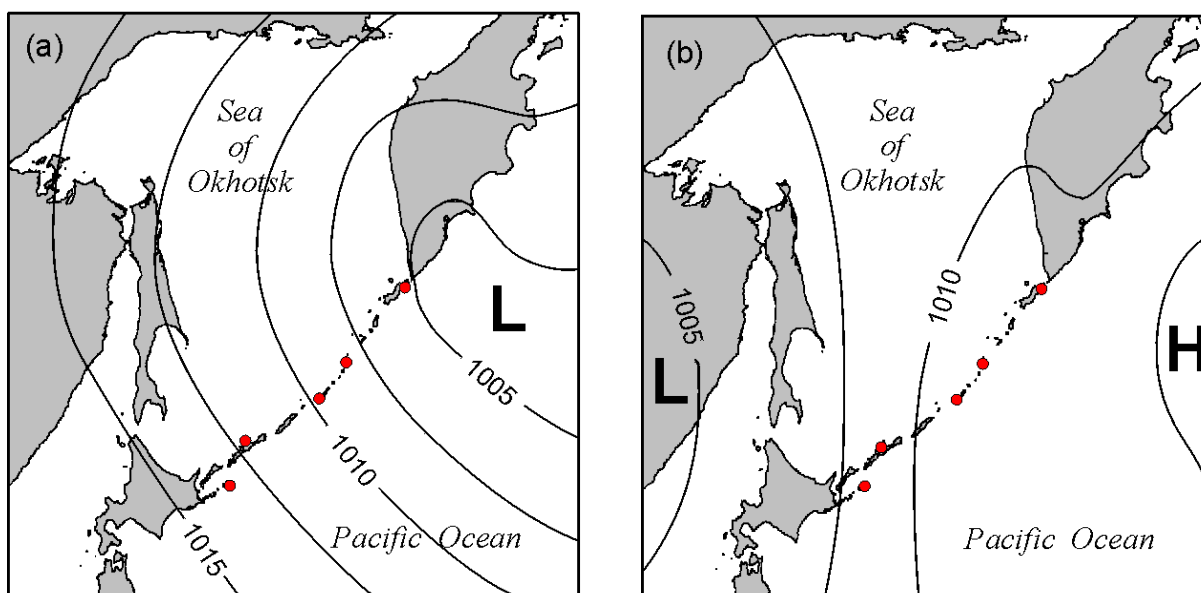


Fig. 3 Typical spatial distribution of sea surface pressure in the area of the Kuril Islands for (a) January and (b) July according to Pacific Ocean (1966).

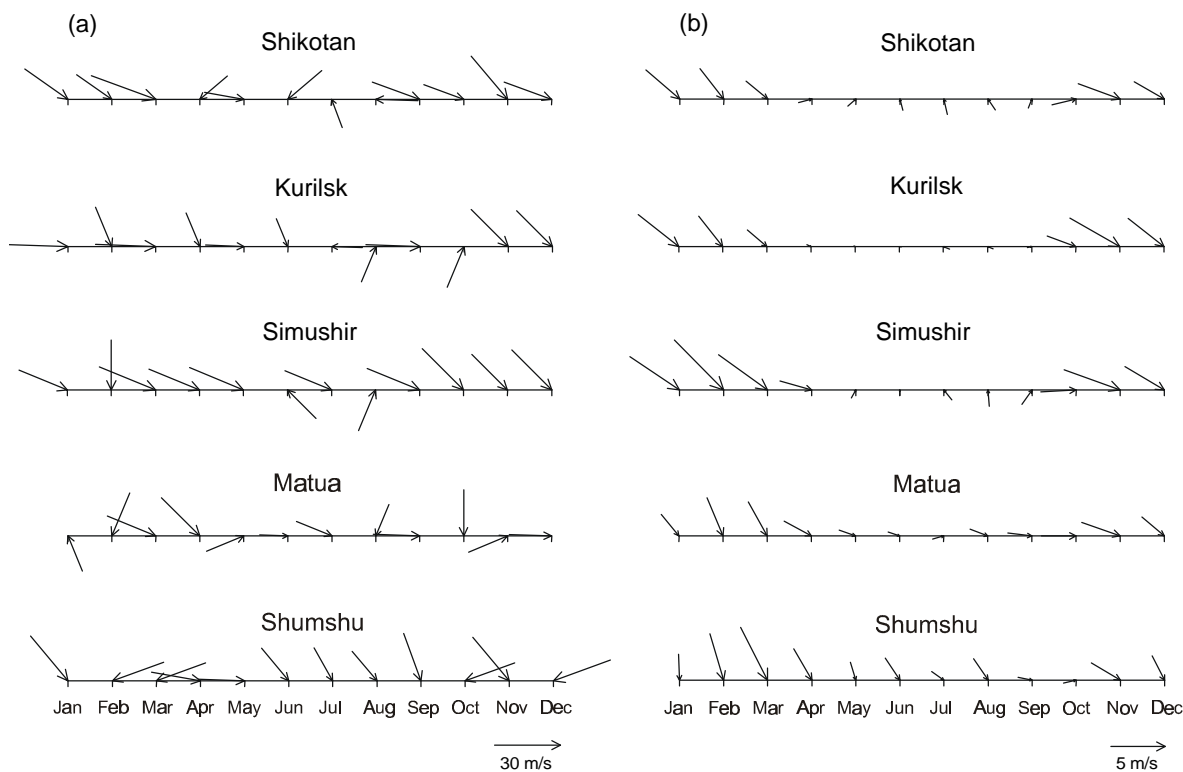


Fig. 4 (a) Maximum monthly and (b) mean monthly winds for the period 1980–1984 for the meteorological stations in the area of the Kuril Islands.

It is interesting to note that the wind velocities near the Kuril Islands are found to be weaker than is usually assumed: according to Climate Guide (1969) extreme wind velocities in this region are up to 50 m/s. Results of the present examination of wind data for the period 1970–1984 showed that none of the five analyzing stations recorded wind velocities exceeding 30 m/s. The total amount of the cases with wind exceeding 20 m/s is rather insignificant, from 0.4% at Matua up to 2.5% at Simushir. These extreme winds with speed up to 28–30 m/s are mainly observed in March or in October and November (Fig. 4a). The strongest winds have northwesterly direction for the southern and central parts of the Kuril Islands, southwesterly at Matua, and northeasterly at Shumshu. These months correspond to the time of the major cyclonic activity in this area. The distribution of the extreme wind shows that the corresponding cyclones cross the chain of the Kuril Islands just in the center, near Matua Island.

The complicated picture of maximum winds is observed in summer. Extreme wind speeds are about 17–25 m/s, the direction of maximum winds

varies significantly from year to year, except at Shumshu where northwesterly winds are dominant, and from station to station. Typhoons which are coming from the tropical Pacific into the area of the Kuril Islands in summer and early fall are probably the reason for destabilizing atmospheric circulation and producing storm winds of various directions.

Monthly mean winds

Spatial and temporal variability of monthly mean winds averaged over 5 years (1980–1984) is clearly seen in Figure 4b. The primary feature of the wind field is the very strong seasonal change of wind velocity. In the cold season (October–March) mean winds are sufficiently strong and steady. For the whole area of the Kuril Islands, they have northwesterly direction; variations from station to station are insignificant. In contrast, in the warm season (April–September), mean winds are much weaker and there is essential difference between the two northernmost stations Shumshu and Matua and the others. At stations Shikotan and Kurilsk in the South Kuril Islands, winds change direction to the southerly and

the southerly and southeasterly, i.e. the wind field takes the character typical for summer monsoon. A similar picture but not so evident is observed also at Simushir. At the same time, monthly mean winds of northwesterly and westerly direction prevail at Matua and Shumshu. The seasonal changes at these stations are manifested mainly in the variations of the velocity magnitude rather than in the direction. This character of seasonal variability of monthly mean wind velocities is in good agreement with the spatial distribution of atmospheric pressure in the area of the Sea of Okhotsk (Fig. 3). Probably, a local area of high atmospheric pressure observed in summer time over the Kamchatka Peninsula influences winds near the North Kuril Islands, causing the difference from the winds in the area of the South Kuril Islands.

We estimated the relation between the variance of the average group values (factorial variance) and the average of the group variances (casual variance), showing the stability of the performance. We found that contribution of the factorial variance is about 70–80% of the total variance except for the east-going (zonal) component of the wind at Matua and Shumshu stations. Seasonal changes of this zonal component of the wind are weak in the area of the Northern Kuril Islands.

Conclusions

The main conclusions of the present analysis are as follows:

- The maximum wind velocities in the area of the Kuril Islands were found to be up to 30 m/s, i.e. significantly smaller than it was assumed according to well-known reference guides mainly based on obsolete weather vane measurements.
- In winter, significant northwesterly winds associated with the Aleutian Low prevail in the area of the Kuril Islands (“winter monsoon”); however there are noticeable differences in distribution of wind directions (“roses of winds”) for various stations.
- In summer, winds are weaker and not stable resulting in the variety of the winds from different directions. A simple model of “summer monsoon” cannot describe summer circulation for the whole area of the Kuril Islands. In fact, there is a boundary between the Simushir and Matua Islands (i.e. in the central part of the Kuril Islands) dividing zones with different character of prevailing winds: northwesterly for the northern stations and southerly to southeasterly for the southern stations.

Acknowledgments

The authors wish to thank Dr. Alexander Rabino- vich, of the Shirshov Institute of Oceanology, Moscow, for valuable advice and discussions, and for his editorial work to help improve this paper. We are grateful to Willie Rapatz for corrections to the English.

References

- Climate Guide of the USSR., Part 3. Wind.* 1969. Gidrometeoizdat, Leningrad. (in Russian)
- Koshinsky, S.D. 1978. *Regime Characteristics of the Strong Winds on the Seas of the Soviet Union.* Gidrometeoizdat, Leningrad. (in Russian)
- Pacific Ocean, Vol. 1. Meteorological Conditions over the Pacific Ocean.* 1966. Nauka, Moscow. (in Russian)

Seasonal variability and specificity of the oceanological conditions in the northern Okhotsk Sea in 1997

Alexander L. FIGURKIN and Igor A. Zhigalov

Pacific Research Institute of Fisheries and Oceanography, Vladivostok, Russia

Introduction

The data obtained from four surveys undertaken in the northern part of the Okhotsk Sea in March–September 1997 (about 900 CTD stations) were analyzed.

The interest in the monitoring experiments carried out by TINRO in the Okhotsk Sea grows considerably at the present time because of discussions of the new “cold” period. The beginning of this cold period was predicted by heliomagnetic cycles happening in the early 1990s (Davydov, 1984) or in the late 1990s (Shuntov, 1985). Shuntov published data on the reorganization of the southern Okhotsk Sea biota and described the same phenomenon observed both with the sea birds and animals (Shuntov, 1994; Shuntov and Dulepova, 1996). In Shuntov’s opinion, these factors were caused by the beginning of a cooling period. The oceanological conditions of recent years up to 1997 in the northern part of the Okhotsk Sea does not confirm this assertion.

Results and discussion

It is known that the severity of winter conditions has significant influence on water structure and temperature of the northern part of the Okhotsk Sea in the layer 0–200 m. According to our data, the correlation of the sea-ice cover maximum with water temperature in spring in different sites of the shelf is characterized by the negative ratio $R = -0.65$ to -0.80 . The temperature anomaly in intermediate cold waters remains as long as the beginning of new winter convection, at a probability of 60–70%. According to the data obtained by Chernyavsky (1992) for the period from 1954 to 1986, the waters with minimal temperature, generated by winter convection in summer are usually divided into four subsurface cold “cores” (temperature $\leq -1^\circ\text{C}$). These are the North-Okhotsk and East-Sakhalin large cold cores, the Shelikhov Bay core and small cold cores off West Kamchatka. The cold core water with a temperature of $\leq -1^\circ\text{C}$ has higher salinity and density and shows cyclonic circulation in the dynamic topography

charts. The large-scale cyclonic circulation is regularly formed around the North-Okhotsk cold core. The westward current, named the North-Okhotsk Current, and the opposite eastward current, named the North-Okhotsk Counter Current, together with the northward flow, called the West-Kamchatka Current (WKC), were observed on the borders of the North-Okhotsk cold core. The variability of size and position of the cyclones depend largely on the cold core seasonal changes, as seen on monthly averaged current charts, drafted by Luchin (1987) (Fig. 1).

A low-ice situation was observed in the Okhotsk Sea after the period 1980–1983. In the winters of 1996 and 1997, there was an unusual decrease in ice cover – down to 25–35%. In April 1997 the WKC transport in the 0–200 m layer was about

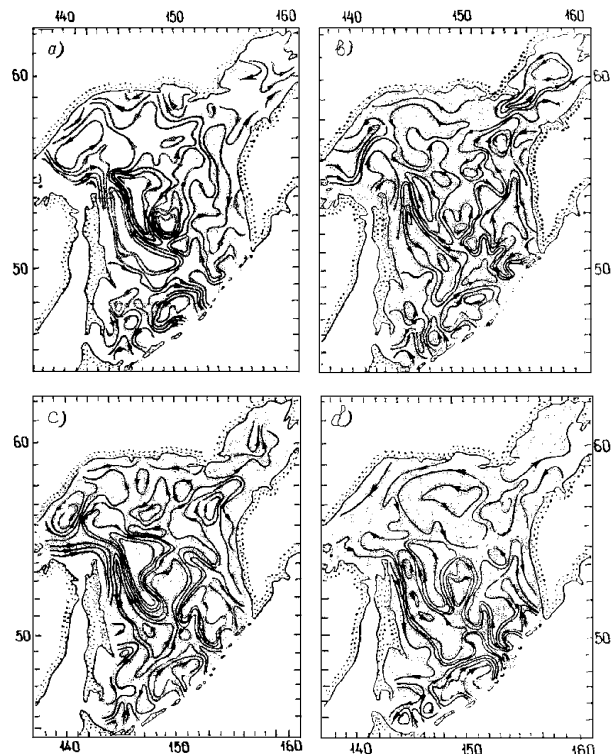


Fig. 1 Seasonal variations of Okhotsk Sea water circulation (from Luchin (1987)). (a) June, (b) August, (c) September, and (d) November.

$0.52 \times 10^6 \text{ m}^3/\text{s}$ (its mid-stream was observed within $154^\circ\text{--}155^\circ\text{E}$, Fig. 2a). The same transport value was noted in April 1984–1986. In the April period from 1987–1995 its value dropped twice and rose again only in 1996, reaching $0.48 \times 10^6 \text{ m}^3/\text{s}$. The weakness of the winter cooling intensity and WKC transport increase caused “warm” and “abnormally warm” thermal conditions throughout the shelf waters in 1997. From May to August 1997 the transport of WKC water into Shelikhov Bay was $0.28\text{--}0.20 \times 10^6 \text{ m}^3/\text{s}$. The Compensatory Current water along the West Kamchatka coast was observed only within $57^\circ50'\text{--}56^\circ30'\text{N}$ in April and between $56^\circ20'\text{--}55^\circ00'\text{N}$ in July.

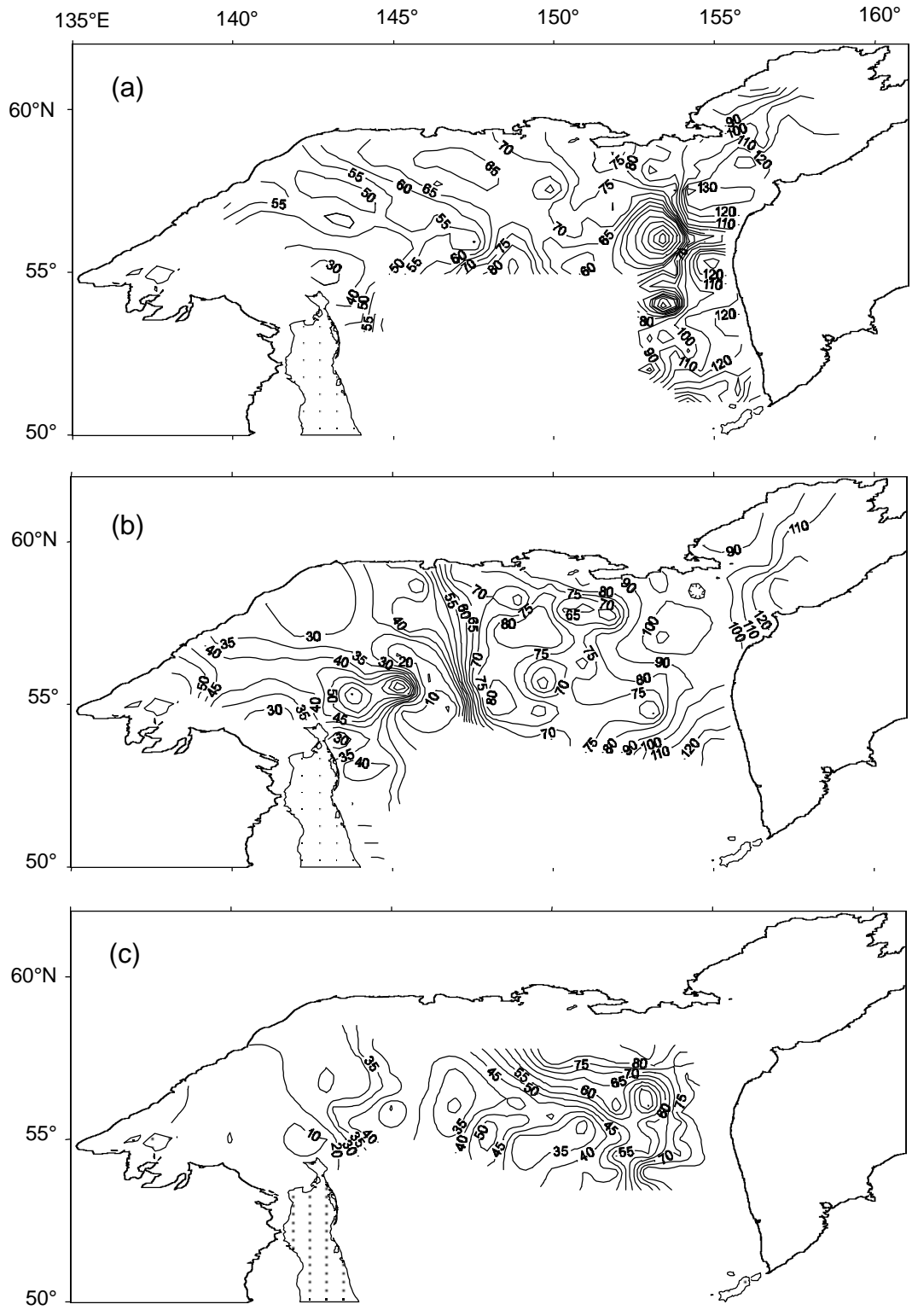
Recent investigations show a significant reduction of the cold core areas. In April 1997, the area with the lowest water temperature of $\leq -1^\circ\text{C}$ covered less than 6% of the total area along West Kamchatka, whereas the average value for 1983–1997 was equal to 41%. In May 1997 the cold core area in Shelikhov Bay was equal to 39%, compared to the average value of 69%. The largest and stable North-Okhotsk cold core usually covered the average annual area of $191 \pm 23 \times (10^3 \text{ km}^2)$ in June, $160 \pm 22 \times (10^3 \text{ km}^2)$ in July, $130 \pm 18 \times (10^3 \text{ km}^2)$ in August, $115 \pm 17 \times (10^3 \text{ km}^2)$ in September, and $79 \pm 15 \times (10^3 \text{ km}^2)$ in October (in the eastern area to 146°E , 1954–1986 according to Chernyavsky’s (1992) observations, and 1987–1997 according to our records). In May 1997, the North-Okhotsk cold core area covered about $75,000 \text{ km}^2$, which was equal to the October-averaged parameters. In July 1997, the North-Okhotsk cold core spread over an area of about $38,500 \text{ km}^2$ and decreased to as low as $1,300 \text{ km}^2$ in September (Fig.3). Its eastern border shifted westward from $151^\circ\text{--}152^\circ\text{E}$ in August to $146^\circ\text{--}148^\circ\text{E}$ in September.

The WKC midstream moved in a similar manner. Its northward water transport in the 0–200 m layer varied from $0.45 \times 10^6 \text{ m}^3/\text{s}$ in August to $0.42 \times$

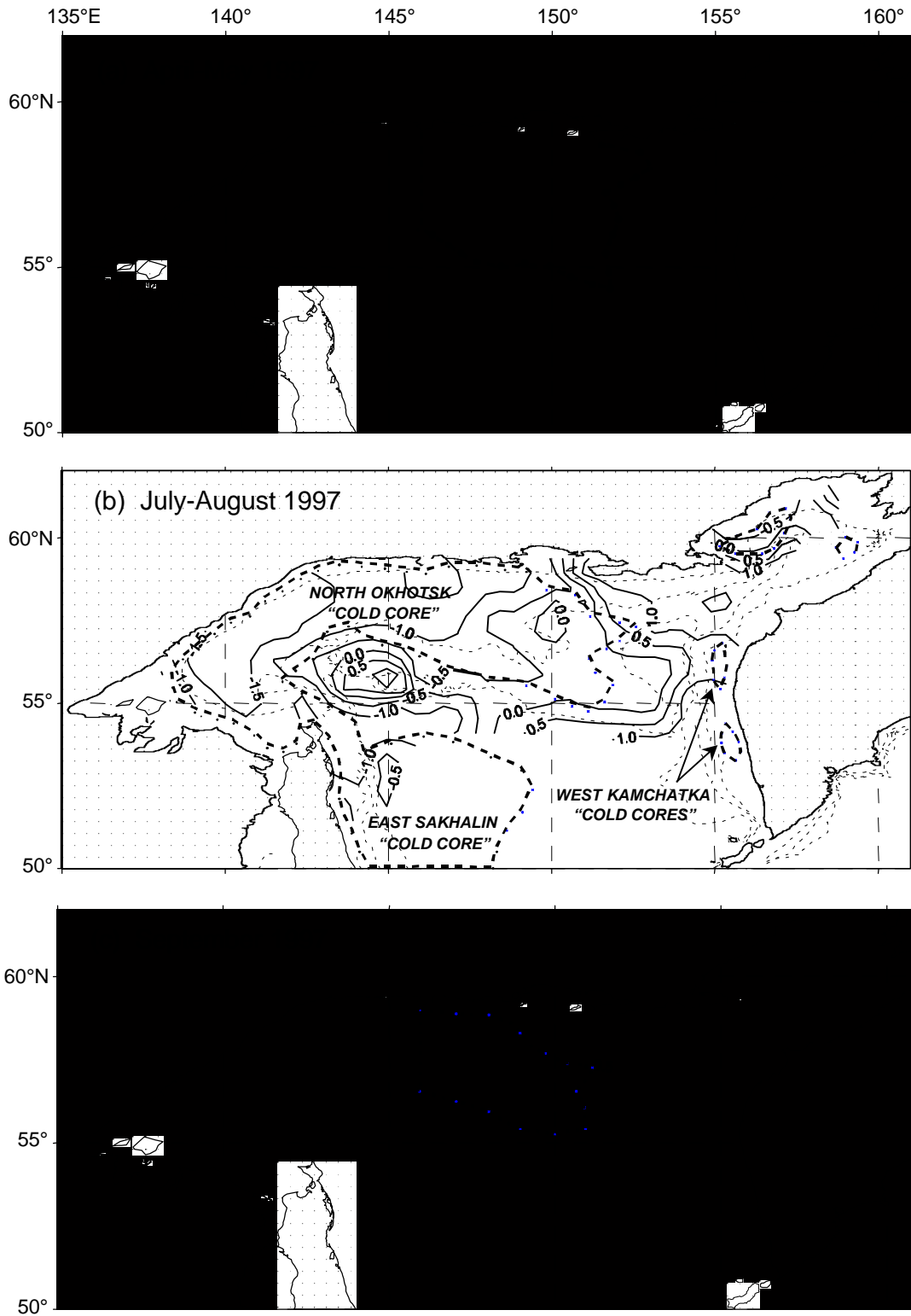
$10^6 \text{ m}^3/\text{s}$ in September. The usually zonally orientated North-Okhotsk Current and its counter-current were not observed. Due to strong cold core destruction, geostrophic currents of the North Okhotsk Sea in July of 1997 were similar to the currents that were usually formed only in September–October as an annual average (Fig. 1c). The most abnormal phenomenon was the formation of the northward flow to the Okhotsk Sea near $143^\circ\text{--}145^\circ\text{E}$ (Fig. 2c). This flow was the North-Okhotsk counter-current which had this unique location and direction due to the abnormal rise of total heat content in the northern Okhotsk shelf waters in 1997.

Moreover, the following factors may also be of importance:

- (1) Shelf water bottom salinity at the 100–200 m isobath dropped by 0.1–0.2 psu from May to September (Fig. 4). A more significant decline of the water salinity was observed in the coastal waters and in the upper layer. The salinity in the “cold halocline” has decreased compared with the data of 1996. The general salinity level of the North Okhotsk Sea has decreased as well compared with the annual average salinity.
- (2) In August the shifting of the eastern border of the North-Okhotsk cold core to the Kashevarov Bank area caused a significant intensification of cyclonic circulation over the Bank.
- (3) In spring 1997, the water transport of the West-Kamchatka Current to the northern Okhotsk shelf was the strongest for the past 10 years. During the summer, the width of the northern flow doubled, but the total transport remained almost unchanged.

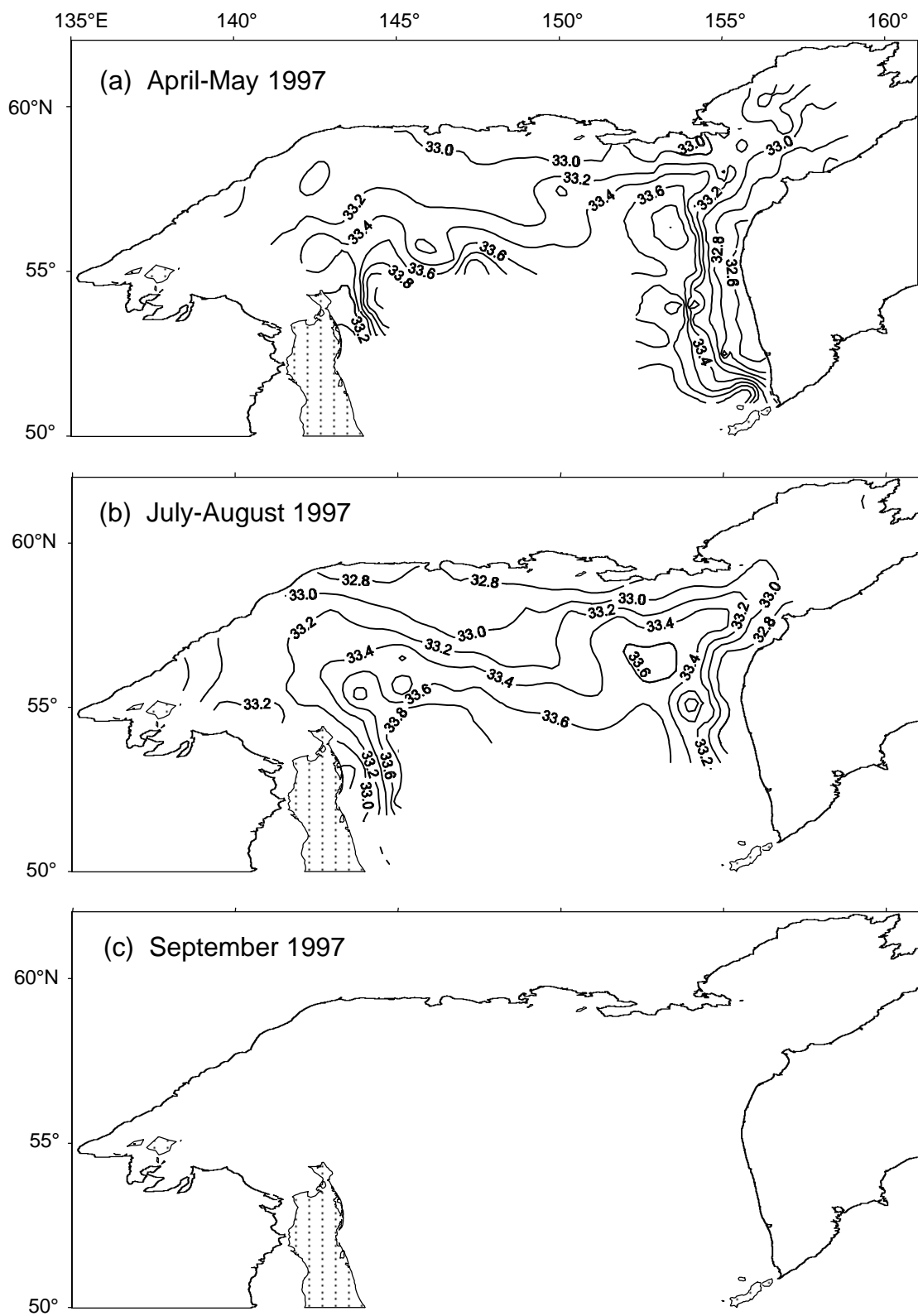


Φιγ. 2
 Γεοστροπηχ χιρχυλατιον ατ τηε συρφαχε, ρελατιψε το 500 δβαρ. (α) Απριλ θυνε 1997, (β)



Φιγ. 3

Διστριβυτιον οφ τη λοωεστ τεμπερατυρε ανδ χολδ χορε λιμιτσ ιν 1997 (δασηεδ αρεα σηοωσ τεμπερατυρε < 1°X). Χολδ χορε λιμιτσ αρε αθεραγεδ φορ 1954 1983 (φορμ Χηερν-



Φιγ. 4 Διστριβυτιον οφ βοττομ σαλινιτυ ιν 1997.

References

- Chernyavsky, V.I. 1984. Thermal characteristics of the north-eastern part of the Okhotsk Sea as the basis for type determination of sea thermal state. *Proc. TINRO*, 109, 94–103. (in Russian)
- Chernyavsky, V.I. 1992. Specificity of the temperature structure formation in the active layer of the Sea of Okhotsk. pp. 91–104. In *Oceanological Base of Biological Productivity in the North-Western Pacific*. TINRO, Vladivostok. (in Russian)
- Davydov, I.V. 1984. On the correlation of development of oceanological conditions in the main fishery areas of the far eastern seas. *Proc. TINRO*, 109, 3–16. (in Russian)
- Luchin, V.A. 1987. Water circulation in the Sea of Okhotsk and its specific interannual changeability as a result of diagnostic circulation. *Proc. FERHRI*, 36, 3–13. (in Russian)
- Shuntov, V.P. 1985. *Biological Resources of the Okhotsk Sea*. Agropromizdat, Moscow. 224 pp. (in Russian)
- Shuntov, V.P. 1994. Once again on the problem of global warming and its impact on the Far-Eastern Seas biota. *Vestnik DVO*, 20, 436–442. (in Russian)
- Shuntov, V.P. and Dulepova, E.P. 1996. Biota of the Okhotsk Sea: Structure of communities, the interannual dynamics and current status. pp. 263–271. In *Proc. Workshop on the Okhotsk Sea and Adjacent Areas, PICES Sci. Rep. No. 6*, Nagata, Y., Lobanov, V.B., and Talley, L.D. (eds.), Sidney, B.C., Canada.

Ventilation of the upper portion of the intermediate water in the Okhotsk Sea

Igor A. ZHABIN

Pacific Oceanological Institute, Far Eastern Branch Russian Academy of Sciences, Vladivostok, Russia

Introduction

Processes determining the ventilation of intermediate water in the North Pacific continue to be of interest, since in the intermediate layer the accumulation and redistribution of carbon dioxide and other gases connected with the greenhouse effect might occur. The direct ventilation of intermediate water occurs only in limited regions of the Northwest Pacific, including the Okhotsk Sea. The cold, low salinity and high oxygen intermediate layer in the Okhotsk Sea differs greatly from the relatively warm, saline and low-oxygen intermediate waters in the adjacent North Pacific. Therefore, these waters are considered as the most significant source for ventilation in the North Pacific (Talley, 1991; Talley and Nagata, 1995; Yasuda, 1997; Kono and Kawasaki, 1997).

The candidates for primary mechanisms that determine direct ventilation and transformation of the intermediate water in the Okhotsk Sea include the following processes (Moroshkin, 1966; Kitani, 1973; Talley and Nagata, 1995; Watanabe and Wakatsuchi, 1998):

1. Formation in winter of brine-enriched Dense Shelf Water (DSW) through surface cooling and freezing in the northern coastal polynyas;
2. Spring inflow of dense Soya Current Water (SCW) through the Laperuz (Soya) Strait;
3. Convection due to winter cooling.

Under the influence of these processes, the ventilation of the upper portion of the intermediate waters in the Okhotsk Sea (potential density 26.7–27.1 σ_q , depths from 150 to 400–700 m) takes place. Moroshkin (1966) named this water mass as the Okhotsk Sea Intermediate Water (OSIW).

This paper describes the ventilation signatures in the upper portion of the intermediate water in the Okhotsk Sea. Temperature, salinity and potential vorticity Q on isopycnal surfaces are analyzed. We also discuss the oceanographic features related to DSW outflow along the east coast of Sakhalin

Island and background conditions for convection in the Soya Current region near the South Kuril Islands.

Data

CTD observations were carried out on board the R/V *Akademik M.A.Lavrentyev* in July–September 1994. The location of stations is shown in Figure 1. A Neil Brown Mark IIIB CTD was used. The CTD data were collected to 1000 m. Conductivity data were calibrated by bottle samples with an accuracy of 0.01 psu in salinity. CTD data were averaged to 1-dbar intervals.

Distribution of temperature, salinity and potential vorticity on isopycnal surfaces

To investigate how ventilated water is distributed in the Okhotsk Sea, we carried out analyses of temperature, salinity and potential vorticity Q within the OSIW density range. To calculate the potential vorticity along isopycnals properties in the 26.8–26.9 and 27.0–27.1 σ_q ranges were used.

The distribution of temperature and salinity (Fig. 2) along isopycnal 26.8 σ_q shows the following features. The warmest and most saline waters were observed in the northeast part of the Kuril Basin. The OSIW in this region is transformed by mixing with Pacific water which flows through the Kruzenshtern Strait. The second area of warm and salty waters were observed off the west coast of the southern Kuril Islands. The surface layer of this area was occupied by the warmest and salty SCW. The coldest and freshest waters connected with DSW were observed along the east coast of Sakhalin Island. In the Kuril Basin spotty distribution of the temperature and salinity related to the presence of mesoscale eddies was observed. The map of dynamic topography (Fig. 3) clearly shows two anticyclonic eddies. The eddy A1 had a cold, fresh core between isopycnals 26.7–26.9 σ_q . For eddy A2 the water between 26.7–26.9 σ_q was warmer and more saline than in the surroundings. Mesoscale eddies are often observed in the Okhotsk Sea (Wakatsuchi and Martin, 1990).

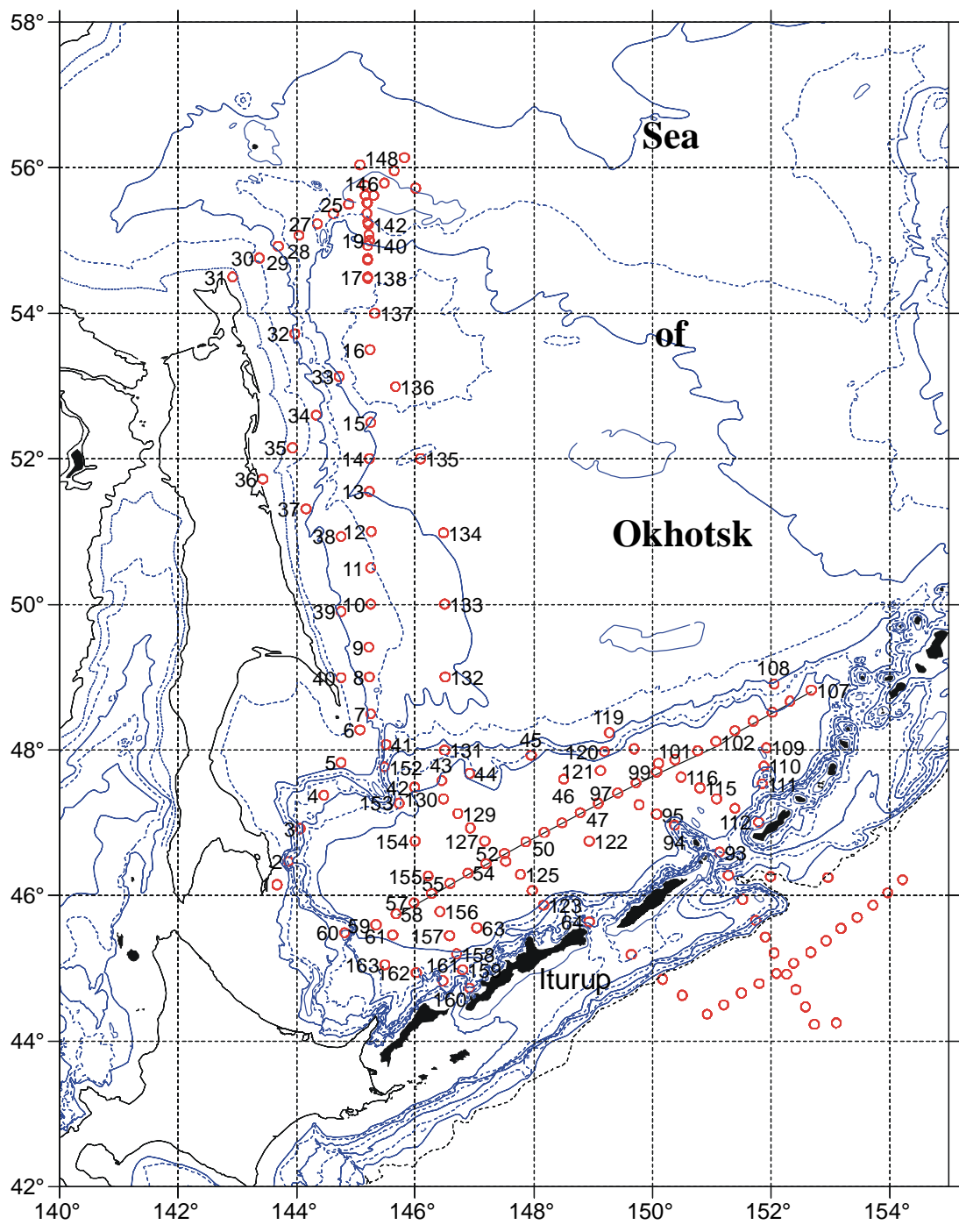


Fig. 1 CTD station locations for the R/V *Akademik M.A. Lavrentyev* survey conducted in summer 1994.

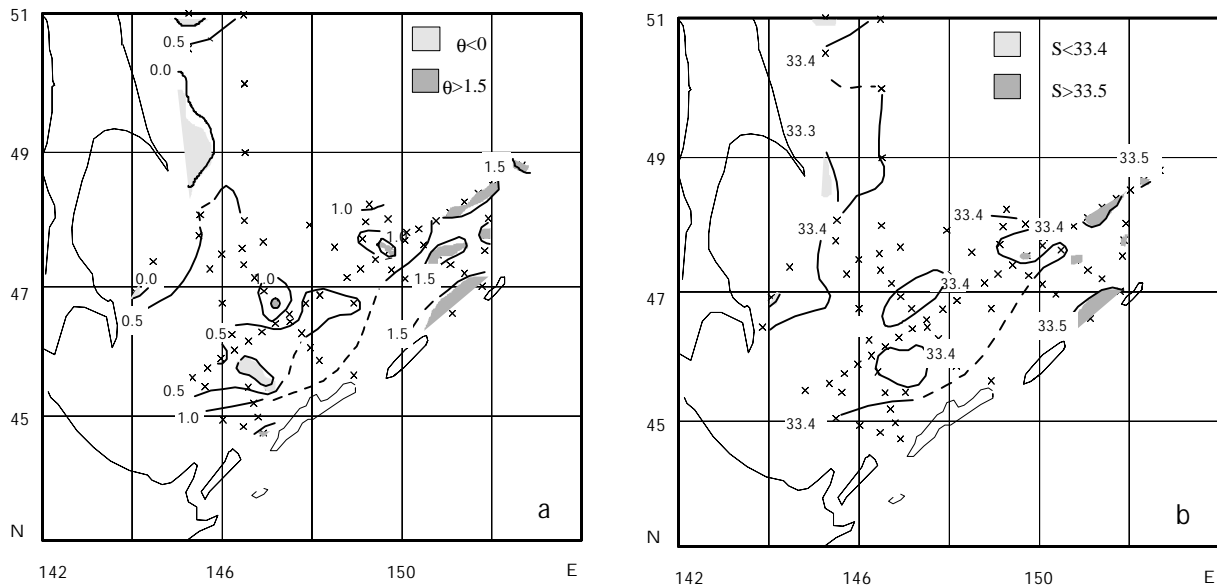


Fig. 2 (a) Potential temperature and (b) salinity at $26.8 \sigma_q$.

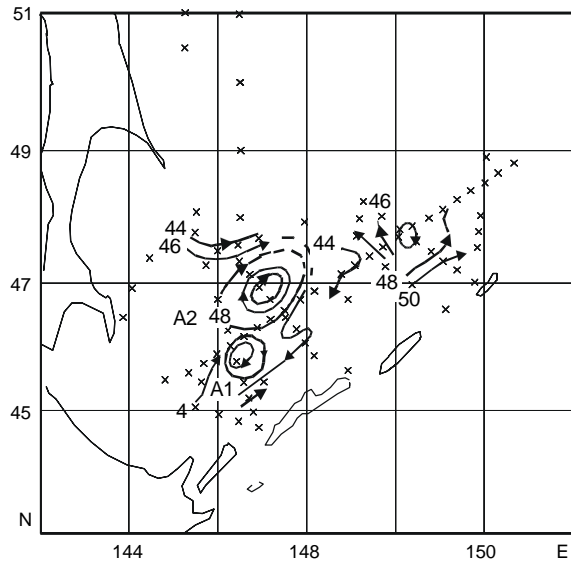


Fig. 3 Dynamic height at 500 dbar relative to 1000 dbar.

Development and decay of eddies in the Kuril Basin can be determined by the surface flow of warm, saline Soya Current Water, the advection of cold, less saline water from the East Sakhalin shelf, and winter cooling and convective mixing (Wakatsuchi and Martin, 1991).

Isopycnal layer thickness, which is locally related to potential vorticity defined as $Q = \mathbf{r}^{-1} f \Delta \mathbf{r} / \Delta z$

($10^{-11} \text{ m}^{-1} \text{ s}^{-1}$), is a useful property to study of the distribution and circulation of the ventilated water mass. Ventilated water can be identified by using potential vorticity minimum (Talley and McCartney, 1982).

According to Freeland et al. (1996) and Yusuda (1997), the vertical distribution of potential vorticity in the Okhotsk Sea has a minimum centered at $26.8\text{--}26.9 \sigma_q$ and a layer of the second maximum Q located between isopycnals 27.0 and $27.1 \sigma_q$. These results suggest that OSIW is a ventilated water mass in the Okhotsk Sea.

A vertical section of Q (Fig. 4) shows that the low potential vorticity layer related to OSIW was observed in the whole deep part of the Okhotsk Sea. The local minima Q were connected with a core of anticyclonic eddies.

In the layer $26.8\text{--}26.9 \sigma_q$ (Fig. 5a), which corresponds to a minimum of potential vorticity (ventilated regime) high- Q water ($Q > 8$) was observed along the Kuril Islands and along the east coast of Sakhalin Island. These are regions with less ventilated (more stratified) water of the intermediate layer. Thus DSW outflows along the east coast of Sakhalin Island can be characterized as high- Q water. It is possible to identify two areas of intermediate- Q water with $6 < Q < 7$, one of which is connected to waters with a strong Pacific compo-

ment flowing through the Kruzenshtern Strait; the second is located near the Terpeniya Bay. Enhanced vertical mixing in these areas results in the reduction of Q . The minima of Q (4–5) related to anticyclonic eddies were observed in the Kuril Basin. This shows that processes of generation and decay of these eddies can be related to pycnostad formation in the Okhotsk Sea.

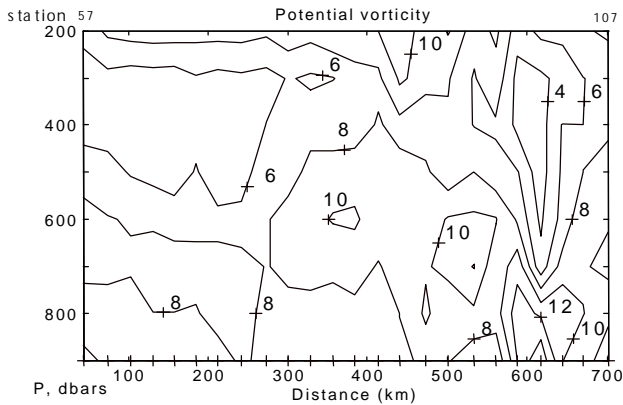


Fig. 4 Potential vorticity Q section across the Kuril Basin. The location of the section is shown in Figure 1. For the estimation of Q , CTD data were averaged to 100-dbar intervals.

The potential vorticity distribution along 27.0–27.1 σ_q (Fig. 5b, potential vorticity maximum) shows the region of high- Q water extending from the Kruzenshtern Strait to the Deryugin Basin. Low- Q water with Q from 6 to 9 was distributed along the central and southern Kuril Islands and near Terpeniya Cape. The formation process of this low- Q water may be associated with boundary mixing. Also, the low- Q band was found in the Kuril Basin.

Dense shelf water along the East Sakhalin Island coast

DSW is formed in winter in the northern coastal polynyas (Kitani, 1973; Alfultis and Martin, 1987). DSW can also be formed in Shelikhov Bay and on the East Sakhalin shelf, including Terpeniya Bay. Dense water is advected from the northwestern shelf to Cape Elizabeth (the northern tip of Sakhalin Island). DSW was observed off Cape Elizabeth as the cold bottom layer between isobaths 70 and 130 m (Fig. 6). Potential density in the bottom layer ranged from 26.94 to 27.02 σ_q . Over the East Sakhalin shelf (bottom depths 60–200 m) the bottom cold layer had potential densities of 26.71–26.85 σ_q . Along the East

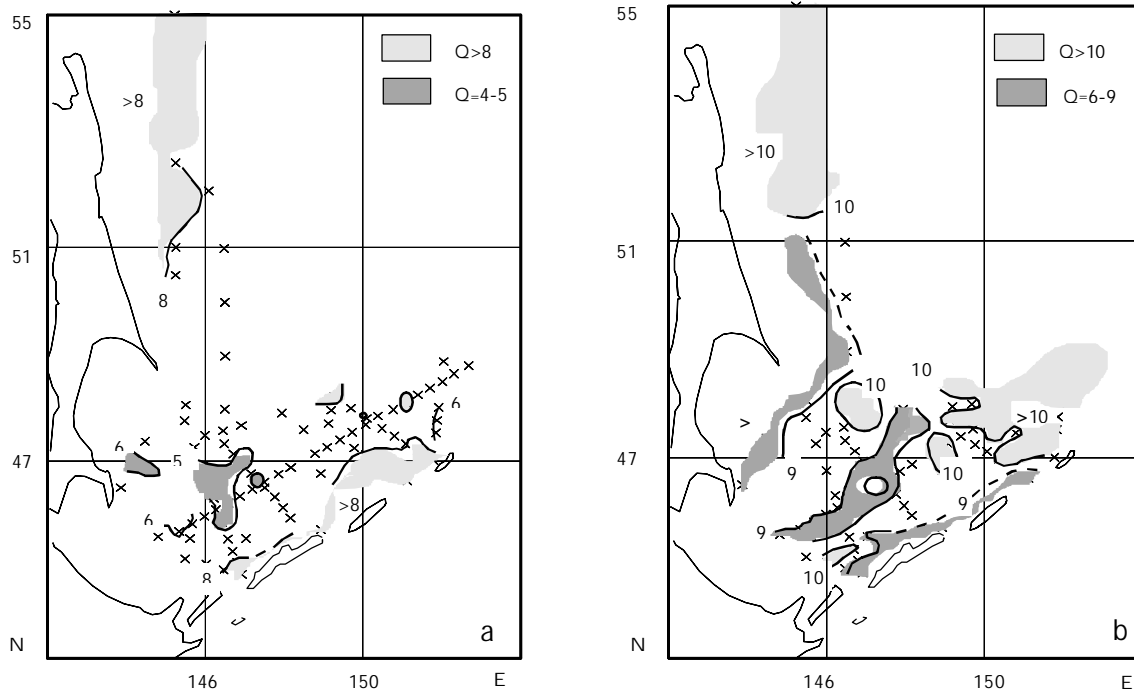


Fig. 5 Isopycnal potential vorticity $(f/r)(\partial r/\partial z)(10^{-11} \text{ m}^{-1} \text{ s}^{-1})$ at (a) 26.85 σ_q and (b) 27.05 σ_q .

Sakhalin Island slope potential density near the bottom ranged from 26.85–26.94 σ_q . This shows that DSW can ventilate the intermediate water at least down to isopycnal 27.02 σ_q .

The outflowing DSW spreads along the east coast of Sakhalin Island. During its movement the DSW mixes with ambient waters. The renewed waters separate from the Sakhalin Island coast near Terpeniya Cape and move into the Kuril Basin. Due to interleaving, numerous cold intrusive layers (lenses) are formed which appear on the vertical profiles as secondary minima of temperature. In Figure 7 the characteristics of the secondary minima of temperature in the region located between the east coast of Sakhalin Island and 147°E are shown. The cold layers had a temperature jump exceeding 0.1°C. DSW leaves the northwestern shelf without significant interleaving with ambient water. Cold intrusions were not found in the region to the north of Cape Elizabeth. Along the east coast of Sakhalin Island this water begins to interleave with waters of the deep part of the sea. The secondary minima of temperature were observed in the layer 150–600 m (26.75–27.10 σ_q). Active interleaving was observed near Terpeniya Cape and in the region of Terpeniya Bay between isopycnals 26.8–27.0 σ_q . The isopycnal and diapycnal mixing of these waters with surrounding water makes the intermediate layer in the Okhotsk Sea colder, less saline and higher in oxygen content.

Intermediate water in the Kuril Basin is also characterized by the high level of finestructure activity. Examination of vertical profiles (Fig. 8) shows that a cold, fresh and rich-in-oxygen intrusion (station 44) originating from the Sakhalin slope and a warm, saline, high-in-oxygen intrusion (station 55), related with dense SCW, were both centered at 26.95 σ_q . These stations were located around the anticyclonic eddy A2.

Conditions for development of convection in the Soya Current region

A vertical potential vorticity minimum was found at intermediate depths everywhere in the Okhotsk Sea. The pycnostad indicates that OSIW can be a convectively formed water mass. Climatic distribution shows that in the Okhotsk Sea the surface winter density does not exceed 26.7 σ_q (Talley, 1991). The cold subsurface (dichothermal) layer

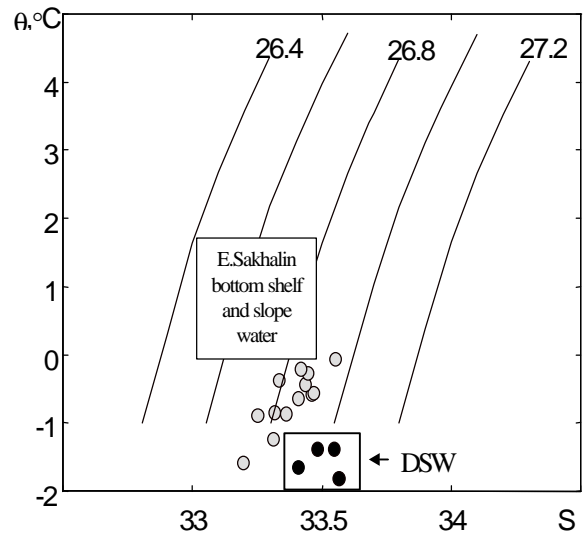


Fig. 6 T–S diagram showing characteristics of DSW off Cape Elizabeth (●) and shelf–slope bottom waters along the east coast of Sakhalin Island (○).

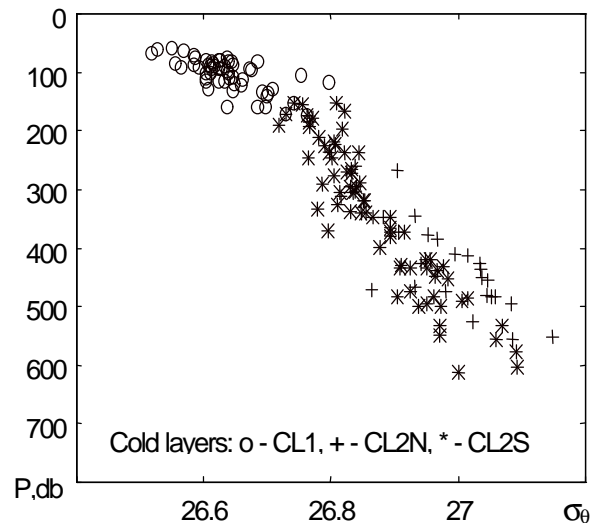


Fig. 7 Characteristics of the cold layers. CL1 refers to subsurface temperature minima, CL2 to secondary minima (N to the north of Terpeniya Cape; S to the south of Terpeniya Bay).

represents a “rest” of a winter mixed layer. Therefore, it is possible to use the density in the core of this layer as the rough estimation of efficiency of direct ventilation in the Okhotsk Sea in winter. A subsurface temperature minimum was identified for all CTD profiles. The core of the cold subsurface layer was centered in the depth

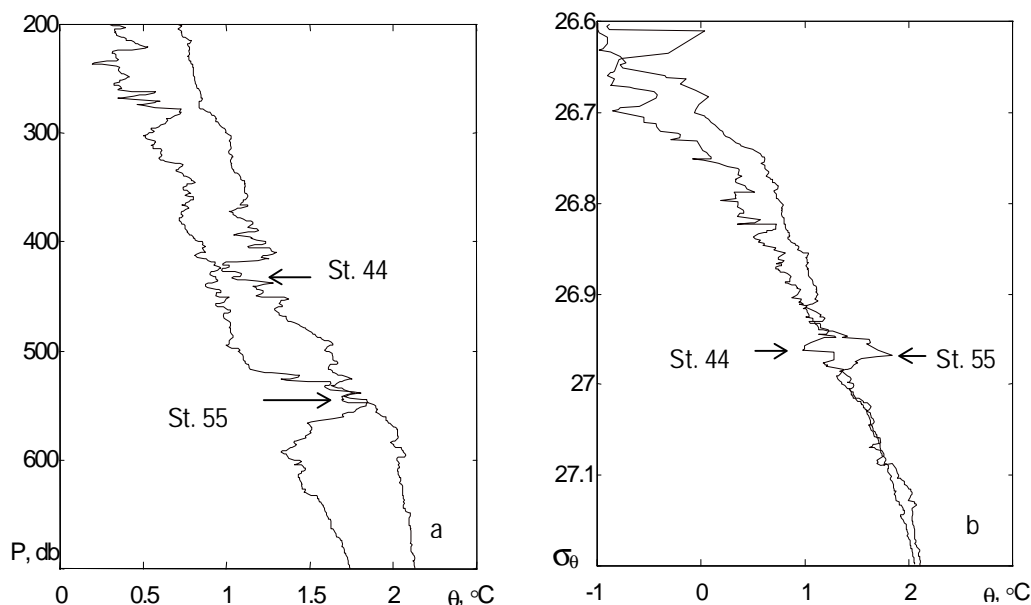


Fig. 8 Profiles of potential temperature (a and b) for stations in the Kuril Basin of the Okhotsk Sea. Arrows mark the cold, fresh intrusion originating from the Sakhalin slope (St. 44) and warm, salt intrusion related to dense Soya Current Water.

range between 60 and 200 m, ranging in potential density from 26.5 to 26.7 σ_q . For only two stations in the southern part of the sea (Stns. 57 and 59) was the core of the cold subsurface layer characterized by high potential density (about 26.75 σ_q). This shows that if intermediate convection takes place in the Okhotsk Sea, the convective renewal of OSIW occurs only in the local region.

The inflow of saline water in the Okhotsk Sea (Soya Current) creates favourable conditions for the development of convection in the southern part of the sea. Saline water enters the Okhotsk Sea from the Japan Sea through the Soya (Laperuz) Strait. During the maximum development of the Soya Current, warm and high-salinity water occupies the narrow region along the northern coast of Hokkaido and the southern Kuril Islands (Takiyawa, 1982). Water with a density of the intermediate layer can be generated due to cooling the surface SCW.

For determination of regions with favourable background conditions of stratification for development of convection, a simple mixed layer model was used. Starting with the observed profiles of temperature and salinity, this model removes from the upper mixed layer a constant amount of heat with each step (0.01°C) and reevaluates the static

stability between the mixed layer and the layer below it. If the mixed layer becomes denser than the water below, the water is completely mixed and the upper layer deepens.

The results of calculations illustrate that in the Okhotsk Sea, at a temperature close to the freezing point, thermal convection can form a mixed layer with a thickness of 40–50 m. A sharp halocline prevents a penetration of convection to large depths. Only in the Soya Current region (Stns. 160 and 161) and in the area of transformation of SCW (St. 162) were the conditions favourable for convection development (Table 1). Warm and highly saline SCW was observed in the surface layer (Fig. 9). Influence of the SCW at St. 160 appears down to a depth of about 300 m. At the bottom of this layer weak salinity and temperature minima were observed. At St. 162 high salinity water occupied only a thin surface layer. These features of the vertical thermohaline structure create favourable conditions for the development of convection. In the SCW area the deepening of the mixed layer begins at relatively high temperature (about 8°C for St. 160) and quickly penetrates to the lower boundary of the warm and salty layer. After further cooling, convective mixing penetrates into the intermediate waters and the

Table 1 Parameters of mixed layer in the Soya Current region after “cooling” to 1.5° and 0.1°C, respectively.

Station	Mixed layer T (1.5°C)				Mixed layer T (0.0°C)			
	ΔH (m)	q (°C)	S (psu)	s_q	ΔH (m)	q (°C)	S (psu)	s_q
160	427	1.53	33.49	26.79	587	-0.07	33.48	26.89
161	220	1.46	33.35	26.69	440	-0.01	33.39	26.81
162	–	–	–	–	246	0.01	33.41	26.82

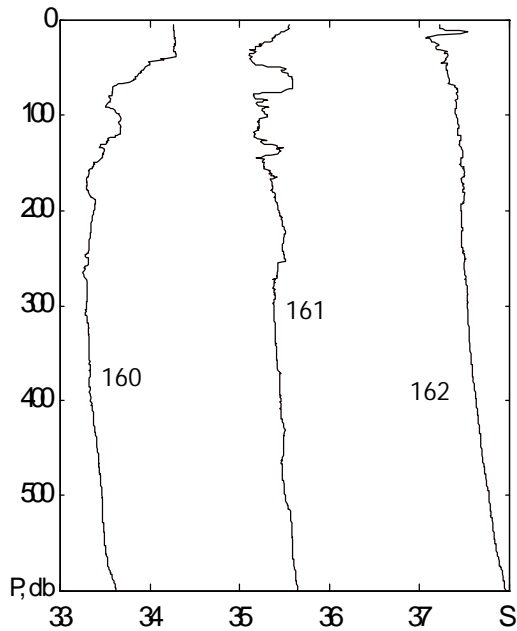


Fig. 9 Profiles of salinity for stations in the Soya Current region. Salinity profiles are offset from each other; scale correct for St. 160.

thickness of a mixed layer continues to be increased. In the area of transformation of the SCW where the contribution of saline water in density stratification is small, convective mixing begins at relatively low temperature (about 0.5°C for St. 162). The thickness of the mixed layer in this area at equal temperature is less in comparison with the SCW area. Calculations of mixed layer parameters at temperatures close to climatology in November and December (Veselova, 1975) have shown (Table 1) that, in the SCW area (St. 160) at $T = 1.53^\circ\text{C}$, the layer thickness is 427 m ($s_q = 26.79$). In the transformation area of the SCW (St. 162) at $T = 0.01^\circ\text{C}$, the thickness of the mixed layer equals 246 m ($s_q = 26.82$). Comparison between profiles of temperature, salinity and dissolved oxygen taken near Iturup Island before and

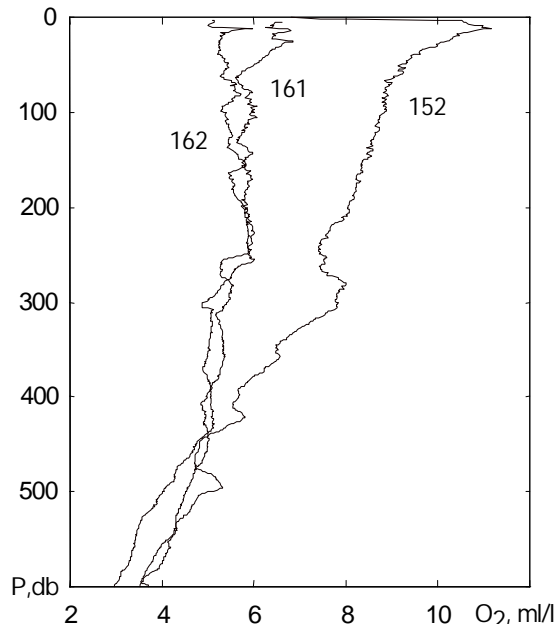


Fig. 10 Vertical profiles dissolved oxygen content in area off the coast of the southern Kuril Islands before (Stns. 160 and 161) and after (St. 152) winter 1994–1995.

after the winters of 1994–1995 (Fig. 10) shows apparent variation in the vertical structure from the surface to 450 m. ($s_q = 26.86$) Thus in the Soya Current region, due to cooling of the saline surface layer and subsequent convection, the intermediate water can be ventilated.

Conclusions

The main results are summarised as follows. The OSIW, in the range of potential density 26.7–27.1 s_q , can be ventilated through the impact of brine-enriched DSW and consequent boundary mixing with ambient water which takes place along the Sakhalin Island shelf and slope. Cold, fresh and high-oxygen water originates from East Sakhalin and the dense SCW ventilated intermediate layer

in the Kuril Basin around $26.95 \sigma_q$. Convection in the Soya Current region along the South Kuril Island can ventilate OSIW down to 26.70 – $26.85 \sigma_q$.

References

- Alfultis, M.A. and Martin, S. 1987. Satellite passive microwave studies of the Sea of Okhotsk ice cover and its relation to oceanic processes, 1978–82. *J. Geophys. Res.*, *92*, 13,013–13,028.
- Freeland, H.J., Bychkov, A.S., Wong, C.S., Whitney, F.A. and Yurasov, G.I. 1996. The Okhotsk Sea component of Pacific Intermediate Water. pp. 36–44. In *Proc. Workshop on the Okhotsk Sea and Adjacent Areas*, *PICES Sci. Rep. No. 6*, Nagata, Y., Lobanov, V.B. and Talley, L.D. (eds.), Sidney, B.C. Canada.
- Kitani, K. 1973. An oceanographic study of the Okhotsk Sea—Particularly in regard to cold waters. *Bull. Far Seas Fish. Res. Lab.*, *9*, 45–77.
- Kono, T. and Kawasaki, Y. 1997. Modification of the western subarctic water by exchange with Okhotsk Sea. *Deep-Sea Res.*, *44*, 689–711.
- Moroshkin, K.V. 1966. Water masses of the Okhotsk Sea. Nauka, Moscow, 68 pp. (Translated from Russian by National Technical Information Services, 1968)
- Takizawa, T. 1982. Characteristics of the Soya Warm Current in the Okhotsk Sea. *J. Oceanogr. Soc. Japan*, *38*, 281–292.
- Talley, L.D. 1991. An Okhotsk Sea water anomaly: Implication for ventilation in the North Pacific. *Deep-Sea Res.*, *38(suppl.)*, S171–S190.
- Talley, L.D. and McCartney, M.S. 1982. Distribution and circulation of Labrador Sea Water. *J. Phys. Oceanogr.*, *12*, 1189–1205.
- Talley, L.D. and Nagata, Y. (eds.) 1995. The Okhotsk Sea and Oyashio region. *PICES Sci. Rep., No. 2*, 227 pp., Sidney, B.C., Canada.
- Veselova, L.E. 1975. Specific features of an annual temperature cycle at the surface of the southern part of the Okhotsk Sea. *Proc. FERHRI*, *50*, 38–56. (in Russian)
- Wakatsuchi, M. and Martin, S. 1990. Satellite observations of the ice cover over the Kuril Basin region of the Okhotsk Sea and its relation to the regional oceanography. *J. Geophys. Res.* *95*, 13,393–13,410.
- Wakatsuchi, M. and Martin, S. 1991. Water circulation of the Kuril Basin of the Okhotsk Sea and its relation to eddy formation. *J. Oceanogr. Soc. Japan*, *47*, 152–168.
- Watanabe, T. and Wakatsuchi, M. 1998. Formation of 26.8 – $26.9 \sigma_\theta$ water in the Kuril Basin of the Sea of Okhotsk as a possible origin of North Pacific Intermediate Water. *J. Geophys. Res.*, *103*, 2849–2865.
- Yasuda, I. 1997. The origin of the North Pacific Intermediate Water. *J. Geophys. Res.*, *102*, 893–909.

Oceanographic conditions over the Kashevarov Bank

Vladimir A. LUCHIN¹ and Alexander L. Figurkin²

¹ Far Eastern Regional Hydrometeorological Research Institute, Vladivostok, Russia

² Pacific Research Institute of Fisheries and Oceanography, Vladivostok, Russia

The abnormal distribution of the oceanographic parameters over the Kashevarov Bank has attracted the attention of many researchers. In warm seasons, the surface waters here keep lower temperature and higher salinity, than those of the surrounding environment. On the contrary, in the subsurface layer, the destruction of the northern Okhotsk “cold core” is observed. All year round, the deep waters over the bank remain unusually homogeneous in temperature, salinity, concentration of dissolved oxygen, and nutrients. Even in the winter, thin ice areas (*polynyas*) are often found in the vicinity of the Kashevarov Bank.

There exist several assumptions today about the mechanism that forms specific hydrological and hydrochemical characteristics of this area. Moroshkin (1966), and Kitani and Shimazaki (1971) noted the abnormal conditions of the water parameters in this region. Akiba et al. (1959) and Kitani (1973) mentioned vertical water mixing as the reason, but did not specify its specific force. Chernyavsky (1970), Veselova (1972), Kovshov and Sinyurin (1982), (Markina and Chernyavsky (1984), and Zhigalov and Matveev (1992), explained the situation by cyclonic water circulation alone, in conjunction with up-welling. Alfultis and Martin (1987), speculated on a dominating role of up-welling over the bank. Some authors, Zhabin and Zuenko (1993), and Kuzmina and Sklyarov (1984), considered tidal mixing and up-welling to be the contributing mechanism.

A theoretical model has been worked out by Karpushin et al. (1996), assuming that the abnormal distribution may be formed by the influence of the anti-cyclonic eddy (a Taylor–Hogg column), with a very small radius and a large cyclonic eddy. Such a circulation may cause intensive up-welling. Rogachev and Kosolapkin (1995) considered that homogeneous structures are formed as a result of summary influence of tidal and non-periodic currents. These authors confirm that mixing together the surface, dichothermal and mesothermal water masses is accompanied by an increase of water

density and by the decline in sea level, as well as by causing the cyclonic circulation.

All the explanations listed above are hypothetical, as it is difficult to differentiate one forcing component from another due to lack of oceanographic data to confirm the assumptions. The largest problem, apparently, is the absence of direct current measurement records, which does not allow researchers to examine the real water circulation and mixing intensity in this area of the sea.

The goal of this work is to analyze all accessible data and to assess the mechanisms that form abnormal conditions over the Kashevarov Bank.

The Kashevarov Bank at the 200 m isobath is located between parallels 55°15′ and 55°57′ N., and meridians 144°45′ and 146°42′ E (Fig. 1). Two tops of the bank are at minimal depths of about 110 and 130 m. The area surrounding the bank has a varied relief. Besides the bank, there are two canyons here. One canyon, with the depths varying from 1300 to 300 m, lies between Kashevarov Bank and Saint Iona Island. The second canyon is located to the east of the bank and its depths vary from 500 to 300 m.

For the analysis, we used all oceanographic stations that lie within parallels 55°00′ and 56°30′ N and meridians 144°00′ and 147°30′ E. In this area, 315 deep-water stations have been occupied since 1937. As a rule, during an expedition 5 to 10 stations were occupied at a distance of 20–30 miles. The section probes that crossed the Kashevarov Bank and its immediate surroundings were purposely carried out only in recent years (1994, 1995 and 1996, Fig. 1). Half of all observations were performed last August (about 90 stations) and September (about 60 stations). During the cold season (from December through April) only individual observations took place there.

In early spring, water temperature around the Kashevarov Bank, taken in the layer of winter con-

vection, is below zero and never exceeds -1.0° to 1.55°C (section A-A, Fig. 2). The salinity varies from 32.9 to 33.2 psu. Below the layer of winter cooling, the water temperature goes up to $+1.5^{\circ}\text{C}$ and the salinity reaches 33.5 to 33.6 psu. Above the top of the Kashevarov Bank, there was noted the homogeneous distribution of hydrological and hydrochemical characteristics was noted. This can be seen in the vertical direction on the lines. Colder temperature water spreads on the slope off the bank, rather than in surrounding waters. At the stations off the bank, the dissolved oxygen concentration at the top of the 50-m layer was 8.5 to 9.2 ml/l, and in shallow waters over the bank it dropped to 7.2 ml/l.

Figure 3 presents a synthetic chart made as a result of 7 expeditions carried out during May from 1983 through to 1996, in which there areas with cyclonic and anti-cyclonic types of water circulation have been observed. Studies have proved that an extensive cyclonic circulation over the Bank and to the north from the 500 m isobath usually predominates in cold periods. Over the deep-water sites of the Deryugin Basin two zones were marked by predominately anticyclonic water circulation. At times, the anticyclonic circulation was observed west of the Kashevarov Bank, over the canyon. This may be caused by the spreading of warm water from the Deryugin Basin.

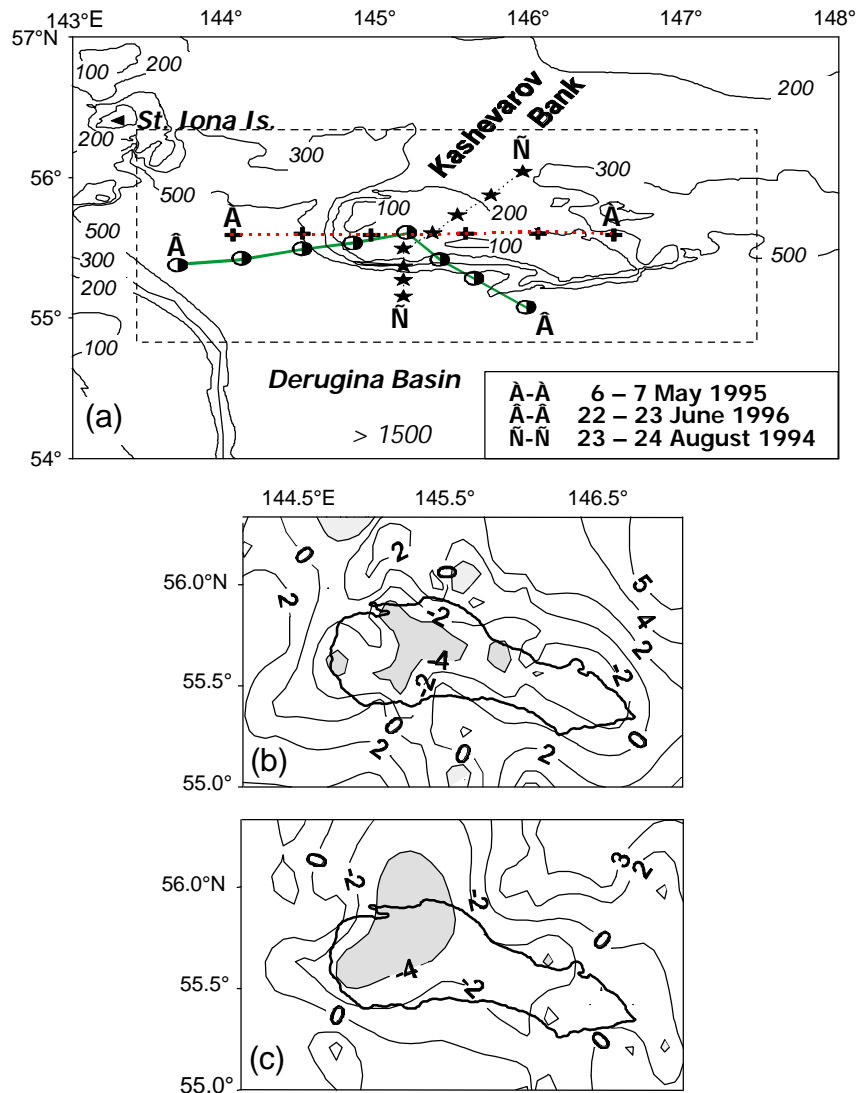


Fig. 1 (a) Bathymetric chart (m) of the Kashevarov Bank area and location of the sections. Averaged spatial surface temperature anomaly ($^{\circ}\text{C}$) in (b) August and in (c) September.

In late spring, around the Kashevarov Bank (see: section B-B, Fig. 2) an intensive freshening influence was observed (water salinity decreased to 27.0–32.0 psu), caused by both ice melting and mainly by the Amur River outflow. The thin upper fresh layer quickly warmed to 7°–10° C, and the temperature was maintained by a bottom strong vertical density gradient. The lowest salinity and highest water temperature were marked southwest of the Kashevarov Bank. The dissolved oxygen concentrations in these waters did not exceed 8.3 ml/l. Dichothermal waters maintained

negative temperatures of about -0.3° to -0.7°C . In late spring, over the Kashevarov Bank, the surface water temperature was about 1.0° to 1.6°C , and temperature over the top of the bank reached -0.5° – -0.8°C . Thus, the basic part of incoming solar heat was redistributed in the water column from the surface through to the bottom. The surface water salinity was nearly same as near the bottom of the Bank (33.16 to 33.2 psu). The range of oxygen concentration between the surface and bottom layers did not exceed 0.1 ml/l.

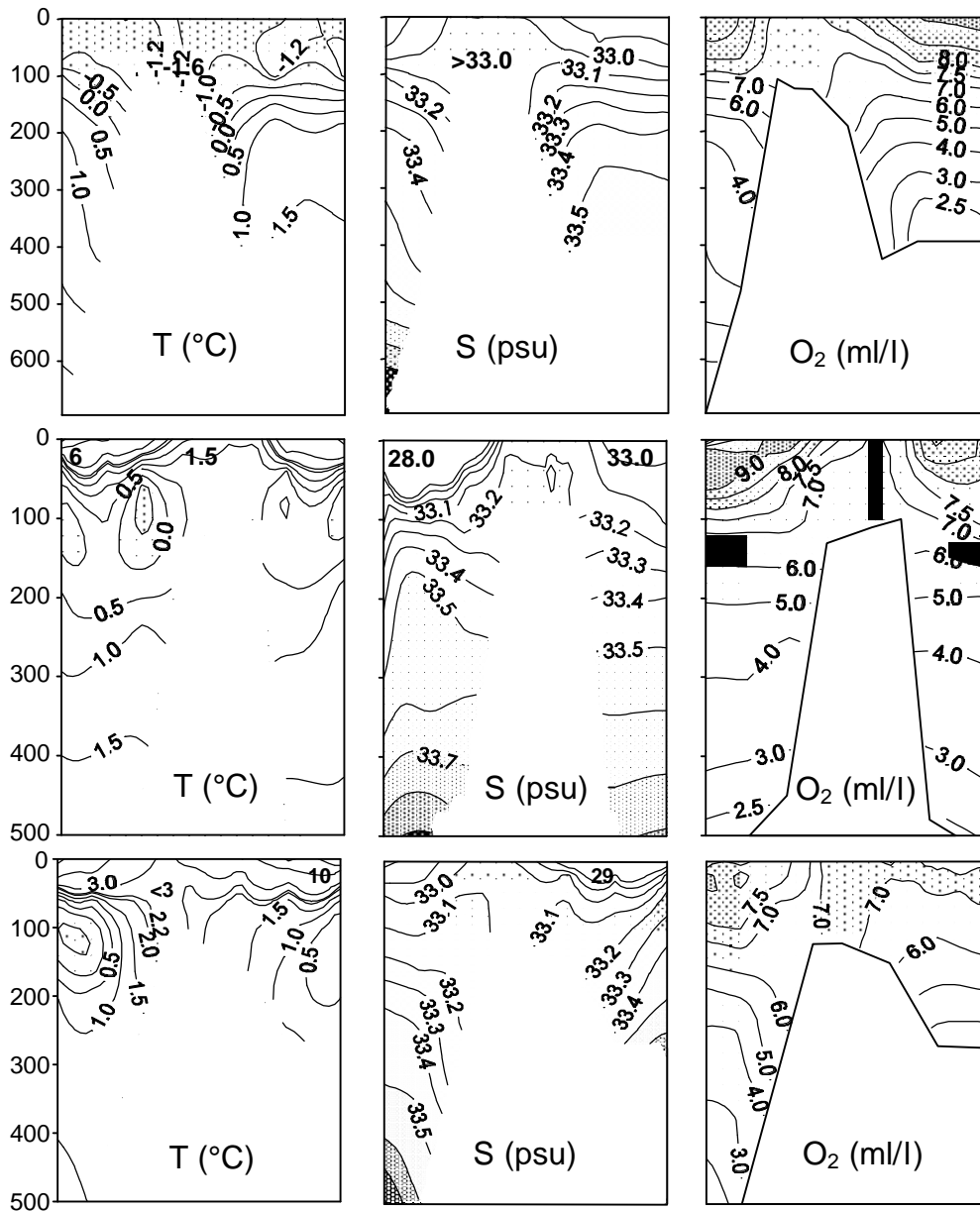


Fig. 2 Distribution of water properties at (top) section A-A for 6–7 May, 1995, (middle) section B-B for 22–23 June, 1996, and (bottom) section C-C for 23–24 August, 1994.

In August (section C-C, Fig. 2), the surface waters around the Kashevarov Bank warmed to 7° to 12°C, while the dichothermal water still maintained negative temperatures. Over the Kashevarov Bank, a thin surface layer with temperature 2.5°–3.0°C and salinity 32.9 up to 33.0 psu was marked. The depth of this layer did not exceed 20–25 m. Below the surface layer, nearly homogeneous waters were found, with temperature ranging from 2.0° to 2.3°C, salinity from 33.05 to 33.2 psu, and oxygen concentration from about 6.5 to 7.2 ml/l. In some years, there was no sign of any thin warm surface layer over the Bank. During these periods, completely homogeneous water was observed over the Bank in all seasons.

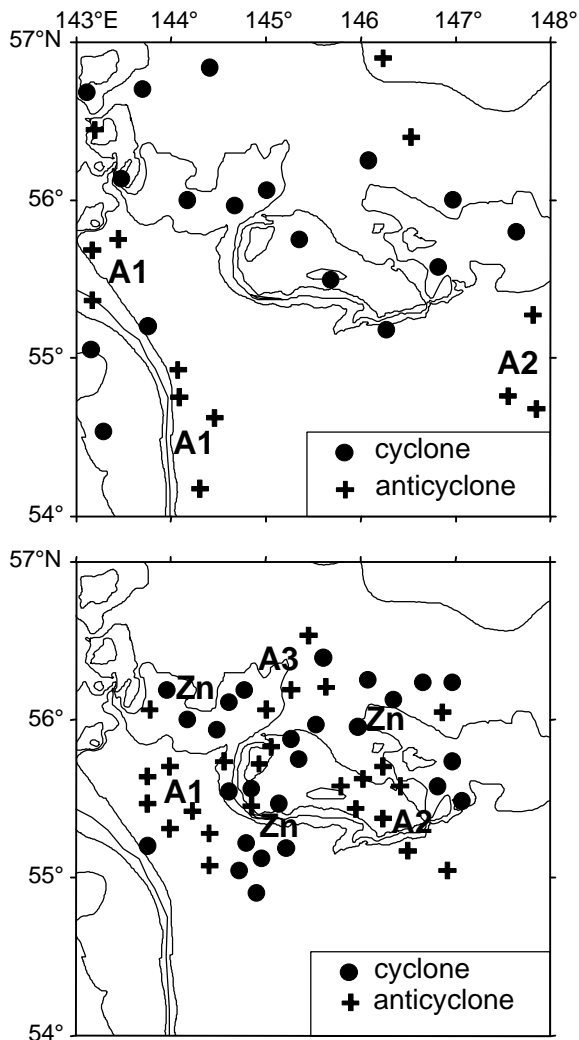


Fig 3 Combined charts of cyclone and anticyclone locations in (top) early spring and (bottom) summer over the Kashevarov Bank.

Figure 4 characterizes the distribution of water temperature at depths 0, 100 and 200 m in August. The temperature was averaged for the period from 1937 to 1996. The points of the highest surface temperature, 11°–13°C are located at some distance in the southwest and north directions from the Kashevarov Bank. As a rule, the locations with the highest temperature overlap the locations with the lowest water salinity. Over the Bank, the surface water temperature drops to 3.5°–5.0°C. The waters over the Bank are colder than surrounding ones, up to a depth of 20 m. At a depth of 30 m this pattern is not observed. From a depth of 50 m, the picture of water temperature distribution is quite the opposite to that of the surface layer: the highest water temperatures (about 1.5°–2.5°C) were observed over the Bank, and the lowest ones (about 0.5°–1.0°C) were marked at some distance from the Bank. A similar distribution of the highest and lowest temperatures was defined at depths from 50 to 200 m. At layer of 300–500 m the temperature conditions are not that clearly determined due to lack of data for accurate averaging. This area is also separated by the Bank slope, which plays a role as well. However, available data show that the August temperature of water in the layer 300–500 m is also higher on the slopes of the Bank, than at a distance away from it.

The September distribution of average water temperatures taken in the course of years is generally similar to the basic August characteristics. However, in September, the depth of the surface layer grows from 20 to 30 m, in which the water temperature over the bank is lower, than that in the surrounding waters.

In August the highest values of water salinity at surface layer (up to 32.90–33.05 psu) are observed over the Kashevarov Bank. The salinity declines with distance from the Bank, and its lowest values (up to 26–28 psu) are observed to the southwest of the Bank. The volume with the highest salinity over the Bank is maintained in the layer from 0 to 75 m. From a depth of 150 m, the salinity over the Bank, compared to surrounding waters, decreases.

The salinity in September is reduced due to the influence of Amur River. The lowest salinity at the surface, 31.14 psu, was marked only to the west of the Kashevarov Bank.

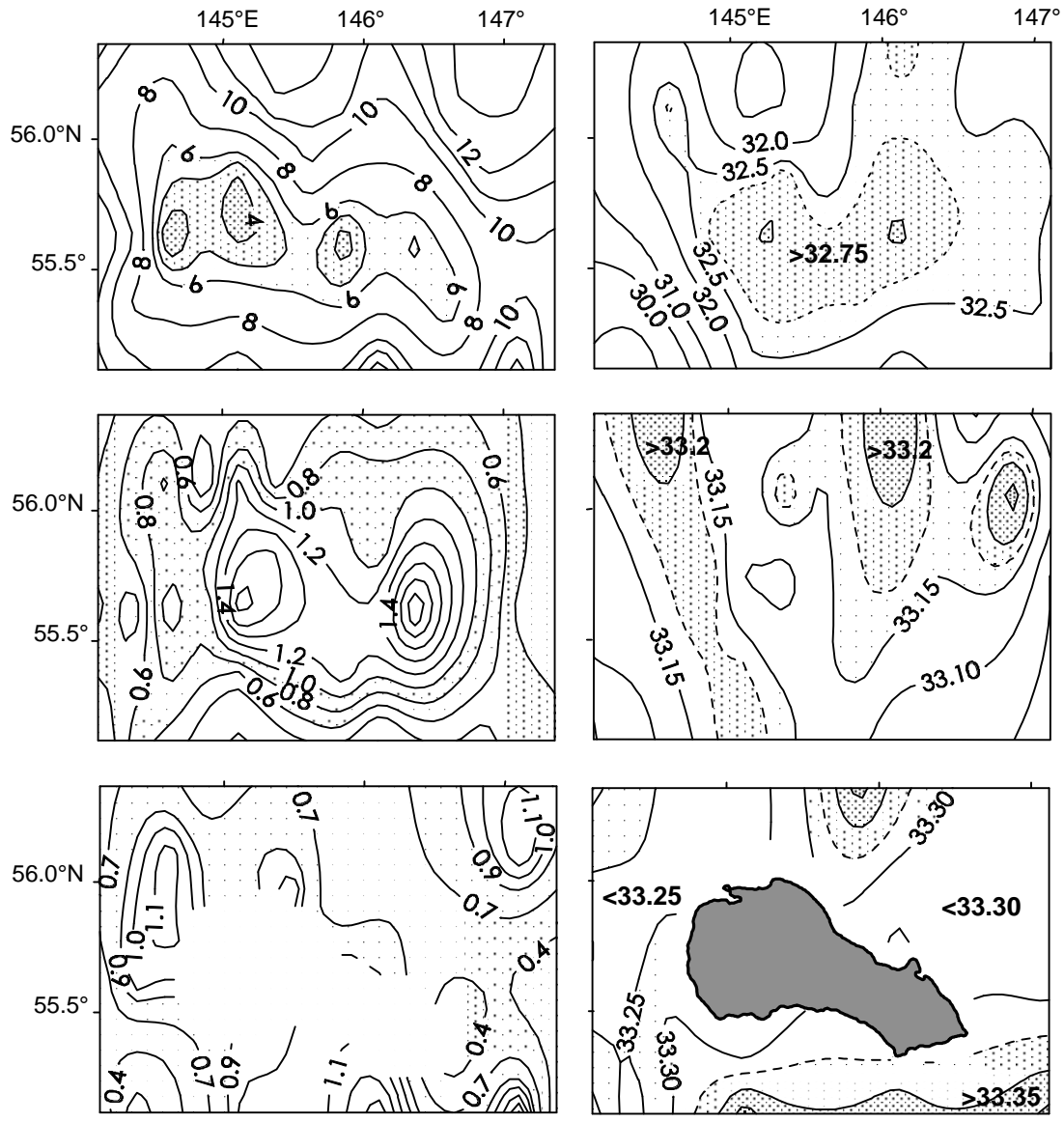


Fig. 4 Distribution of (left column) water temperature (°C) and (right column) salinity (psu) in August (averaged data) at different depths: (top) 0 m, (middle) 100 m, and (bottom) 200 m.

The charts of geostrophic circulation have shown that in warm seasons of the year the top layer (0–30 m) contributes to the dominant cyclonic circulation over the Bank. It is natural, as this is the layer where the highest values of temperature and salinity have been marked. Figure 5 shows two dynamic topography charts for August 1983. On the left-hand charts, the dynamic topography was calculated for the layer from the surface down to 300 m, and an extensive area with cyclonic water circulation was observed. On the right-hand charts, the dynamic topography was calculated for the layer from 30 down to 300 m, and it is evident that the cyclonic circulation area has broken up into a pair of cyclonic and a pair of anti-cyclonic

areas. A similar phenomenon was observed when we analyzed the data from the other expeditions, as well as the averaged data for August and September (Fig. 5). Thus, when we take into account the distribution of density in the top layer 0–30 m, we see the prevalence of a cyclonic-type circulation over the Kashevarov Bank. In the other case, the area of cyclonic circulation decreases considerably, and the chart of currents does not look as simple.

Three areas with a prevalence of cyclonic circulation and three areas with a prevalence of anti-cyclonic circulation in the layer from 30 to 300 m depth were observed as typical for warm seasons

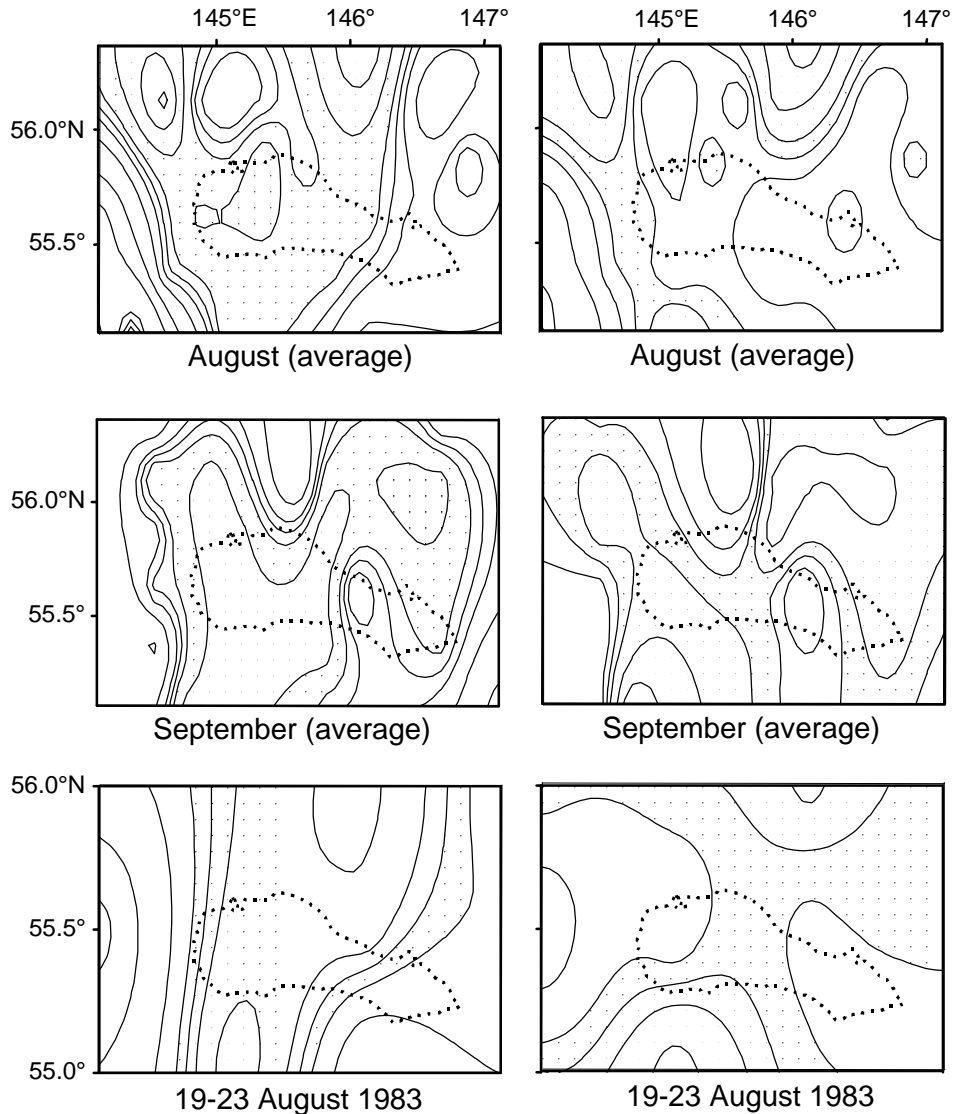


Fig. 5 An example of dynamic topography charts in the Kashevarov Bank area. (Left column) isopleths calculated with surface layer and (right column) calculated without surface layer. Dashed line indicates the area of cyclonic circulation.

(Fig. 3, bottom panel). Areas of cyclonic circulation were marked (Z) and anti-cyclonic circulation were marked (A), and were conditionally numbered. Compared to the similar chart for spring, the area with cyclonic water circulation has noticeably decreased, and the warm waters of the Deryugin Basin (marked as A1 and A2) have moved to the north. It is interesting to note that in summer the anti-cyclonic type of water circulation is usually registered in the eastern part of the Kashevarov Bank (A2). Warmed waters with anti-cyclonic circulation (A3) are often found to the north of the Bank, where they reach by spreading along the deepest curves of the canyon bottom.

Apparently, the real charting of currents over the Kashevarov Bank is more complicated than it is usually thought and its parameters may vary, depending on the season. During warm seasons, the density distribution in the surface layer plays active role in the formation of cyclonic circulation.

Regarding the reasons for anomalous formations found over the Kashevarov Bank, a number of authors consider up-welling and tidal mixing as the basic mechanisms capable of producing a nearly homogeneous water structure which is typical of the Bank.

As for the arguments for or against the up-welling, there are several factors to consider. In the case of up-welling, during the cold period of the year, temperature is expected to be higher over the Bank than in adjacent waters. However, during these periods, as a rule, the water temperature over the Bank is colder than that of the surrounding waters. It is also difficult to explain why winter convection is not restrained by the up-welling but penetrates deeper than that in waters surrounding the Bank. These facts testify that, in addition to the convection, some other processes intensify vertical exchange (for example, tidal mixing).

Up-welling can hardly explain why water salinity is lower in the layer between 150 m and the top of the Bank than that in surrounding waters.

In Figure 1b and c, the spatial anomalies of the surface temperature in August and September are shown. It is clearly shown here that, as a rule, the location of the maximal anomalies zone maintains within the limits of the 200 m isobath. In case of up-welling along the Bank slope, the maximal anomalies are assumed to lie under some slope of the Bank rather than over the Bank.

In the case of up-welling at intermediate depths, the convexity of isolines in upward direction is assumed in the section over the Bank. It is interesting to note that, in this case, we see two opposite directions of isolines – up to the surface and down to the bottom. A similar picture with isolines over the Bank was observed by Zuenko and Zhabin (1993). They explained this phenomenon by intensive tidal water mixing over the Bank. This conclusion was confirmed by the results obtained from Bowden's investigations. Bowden (1988) has shown that the same type of isolines is typical of the range between stratified and well-mixed water. The depth of the mixed layer correlates with the parameter that is supposed to be equal or less than P , giving $P = H/U^3$, where H is the depth of a site (m) and U is the current speed (m/s).

Bowden has calculated that the parameter P varies from 70 to 100. The parameter P is proportional to H and is back proportional to U^3 . Thus, by knowing the actual thickness of a homogeneous layer over the Kashevarov Bank, it is possible to assume the speeds of tidal currents in this area to be not less than 110 cm/s. Although we have no actual records of tidal currents, we still can borrow facts

obtained by Kanari and Suzuki (1986). They calculated that the model tidal speed was about 40–50 cm/s and actual only for daily harmonics (K_1 and O_1). Thus, we can estimate that the total speed equals or is greater than 110 cm/s in the Kashevarov Bank area, which seems quite possible.

We have calculated weighted average values of temperature, salinity, concentration of dissolved oxygen and nutrients at the stations that were carried out off the Bank (i.e. in the zone with significant stratification). In the first approximation, the weighted average value is equal to the value of complete mixing in the tested layer. The probes were taken from the surface and down to a depth where the weighted average values were equal to the values of mixed waters over the Kashevarov Bank. It appeared that the values of all parameters (temperature, salinity, oxygen and biogenes) over the Kashevarov Bank could be equal to those of weighted average values, in case where the waters outside the Bank were mixed from the surface down to a depth of 170–220 m.

The arguments listed above allows us to conclude that tidal mixing effects serve as a more realistic reason for a nearly homogeneous water structure over the Kashevarov Bank, rather than up-welling. Water mixing results in the lowering of a surface level and in causing cyclonic circulation, at least over a significant part of the Bank. The cyclonic circulation causes divergence of the surface waters outside the bank area, which explains the phenomena of polynyas over the Bank.

References

- Akiba, Y., Yamamoto, S. and Ueno, M. 1959. On the oceanographical conditions of the Okhotsk Sea in summer of 1958. *Bull. Fac. Fish. Hokkaido Univ.*, 10(1), 37–46.
- Alfultis, M.A. and Martin, S. 1987. Satellite passive microwave studies of the Sea of Okhotsk ice cover and its relation to oceanic processes 1978–1982. *J. Geophys. Res.*, 92(C12), 13,013–13,028.
- Bowden, K.F. 1988. *Physical Oceanography of the Coastal Waters*. Mir, Moscow. 324 pp. (in Russian)
- Chernyavsky, V.I. 1970. On the factors causing high biological productivity in the northern Sea of Okhotsk. *Proc. TINRO*, 71, 13–22. Vladivostok. (in Russian)

- Kanari, S. and Suzuki, K. 1986. Tidal simulation of the Sea of Okhotsk. *Kaiyo Kagaku*, 18(7), 455–463. (in Japanese)
- Karpushin, M.A., Sapozhnikov, V.V and Tolmachev, D.O. 1996. Hydrochemical structure and vertical biogens fluxes over Kashevarov Bank. *Oceanology*, 36(6), 868–874. (in Russian)
- Kitani, K. 1973. An oceanographic study of the Okhotsk Sea – Particularly in regard to cold waters. *Bull. Far Seas Fish. Res. Lab.*, 9, 45–76.
- Kitani, K. and Shimazaki, K. 1971. On the hydrography of the northern part of the Okhotsk Sea in summer. *Bull. Fac. Fish. Hokkaido Univ.*, 22(3), 231–242.
- Kovshov, V.A. and Sinyurin, Y.N. 1982. Permanent sparseness of ice cover in open areas of the Okhotsk Sea. *Meteorol. Gidrol.*, 11, 76–81. (in Russian)
- Kuzmina, I.P. and Sklyarov, V.E. 1984. Drifting ice as a tracer for the studies of peculiar water circulation of the Pacific marginal seas. pp. 16–25. In *Investigation of the Earth from the Space.1.* (in Russian)
- Markina, V.V. and Chernyavsky, V.I. 1984. Quantitative distribution of plankton and benthos in the Sea of Okhotsk. *Proc. TINRO*, 109, 109–119. Vladivostok. (in Russian)
- Moroshkin, K.V. 1966. *Water Masses of the Sea of Okhotsk.* Nauka, Moscow. 65 pp. (in Russian)
- Rogachev, K.A. and Kosolapkin, G.Y. 1995. Water mixing over Kashevarov Bank. *Meteorol. Gidrol.*, 3, 96–104. (in Russian)
- Veselova, L.E. 1972. Spatial temperature distribution in the surface waters of the Sea of Okhotsk. *Trudy DVNIGMI*, 37, 13–28. (in Russian)
- Zhigalov, I.A. and Matveev, V.I. 1992. Spatial structure of Okhotsk Sea surface water. pp. 40–46. In *Oceanological Base of Biological Productivity in the North-Western Pacific.* TINRO, Vladivostok. (in Russian)
- Zuenko, Y.I. and Zhabin I.A. 1993. T-S conditions in the tidal shelf regions of the Okhotsk Sea. pp. 104–111. In *Geographical Researches of the Far Eastern Sea's Shelf.* Far Eastern University, Vladivostok. (in Russian)

Tidal exchange through the Kuril Straits

Toshiyuki AWAJI¹, Tomohiro Nakamura¹, Takaki Hatayama¹,
Kazunori Akitomo¹ and Takatoshi Takizawa²

¹ Department of Geophysics, Kyoto University, Kyoto, Japan

² Japan Marine Science and Technology Center, Yokosuka, Japan

Abstract. The tidal exchange between the Okhotsk Sea and the North Pacific Ocean is studied numerically with particular emphasis on the predominant component, the barotropic K_1 tide. Since the K_1 tide is subinertial in the Okhotsk Sea, topographically trapped waves are effectively generated, contributing to strong tidal currents with a maximum amplitude of over 1.5 m s^{-1} in the Kuril Straits. The structures of tide-induced mean flows in most passages of the Straits are characterized by “bi-directional currents” (in which the mean flow exhibits a reversal in direction across the passages). The mean transport shows significant net exchange of water via several straits in the Kuril Islands, whose amount is over 5.0 Sv toward the North Pacific. Therefore, the tidal current is thought to play a major role in water exchange processes between the Okhotsk Sea and the North Pacific. Our analysis reveals that the bi-directional mean currents at shallow passages are produced through the well known process of tidal rectification, whereas in deep passages, the propagating trapped waves along islands are essential for generating the bi-directional mean currents.

Introduction

The Okhotsk Sea (Fig. 1) is thought to have a significant impact upon the North Pacific. For example, Talley (1993) and Yasuda et al. (1996) commented that the Okhotsk Sea supplies low salinity water to the North Pacific Intermediate Water (NPIW) characterized by a salinity minimum centered at $26.8\sigma_\theta$. Thus, a clarification of the exchange processes through the Kuril Straits is indispensable for a better understanding of water mass formation in the North Pacific (such as the NPIW). Past studies regarded the current in the Okhotsk Sea as part of the cyclonic subarctic circulation which predominantly flows into the Okhotsk Sea through the Kruzenshtern Strait and out through the Bussol Strait. However, recent observational studies suggest that there is great difficulty in explaining this in/outflow in terms of geostrophic balance. One reason for this is that the overall surface dynamic height is higher in the Okhotsk Sea than in the northwestern North Pacific (Kawasaki and Kono, 1992). Another reason is that due to the weak stratification, the Oyashio extends to such depths that it tends to flow along the continental shelf slope along the Kuril Islands ($2000 \sim 3000 \text{ m}$ deep) and is plausibly unable to pass over the shallow sills in the Kuril Straits. Moreover, Leonov (1960) and Moroshkin (1966) mentioned that bi-directional currents occur in most passages. This picture is clearly seen in the NOAA 12 AVHRR imagery (not

shown). Such current structures cannot be explained by large-scale wind-driven geostrophic flow. These observational results strongly suggest the importance of non-geostrophic components. In fact, tidal currents, especially diurnals, are dominant in and around the Kuril Straits, and their speeds reach a few knots. According to previous studies on tidal exchange (Awaji et al., 1980), such strong tidal currents are expected to induce significant mean transport, even if there are sills in the straits. Moreover, tide-induced mean currents allow us to explain the bi-directional structure of the (local) mean currents in the passages. Thus, as a first step toward understanding the transport process, we have investigated numerically the characteristics of the tides and tidal currents around the Okhotsk Sea.

Model

The model region (Fig. 1) covers the entire Okhotsk Sea and part of the North Pacific. The open boundaries are set away from the Okhotsk Sea in order to reproduce tidal wave propagation from the North Pacific. We resolved the topography of the model region using $5 \text{ km} \times 5 \text{ km}$ grids. The numerical model is the same as that used by Hatayama et al. (1996) with the familiar barotropic global tidal equations (e.g., Schwiderski, 1979a). The boundary conditions are set as follows. A no-slip condition is imposed at the land boundaries. At the open boundaries, the tidal elevation for K_1 and M_2 is specified

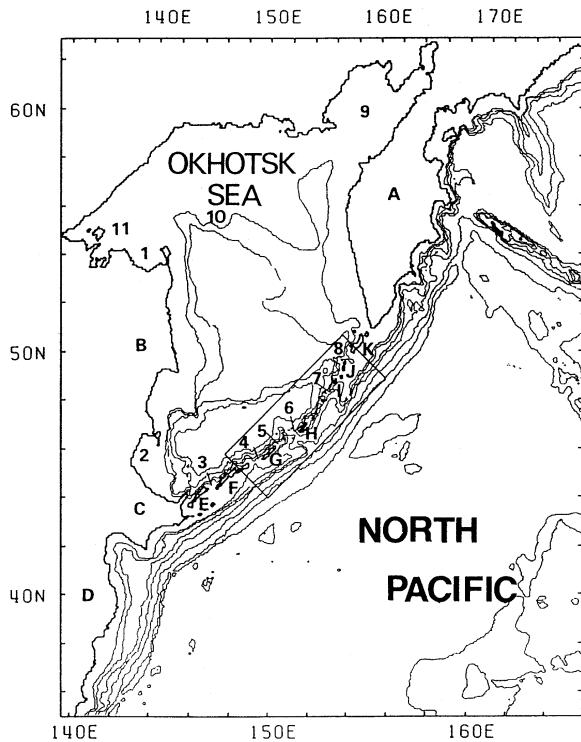


Fig. 1 Model domain and topography. Main straits of the Kuril (3–8, E–K) are the Bussol (6), Kruzenshtern (7), Chetvertyi (8) Straits. The Kashevarov Bank and Kamchatka Peninsula are indicated by 10 and A, respectively.

separately using previous results (e.g., Schwiderski, 1979a,b). Thus, the model is forced by these boundary oscillations in addition to the effects of the tide generating potential, the Earth tide, and the ocean loading tide. We performed 24 cycles of the integration, by which time the model ocean reached an almost steady oscillation and the final cycle of simulation is used for the analysis described below.

Tidal fields in the Okhotsk Sea

The harmonic constants (sea-level amplitude and phase) are calculated at every grid point, and the spatial distributions of the co-amplitude and co-phase lines obtained for K_1 and M_2 tides (not shown) are qualitatively consistent with previous studies (Mazzeaga and Bérge, 1994), respectively. To check the calculated fields quantitatively, we made a comparison with the International Hydrographic Office (IHO) tidal harmonic constants. For the predominant component K_1 tide, the correlation coefficients between the calculated and the observed harmonic constants are high (0.904 for phase and 0.976

for amplitude). For the M_2 tide, the correlation coefficients are also high (0.825 for amplitude and 0.929 for phase). Thus it can be said that the calculated tidal fields have good similarities compared to those observed and the current fields are expected to be fairly reliable. To study the features of the tidal currents in the Okhotsk Sea, we calculated the ellipse parameters shown in Figure 2. The K_1 tide has the greatest current speed. The currents are strong and their tidal ellipses are circular around topographic features, such as the Kuril Straits and the Kashevarov Bank. For example, the peak velocity in the northern part of the Kuril Straits reaches about 1.6 m s^{-1} . These features are associated with the fact that the period of the K_1 tide is longer than the inertial period around the Kuril Straits. Since subinertial tidal currents generate subinertial waves trapped at islands and/or submarine banks, the topographically trapped waves are subjected to continuous forcing and are enhanced until damping by friction or viscosity becomes important. The resulting amplification of trapped waves is most effective when the resonance occurs but is significant for a wide range if the tidal frequency is subinertial. Therefore the K_1 tide is expected to cause significant tide-induced mean flow around the Straits. On the other hand, the M_2 tide is significantly smaller in current speed than the K_1 tide, despite the fact that their elevation amplitudes are comparable. In fact, the maximum value around the Kuril Straits is only 0.6 m s^{-1} . The tidal ellipses are not circular around the Kuril Straits. Since the M_2 tide is superinertial, amplification hardly occurs and the currents are weak in the Kuril Straits, indicating that the mean currents induced by the M_2 tide are probably not significant.

Eulerian mean currents and estimates of tidal exchange through the Kuril Straits

Based on the depth-averaged velocity vectors of the Eulerian time-averaged currents over a cycle, we calculated the stream function of the mean volume transport ψ , which is defined as

$$(\bar{u}, \bar{v}) = \left(-\frac{1}{H} \frac{\partial \psi}{\partial y}, \frac{1}{H} \frac{\partial \psi}{\partial x} \right) \quad (1)$$

with the zero point taken at the Kamchatka Peninsula. The result for the K_1 tide is shown in Figure 3. In general, the mean currents are almost parallel to the isobaths and form clockwise mean currents around the islands, leading to bi-directional mean currents in most passages and strong clockwise along-sill (or along-island) mean currents. Tak-

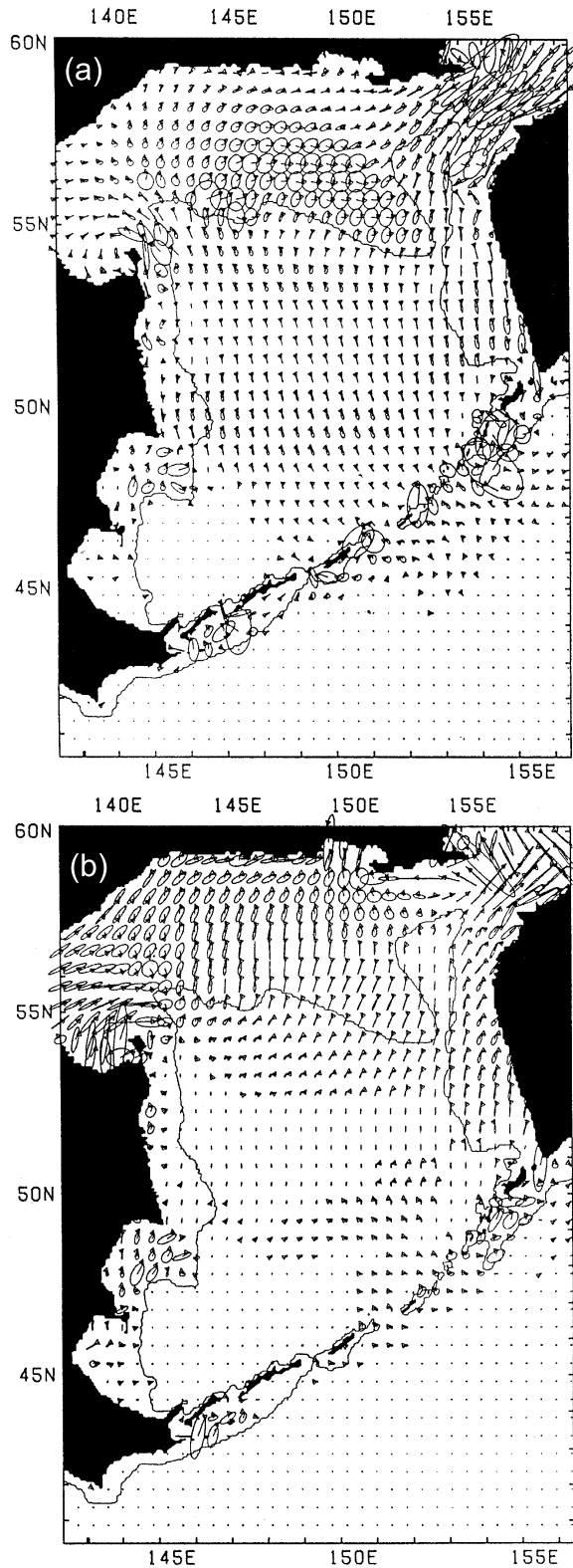


Fig. 2 Calculated tidal ellipses for (a) the K_1 tide and (b) the M_2 tide. The magnitude of velocity for (a) is 15 cm s^{-1} and for (b) is 30 cm s^{-1} .

ing the bi-directional currents into account, we estimated the total transport for all the straits with this mean current field. For K_1 (Fig. 4), most of the exchange occurs at the Bussol Strait and the northeastern part of the Kuril Straits. In terms of magnitude, the net transport of about 5.0 Sv from the Okhotsk Sea to the North Pacific occurs mainly through the Bussol (2.4 Sv), Kruzenshtern (0.8 Sv) and Chetvertyy (0.8 Sv) Straits. Inflow transport is largest (1.45 Sv) through the Bussol Strait followed by 1.2 Sv through the Kruzenshterna Strait. When neglecting the bi-directional flow, the total transport comes to 2.2 Sv, indicating that current meter deployment capable of resolving the bi-directional current structure is required to estimate the total transport observationally. Transport estimates made with the O_1 , P_1 , M_2 , and S_2 tides are 3.5, 1.0, 0.3, and 0.1 Sv, respectively, showing that transport induced by diurnal tides is much greater than that by semidiurnal tides.

Formation mechanism of bi-directional mean currents

Figure 5 shows the Eulerian mean relative vorticity over a cycle around the Kuril Straits. According to previous studies of tidal rectification (Robinson, 1981), the mean vorticity generally acquires negative values on the sill top and positive values at the base

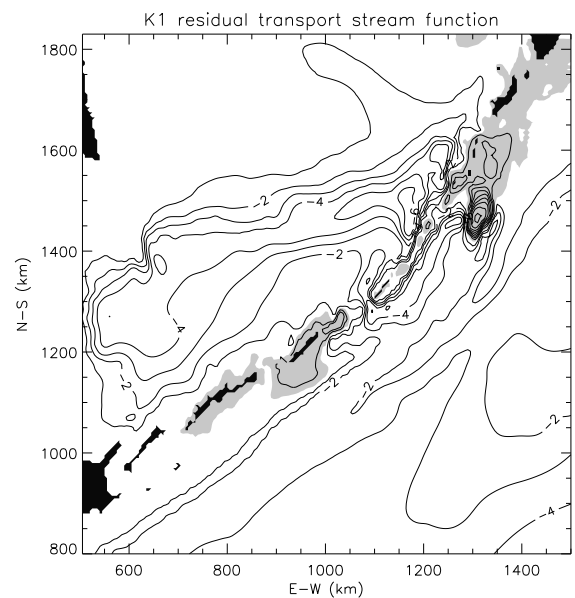


Fig. 3 Mean transport stream function for the K_1 tide, which is set to be zero at the Kamchatka Peninsula. The contour units are 0.4 Sv and values in shaded areas are positive.

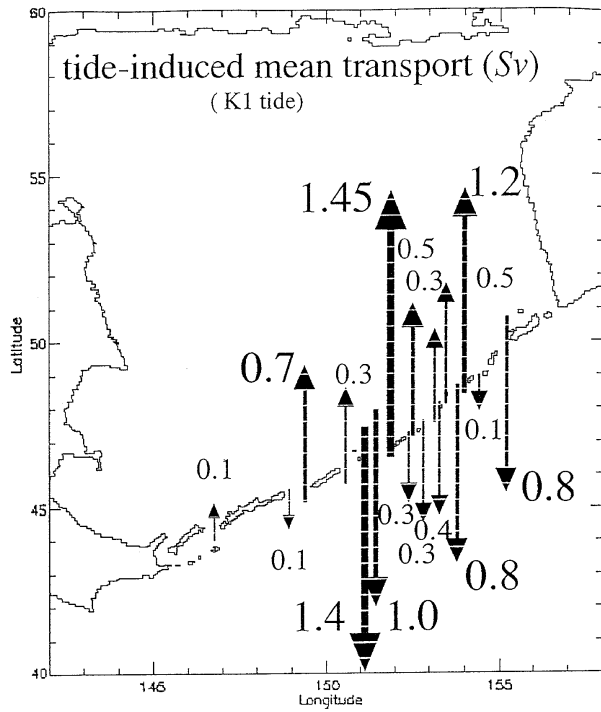


Fig. 4 The estimate of the mean transport through the Kuril Straits induced by the K_1 tide. Upward and downward arrows represent inflow and outflow, respectively.

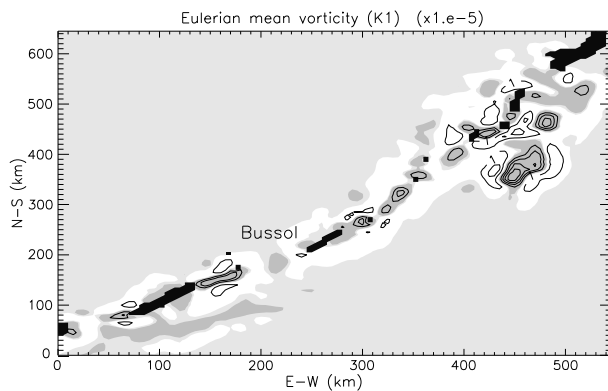


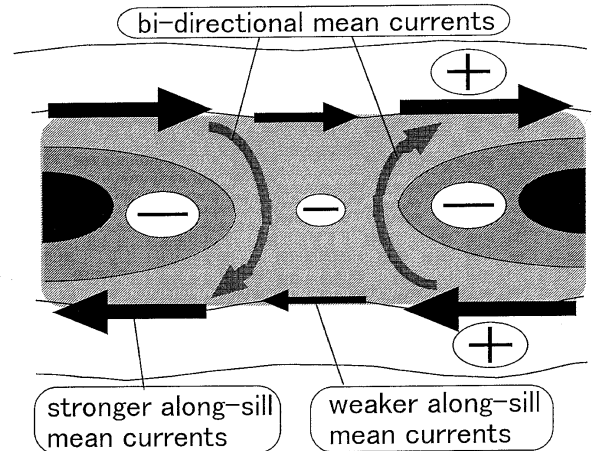
Fig. 5 The Eulerian mean relative vorticity over one cycle around the Kuril Straits for the K_1 tide. The contour interval is $1 \times 10^{-5} \text{ s}^{-1}$. Values in unshaded areas and the dark shaded areas are positive and negative, respectively, and the absolute values in the light shaded areas are less than $1 \times 10^{-6} \text{ s}^{-1}$.

of the sill, which, in turn, produce a clockwise mean current along the sill. Such a pattern is clearly seen in shallow straits (200 ~ 600 m depth), and as the sill gets higher in the vicinity of the islands, the magnitude of the negative mean vorticity on top of the sill becomes larger. Supposing mass conservation of

the along-sill mean currents, such vorticity changes in shallow straits lead to clockwise mean circulation on island scales, thus creating bi-directional mean currents in shallow straits as shown schematically in Figure 6. In deep straits, on the other hand, the mean vorticity distribution on the sill top has positive values near the islands. This vorticity pattern differs greatly from that in shallow straits in spite of the presence of similar bi-directional currents. To investigate this problem, we direct our attention to the Bussol Strait, where the sill is very deep, bi-directional currents are dominant, and hence most of the outflow from the Okhotsk Sea occurs.

To examine the cause for the different vorticity distribution between deep and shallow straits, we diagnose the vorticity balance in a similar way to Ridderinkhof (1989). The result shows that, as in past studies, the stretching/squeezing effects are basically dominant in vorticity generation. These fea-

(a) in shallow straits



(b) in deep straits (e.g., Bussol Strait)

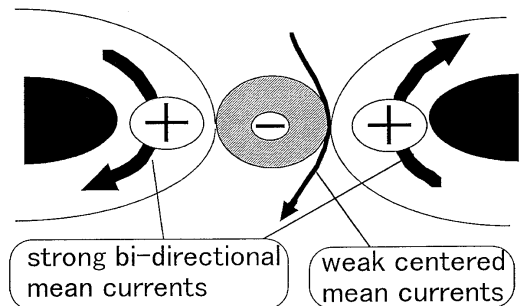


Fig. 6 Schematic illustrations of mean currents associated with the mean vorticity distribution in (a) shallow straits (200 ~ 600 m depth) and (b) deep straits (the case of the Bussol Strait).

tures are present at most straits. Thus, the vorticity balance for generating bi-directional mean currents is the same in both shallow and deep straits, despite the fact that their vorticity distribution differs mutually. This implies the presence of a different mechanism from the previous tidal rectification theory for the formation of the mean circulation in deep straits. The most likely candidate for this is the effect of topographically trapped waves, because it is anticipated that for subinertial tides the transport of vorticity anomaly by the waves becomes effective in the vorticity balance. Detailed analysis using the vorticity equation revealed that the transport of vorticity anomaly around the Kuril Islands is basically determined by the following equation:

$$\begin{aligned} & \left(\frac{\partial}{\partial t} + (\mathbf{u}_{across} + \mathbf{u}_{along} + \mathbf{c}) \cdot \nabla \right) \omega_{wave} \\ & + \left(\frac{\partial}{\partial t} + \mathbf{u} \cdot \nabla \right) (\omega - \omega_{wave}) \\ & = -\frac{f}{H} \nabla H \cdot \mathbf{u}_{across}^{irr} + \text{damping}, \end{aligned} \quad (2)$$

where $\mathbf{c} = (c_x, c_y)$ is the phase velocity of a nondivergent linear topographic Rossby wave given as

$$c_x = \frac{H_y}{k^2 + l^2} \frac{f}{H}, \quad c_y = -\frac{H_x}{k^2 + l^2} \frac{f}{H}. \quad (3)$$

The term ω_{wave} is the vorticity associated with the wave component. This equation shows that the vorticity component $(\omega - \omega_{wave})$ is transported only by tidal currents and causes the well known process of tidal rectification. On the other hand, the vorticity anomaly ω_{wave} is transported not only by the currents $(\mathbf{u}_{across} + \mathbf{u}_{along})$ but also by topographically trapped waves propagating with a phase velocity \mathbf{c} (thus, there are additional vorticity changes caused by the propagation of topographically trapped waves at any location along the island chain). Accordingly, topographically trapped waves are able to affect the mean field at locations well away from the generation region of vorticity. In the northern hemisphere, the phase velocity \mathbf{c} of topographically trapped waves is in the along-isobath direction with shallower regions on the right. The along-sill (along-isobath) current flows with positive and negative values of vorticity to their left and right, respectively (not shown). On the positive vorticity side of the sill, the along-sill current is in the same direction as the phase velocity \mathbf{c} of the topographically trapped waves of positive vorticity. In contrast, on the negative vorticity side of the sill, the along-sill current is in the opposite direction to the propagation of topographic waves of negative vorticity. Consequently, the topographically

trapped waves of positive vorticity move faster than those of negative vorticity. This means that the magnitude of the positive vorticity flux created by topographically trapped waves in the along-isobath direction is larger than that of the negative vorticity flux over a tidal cycle, and eventually leads to the presence of a net flux of positive vorticity in a clockwise sense around the islands. In shallow straits, since topographically trapped waves hardly cross the shallow sills, this process has little effect on the formation of mean vorticity. In contrast, in deep and wide straits such as the Bussol and Kruzenstern Straits, mean vorticity generation through the tidal rectification process is small but the topographically trapped waves coming from shallow straits can cross the deep sills, thus producing positive mean vorticity. This leads to the formation of the bi-directional mean current structures around both ends of the deep sills.

Summary and discussion

Our regional model has shown that the Eulerian mean outflow from the Okhotsk Sea can reach the significant value of 5.0 Sv for the K_1 tide, the main part of which is conducted through the Bussol, Kruzenstern, and Chetverty Straits. This significant tidal exchange is produced by bi-directional mean currents in the Straits, which are consistent with the current structure observed in infrared images taken by NOAA 12 and mentioned in earlier work by Moroshkin (1966) and Leonov (1960). Therefore, it is suggested that tidal currents play an important role in water exchange between the Okhotsk Sea and the North Pacific, although precise quantitative discussions will await future observations. We showed that the mean currents are produced through the effects of topographically trapped waves as well as through well known tidal rectification. In shallow straits (200 ~ 600 m depth), tidal rectification mainly due to advection, vorticity generation by the stretching/squeezing effect, and damping by bottom friction produces the strong along-sill and weak bi-directional mean currents. On the other hand, in deep straits such as the Bussol Strait, a net flux of positive vorticity from the adjacent shallow straits to the deep strait is caused by topographically trapped waves and produces strong bi-directional mean currents there. This net flux is caused by the fact that the along-isobath currents are in the same direction as the phase velocity of the topographically trapped waves with positive vorticity, and are in the opposite direction to that with negative vorticity. We have clarified the outline of the horizontal exchange induced by the tidal currents.

However, since we use a two-dimensional barotropic model, the vertical structure is still unclear. Therefore, an investigation of the vertical structure of tidal currents around the Straits, which includes the baroclinic effect, may be important for our understanding of the detailed transport processes as well as the effect of wind-driven large-scale geostrophic flow and eddies on water exchange and mixing around the Kuril Straits.

References

- Awaji, T., Imasato, N. and Kunishi, K. 1980. Tidal exchange through a strait: A numerical experiment using a simple model basin. *J. Phys. Oceanogr.*, *10*, 1499–1508.
- Hatayama, T., Awaji, T. and Akitomo, K. 1996. Tidal currents in the Indonesian Seas and their effect on transport and mixing. *J. Geophys. Res.*, *101*, 12,353–12,373.
- Kawasaki, Y. and Kono, T. 1992. Baroclinic water exchange in the Kuril Basin and the northwestern Pacific in summer. *Sea and Sky*, *68*, 41–54. (in Japanese)
- Leonov, A.K. 1960. *Regional Oceanography. Part 1*. Gidrometeoizdat, Leningrad, pp. 226–229.
- Mazzege, P. and Bergé, M. 1994. Ocean tides in the Asian semienclosed seas from TOPEX/POSEIDON. *J. Geophys. Res.*, *99*, 24,867–24,881.
- Moroshkin, K.V. 1966. Water masses of the Sea of Okhotsk. U.S. Department of Commerce, Clearing-house for Federal Scientific and Technical Information, Joint Publication Research Service, *43*, 942. 98 pp.
- Ridderinkhof, H. 1989. Tidal and residual flows in the Western Dutch Wadden Sea: Vorticity balances. *Neth. J. Sea Res.*, *24*, 9–16.
- Robinson, I.S. 1981. Tidal vorticity and residual circulation. *Deep-Sea Res.*, *28a*, 195–212.
- Schwiderski, E.W. 1979a. Global Ocean Tides, II: The semidiurnal principal lunar tide (M_2). In *Atlas of Tidal Charts and Maps, Naval Surface Weapons Center NSWC-TR*.
- Schwiderski, E.W., 1979b. Global Ocean Tides, IV: The diurnal luni-solar declination tide (K_1). In *Atlas of Tidal Charts and Maps, Naval Surface Weapons Center NSWC-TR*.
- Talley, L.D. 1993. Distribution and formation of North Pacific Intermediate Water. *J. Phys. Oceanogr.*, *23*, 517–537.
- Yasuda, I., Okuda, K. and Shimizu, Y. 1996. Distribution and formation of North Pacific Intermediate Water in the Kuroshio-Oyashio interfrontal zone. *J. Phys. Oceanogr.*, *26*, 448–465.

Vertical mixing induced by tidally generated internal waves in the Kuril Straits

Tomohiro NAKAMURA¹, Toshiyuki Awaji¹, Takaki Hatayama¹,
Kazunori Akitomo¹, Takatoshi Takizawa²
and Masao Fukasawa³

¹ Department of Geophysics, Kyoto University, Kyoto, Japan

² Japan Marine Science and Technology Center, Yokosuka, Japan

³ School of Marine Science and Technology, Tokai University, Shizuoka, Japan

Abstract. Numerical experiments are performed to investigate the vertical mixing induced by tidally generated internal waves in the Kuril Straits. The results show that in contrast to previous theories, intense short internal waves generated at the sill breaks by the subinertial K_1 current can propagate upstream as the tidal current slackens. Our theoretical considerations identify these short waves as unsteady lee waves, which tend to be trapped at the generation region and grow into large-amplitude waves. Superposition of a propagating unsteady lee wave and a newly generated lee wave over a sill causes significant wave breaking leading to a maximum vertical diffusivity of $\sim 10^3 \text{ cm}^2 \text{ s}^{-1}$. This quite intense mixing reaches down to the density layer of the NPIW, thus suggesting that lee waves generated by interactions between the K_1 current and the bottom topography of the Kuril Straits play an important role in the formation of the NPIW.

Introduction

Recent observations (e.g., Kawasaki and Kono, 1994) show the presence of strong vertical mixing in the Kuril Straits, implying that such strong vertical mixing is one of the major factors in supplying low salinity water required for the production of the NPIW (Talley, 1991). Several studies suggested that tidal mixing is responsible for this intense vertical mixing. However, the actual physical mechanisms are still unknown. According to observations, the currents are dominated by the diurnal tidal components in the Kuril Straits, and the semidiurnal components are rather weak. Swift K_1 currents have been thought to cause intense vertical mixing by interactions with large-amplitude sills in the Kuril Straits. However, this situation is out of the range of previous theories for the growth of oceanic internal waves, which assume that an oscillating tidal flow over an obstacle excites only internal waves at its tidal frequency (internal tides). Since the diurnal tides are subinertial around this high latitude ($\sim 47^\circ \text{ N}$), internal tides at the K_1 tidal frequency are not freely propagating waves. This fact prevents us from using the previous theoretical models. For example, Hibiya's (1986) theory assumes that internal tides propagating upstream are trapped at the generation region and amplified when the barotropic flow is critical (i.e., when the Froude number F_n is unity where F_n is the ratio of the barotropic tidal

flow speed to phase speed of n th mode). Thus, as a first step toward clarifying the physics responsible for the vertical mixing in the Kuril Straits, we have performed numerical simulations of tidally generated internal waves and have estimated the vertical mixing induced by those waves.

Numerical model

The model bottom topography is representative of the sills in the northeastern part of the Kuril Straits, where tidal currents are so strong that they can cause considerable mixing (Fig. 1). In order to simulate vertical mixing by internal waves, we used a vertically two-dimensional nonhydrostatic f -plane model with horizontal and vertical grid sizes of 500 m and 10 m, respectively. The horizontal and vertical eddy viscosity coefficients are assigned the relatively small values of $2 \times 10^5 \text{ cm}^2 \text{ s}^{-1}$ and $0.1 \text{ cm}^2 \text{ s}^{-1}$, respectively, so that their effect on mixing is small enough to demonstrate the wave mixing clearly. As basic forcing terms for internal wave generation, barotropic K_1 and M_2 currents are given at both lateral boundaries. Their maximum speeds at the sill top are 0.5 m s^{-1} for the K_1 case and 0.2 m s^{-1} for the M_2 case, as determined from our preceding barotropic tidal simulations (Awaji et al., 1999). We took account of the effect of rotation to distinguish the physics of waves generated by the subinertial K_1 flow from that of the superinertial M_2

flow in the Kuril Straits. At the bottom boundary, a no-slip condition is imposed in the sill region and a free-slip condition is imposed in the deep region with the flat bottom. A rigid-lid approximation is used at the surface to restrict our attention to internal processes. The initial vertical profiles of potential temperature and salinity are from the summertime climatology in the Kuril Basin of the Okhotsk Sea (not shown). With these vertical profiles, model calculations start at the beginning of rightward flow so that wave generation processes can be seen clearly.

Model results

Figure 2 shows the map of the internal mode stream function defined by Lamb (1994) during the second cycle in the M_2 case. As past studies show, first-mode internal waves are generated on the slopes of the sill (Fig. 2a), and propagate away from the sill. Wave generation on the sill slopes by rightward flow continues for up to 1.5 periods when the flow stops (Fig. 2b), and the generated waves propagate away from the sill after 1.75 periods. In the half period of leftward flow (Figs. 2c and d), almost the same sequence of events can be observed, but with their phase reversed. The linear dispersion relation gives the frequency of first-mode waves of $1.4 \times 10^{-4} \text{ s}^{-1}$, almost equal to the M_2 frequency. Thus the first mode waves seen in Figure 2 can be identified as typical internal tides at the M_2 frequency. Since most of internal mode energy generated by the M_2 flow propagates away as first-mode internal tides, large-amplitude internal waves are not formed and breaking is absent in the M_2 case. Consequently, vertical mixing induced by waves generated by the M_2 flow is probably not strong enough to cause significant freshening in the Kuril Straits. The time series of the internal mode stream function in the K_1 case (Fig. 3) shows quite different behavior from that of the M_2 case primarily because the Kuril Straits are located over the critical latitude for the K_1 tide. For example, sill-scale cells do not propagate away, and, in contrast to the M_2 case, intense disturbances

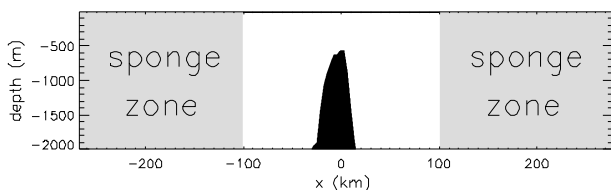


Fig. 1 The model topography, representing the vertical cross-section of a strait in the northeastern part of the Kuril Islands, where tidal currents are strong enough to cause considerable mixing.

exist on small scales. We direct our attention to intense smaller-scale disturbances detected in Figure 3. These short waves may cause considerable mixing because shorter wavelengths induce stronger dissipation and so release energy for mixing, and because the process of wave breaking takes place at smaller amplitudes for waves of shorter wavelength. Figure 3 clearly shows the movement of small-scale disturbances labelled as A_1, B_1, A_2, B_2, a_1 , and b_1 from left to right, with the tidal period during which they are produced indicated by subscripts and with the direction of the tidal flow at the time of their production indicated by capital (rightward) and small (leftward) letters. The propagation speeds of these small-scale disturbances estimated from Figure 3 ($0.3 \sim 1.4 \text{ m s}^{-1}$) are different from the tidal flow speed (less than 0.125 m s^{-1}). This fact means that they are freely-propagating internal waves. Thus,

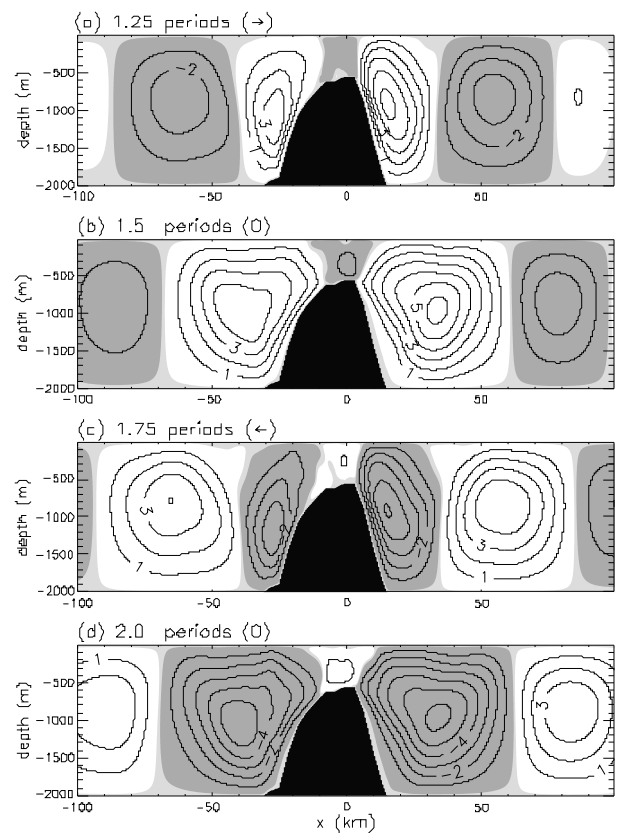


Fig. 2 The time series of the internal mode stream function in the M_2 case during the second tidal period; after (a) 1.25, (b) 1.5, (c) 1.75, and (d) 2.0 periods. The contour interval is $1.0 \times 10^5 \text{ cm}^2 \text{ s}^{-1}$. Values in unshaded areas and the darkly shaded areas are positive and negative, respectively, and the absolute values in the lightly shaded areas are less than $1 \times 10^4 \text{ cm}^2 \text{ s}^{-1}$.

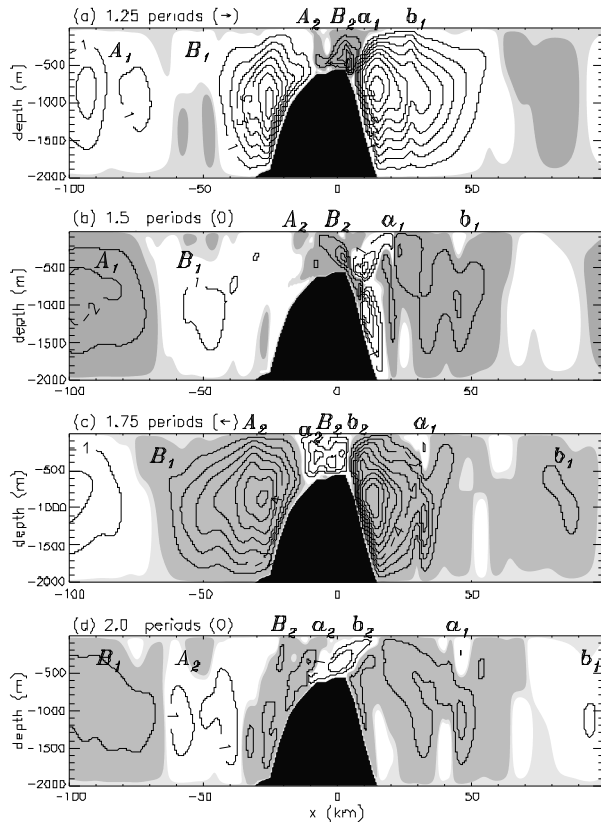


Fig. 3 Same as in Figure 2 but for the K_1 case.

their frequencies must be larger than the inertial frequency, despite the fact that the K_1 frequency is subinertial. Therefore, previous theoretical models cannot explain the generation of such intense short waves as described earlier. Furthermore, these features are produced by rightward (leftward) flow and propagate leftward (rightward), indicating that they move only in the upstream direction as determined at their generation time. This is also inconsistent with the character of internal tides which propagate in both directions. From these considerations, it is inferred that the intense short waves in our model must represent another class of wave, and thus we reinvestigate the excitation mechanism of internal waves by a tidal flow in the next section.

The excitation mechanism of unsteady lee waves

To investigate the wave excitation properly, it is necessary to consider the total time variation of the forcing to which fluid parcels are subjected. Representing the forcing as F , the total time variation of the forcing DF/Dt is given in Eulerian variables as,

$$\frac{DF}{Dt} = \frac{\partial F}{\partial t} + U_i \frac{\partial F}{\partial x_i}, \quad (1)$$

where U_i represents the velocity of the basic flow in the x_i direction. Most of the previous theories of internal waves generated by an oscillating tidal flow have neglected the advection effect (the second term) in wave excitation. However, Eq. (1) shows that in regions where the tidal flow is strong and the horizontal scale of forcing is small, such as sill tops or shelf breaks, wave excitation cannot be fully comprehended unless the advection effect on wave excitation is incorporated. To easily specify the nature and structure of tidally generated internal waves, our discussion is restricted to the vertically two-dimensional case ($\partial/\partial y = 0$), and we assume that the flow varies as a single harmonic component of frequency σ_f in time. Then, the vertical velocity W at the bottom is given by

$$W = W(x, t) = e^{i\sigma_f t} \int_{-\infty}^{\infty} \hat{W}_0(k) e^{-ikx} dk, \quad (2)$$

using a Fourier transformation. We can describe the wave forcing (2) in the neighborhood of $x = x_0$ and $t = t_0$ in the moving frame X . After some manipulation, the vertical velocity W splits into the sum of traveling waves propagating with two different phase velocities as

$$\begin{aligned} W(x, t) &= \int_0^{\infty} \hat{W}_0(k) e^{i\sigma_f t_0} \{ \exp[-i(kX + (kU(x_0, t_0) + \sigma_f)\tau)] \\ &\quad - \exp[+i(kX + (kU(x_0, t_0) - \sigma_f)\tau)] \} dk. \end{aligned} \quad (3)$$

This expression shows that the internal wave excited in the neighborhood of $x = x_0$ and $t = t_0$ by the basic flow (U, W) is composed of a sum of monochromatic waves with frequency of $-kU(x_0, t_0) \pm \sigma_f$ and horizontal wavenumber of k . Thus, according to the nondimensional parameter kU_0/σ_f , we can classify internal waves excited by an oscillating flow into unsteady lee waves (when $kU_0/\sigma_f \gg 1$) and “mixed tidal lee waves” (when $kU_0/\sigma_f \sim 1$), in addition to internal tides (when $kU_0/\sigma_f \ll 1$) which previous theoretical models have considered. These three types of “topographic internal waves” have the following properties: Unsteady lee waves have the frequencies of $-kU(t)$, and their phase velocities are $-U(t)$. Thus, unsteady lee waves can propagate in the upstream direction at their excitation time. The amplitudes of unsteady lee waves depend on the magnitude of the forcing at the time of their excitation, so that the waves generated around the time of maximum flow have maximum amplitudes. Such

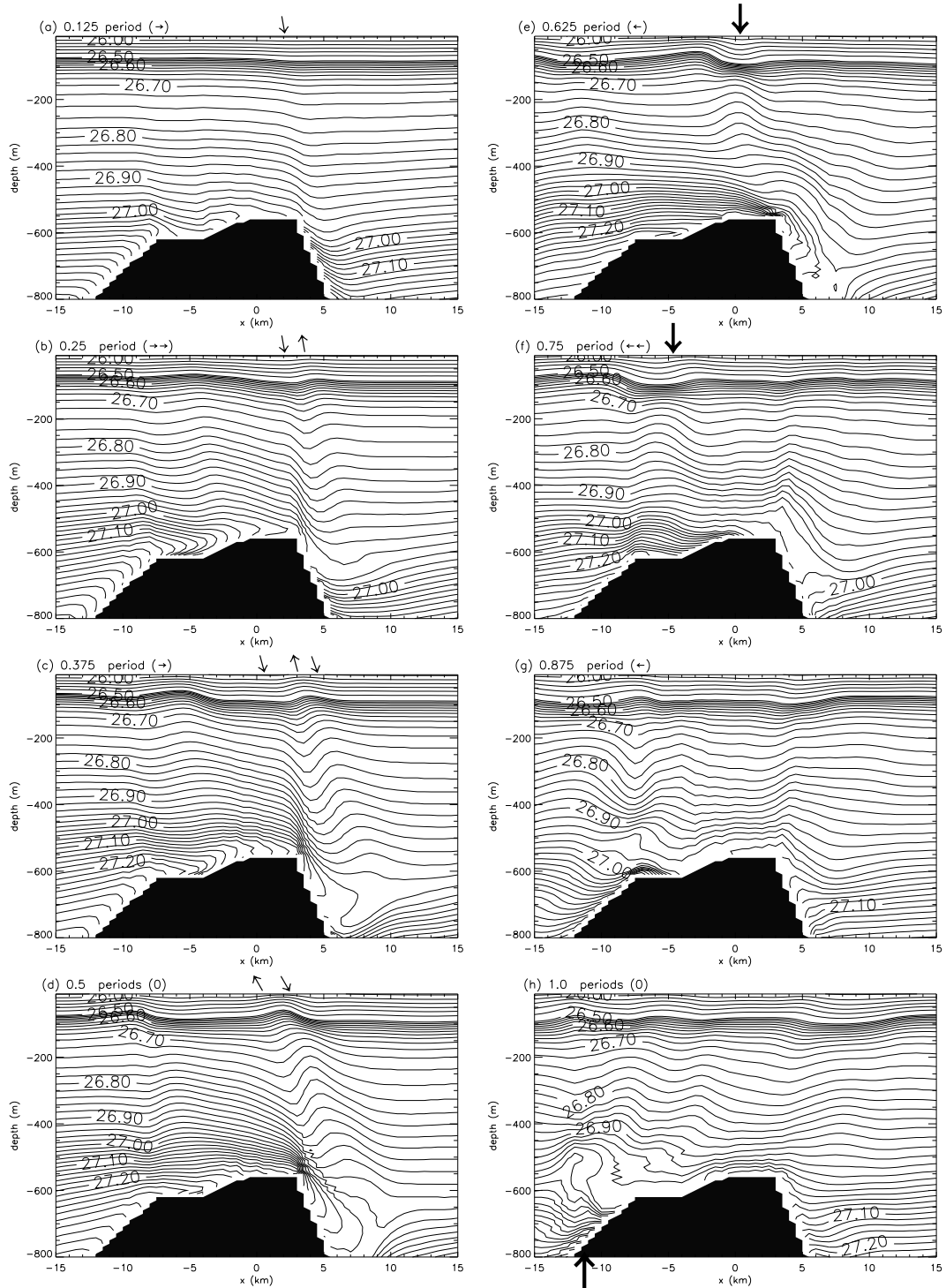


Fig. 4 The evolution of potential density (σ_θ) around the sill top in the K_1 case, during the first period, after (a) 0.125, (b) 0.25, (c) 0.375, (d) 0.5, (e) 0.625, (f) 0.75, (g) 0.875, (h) 1 period, when the generation process of the large-amplitude unsteady lee wave can be clearly seen. For $\sigma_\theta < 26.5$, the contour interval is 0.1 σ_θ . For $\sigma_\theta \geq 26.5$ the contour interval is 0.02 σ_θ .

unsteady lee waves are excited in a region where the curvature of topography is sufficiently large, such as shelf breaks. In contrast, internal tides have a frequency of σ_f and a constant phase velocity of $\pm\sigma_f/k$, and propagate in both directions, as shown in previous studies. In the intermediate range, excited waves have intermediate properties between those of lee waves and internal tides, and we name such waves “mixed tidal lee waves”. Consideration of the frequency of these new waves allows us to explain the reason why the subinertial K_1 flow can generate freely-propagating internal waves at the sill top. The co-phase lines of the internal wave generated at the break (not shown) extend only in one direction, consistent with the character of unsteady lee waves. Thus, we conclude that the intense short waves simulated in the K_1 case are unsteady lee waves.

The evolution of large-amplitude unsteady lee waves

Figure 4 shows the evolution of potential density (σ_θ) in the K_1 case up to 1 period, where the generation process of the intense short waves can be seen clearly. As expected from our theoretical model, small-scale vertical velocity distributions produced at sudden changes in the sill slope generate a relatively large depression of small horizontal length at the right-hand break and adjacent weak elevation and depression over the left-hand break and sill top. The displacement at the right-hand break continues to grow until the end of the rightward flow to form a large-amplitude (~ 100 m) unsteady lee wave (Fig. 4d). As the rightward flow vanishes after 0.5 period, the large-amplitude unsteady lee wave begins to propagate in the upstream direction at the generation time (leftward). When propagating across the sill, this large-amplitude wave encounters an unsteady lee wave newly generated at the left-hand break by the leftward flow. These lee waves are superposed and interact with each other (after 0.875 period). As the flow turns to the right, the large-amplitude elevation at the foot of the lee wave gradually breaks, propagating rightward, and causes vigorous vertical mixing over the sill top. In this way, large-amplitude unsteady lee waves induce intense vertical mixing, and relatively vertically uniform water is produced over and around the sill top in the K_1 case as seen in Figure 5a. The feature of this map has good similarities with that of observations (Fig. 5b), supporting our model’s realism.

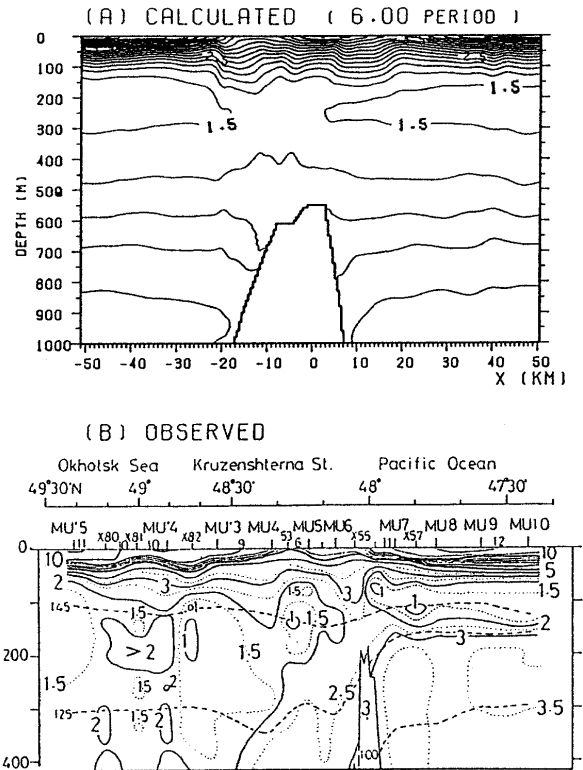


Fig. 5 (a) The calculated potential temperature distribution after 6 periods, and (b) the observed potential temperature distribution in the Kruzenshterna Strait.

Vertical mixing induced by internal waves

Here, we estimate the intensity of the resulting vertical mixing in terms of diffusivity. To relate the result to the parameterizations used in general circulation models, we estimate the vertical diffusivity K_z^E from an Eulerian point of view with the following Fickian formulation,

$$K_z^E = \left| \frac{\overline{S'w'}}{dS_0/dz} \right| \quad (4)$$

where dS_0/dz is the vertical gradient of the initial salinity profile, and $\overline{S'w'}$ is salinity flux induced by perturbations, averaged over one tidal period. In the M_2 case, the estimated diffusivity using the calculated velocity fields in the second period is not so large ($\sim 10 \text{ cm}^2 \text{ s}^{-1}$), as expected earlier. In contrast, the value in the K_1 case is very large around the sill ($\sim 10^3 \text{ cm}^2 \text{ s}^{-1}$) and relatively small in other regions. This is mainly due to large-amplitude unsteady lee waves propagating over the sill and their superposition on unsteady lee waves newly generated by

the reversed flow leading to significant wave breaking.

Summary

In order to clarify the role played by intense vertical mixing in the Kuril Straits on the modification of water properties, we numerically investigated internal waves generated through the interaction between the tidal currents and the sill and their effect on mixing, using a nonhydrostatic f -plane model. The model results reveal the following. Internal waves at the tidal frequency (internal tides) generated by the K_1 flow are trapped to the sill, because the K_1 tide is subinertial in the Kuril Straits. Since the strong barotropic flow is further intensified near the bottom by the trapped internal tides, large-amplitude free-propagating internal waves of short wavelengths are repeatedly generated and break around the sill top, thus producing relatively vertically uniform water over and around the sill top. On the other hand, in the M_2 case, since most of the generated internal waves propagate away as first-mode internal tides, their amplitudes do not become so large. As a result, the M_2 tidal current does not have the potential to cause significant vertical mixing to explain the freshening in the Kuril Straits. Our theoretical consideration identifies the large-amplitude short waves in the K_1 case as unsteady lee waves, whose existence has been neglected in previous oceanic internal wave theories. Interestingly, the superposition of a propagating unsteady lee wave and a newly generated lee

wave over the sill generates a large-amplitude internal wave, which causes wave breaking and induces intense vertical mixing over the sill top.

References

- Awaji, T., Nakamura, T., Hatayama, T. and Akimoto, K. 1999. Tidal exchange through the Kuril Straits. pp. 77–82. In *Proc. Second Workshop on the Okhotsk Sea and Adjacent Areas, PICES Sci. Rep. No. 12*, Labonov, V.B., Nagata, Y. and Riser, S.C. (eds.), Sidney, B.C., Canada.
- Hibiya, T. 1986. Generation mechanism of internal waves by tidal flow over a sill. *J. Geophys. Res.*, *91*, 7696–7708.
- Kawasaki, Y. and Kono, T. 1994. Distribution and transport of subarctic waters around the middle of Kuril Islands. *Sea and Sky*, *70*, 71–84. (in Japanese)
- Lamb, K.G. 1994. Numerical experiments of internal wave generation by strong tidal flow across a finite amplitude bank edge. *J. Geophys. Res.*, *99*, 843–864.
- Talley, L.D. 1991. An Okhotsk Sea water anomaly: Implications for ventilation in the North Pacific. *Deep-Sea Res.*, *38*(Suppl. 1), S171–190.
- Talley, L.D. 1993. Distribution and formation of North Pacific Intermediate Water. *J. Phys. Oceanogr.*, *23*, 517–537.

Water exchange between the Okhotsk Sea and the North Pacific Ocean estimated by simple models

Katsuro KATSUMATA and Ichiro Yasuda

Department of Earth and Planetary Physics, Graduate School of Science,
The University of Tokyo, Tokyo, Japan

Introduction

Water exchange between the Okhotsk Sea and the North Pacific Ocean plays an important role in the formation process of the North Pacific Intermediate Water (e.g., Talley and Nagata, 1995; Yasuda, 1997). However, the detailed mechanism of the exchange has not yet been clarified. We estimate the rate of the water exchange by using two simple models. One model is similar to Minato and Kimura (1980) which is used to estimate the flow rate of the Tsushima Current, and the analytical result is discussed by the Island Rule derived by Godfrey (1989), Pedlosky (1994), and Pedlosky et al. (1997). The other is a hydraulic theory derived by Gill (1977), and this hydraulic theory is applied to the Bussol Strait to estimate the flow rate.

Island rule

We use a single layer of homogeneous fluid over a passive quiescent fluid (one-and-a-half layer model), and the Okhotsk Sea and the North Pacific Ocean are modeled as rectangular basins separated by a vertical thin wall except for two gaps as shown in Figure 1: the northern gap corresponds to the Kruzenshterna Strait and the southern gap to the Bussol Strait. The islands between these two straits are replaced with a single island, and this part will be called “the island” hereafter. The sill depths of the straits are assumed to be deeper than the bottom of the surface layer. Since we are discussing only the volume transport, the size of the sea and ocean is not a determinative factor, except for the integration route of wind stress over the Pacific Ocean.

A similar model was used by Minato and Kimura (1980) to estimate transport between the Japan Sea and the Pacific Ocean. By checking their result, it is found that their estimated transport depends strongly on their treatment of the friction term near the strait. They parameterized the frictional effect by “the effective distance from the channel in which the pressure gradient is dominant”. This parameter is not clearly defined, and is hard to estimate from observations. A different parameterization is used in this paper.

By using the rectangular coordinates and taking

x eastward and y northward, the horizontal momentum equations of the surface homogeneous layer can be expressed in the form:

$$\frac{\partial \vec{u}}{\partial t} + (\zeta + f)\hat{k} \times \vec{u} = -\nabla \left(g'D + \frac{|\vec{u}|^2}{2} \right) + \text{Diss}(\vec{u}) + \vec{T} \quad (1)$$

where \vec{u} is the horizontal velocity (u, v), ζ the vorticity ($= \partial v/\partial x - \partial u/\partial y$), f the Coriolis parameter, \hat{k} the upward unit vector, g' the reduced gravity, and D the thickness of the surface layer. $\text{Diss}(\vec{u})$ represents the dissipation term, and \vec{T} the wind stress per unit density divided by the fluid depth. The first term of the right-hand side of (1) disappears by

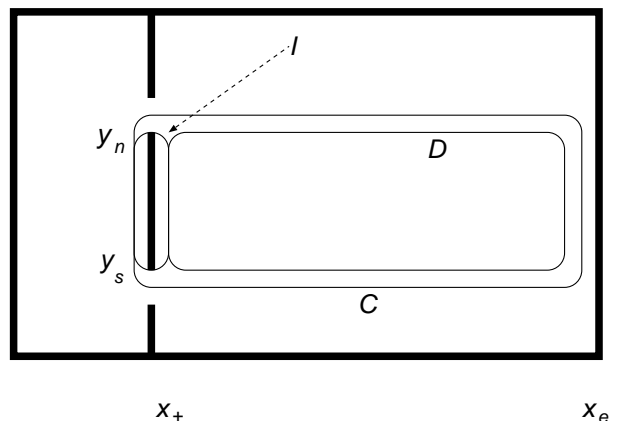


Fig. 1 Schematic view of the model. A square basin is separated by a thin wall with two gaps. The wall represents the Kuril Islands, and the northern gap represents the Kruzenshterna Strait and the southern gap the Bussol Strait. The right larger basin is the Pacific Ocean, and the left smaller basin the Okhotsk Sea. The terms y_n and y_s denote the latitudes of the northern and southern tips of the island, respectively, and x_+ and x_e denote the positions of the western and eastern coasts of the Pacific. Three integration contours used in the text are schematically shown with I , C , and D : the zonal parts of C run at y_n and y_s , and the western meridional part of D and the eastern part of I should be taken just at the eastern side of the island coast (x_+) of I and D .

integrating around the circuit C in Figure 1, and we have

$$\begin{aligned} \frac{\partial}{\partial t} \oint_C \vec{u} \cdot d\vec{t} + \oint_C (\zeta + f) \vec{u} \cdot d\vec{n} \\ = \oint_C \text{Diss}(\vec{u}) \cdot d\vec{t} + \oint_C \vec{T} \cdot d\vec{t} \end{aligned} \quad (2)$$

where $d\vec{t}$ is the infinitesimal vector along C and $d\vec{n}$ is the infinitesimal vector normal to C such that $d\vec{t} \times \hat{k} = d\vec{n}$. We assume that the flow is steady. Under the quasi-geostrophic assumption, ζ is negligible ($\zeta \ll f$) and the dissipation is also negligible as the circuit C does not reach the western boundary layer. D , which is implicitly included in \vec{T} , can be approximated by the surface layer thickness averaged over the whole modeled basin D_0 under the quasi-geostrophic assumption. Multiplying (2) by D_0 , we have

$$(f_n - f_s)\Phi = -D_0 \oint_C \vec{T} \cdot d\vec{t} \quad (3)$$

where Φ is the transport through each channel or the meridional transport between the island and the eastern boundary of the North Pacific, and f_n and f_s are the Coriolis parameters at the latitudes of the north and the south ends of the island, respectively. This corresponds to the Island Rule obtained by Godfrey (1989). We introduce the Sverdrup stream function

$$\beta \Psi_s = - \int_x^{x_e} \hat{k} \cdot \nabla \times D_0 \vec{T} dx \quad (4)$$

where x_e is the zonal position of the eastern boundary (Fig. 1). The integral circuit C can be replaced by two circuits, I and D , as shown in Figure 1. The right-hand side of (3) can be written as

$$\begin{aligned} \oint_C D_0 \vec{T} \cdot d\vec{t} &= \left(\oint_I + \oint_D \right) D_0 \vec{T} \cdot d\vec{t} \\ &= \oint_I D_0 \vec{T} \cdot d\vec{t} - \beta \int_{y_s}^{y_n} \Psi_s(x_+, y) dy \end{aligned}$$

where y_n ($\approx 48^\circ$) and y_s ($\approx 46^\circ$) are the meridional positions of the northern and southern tips of the island, respectively (Fig. 1), and x_+ is the position of the eastern coast of the island. Since the island is thin, the integration in the first term on the right-hand side is much smaller than that of the second term, and (3) becomes

$$\Phi = \frac{1}{y_n - y_s} \int_{y_s}^{y_n} \Psi_s(x_+, y) dy \quad (5)$$

This is the Island Rule obtained by Pedlosky (1994).

Assuming the Sverdrup balance (4), Ueno (personal communication) calculated the stream function in the North Pacific Ocean (Fig. 2) using the wind field given by Hellerman and Rosenstein (1983). The resulting value of the stream function along the east coast of the island is applied to (5), and the outflow transport through the Bussol Strait is estimated at about 10 Sv (1 Sv = $10^6 \text{ m}^3 \text{ s}^{-1}$). Ueno also estimated the streamfunction in the North Pacific from the Levitus climatological density field, under several assumptions (the result is not shown here). If we use Ueno's result, the volume transport through the strait becomes 8 Sv if the reference level is taken at 1500 dbar and 10 Sv if the level taken at 2000 dbar.

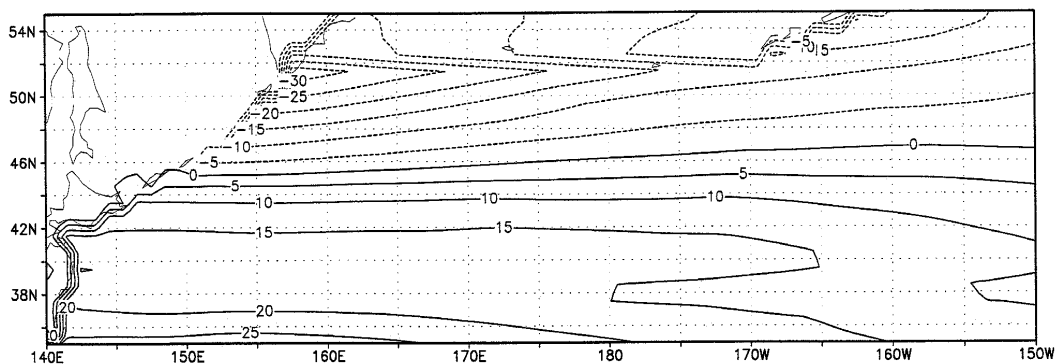


Fig. 2 Stream function (in Sverdrups) in the North Pacific Ocean which is calculated from the Hellerman and Rosenstein (1983) wind field under the assumption of the Sverdrup balance. The contour of the stream function is drawn so that the transport between two adjacent lines indicates 5 Sv, and the value at the east coast is set to zero.

Hydraulic theory

An example of a density cross-section from the Okhotsk Sea to the Pacific Ocean is shown in Figure 3 (Yasuda, 1997). The thickness of the surface layer (see the depth of $27.0 \sigma_\theta$) in the Okhotsk Sea is much greater than that in the Pacific Ocean, and a steep slope is seen just at the position of the strait. If the flow direction is from left to right, this sharp slope may represent that the flow state changes from subcritical to supercritical at the narrowest portion of the strait, and the flow may be controlled by hydraulic effect. In the case of the controlled flow and in the case that the flow is vertically uniform (one-layer flow), the volume transport and the Bernoulli function (or energy) are not independent near and upstream of the strait, and the transport can be given by the Bernoulli function and by the topography.

Whitehead et al. (1974) extended the idea of controlled flow in a rotating frame. They considered the case where potential vorticity is zero, and discussed the controlled behavior of a bottom flow. Gill (1977) analyzed a flow with uniform potential vorticity. Here, Gill's model is used to estimate the

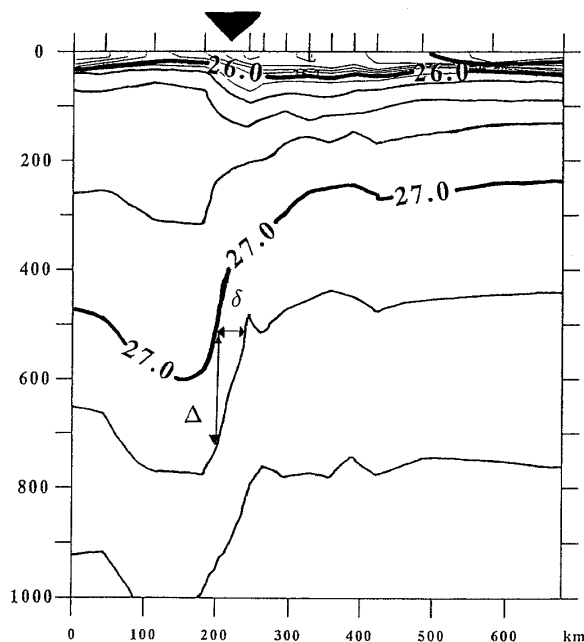


Fig. 3 An example of the density cross-section from the Okhotsk Sea to the Pacific Ocean (Yasuda, 1997). The position of the Kuril Islands is shown by a black triangle above the figure. The depth in meters is taken in the ordinate, and the horizontal distance in kilometers is taken in the abscissa. The values δ and Δ show the horizontal and vertical differences used in the Discussion.

transport through the Bussol Strait. Since the deformation radius at the strait (roughly 20 km) is comparable to the width of the Strait (roughly 20 km for 1000 m depth), the flow would feel the rotation.

The y -axis is taken in the flow direction (along the center of the strait), and the topography is assumed to be symmetrical to the y -axis (see Figure 4). The x -coordinate is taken horizontally and perpendicular to the y -axis. The right and left coasts are denoted by $x = \pm w(y)$. Starting from the steady inviscid equation of one-layer flow

$$-(f + \zeta) \frac{\psi_x}{D} = -B_x, \quad (6)$$

$$-(f + \zeta) \frac{\psi_y}{D} = -B_y \quad (7)$$

where D is the thickness of the layer and ψ is the stream function:

$$Du = -\psi_x,$$

$$Dv = \psi_y,$$

ζ is the vorticity ($\zeta = v_x - u_y$) and B is the Bernoulli function

$$B = \frac{u^2 + v^2}{2} + g'D.$$

Two equations governing the flow of a constant potential vorticity (f/D_∞ where D_∞ is the layer thickness at the center of the far upstream region) under the assumption that flow varies gradually enough ($u \ll v$ and $u_y \ll v_x$). (See Gill (1977))

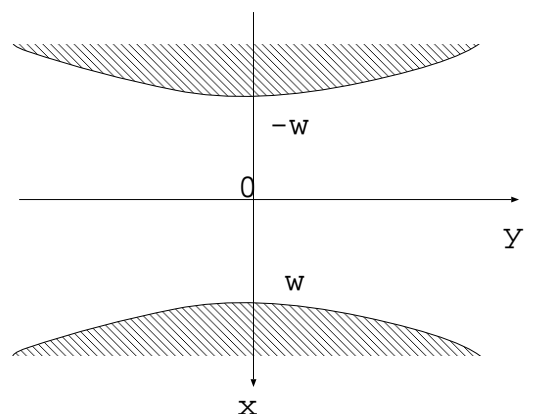


Fig. 4 Schematic view of flow through a strait (Gill's hydraulic model, 1977). The fluid flows from left to right in the y direction; x is taken perpendicular to y . The coasts are set symmetrical to the y -axis. The right coast (looking downstream) is denoted by $x = w(y)$.

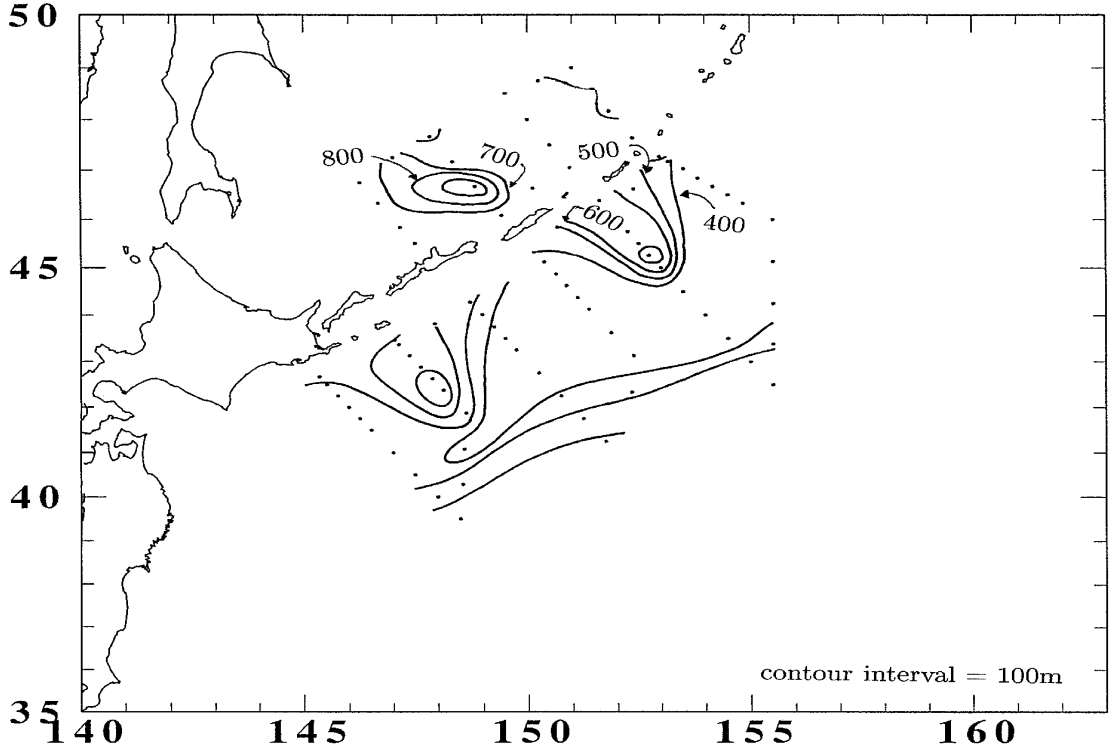


Fig. 5 The depth distribution of the isopycnal surface of $\sigma_\theta = 27.1$ from CTD observation of the R/V *Hokko-maru* in August–September 1991 (Kawasaki and Kono, 1992). Only the contours around the Bussol Strait are numbered. Contour interval is 100 m. Dots show the observation points.

for the detailed derivation.)

$$\delta D \cdot \bar{D} = -\frac{f}{2g}\Phi \quad (8)$$

$$(\bar{D} - D_\infty)^2 t^2 + \delta D^2 t^{-2} + 2D_\infty \bar{D} = \frac{f}{g}\Phi + 2D_\infty B_u/g \quad (9)$$

where $2\delta D$ and $2\bar{D}$ is the difference between and the sum of the water depths at the right (looking downstream) coast and the left coast, respectively, Φ is the transport, and B_u the value of B on the right wall in the far upstream region. The term t is a non-dimensional width and $t = \tanh(wf/\sqrt{g'D_\infty})$. The condition to realize the controlled flow is given by

$$\frac{\partial}{\partial \bar{D}}[\text{Equation (9)}] = 0. \quad (10)$$

If the controlled flow is determined, Φ can be determined by three parameters, t , D_∞ , and B_u .

Equation (9) requires that the flow in the upstream region takes the form of boundary jets along the both coasts. The depth D_∞ can be defined in the quiescent region away from the boundary. Denoting the thickness of the layer upstream at the right coast with D_u , the transport (Q_u) of the jet along to the right coast is $g'(D_u^2 - D_\infty^2)/(2f)$, and B_u is given by $B_u = g'(D_u^2 + D_\infty^2)/(2D_\infty)$.

An example of the depth distribution of the isopycnal surface of $\sigma_\theta = 27.1$ is shown in Figure 5 from CTD observations on board the R/V *Hokko-maru* in August–September 1991 (Kawasaki and Kono, 1992). The value of the surface layer thickness in the far upstream region (D_∞) is assumed to be 700 m, from Figure 5. The densities of the surface and bottom layers are $26.8 \sigma_\theta$ and $27.4 \sigma_\theta$, respectively, assumed from the density distribution shown in Figure 3. Then, the reduced gravity g' becomes $5.7 \times 10^{-3} \text{ m s}^{-2}$. The term w is taken as 20 km from the width of the Bussol Strait.

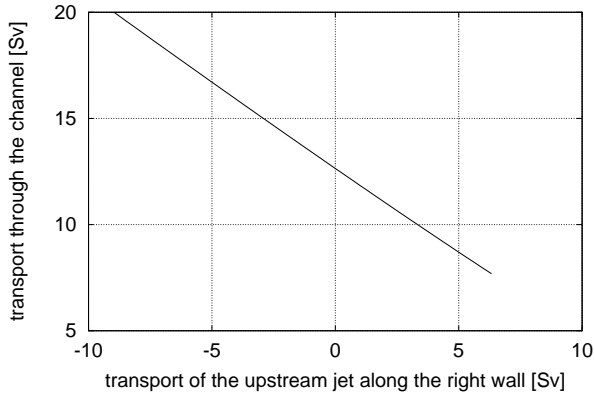


Fig. 6 Transport through the strait as a function of the transport of the upstream jet along the right side of the coast. The estimation is based on Gill's hydraulic model (1977) of constant potential vorticity flow. See the text for details.

The undetermined values are \bar{D} , B_u and Φ , and we have two equations (9) and (10). So, we have only one independent variable, and we select the transport of the jet along the right coast (Q_u) as the independent variable. The relation between Q_u and Ψ (the transport through the channel) is shown in Figure 6. If Q_u is positive and very large, the jet separates from the left coast. The curve is not shown beyond this separation point.

The Okhotsk Sea Water is generally flowing out through the Bussol Strait. If Q_u is taken to be positive, the transport through the Bussol Strait is less than 12 Sv and greater than 8 Sv, depending on the strength of the incoming jet. The northeastward jet in the Okhotsk Sea along the Kuril Islands south of the Bussol Strait is not so prominent, and the upstream jet along the right coast may be weak. Then the transport through the strait would be about 10 Sv, although the model would not be applicable directly to the real Bussol Strait.

Discussion

If the flow is always subcritical, hydraulic theory cannot be applied. The Island Rule is basically applicable to subcritical flow. However, the Island Rule does not give any detailed structure near the strait such as the asymmetric density field in the strait. If the flow is subcritical, the eminent slopes of the isopycnal surfaces through the Bussol Strait would be explained by the advection–diffusion balance.

An advection–diffusion balance of the density is

$$u \frac{\partial \rho}{\partial x} = \kappa \frac{\partial^2 \rho}{\partial z^2}$$

where u is the horizontal velocity in the along-channel direction, κ is the vertical diffusivity, and vertical velocity is assumed to be very small compared with horizontal velocity. A rough estimate of the vertical diffusivity κ is given by

$$\kappa \sim \frac{\delta \rho}{\Delta \rho} \frac{\Delta z^2}{\delta x} u$$

where δ and Δ denote the horizontal and vertical finite differences, respectively. Typical values of δ and Δ may be given from the density field in Figure 3 ($\Delta z \sim 100$ m, $\delta x \sim 30$ km). If u is chosen to be 1 m s⁻¹, κ becomes 0.3 m² s⁻¹. This estimated value appears to be too large, but the strong tidal mixing in the strait might provide such a large mixing.

When the diffusion effect is very large, the dissipation would contribute significantly in the integral (2). Pedlosky et al. (1997) discussed the frictional effect near the strait in the Island Rule (5). If we take Δ as the channel width, δ_M as the diffusive boundary layer width, and α as the ratio of the channel length to the meridional extent of the island, the parameter

$$R_\Delta = \frac{\Delta}{\delta_M \alpha^{1/3}}$$

becomes a determinative parameter. When it is less than 1.5, significant reduction of the transport would occur. For the Bussol Strait, $\Delta \sim 20$ km, $\delta_M \sim 50$ km, and $\alpha \sim 0.1$. So, R_Δ is 0.9, and the reduction due to diffusion would be significant. According to Pedlosky et al. (1997), the transport may become half of that estimated by the Island Rule without diffusion, discussed in the previous section. Then, the transport through the Bussol Strait would be about 5 Sv.

The Island Rule may be modified to be applicable for the hydraulically controlled flow. In the derivation of the Island Rule (2) from (1), it is implicitly assumed that $B = g'D + |\bar{u}|^2/2$ is continuous and is single-valued and that it vanishes when integrated along a closed circuit. Under the hydraulically controlled condition, the flow just downstream of the strait is supercritical, and a hydraulic jump should exist in order that the supercritical flow is connected to the subcritical flow further downstream. The transport and momentum are conserved across the jump, but the energy is dissipated at the jump. If we denote this energy dissipation with $-\delta B$, we have

the modified Island Rule

$$\Phi = \frac{\int_{y_s}^{y_n} \Psi_s(x_+, y) dy - \delta B / \beta}{y_n - y_s}. \quad (11)$$

The relative contribution of the hydraulic effect is stronger for shorter islands or for stronger energy dissipation.

Conclusion

In this paper, transport through the Bussol Strait is estimated by using simple models. Both the global constraint (Island Rule) and local constraint (hydraulics) yield estimates of transport from 5 to 10 Sv. The models can be improved if an active lower layer is added, and if a seasonal or shorter variability term is considered. However, much more elaborate observations are needed to model the oceanic state under consideration.

Acknowledgments

The authors wish to express their thanks to Dr. Yutaka Nagata of the Marine Information Research Center, JHA for his valuable comments and suggestions. Thanks are due to Mr. Hiromichi Ueno of University of Tokyo for providing his results about the distribution of the stream function in the North Pacific Ocean.

References

Gill, A.E. 1977. The hydraulics of rotating-channel flow. *J. Fluid Mech.*, 80, 641–671.

- Godfrey, J.S. 1989 A Sverdrup model of the depth-integrated flow from the world ocean allowing for island circulations. *Geophys. Astrophys. Fluid Dyn.*, 45, 89–112.
- Hellerman, S. and Rosenstein, M. 1983. Normal monthly wind stress over the World Ocean with error estimates. *J. Phys. Oceanogr.*, 13, 1093–1104.
- Kawasaki, Y. and Kono, T. 1992. Baroclinic water exchange in the Kuril Basin and in the northwestern Pacific in summer. *Umi to Sora*, 68, 41–54.
- Minato, S. and Kimura, R. 1980. Volume transport of the Western Boundary Current penetrating into a marginal sea. *J. Oceanogr. Soc. Japan*, 36, 185–195.
- Pedlosky, J. 1994. Stratified abyssal flow in the presence of fractured ridges. *J. Phys. Oceanogr.*, 24, 403–417.
- Pedlosky, J., Pratt, L.J., Spall, M.A. and Helfrich, K.R. 1997. Circulation around islands and ridges. *J. Mar. Res.*, 55, 1199–1251.
- Talley, L.D. and Nagata, Y. (eds.) 1995. The Okhotsk Sea and the Oyashio Region. *PICES Sci. Rep.*, 2, 227 pp., Institute of Ocean Sciences, Sidney, B.C., Canada.
- Yasuda, I. 1997. The origin of the North Pacific Intermediate Water. *J. Geophys. Res.*, 102, 893–909.
- Whitehead, J.A., Leetmaa, A. and Knox, R.A. 1974. Rotating hydraulics of strait and sill flows. *Geophys. Fluid Dyn.*, 6, 101–125.

Oyashio west path culmination as the consequence of a rapid thermohaline transition in the Pacific Subarctic

Konstantin ROGACHEV

Pacific Oceanological Institute, Vladivostok, Russia

Abstract

Oyashio and Kamchatka Currents are western boundary currents of the Pacific subarctic gyre. The Kamchatka Current transports fresh water in the surface layer to the Sea of Okhotsk. Large Oyashio eddies propagate against the current and bring warm subtropical water in their cores up to the Strait of Boussole. Here, I present the evidence of the recent rapid change of stratification in the Oyashio and Sea of Okhotsk during the last decade. There were significant changes in the thermohaline structure in the Western Subarctic during the period from 1990 to 1997. The transition began during the reinforcement of the Coastal Oyashio. The main consequences of this thermohaline transition from one ocean state to another are changes of the Oyashio path and restratification of its water. It indicates that the ocean climate in the Western Subarctic depends strongly on the Oyashio path.

Introduction

The waters of the Kamchatka Current, having warm water at depth of 200–300 m, enters the Sea of Okhotsk through the deep Kuril Straits (Fig. 1). This current brings cold and fresh water in the surface layer (0–100 m). Kamchatka Current water, penetrating through these Straits, forms a cyclonic circulation inside the Sea and mixes with Soya Current water (SC in Fig. 1) in the Kuril Basin (Alfultis and Martin, 1987). There is significant cooling of the Kamchatka Current water in the Sea of Okhotsk. While the Alaska Current brings warm water to the Western Subarctic, most of the water is of the Western Subarctic formed by the lateral mixing of the Kamchatka Current water and cold water of Okhotsk Sea origin (Ohtani, 1970). Therefore, the exchange between the Sea of Okhotsk and North Pacific is essential for cooling, freshening and change of stratification at intermediate depths (100–800 m). The Soya Current flows along the Hokkaido coast and brings the warm Japan Sea water into the sea (Takizawa, 1982). This current is known to be driven by a large difference in sea level between the Japan and Okhotsk Seas (Takizawa, 1982; Ohshima, 1994). The seasonal cycle of this current is clear, and Soya inflow is not observed from December to March, due to either higher Okhotsk Sea levels or the low difference of the sea level across the Strait.

A principal feature of the Pacific Subarctic is its high stratification. Wintertime convection there seems to be limited to the upper 150 m (Reid,

1973). This is quite different compared with the northern North Atlantic. The reason for no deep convection in the northern North Pacific is that the surface water is too fresh. According to Warren (1983), the low surface salinity is due partly to a low evaporation rate, which in turn, is due to a relatively low surface temperature.

Recently, the Sea of Okhotsk interannual cycle was studied by Yang and Honjo (1996). They found its hydrographic structure is sensitive to interbasin exchanges between the Japan and Okhotsk Seas. The doubling of the Soya Current transport (SC on Fig. 2) results in higher salinity in the surface and deepens vertical mixing. Reducing the Soya Current leads to more freshening of the mixed layer, restricting deep vertical mixing.

Here, I consider a case of the rapid thermohaline transition from low stratified periods with different thermohaline structure in the western Subarctic. The first one was observed 7–8 years ago prior to the thermohaline transition in the North Pacific which occurred in 1990–1997. I described this case using the INPOC (International North Pacific Ocean Climate Study; see Rogachev et al. (1996a,b, 1997)) array of CTD stations in the Oyashio. One of the basic findings of this project was the discovery of the thermohaline transition in the subarctic Pacific. This means there are rapid and significant changes in the water column properties to a depth of 1000 m in western subarctic boundary currents. A main consequence of this transi-

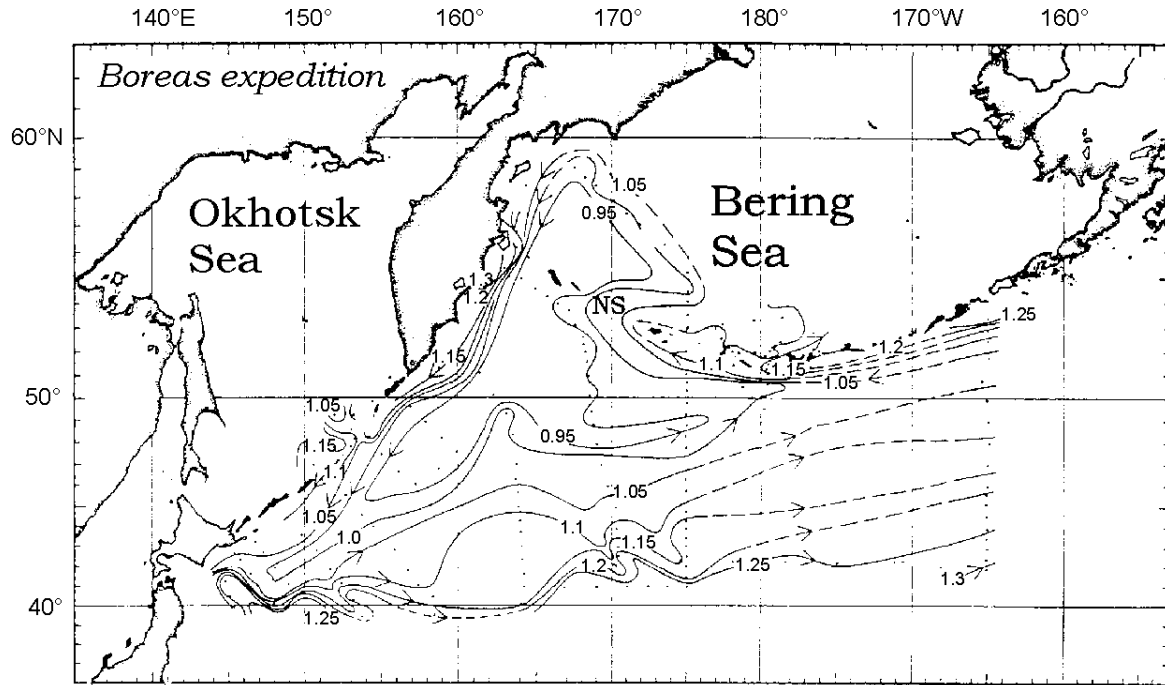


Fig. 1 Geopotential anomaly at the sea surface relative to 1000 dbar (10 J/kg) (after Reid (1973)). NS is Near Strait.

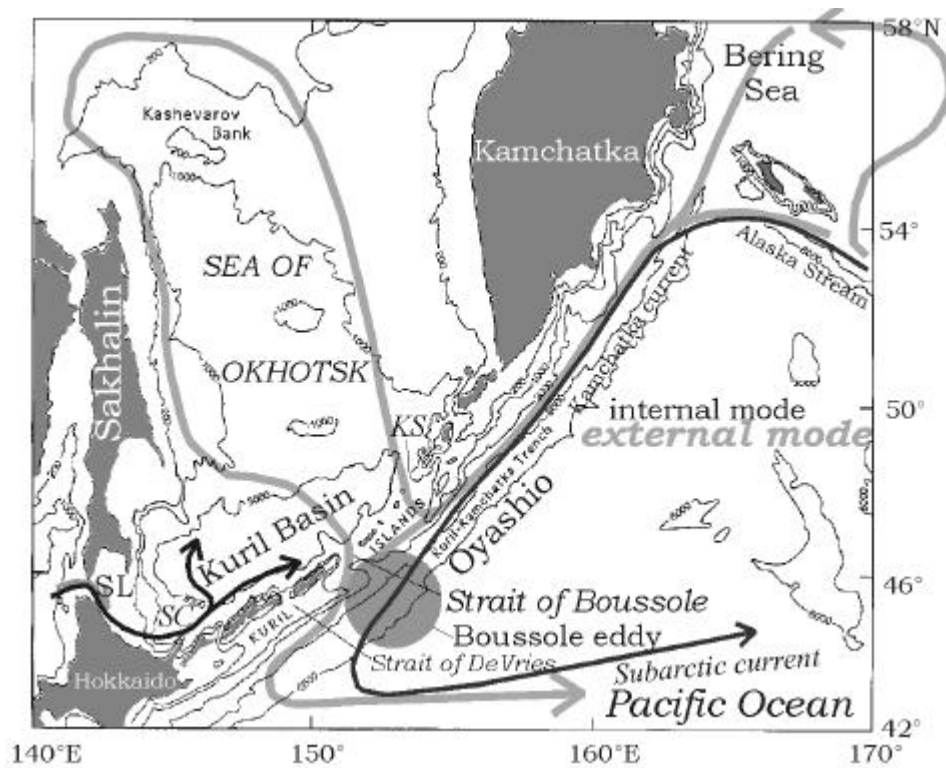


Fig. 2 Scheme of the two circulation modes based on the recent thermohaline transition in the western subarctic. Black and grey lines represent internal and external modes, or different circulation regimes. KS is Krusenshtern Strait, SL is Strait of Laperouse, SC is Soya Current.

tion is the change of the Oyashio path and restratification of its water. The stratification was destroyed before the transition due to a high inflow of saline subtropical waters to the Sea of Okhotsk and Oyashio in 1990 and a weak transport of the subarctic water by the coastal Oyashio (Rogachev, 1997). However, during the transition there was a significant change of water mass thermohaline structure and a change of the main Oyashio path (Fig. 3). It appears that notable changes have occurred also within large areas of the Arctic Ocean and subarctic Pacific during the past decade (Latif and Barnett, 1996; Qüadfasel et al., 1991)

Data and method

The initial data were collected while carrying out the INPOC project (Rogachev et al., 1996a,b, 1997). The program involved four cruises in the Oyashio from 1990–1992 and was continued by the Pacific Oceanological Institute (POI) in 1993, 1994 and 1996. Most of those cruises covered the area with a high resolution station grid (the distance between stations was 18–20 km). From the analysis of these data it is possible to determine the horizontal structure of the Oyashio fresh-core eddies, which are the major features of the region (Rogachev and Goryachev, 1991; Rogachev et al., 1996a,b). The

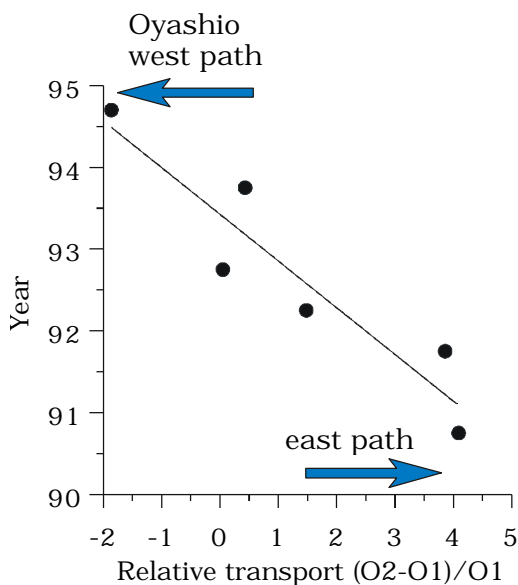


Fig. 3 Transport difference between offshore (O2) and coastal Oyashio (O1) relative to the coastal Oyashio in 1990. Note a shift to the Oyashio west path.

added data I used is the study conducted on board the R/V *Hokko Maru* under the joint project of the Hokkaido National Fisheries Research Institute (HNFRI) and the Pacific Research Institute of Fisheries and Oceanography (TINRO) (Kono and Kawasaki, 1997). I used potential vorticity as the property of the stratification, which is determined as $Q = f/r(\partial s_q/\partial z)$, where f is the Coriolis parameter, r the density, z is the vertical coordinate, and s_q is sigma theta. To estimate Q , the density was calculated at standard depths.

Results

Rapid changes in the western subarctic

For the past 7 years, evidence of the thermohaline transition event has appeared within the core of the Pacific and Soya waters entering the Sea of Okhotsk. In 1997 the Pacific water almost completely displaced warm and salty Japan Sea water, whereas the opposite situation was observed in 1990. For instance, high salinity water flowed out to the Pacific Ocean through the Strait of Boussole in 1990. However, the high salinity area was limited by a narrow zone in 1996 and 1997. While Soya warm water inflow was weak, the low salinity subarctic water area enlarged. More dramatic events occurred at the ocean side of the Kuril Islands. For instance, Figure 4 shows rapid penetration of the cold upper layer at sigma- $T = 26.3$ from Kamchatka to Hokkaido during the 7-yr period. A major consequence of this transition are changes in the stratification and the main Oyashio path from offshore to coastal (Rogachev, 1996b, 1997). I call it Oyashio west path culmination (Fig. 3). Potential vorticity time series show a six-fold increase at 500 db (Fig. 5). In particular, there was a minimum of potential vorticity at 400–500 db in 1990 which, seven years later, became a maximum of the potential vorticity in 1996. This change of potential vorticity vertical distribution reflects variations of the stratification in the Oyashio and its fresh-core eddies.

Discussion

The present data show that there was a thermohaline transition in the western subarctic during 1990–1997, which is evident in the change of the Oyashio path and its thermohaline structure. There was a prominent penetration of salty Soya Current water to the Sea of Okhotsk in 1990. This process changed stratification and surface salinity.

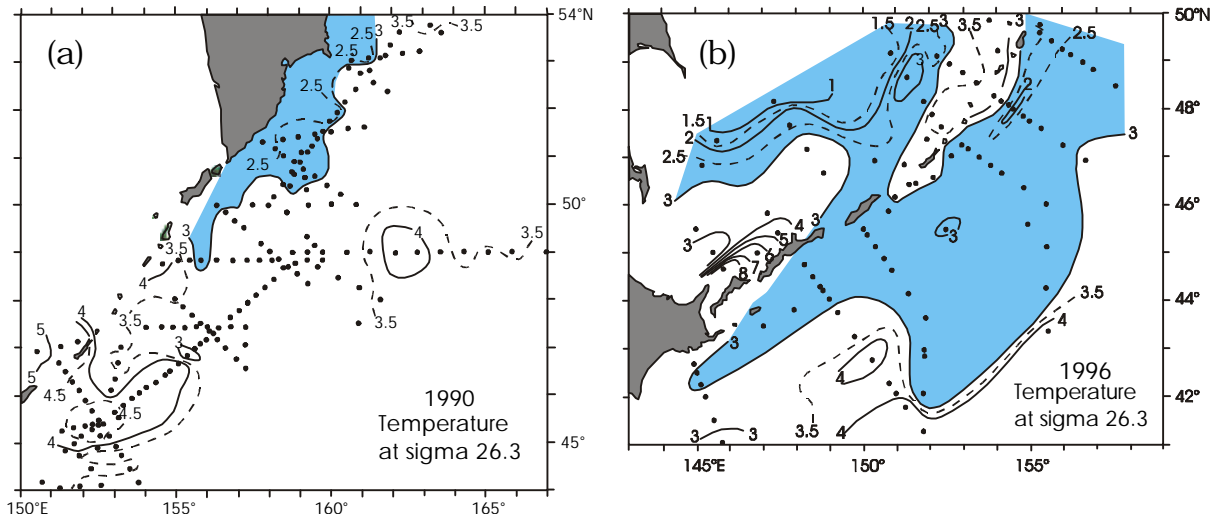


Fig. 4 Cooling at the surface layer during a thermohaline transition. Temperature at sigma- $T = 26.3$ in (a) August 1990 and (b) August–September 1996. Low-temperature area is shaded.

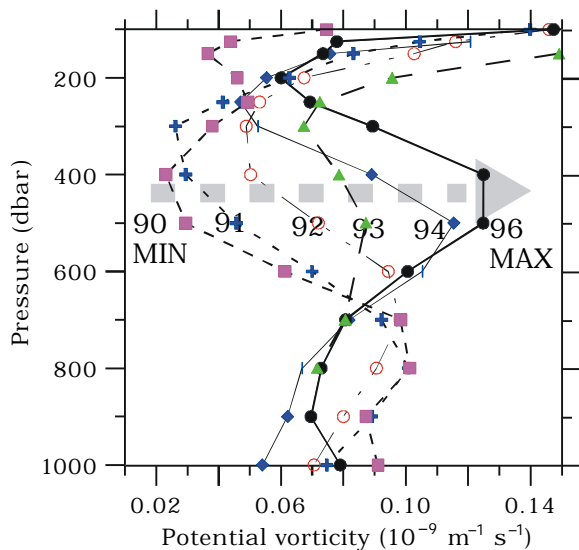


Fig. 5 Potential vorticity profiles for the central stations in Boussolle eddies during the thermohaline transition. Arrow shows increase of stratification from 1990 to 1996.

Stratification was initially destroyed in 1990 by the increased influx of salty water and low southward transport by the Western Subarctic boundary currents (Rogachev, 1997). The vertical profiles of the salinity in the Kamchatka Current have a very sharp halocline at 100–200 m depth (Nagata and Ohtani, 1989). A distinct mesothermal layer (warm subarctic intermediate layer) is associated with this halocline. The halocline off the southern Kuril Islands is almost erased, and salinity decreases much more gradually. The mesothermal

layer becomes unclear and its depth is increased in comparison with the Kamchatka Current region. Therefore, the fresh water budget of the Okhotsk Sea should affect the interbasin water exchange between Japan and Okhotsk seas.

The recent Oyashio west path culmination is associated with the cooling of the surface layer (Fig. 4). This cooling of the surface layer provides a feedback for the decrease of evaporation which may sustain the salinity anomalies.

Acknowledgments

This work was partially supported by the Russian Fund for Basic Research. E. Carmack, B. Lake and J. Love from the Institute of Ocean Sciences, Canada, made significant contributions to the INPOC study. M. Kashiwai and Y. Kawasaki from the Hokkaido National Fisheries Research Institute, Japan, kindly permitted us to use the R/V *Hokko Maru* data for this research.

References

- Alfultis, M.A. and Martin, S. 1987. Satellite passive microwave studies of the Sea of Okhotsk ice cover and its relation to oceanic processes, 1978–82. *J. Geophys. Res.*, 92, 13,013–13,028.
- Kono, T. and Kawasaki, Y. 1997. Modification of the western subarctic water by the exchange with the Okhotsk Sea. *Deep-Sea Res.*, 44, 689–712.

- Latif, M. and Barnett, T.P. 1996. Decadal climate variability over the North Pacific and North America : Dynamics and predictability. *J. Climate*, 9, 2407–2423.
- Nagata, Y. and Ohtani, K. 1989. The gap in research plans for the subpolar region in the north Pacific. pp. 57–112. In *The Third Japan–US WOCE Workshop*, Kyoto, Japan.
- Ohtani, K. 1970. Relative transport in the Alaskan Stream in winter. *J. Oceanogr. Soc. Japan*, 26, 271–282.
- Oshima, K.I. 1994. The flow system in the Japan Sea caused by a sea level difference through shallow straits. *J. Geophys. Res.*, 99, 9925–9940.
- Quadfasel, D. Sy, A. Wells, D. and Tunik, A. 1991. Warming in the Arctic. *Nature*, 350, 385.
- Reed, R.K. and Stabeno, P.J. 1993. The recent return of the Alaskan Stream to Near Strait. *J. Mar. Res.*, 51, 515–527.
- Reid, J.L. 1973. *Northwest Pacific Ocean Waters in Winter*. The John Hopkins University Press, Baltimore, 96 pp.
- Rogachev, K.A. 1997. Recent speeding up of the Pacific subarctic circulation. *International WOCE Newsletter*, 26, 40–42.
- Rogachev, K.A. and Goryachev, V.A. 1991. Mixing in warm-core rings of the Kuroshio. *J. Geophys. Res.*, 96, 8773–8777.
- Rogachev, K.A., Tishchenko, P.Ya., Pavlova, G.Yu., Bychkov, A.S., Carmack, E.C. Wong, C.S. and Yurasov, G.I. 1996a. The influence of fresh-core rings on chemical concentrations (CO₂, PO₄, O₂, alkalinity, and pH) in the western subarctic Pacific Ocean. *J. Geophys. Res.*, 101, 999–1010.
- Rogachev, K.A., Salomatin, A.S. and Carmack E.C. 1996b. Concentration of pelagic organisms at mesoscale fronts in the western subarctic Pacific: Small fish on long waves. *Fish. Oceanogr.*, 5(3/4), 153–162.
- Takizawa, T. 1982. Characteristics of the Soya Warm Current in the Okhotsk Sea. *J. Oceanogr. Soc. Japan*, 38, 281–292.
- Warren, B.A. 1983. Why is no deep water formed in the North Pacific? *J. Mar. Res.*, 41, 327–347.
- Yang, J. and Honjo, S. 1996. Modelling the near-freezing dichothermal layer in the Sea of Okhotsk and its interannual variations. *J. Geophys. Res.*, 101, 16,421–16,433.

On the Year-to-Year Change in Subarctic Water Characteristics Around the Kuril Islands

Yasuhiro KAWASAKI

Hokkaido National Fisheries Research Institute, Kushiro, Japan

A counterclockwise circulation centered approximately at 50°N 165°E is seen in the western Subarctic Pacific Ocean. The Oyashio makes up the southwestern rim of this circulation, and flows southwestward along the Kuril Islands and the eastern coast of Hokkaido. The water characteristics of the Oyashio show a considerable seasonal change due to the direct influence by the Okhotsk Sea (Kono and Kawasaki, 1997). The seasonal change in subsurface waters beneath the pycnocline is less than those above the pycnocline, and we consider only the data taken in the same seasons every year. We confine our attention to the subarctic dichothermal (inter-cooled) water, which shows considerable year-to-year change due to the yearly variations in winter cooling and in global climate conditions. In this study, we analyze the data of subsurface water deeper than pycnocline depth observed around the Kuril Islands, and discuss the yearly change in water characteristics of the subarctic.

region, salinity is more uniform on isopycnals than potential temperature, as the salin-

Bussol Strait, the sill depth of which is 2200 m, is one of the main straits connecting the North Pacific Ocean with the Okhotsk Sea. The Hokkaido National Fisheries Research Institute (HNFRI) is continuing observations along a line which passes through Bussol Strait (NU-line) by using the R/V *Hokko-Maru* belonging to HNFRI, every year since 1988. The location of the observational stations are shown in Figure 1. Annual observations are made from late August to early September. Kawasaki and Kono (1994) discussed the characteristics of subarctic waters of the Western North Pacific Ocean and of the Okhotsk Sea and showed that they are distinguished by maxima and minima of water temperature in particular density surfaces. The difference of the water characteristics is discussed here by comparing their potential temperature on isopycnal (isosteric) surfaces. In the subarctic

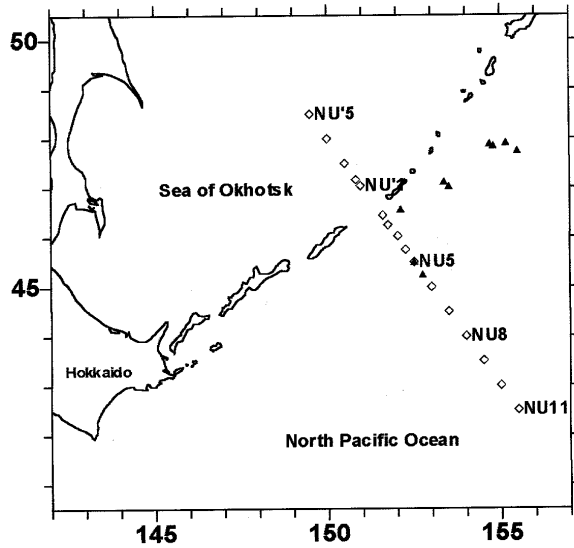


Fig. 1 Location of stations on the NU-line, 1987-1997, *R/V Hokko-maru*. Triangles denote the stations which were used for the East Kamchatka Current water (see text).

ity effect on water density is much larger than temperature.

The distributions of potential temperature ($^{\circ}\text{C}$) averaged over 10 cruises (1988-1997) and its standard deviation along the NU-line are shown in Figure 2. The potential density (σ_{θ} : left axis) and the thermocline anomaly (Δs_{θ} : right axis) are given on the ordinate. The station NU9 corresponds to the Subarctic Front. Water characteristics in the subtropical region (NU10-11) are evidently different from those in the subarctic region (NU8-NU'5). The water in the subarctic region may be divided into the Okhotsk Sea water (NU'2-5), the Kuril water (NU'1-NU2), and the Western Subarctic Pacific water (NU3-8). A dichothermal (inter-cooled) structure is observed both sides of Bussol Strait: 26.5-26.8 σ_{θ} layer (75-150 m in

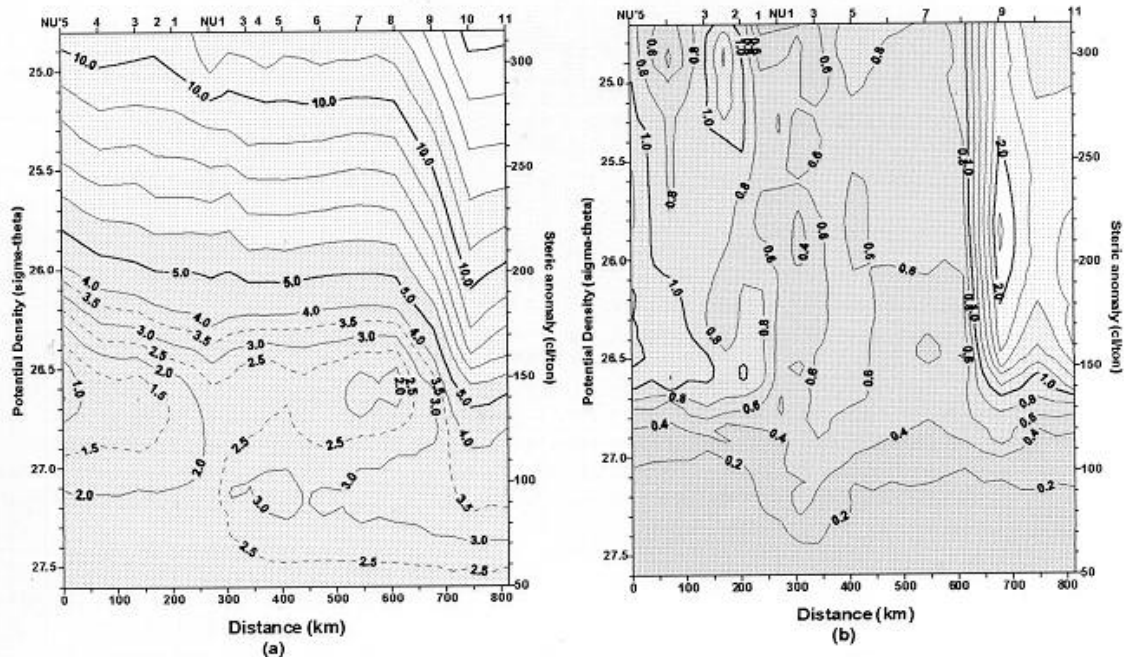


Fig. 2(a) Potential temperature distribution ($^{\circ}\text{C}$) along NU-line averaged for ten years from 1988 to 1997. The potential density or the steric anomaly is taken in the ordinate. The distance (in km) measured from NU'5 is taken in the abscissa. **Fig. 2(b)** Same as 2(a) except for the averaged standard deviation ($^{\circ}\text{C}$) of the potential temperature.

water depth) in the Pacific side, and 26.5-27.0 σ_{θ} layer (50-300 m in water depth) is seen on the Okhotsk side. A methothermal (inter-warmed) structure is observed in 26.9-27.2 σ_{θ} layer (200-400 m in water depth) in the Pacific side, while a deep warm water in 27.3-27.4 σ_{θ} layer (900-1100 m in water depth) is seen on the Okhotsk side. High standard deviations ($> 1.5^{\circ}\text{C}$) are found near the Subarctic Front (NU9) in Figure 4b. This high variance seems to be caused by the fluctuation of the position of the front. Other high standard deviation values ($> 1.0^{\circ}\text{C}$) appear in the subsurface layers of the northern stations (NU'3-5). This high variance would be caused by inflow of a very cold water lower than 0°C , which seems to originate from the East Sakhalin Current Water. Beneath the 26.7 σ_{θ} layer (lower part of dichothermal layer), the standard deviation value decreases monotonically with depth, indicating that yearly temperature variations hardly penetrate into deeper layers. However, relatively high value tends to penetrate into deeper

depths around Bussol Strait (see, for example, isopleths of 0.4 and 0.2). This would indicate that active mixing reaches deeper layers near Bussol Strait.

In order to remove the considerable variation of the standard deviation in the cross-section, and in order to exaggerate the temperature variation beneath the pycnocline, the temperature deviations from the mean values (Fig. 2a) for each year were normalized by the mean standard deviation (Fig. 2b). Distributions of this normalized temperature deviation are shown in Figures 3a-c for the years of 1990, 1993, and 1996, respectively. Conspicuous negative deviations are found in the subsurface layers of the Pacific side in 1990 (Fig. 3a) and 1991 (not shown), and in the Okhotsk side in 1993 (Figure 3b). In 1993, many positive and negative deviation domains having small spatial scales appear in complicated ways in the Pacific side. On the other hand, the conspicuous positive deviation appears in almost the whole cross-section in the layer below 26.6 density surface in 1996 (Figure 3c), though

the thickness of the positive deviation region on
the Okhotsk side

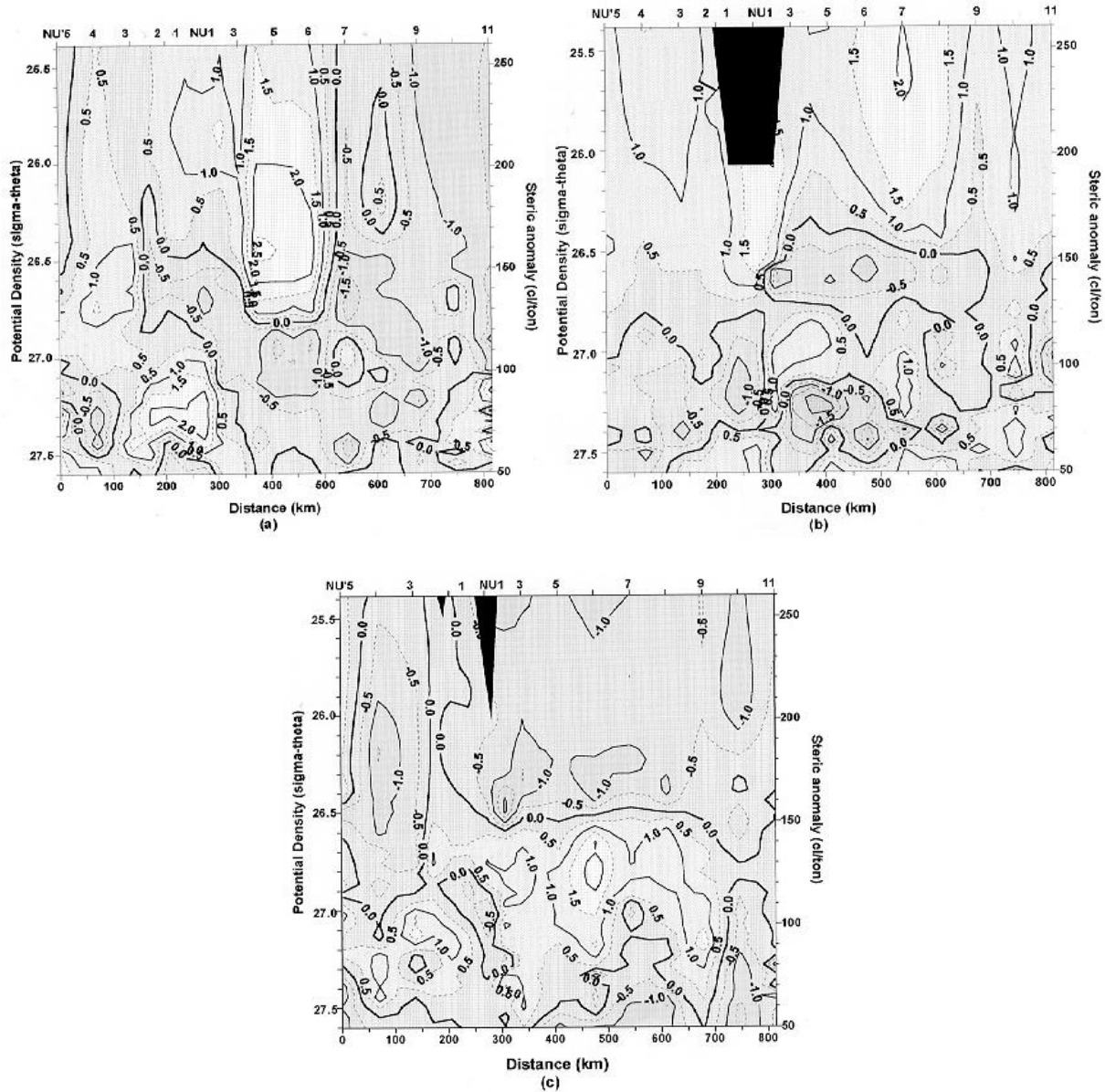


Fig. 3 As in Figure 2a except for the normalized temperature deviation in (a)1990, (b) 1993 and (c) 1996. See text for the definition of normalized temperature deviation.

(NU'5 and NU'4) is rather limited. A similar distribution is also seen in 1997 and the thickness of the positive region increases considerably in 1997, just as on the Pacific side in 1996. The density range (26.6-27.3), where conspicuous deviations are seen, corresponds to the lower part of the dichothermal layer and the methothermal layer.

Yearly changes of the normalized temperature deviations are shown in Figure 4 for two observation points, NU'4 and NU 8. NU'4 is located at the center of the Kuril Basin in the Okhotsk Sea (48°N 150°E), and NU8 at the center of the Western Subarctic Circulation in the North Pacific (44°N 154°E). Relatively large negative deviations are seen in the layer of 27.3-27.5 density in 1990 at NU'4 (Figure 4a).

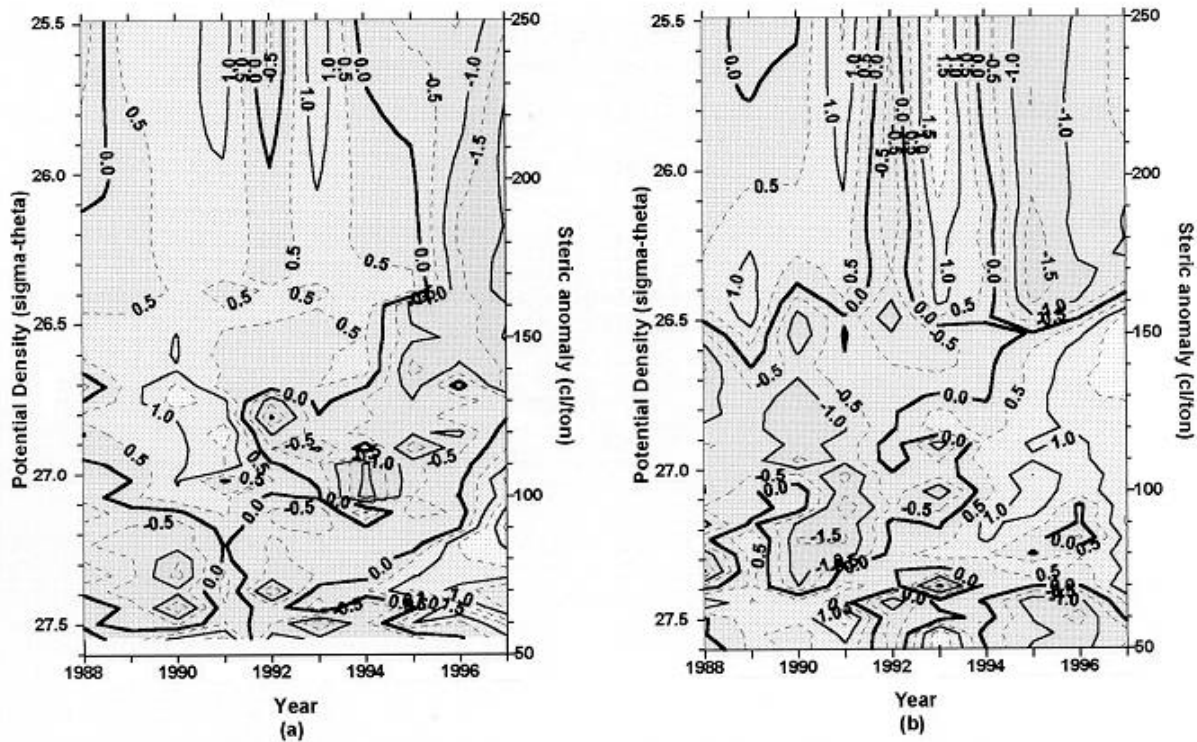


Fig. 4 Temporal change of the normalized temperature deviation: (a) at NU4 (the center of the Kuril Basin in the Okhotsk Sea) and (b) at NU8 (the center of the western subarctic circulation in the North Pacific Ocean).

This negative domain is seen near the lower left corner in Figure 3a. Though the spatial extent of this domain is very limited in the 1990 cross-section (Figure 3a), its time scale (or persistency) appears to be considerably large: no such domain is seen in 1991, but the similar distribution is also seen in 1992 and 1993. This domain shifts towards lower density ranges during the period from 1993 to 1997. Instead, the positive deviation domain was created in the 27.4-27.5 density layer in 1993, and this positive domain increased its magnitude and its thickness continuously afterward, as seen in the cross-section in 1996 (Fig. 3c).

As we are discussing the temperature deviation from mean value (the average value for all cross-section and for all period would be very small even normalized by standard deviation), the situation at NU8 (the center of the Western Subarctic Circulation) tends to behave just oppositely in general: the positive deviation domain found in

the 27.2-27.5 density layer in 1992 or in 1993 shifted towards lower density range, and its thickness tends to increase after 1993. It should be noted that the yearly change of the temperature deviation in the subsurface layer between 26.5 and 27.0 density surfaces is more clearly seen in Figure 4b than Figure 4a. The temperature deviation in Figure 4b before 1992 or 1993 is negative in this layer, and positive after. The subsurface water in the Western Subarctic Circulation region appears to be significantly warmed in recent years.

We selected the observation points which were identified to be in the East Kamchatka Current Region from available spatial distribution of water quantities for the period from 1988 to 1997. The distribution of the selected points are shown with closed triangles in Figure 1. Though the positions are distributed in rather wide area, the data

Influence of oceanological conditions of the West Kamchatka shelf waters on spawning grounds and on pollock egg distribution

Alexander L. FIGURKIN and Evgeniy E. Ovsyannikov

Pacific Research Institute of Fisheries and Oceanography, Vladivostok, Russia

Introduction

From 1983 until the present the Pacific Research Institute of Fisheries and Oceanography (TINRO) has been carrying out a series of observations in areas of Pollock spawning grounds. These standard investigations spread over the basic shelf area of the Okhotsk Sea. We have analysed the data obtained from 21 expeditions near western Kamchatka (16 cruises were undertaken in April, and 5 cruises were held in March and in June). The data collected at more than 2000 stations have been processed. The water circulation has been analysed by dynamic topography method.

This study was done in order to pursue the following goals:

- ⌚ to study the currents in western Kamchatka in early spring, as there is a lack of published information for this period,
- ⌚ to determine the clusters of years with similar oceanological conditions,
- ⌚ to analyse how much the spawning ground sites and pollock egg distributions differ from cluster to cluster of years, given similar oceanological conditions.

As the names given to the same currents by different authors vary, we accept the following terms: the West Kamchatka Current (WKC) for the northward warm flow along the Kamchatka slope and the Compensatory Current (CC) for the southward coastal counter-current, (in accordance with the names given by Davydov (1975) and Luchin (1982)).

Results and discussion

In early spring the basic elements of water circulation, as seen on the dynamic topography charts, are the following: anticyclonic circulation of warm water of the WKC; cyclonic circulation of cold northern Okhotsk shelf waters – on the western periphery of the WKC, and the circulation of cold

coastal waters, where the CC was observed in some years (Fig. 1).

Many features typical of the WKC are well known. From dynamic topography charts the WKC water looks like a system of anti-cyclonic eddies or like areas with anti-cyclonic curvature of streamlines. In the observed regions the surface current velocities were observed between 54°–57°N, in the area where the warm WKC water meets with cold water from the northern Okhotsk shelf. To the south of 53°N, the velocity of WKC is usually slow, as its streamline runs to the west from study area.

Moroshkin (1964), Luchin (1982) and Chernyavsky (1981) determined that the usual location of the WKC streamline to the north of the 500-m isobath varies between 152° and 154°E during the warm period. Our charts show that in April the WKC flows between 153°10'–154°20'E, that is, more to the east, than in warm seasons. This shift can be explained by seasonal variability of water density after long winter cooling, which reduces the zone of influence by the warm WKC water.

Very little data have been obtained about the CC. In 1910 Zhdanko published information about the drift of bottles southward along western Kamchatka. Kajiura (1949) and Leonov (1960) showed a southward current along western Kamchatka, too. From Moroshkin's (1964) charts and those of Davydov (1975) and Chernyavsky (1981), the CC was not shown and the WKC water moved in a northern direction between the coast and the slope. In 1982 Luchin confirmed the existence of the cold CC. He used Sarkyisyan's (1977) diagnostic model for current computation. Luchin assumed that the CC originated in shallow water to the south of Cape Utkolokskiy. In the summer, the CC is neither wide nor intensive, but these parameters increase from the summer to the autumn. Luchin (1987) explained the seasonal growth of the CC intensity both by a weakening of the WKC and by a strengthening of northeastward winds,

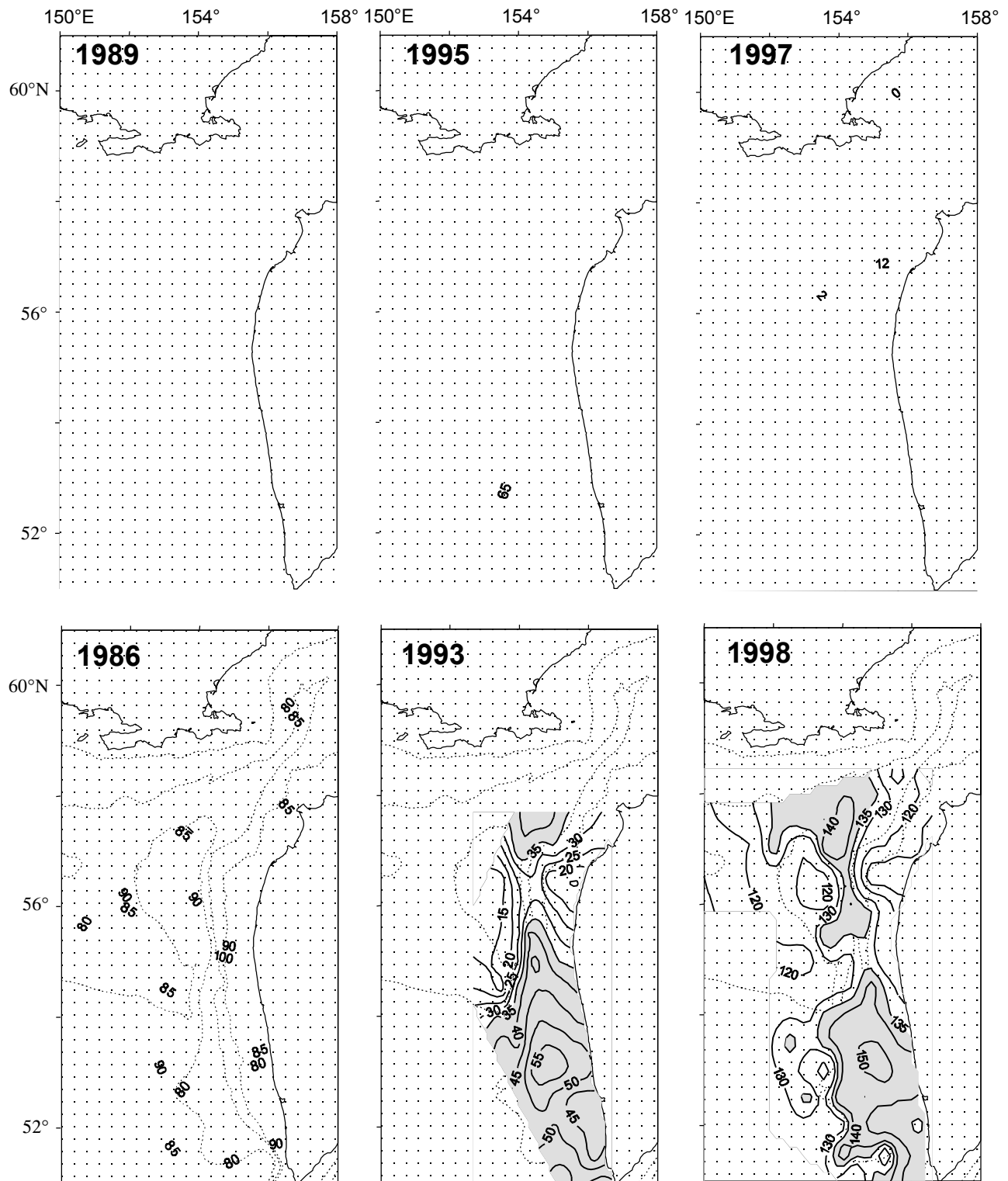


Fig. 1 Typical water circulation in April showing (top) the years with an absence of the Compensatory Current (CC) and (bottom) the years with an intensive CC. Dashed is area of the West Kamchatka Current (WKC).

which cause an additional coastal southward flow from Shelikhov Bay.

Our charts of dynamic topography show that in April during 1983–1998 the CC was not formed in each year. The intensive CC, traced along a significant part of the western Kamchatka coast, was observed in 9 of 16 years: in 1985, 1986, 1988, 1991, 1993, 1996, 1998 and, probably, in 1987 and 1994 (the absence of data on salinity did not allow us to complete the current calculations for these years). In other years the CC was not observed or did not reach farther south than 56°–57°N (1984, 1989, 1990, 1992, 1995, 1997 and 1983, presumably, Fig. 1).

Studies were continued in order to analyze and compare particular oceanological conditions in a cluster of years with the intensive CC and in a cluster of years without the current.

According to our calculations, the southward water transport during the years of a weak CC was 0.005 Sv. During the years with an intensive CC, the typical value of southward transport increased more than 10 times – about 0.1 Sv (Fig. 2). It is worth mentioning, that the values of transport and velocity obtained by the dynamic height calculation method are sufficient only for comparison, but do not work for calculation of exact values. Transport grew due to the increase of flow width, usually up to the 70–100 m isobath, to a maximum, up to the 150–170 m isobath.

Cyclonic circulation of coastal water is the main marker of the CC on dynamic topography charts. In the years when the CC was not found, the anticyclonic circulation of the WKC water was observed from the slope up to the coastline of western Kamchatka.

The cyclonic circulation of the CC means that the integrated density of its water is higher than the density of WKC waters. It is established that the lower temperature of the coastal water, as compared to the temperature of the WKC water, is not a sufficient condition for the formation of an intensive CC. Analysis has shown that coastal water salinity was usually higher or equal to the salinity of WKC waters in the years with an intensive CC (Fig. 3). In other years, when WKC water dominated along the coast, the salinity increased gradually with distance from the coast. The salinity of coastal waters in the years of an intensive CC is

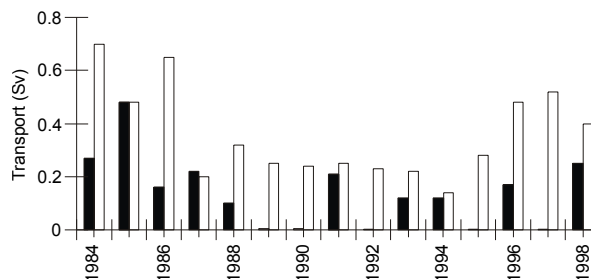


Fig. 2 Water transport (Sv) in April for the layer for the layer 0–200 m (between West Kamchatka and 153°E). White bars denote transport of the WKC; black bars indicate transport of the CC. The years with intensive CC (transport ≥ 0.1 Sv) in April: 1985, 1986, 1988, 1991, 1993, 1996, 1998 and probably 1987 and 1994. The years with absence or weak CC (transport ≤ 0.005 Sv) in April: 1984, 1989, 1990, 1992, 1995 and 1997.

0.3–0.6 psu higher than the salinity in the years when the CC was not found.

It is also known that in the Arctic seas salinity may increase due to ice formation or due to upwelling. The most intensive process of highly saline water formation took place in the upper part of the northwestern Okhotsk shelf and in the northern part of Shelikhov Bay (in areas with polynyas). Any increase of coastal water salinity due to local ice formation takes place in the winter along the Kamchatka coastline. Nevertheless, the local conditions solely can neither cause nor maintain high values of salinity that were observed here in the years with the intensive CC.

As noted on the dynamic topography charts, highly saline coastal water originated in the areas of Shelikhov Bay. This water reaches the West Kamchatka coast either with the flow moving in a southern direction from Gizhiginskaya Guba along Pyagina Peninsula or along the Kamchatka coast. In both cases, the WKC cannot bring its waters to Shelikhov Bay along the coast. It is interesting to note that the maximal value of high salinity of bottom waters in Gizhiginsky Bay was about 33.4–33.6 in the years with an absence of the CC and increased to 33.7–33.9 (up to 34.1) in the years with an intensive CC. The year-to-year variability of bottom water salinity in Gizhiginsky Bay correlates with the salinity in the shore zone of northern and central West Kamchatka with coefficient $R = 0.90$ – 0.70 .

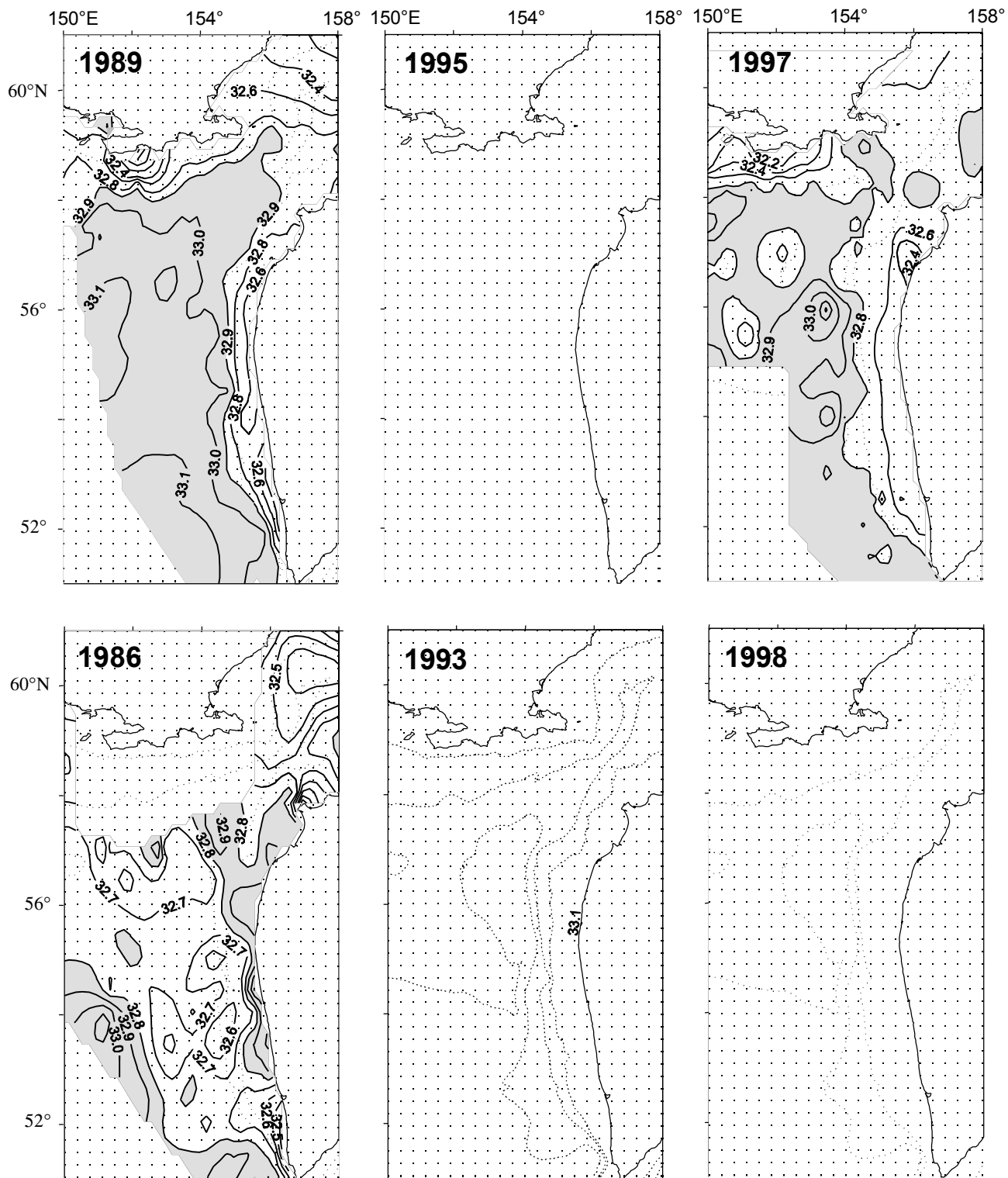


Fig. 3 Typical distribution of surface salinity (psu) in April: (top) in the years with an absence of the CC and (bottom) in the years with an intensive CC. Shaded areas show higher salinity water.

The availability or absence of the CC significantly influences the water temperature in the convective layer from the surface to depths of 100–150 m. In April, the temperature of these depths and bottom temperature between the coast and the 100-120 m isobath is lower in the years with an intensive CC than in the years of its absence. For example, the temperature at 100 m was defined as “warm” or “normal” in the years with an absence of the CC and was defined as “cold” or “normal” in the years with an intensive CC. In other warm periods, the temperature anomaly was in the dichothermal layer with a probability of about 60–70%. If the Compensatory Current was stable and available in the summer months, the significant negative temperature anomalies and high positive salinity anomalies were observed in all water layers between the coast and 70–100 m isobath.

The combined charts of areas with cyclonic or anticyclonic water circulation were drawn for specified clusters of years. The analysis allowed us to conclude that the central location of cyclonic circulation in the northern Okhotsk shelf shifted to the south in the range of from 54°50′N–56°30′N to 53°20′N–56° 00′N – in cold years with an in-

tensive CC (Fig. 4). The centres of anticyclonic circulation were between 155°E and the coast in the years with an absence of the CC. In this case, in the summer, the highest values of surface layer temperature and thickness as well as accumulation of river discharge were observed there. The areas with these parameters shifted to 30–50 miles from the coast in the years with an intensive CC, followed by the displacement of anti-cyclonic circulation

The vorticity of the current varied considerably from year to year. The number of the closed and semi-closed eddies from dynamic topography charts grew from 4–7 to 11–20, in case of an intensive CC. Davydov (1975) also noted that eddying increased during cold years in area west of the WKC. He explained this fact by a weakening of the WKC. We have not found the same direct correlation. Eddying and temperature variability depend on the intensity of both Currents, but the temperature range of the convective layer in spring and the temperature range of the dichothermal layer in summer depend rather more on the CC intensity than on the intensity of the WKC.

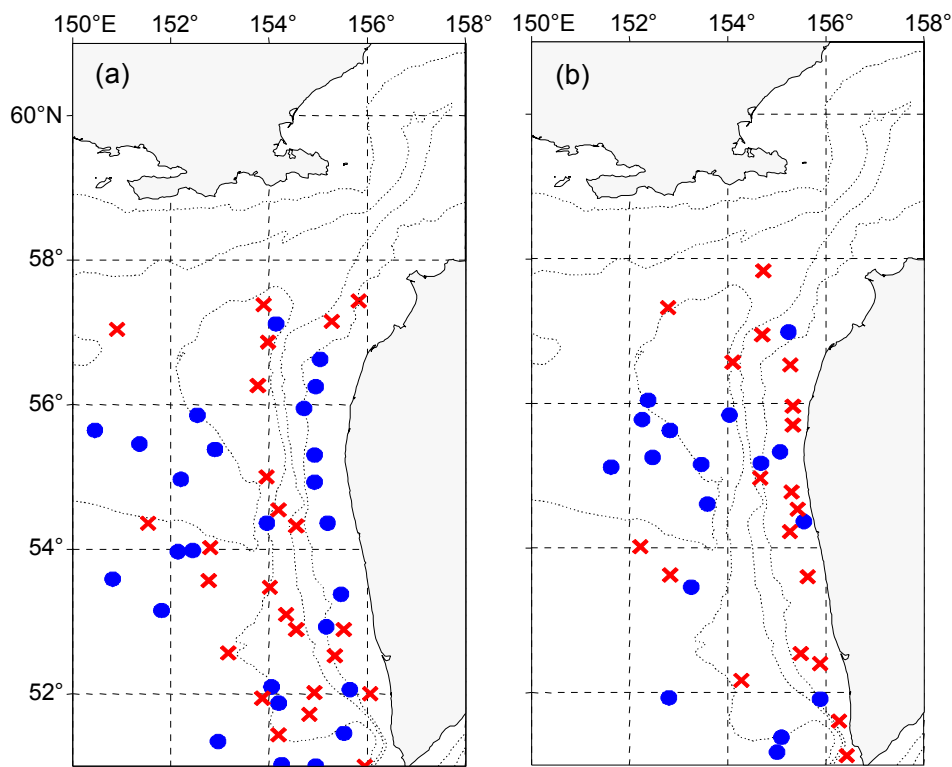


Fig. 4 Combined locations of cyclones (solid circles) and anti-cyclones (crosses) in April in (a) years with an intensive CC and (b) years with the absence of the CC.

It is common knowledge that the variability of oceanological conditions influences the distribution and reproduction of living organisms. The conditions in a coastal zone play a special role because it is a place of spawning and an environment for eggs, larvae and younger generations of many species. We have found that the availability or absence of the coastal CC influences the oceanological conditions in this zone. Further, we have analysed spawning ground sites and pollock egg distributions in the years with intensive parameters and those with a weak CC. The distribution of pollock eggs of the first embryogeny stage was used as an indirect indicator of spawning ground locations. The distribution of eggs of the later stage was used to determine the direction of its drift. Some data on pollock egg distributions in all stages of growth in the years with an intensive or weak CC are presented in Figure 5. The following conclusions have been drawn:

1. In the years with an intensive CC, the main pollock spawning grounds were located to the south of 55° – 54.5° N. In the years with an absence of the CC the main pollock spawning grounds were found north of 55° N.
2. In the years with an absence of the CC, spawning takes place at the 40–100 m isobath; in the years with an intensive CC spawning occurs at 60–150 m.
3. The more northern the spawning grounds lie, the deeper spawning takes place. It is well correlated with the location of a pre-bottom frontal zone formed by the lower edge of the convective layer.
4. Repeated observations show that pollock eggs are more often advected in the southern direction and farther off the coast in the years with an intensive CC. In the years with an absence

of the CC, pollock eggs more often drift northward and towards the coast.

5. It is possible to assume that upwelling and divergence of water both accompany the cyclonic circulation of CC water, and may move some eggs not only from the coast, but also to the surf wave zone. Upwelling, together with the higher density of CC water, may keep pollock eggs in the surface layer longer than in years of CC absence.

In the years with an absence of the CC, productivity of young pollock generations had “normal” or “high” levels. In the years with an intensive CC, productivity of young pollock generations had “normal” or “low” levels.

In conclusion, some words about the probable reasons for CC formation are offered. The first and only hypothesis is hinted at by the name of the current – it partially compensates the transport of WKC water. However, an intensive CC was observed in the years with small, as well as large transport of WKC water to the northern part of the Okhotsk Sea. Probably the intensity of the CC depends rather on the inflow of WKC waters into Shelikov Bay. This needs further investigation.

It is interesting to note the regular concurrence of years with an intensive CC and the bottom salinity increase in Gizhiginsky Bay. Probably these phenomena are caused by specific atmospheric influences. For example, the increase of northern winds in winter over the Okhotsk Sea can cause sea level lowering and wind-induced upwelling along West Kamchatka, and polynya formation along the northern coast of the Sea. The latter serves as a favorable condition for the intensive formation of salty bottom water, including that in Gizhiginsky Bay. We plan to make this the subject of the further research.

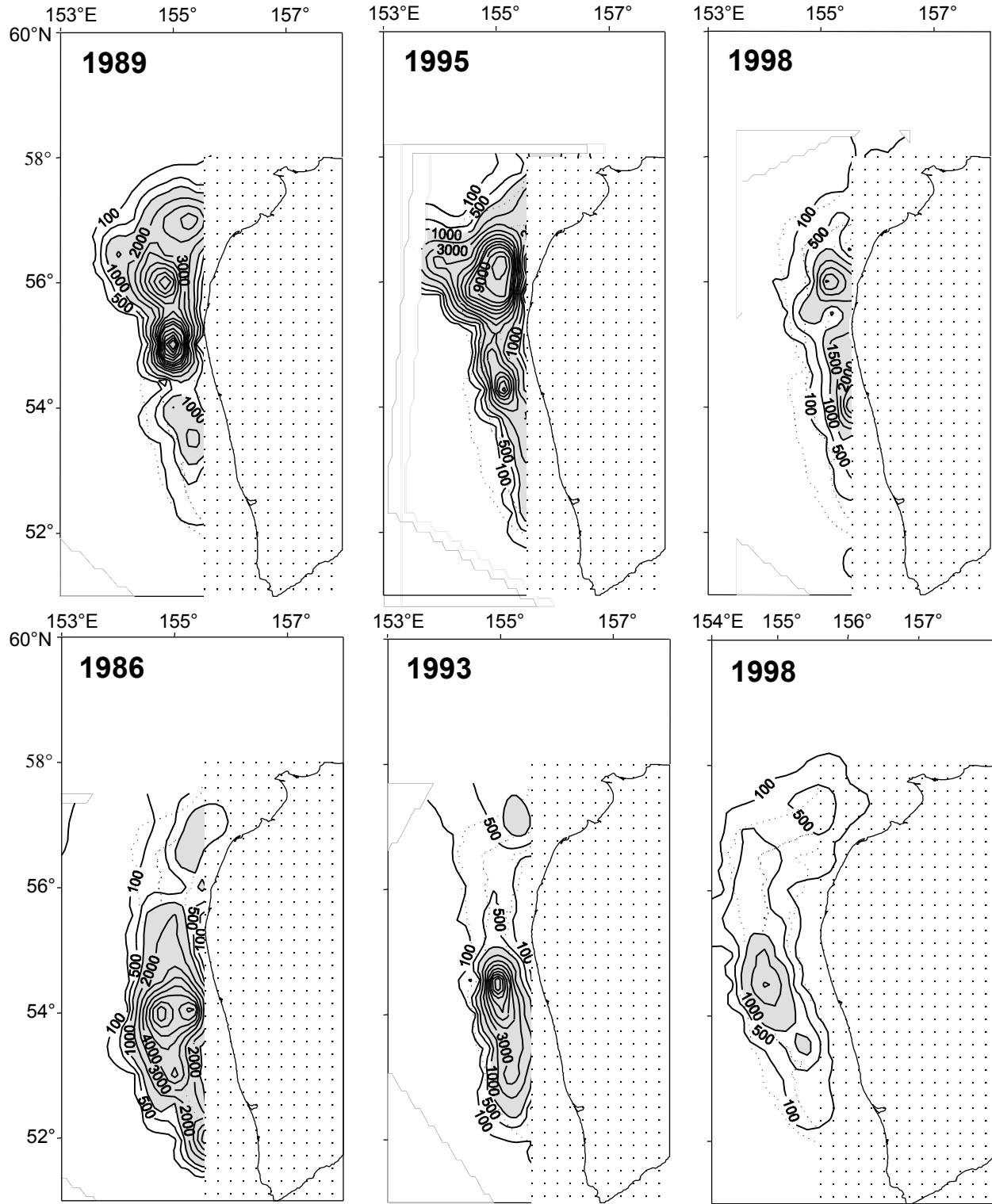


Fig. 5 Typical distribution of pollock eggs in April in (top) the years with an absence of the CC and (bottom) the years with an intensive CC.

References

- Chernyavsky, V.I. 1981. Circulation systems in the Sea of Okhotsk. *Proc. TINRO*, 105, 13–19. (in Russian)
- Davydov, I.V. 1975. The water regime of the West-Kamchatka shelf and certain features of the behaviour and reproduction of commercial fishes. *Proc. TINRO*, 97, 63–81. (in Russian)
- Kajiura, K. 1949. On the hydrography of the Okhotsk Sea in summer. *J. Oceanogr. Soc. Japan*, 5, 19–26. (in Japanese)
- Leonov, A.K. 1960. The Sea of Okhotsk. In *Regional Oceanography. Part 1*. Gidrometeoizdat, Leningrad, 765 pp.
- Luchin, V.A. 1987. Water circulation in the Sea of Okhotsk and its specific interannual changeability as a result of diagnostic circulation. *Proc. FERHRI*, 36, 3–13. (in Russian)
- Sarkisyan, A.S. 1977. The diagnostic calculations of a large-scale oceanic circulation. pp. 363–458. In *The Sea, Marine Modelling, Vol. 6*, John Wiley, New York.

Transport and turbulence characteristics for the northeastern Sakhalin shelf conditions

Igor E. KOCHERGIN and Alexander A. Bogdanovsky

Far Eastern Regional Hydrometeorological Research Institute, Vladivostok, Russia

Introduction

To understand the dynamics of pollutants, one should know their transport characteristics (conditioned by velocities of currents and particles) and calculated turbulent parameters (vertical and horizontal turbulence caused by shift instability, surface disturbance, near-bottom friction, and other factors).

Transport characteristics, responsible for the trajectory of pollution migration, can be accurately calculated for the set of hydrometeorological situations by means of wind and current characteristics and other factors.

Determination of turbulent parameters is a more complicated task, as, due to the absence of unified descriptive methods, much depends on a modeler's expertise and approach to the problem. For applied purposes, turbulent parameters can be calculated by two approaches, analogous to Euler and Lagrange media equations. For numerical modeling, the method of "Monte-Carlo" (Lagrange equation), using turbulent parameters set up as the rate of turbulent fluctuations, provides many more possibilities. Turbulence parameters of a definite zone are conditioned by hydrometeorological and hydrological factors, with sea water temperature, salinity, density, surface waves, currents and wind being the most important.

Model description

Pollutant transport and the sedimentation zone have been calculated by means of a three-dimensional advective-diffusive model based on the "Monte-Carlo" method using the generator of random numbers for non-determined processes imitation in accordance with Ozmidov (1986).

The basic equations describing the trajectories of migrating markers are as follows:

$$\frac{dx}{dt} = u(x_i, y_i, z_i, t) + u'(x_i, y_i, z_i, t);$$

$$\frac{dy}{dt} = v(x_i, y_i, z_i, t) + v'(x_i, y_i, z_i, t); \quad (1)$$

$$\frac{dz}{dt} = w(x_i, y_i, z_i, t) + w'(x_i, y_i, z_i, t) + w_0(x_i, y_i),$$

where,

- x_i, y_i, z_i - coordinates of the i -marker;
- u, v, w - velocity components of water motion (currents);
- u', v', w' - rate components of turbulent fluctuations;
- w_0 - sedimentation rate of TSS (total suspended solids).

Concentration of pollutants in volume V is determined in accordance with weight and distribution of markers.

$$C = \frac{\Delta n \cdot P}{\Delta V \cdot m}, \quad (2)$$

where,

- Δn - number of markers in volume ΔV ;
- P - source capacity (kg/s);
- m - number of markers released in a time unit.

The conditions set at the boundaries are partial sedimentation, evaporation, or reflection, depending on the specific characteristics of these boundaries and pollutants. Reflection or sedimentation numbers are conditioned by the adhesion coefficients. For the bottom boundary these coefficients are determined in accordance with Beloshapkov (1994a,b).

The sedimentation rate of the TSS phase w_0 for light and medium fractions in (1) is found over the balance equation of three forces for ball-shaped particles of the given equivalent radius (Kurganov, 1973):

$$W_0 = \frac{g(\mathbf{r}_i - \mathbf{r}(z))l_i^2 \sqrt{1 + 0.862 \lg k}}{\mathbf{m}(\mathbf{r}(z))(18 + 0.61\sqrt{g(\mathbf{r}_i - \mathbf{r}(z))l_i^3 / (\mathbf{m}^2 \mathbf{r}(z))}} \quad (3)$$

where,

- l_j - characteristic diameter of a particle;
- r_i - specific weight of a particle;
- $r(z)$ - water density;
- k - geometric shape coefficient;
- μ - viscosity coefficient determined from the empirical equation; for fresh water it is as follows:

$$m = \frac{0.01775}{1 + 0.0337t + 0.000221t^2}, \quad (4)$$

where, t - temperature ($^{\circ}\text{C}$).

Based on the concept of normal spectrum distribution of ocean turbulence, one can write the equation of fluctuating rate components in (1) for each statistic test:

$$\begin{aligned} u' &= \mathbf{s}_u \sqrt{-2 \cdot \ln P} \cdot \text{sgn}(\mathbf{I}); \\ v' &= \mathbf{s}_v \sqrt{-2 \cdot \ln P} \cdot \text{sgn}(\mathbf{I}); \\ w' &= \mathbf{s}_w \sqrt{-2 \cdot \ln P} \cdot \text{sgn}(\mathbf{I}), \end{aligned} \quad (5)$$

where,

- P - random value uniformly dispersed in interval $\{0;1\}$;
- \mathbf{I} - randomly takes the values 1 and -1 .

The equations of root-mean-square deviations are derived from the assumption that the basic dispersion value is directly conditioned by the current (Pukhtyar, 1981) together with wind and near-bottom corrections produced by in-a-row expansion of parametrization of the wind waves effect (t) on turbulence $a \approx k_1 z t \exp(-k_2 z)$ and parameterization of the near-bottom friction effect (near-bottom friction is proportional to $(z-h)^2$).

Thus, the equation of the turbulent fluctuation rate is as follows:

$$\begin{aligned} \dot{\sigma}_u &= \sqrt{2 + 0.196v_x^2 + 0.076v_y^2} \\ &\quad * (K_1 + K_2 \exp(-Az) + \frac{K_3}{\hat{\alpha}h - z)^2 + 1}); \\ \dot{\sigma}_v &= \sqrt{2 + 0.196v_y^2 + 0.076v_x^2} \\ &\quad * (K_1 + K_2 \exp(-Az) + \frac{K_3}{\hat{\alpha}h - z)^2 + 1}); \\ \dot{\sigma}_w &= \sqrt{\dot{\sigma}_u^2 + \dot{\sigma}_v^2} * f(Ri), \end{aligned} \quad (6)$$

where,

- v_x, v_y - liquid current velocities (cm/s);
- K_1, K_2, K_3 - parameters of relative contribution of various processes into agitation;
- α - scale of the surface disturbance effect (wind waves);
- β - near-bottom conditions effect (sea floor features);
- γ - transition parameter characterizing the mean relation between horizontal and vertical diffusion (0.083 number is used)
- $f(Ri)$ - function determined by the Richardson criterion, that decreases turbulent mixing under stable stratification and intensifies it under unstable stratification conditions.

General pollution transport tendencies in the area of the northeastern Sakhalin shelf

Accidental spills are dangerous by over-the-sea-surface migration of pollutants with positive floatability (oil spills). The sedimentation rate of the pollutants with negative floatability is high and they easily precipitate and mix in the sea water column, thus impacting a smaller area. However, the role of turbidity tails produced by drilling mud and cutting in oil drilling operation must be estimated by the impact assessment provided.

Generalization of hydrometeorological data collected in the area of northeastern Sakhalin shelf helped to distinguish the following typical seasons:

- Summer, July–September (September – the highest mean sea water temperature, although wind regime tends to change);
- Autumn, October–December (characterized by intensive northwestern winds and the absence of unbroken ice cover);
- Winter (ice), January–April (fast ice and unbroken ice cover);
- Spring, May–June (ice cover destruction and the beginning phase of summer thermohaline structure formation).

The wind regime has been characterized, statistics have been analyzed, and duration characteristics of situations and correlation of one-into-another-situation transits have been studied for summer and autumn. Figures 1 and 2 illustrate the reoccurrence distribution and characterization of situations for summer and autumn. For the distinguished wind situations, the total current fields have been constructed. Modal long-time data rows have been constructed with the help of reoccurrence characteristics and the total component of currents. Comparative reoccurrence characteristics of the model current and observation row data for autumn are shown in Figure 3.

The northeastern Sakhalin shelf is characterized by intensive currents with predominant along-shoreline transport and high tidal current velocities. In summer winds get weaker, the predominant vectors are south and southeastern. The possibility exists for pollutants to migrate slightly northward. Weak and moderate winds can cause the pollutants transported by surface currents to migrate westward (to a shoreline) rather than eastward. This was also proved by the correlation analysis of synchronous observations of wind and currents. Due to greater reoccurrence of strong winds directed eastward, the probability for pollutants to migrate to a shoreline can increase. During a 10-day period an oil spill can transfer at a distance of 200 km.

In autumn, winds intensify and change their direction, northern and western components become

predominant. Accordingly, an oil spill transported by surface currents will migrate south and south-eastward. The probability for pollutants to migrate to a shoreline is 1.5–2 times greater than in summer. Under the influence of typical autumn northwestern winds, an oil spill can cover 400 km in 10 days.

In winter, when the sea in the area under discussion is clean and semi-clean, the tidal currents tend to slow down with transport direction and turn southward. With mean velocity 20 cm/s, the total transport can cover 150 km to the south in 10 days.

Sedimentation rate of TSS

The sedimentation rate of TSS depends mostly on grain size and less on sea water density. The characteristic diameter of bottom soil, drilling mud and cutting grains ranges between 1.5 and 0.005 mm with the main bulk of solids being over 0.1 mm in diameter. For this size variety of grains, the characteristic sedimentation rate ranges between 5 and 0.0005 cm/s. Intensive summer stratification may have a different sedimentation rate of TSS in the surface and near-bottom layers which depends on hydrology. In the surface layer it may be 20% higher than in the near-bottom layer. It should be stressed that when very large volumes are discharged, the sedimentation rate increases due to the “lump” effect, where the main bulk of discharged solids precipitates as a relative body large in size. Thus, sedimentation characteristics and the dimensions of the zones impacted due turbulence depend mainly on fractional composition and process intensity. Calculations showed that most (80%) of the drilling mud and cutting discharged in course of drilling operations precipitate within several hundred meters around the source, which agrees with the results of other model applications (O’Reilly, 1989).

Parameters of turbulent fluctuation rate

The dispersion of meridional, zonal, and vertical components of turbulent fluctuations was calculated from equations (6) for the surface and near-bottom horizons. Parameter α has been selected as the value to be inversely proportional to the characteristic scale of wind waves effect, $0.25 L$, where L is the characteristic wind wave length. For deep water, the wavelength is calculated from

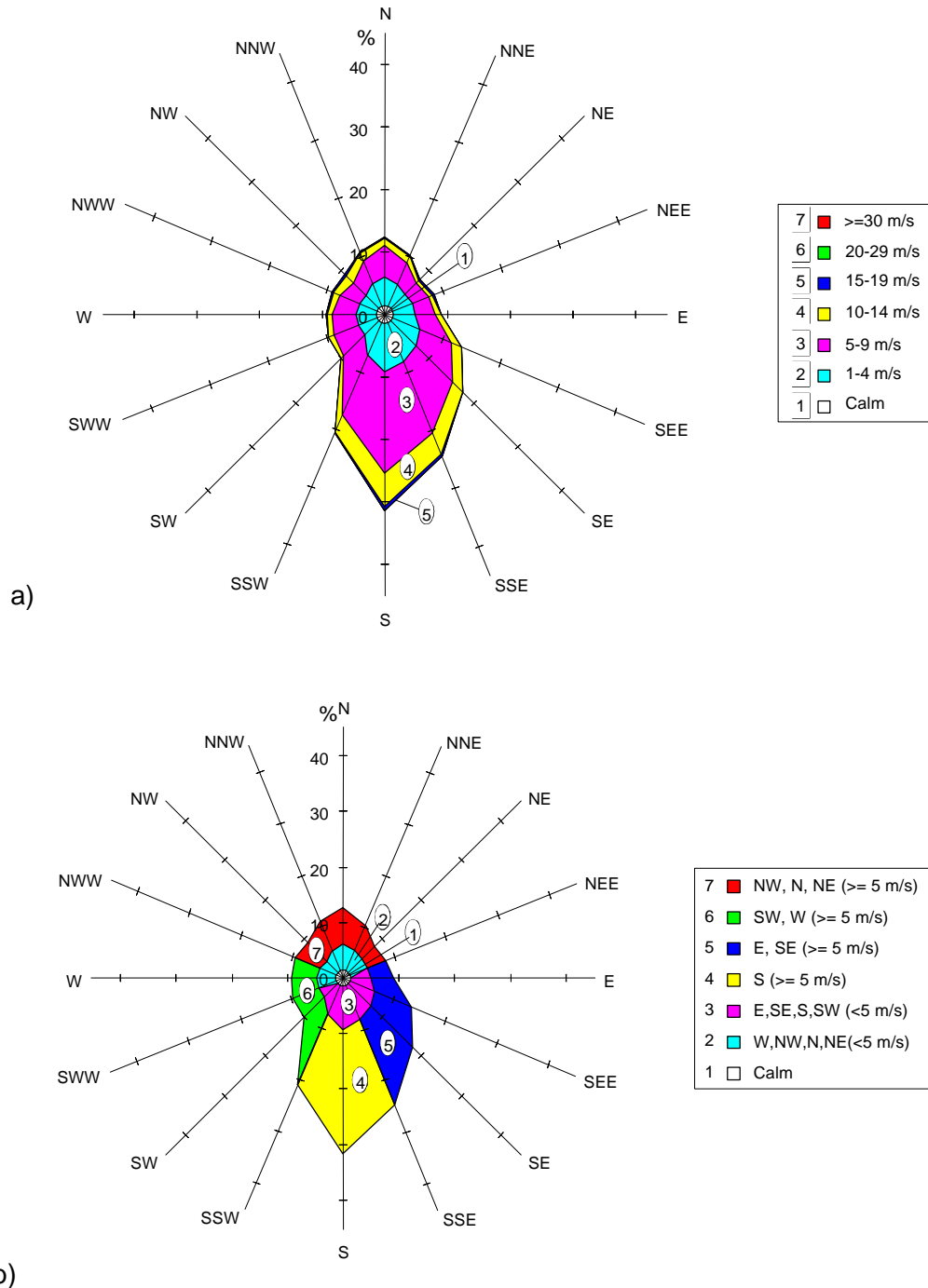


Fig. 1 (a) Summer recurrence of wind vectors and velocity (based on on-route ship observations) and (b) typical wind situations over the direction and velocity parameters for a summer season

relation $L=T^2 * g / 2p$, where T is the period of wind waves. Parameter **b** characterizes the thickness of the bottom boundary layer. For mean velocities of near-bottom currents this parameter is assumed equal 0.16. Coefficient K_1 was determined experimentally, and was found to be in the range 0.5–1.0. Coefficient K_2 was

estimated in the range 0.1–0.5 over wind characteristics (we used 0.03 as wind velocity magnitude). Coefficient K_3 was assumed equal to 0.1–0.2.

An exponential equation for stable stratification characteristics usually proved to be the best. So,

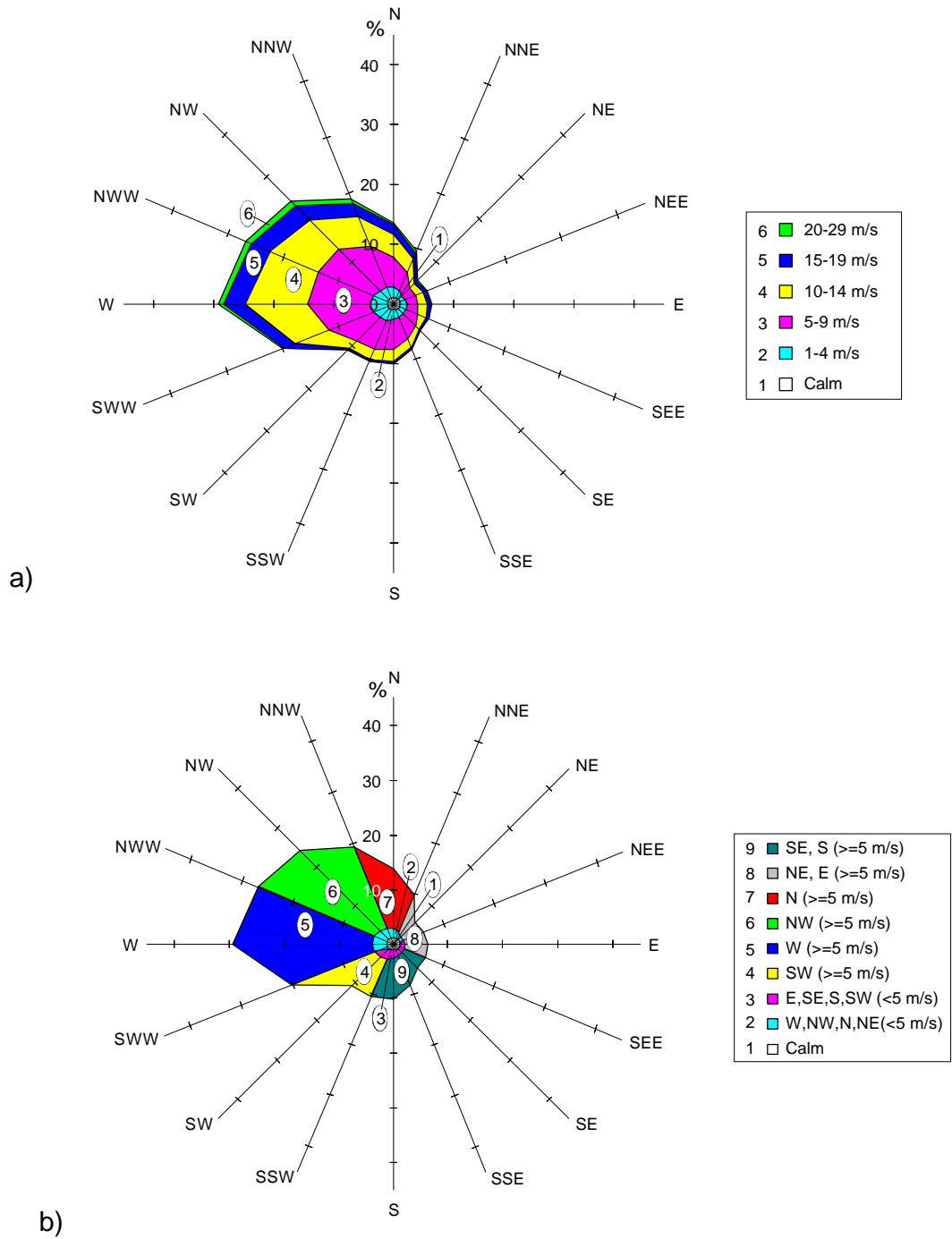


Fig. 2 (a) Autumn reoccurrence of wind vector and velocity (based on on-route ship observations) and (b) typical wind situations over the direction and velocity parameters for an autumn season

we assumed $f(Ri) = \exp(-1.1 * Ri)$.

Variability intervals of current velocity magnitude for the northeastern Sakhalin shelf are:

- summer season - 20–70 cm/s;
- autumn season - 25–100 cm/s;
- winter season - 10–30 cm/s.

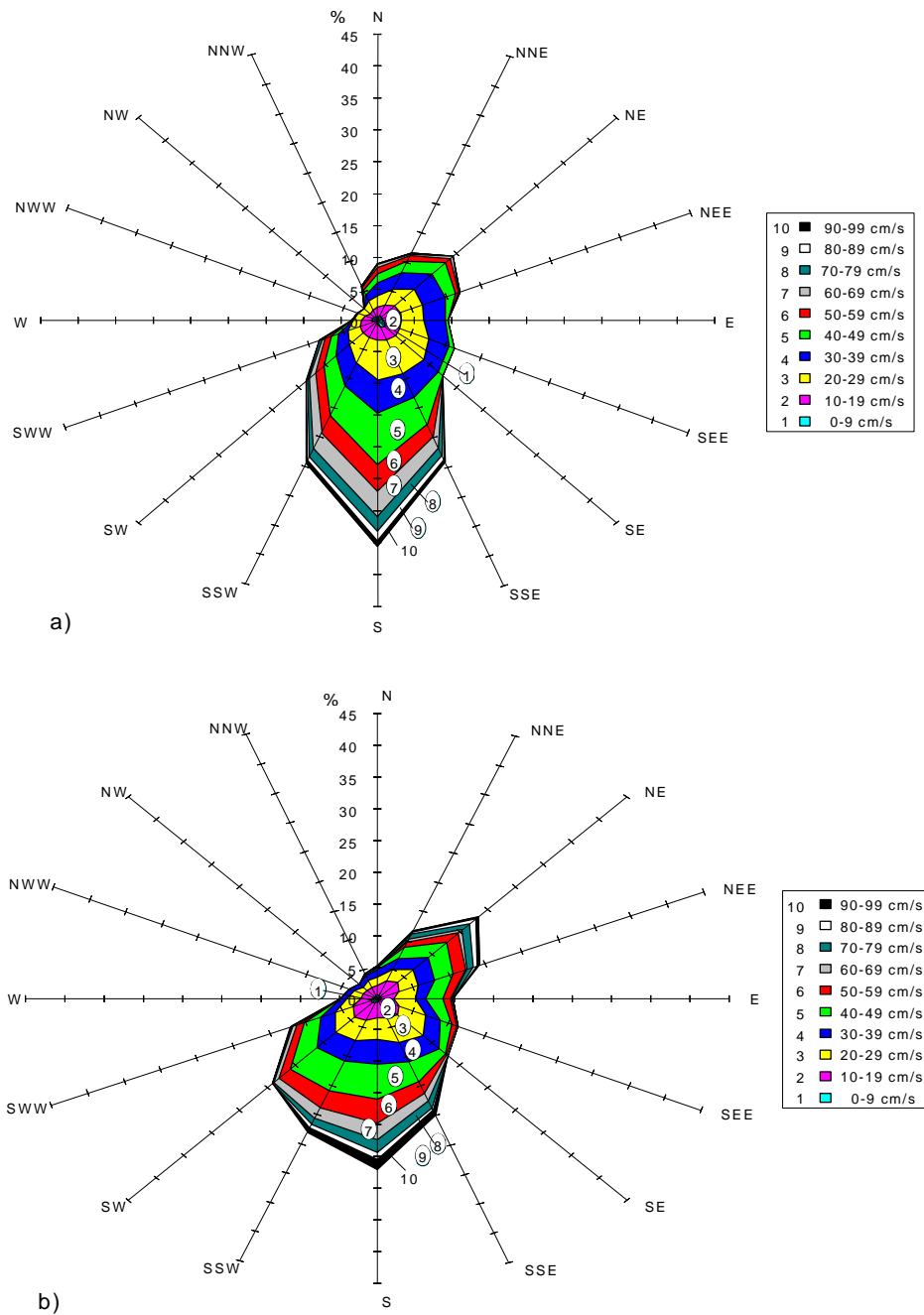


Fig. 3 Autumn reoccurrence of total currents in the area of the Arkutun-Dagi oil field calculated for a typical wind situation (a) and the comparative reoccurrence table of current direction and velocity developed on the basis of real data collected in September–October 1996 (b).

Figure 4 demonstrates the calculated graphs of mean seasonal dispersions of turbulent fluctuations, used in equations (1).

The analysis of instrumental data series added some understanding to the observed dispersion

although the analyzed information was not sufficient to assess the turbulent properties of the characteristic surface waves. The method of instrumental data series processing included:

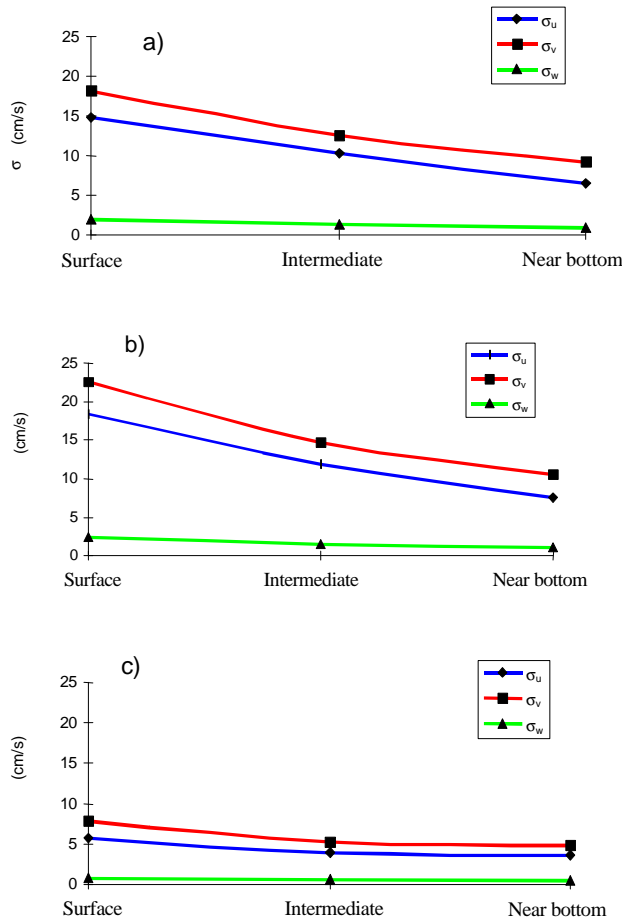


Fig. 4 Mean turbulence dispersion: (a) in summer, (b) in autumn and (c) in winter.

- distinguishing of tidal component;
- analysis of the time needed to reconstruct the fields of tidal currents under the influence of meteorological factors (determination of the time lag row coefficient);
- smoothing of a non-tidal data row by filtration methods with a characteristic time lag;
- distinguishing of the smoothed trend from a non-tidal data row;
- dispersion analysis (components inclusive).

Characteristic values of turbulence fluctuation components (velocity dispersion), obtained by means of the above-described technology with

the help of instrumental observations are as follows:

- in summer - 3–6 cm/s;
- in autumn - 5–11 cm/s.

Different approaches to the turbulence problem may produce different dispersion values. However, the reported dispersion assessments generally describe seasonal and weather conditions. These assessments were tested with experimental results and compared with calculations from different models.

Acknowledgment

The authors acknowledge Sakhalinmorneftegas Shelf JS Co. Ltd. for the support it rendered to get the transport model verified.

References

- Beloshapkova, S.G. and Beloshapkov, A.B. 1994a. Mechanics of particle separation under the influence of coherent structures in water currents (model of filtration suspension). *Oceanologiya*, 34(1), 127–132.
- Beloshapkova, S.G. and Beloshapkov, A.B. 1994b. Mechanics of particle separation under the influence of coherent structures in water currents (overturning model). *Oceanologiya*, 34(4), 527–532.
- Kurganov, A.M. and Fedorov, N.F. 1973. *Reference Book of Hydraulic Assessments for Water Supply and Canalization Systems*. Stroyizdat, Leningrad, 408 pp.
- O'Reilly J.E., Sauer, T.C., Ayers, R.C., Brandsma, M.G. and Meek, R. 1989. Field verification of the OOC mud discharge model. *Drilling Wastes*. New York, pp. 647–665.
- Ozmidov, P.B. 1986. *Diffusion of Suspended Matter in the Ocean*. Gidrometeoizdat, Leningrad, 280 pp.
- Pukhtyar, L.D. and Osipov, Yu.S. 1981. Turbulent characteristics of the coastal sea. *Proc. State Oceanogr. Inst.*, 158, 35–41.

Modeling of oil spills for the shelf conditions of northeastern Sakhalin

Igor E. KOCHERGIN¹, A.A. Bogdanovsky¹, V.D. Budaeva¹, V.G. Makarov¹,
V.F. Mishukov², S.N. Ovsienko³, V.F. Putov⁴, L.A. Reitsema⁵, J.W. Sciallabba⁵,
O.O. Sergusheva⁵ and P.V. Yarosh²

¹ Far Eastern Regional Hydrometeorological Research Institute, Vladivostok, Russia

² Pacific Oceanological Institute, Vladivostok, Russia

³ State Oceanographic Institute, Moscow, Russia

⁴ Ecological Company of Sakhalin, Yuzhno-Sakhalinsk, Russia

⁵ Sakhalin Energy Investment Co. Ltd., Houston, USA/Yuzhno-Sakhalinsk, Russia

Introduction

Shelf oil and gas fields of northeastern Sakhalin to be developed in the near future bring forth the risk of oil spills which may occur in the course of oil production and transportation. Oil field behavior modeling has been carried out for potential sources located in the area of the Piltun-Astokhskiye oil field and Terpeniye Cape along the route of oil transportation. Statistical regularities of oil spill migration have been studied on the basis of 158 ten-day hydrometeorological scenarios modeled for summer and autumn seasons.

Methods and models

Various models and methods have been used to develop scenarios of ecological situations in the case of accidental oil spills, as well as their migration and evolution. The most important and complex models used to determine the dynamics and physical-chemical characteristics of an oil spill are as follows:

The model is used to construct the scheme of currents to determine the basic environmental parameters for spatial dynamics of oil spill migration under various hydrometeorological situations. The technology of current scheme estimation includes the model of non-tidal currents (Budaeva, 1997) and the technology of tidal current estimation over calculated harmonics;

the trajectory model of oil spill dynamics (describes oil spill migration under set hydrometeorological situations) (Harlow, 1964; Zatssepa, 1992);

the oil evolution model (describes physical-chemical processes taking place in a spill, such as evaporation, dispersion, emulsification, etc.) (Kuipers, 1981; Michoukov, 1997; Zatssepa, 1992).

Besides the above mentioned, the following models and methods were also used in calculations:

Statistical, correlation and interpolation methods for estimation of meteorological fields (re water, wind);

correlation methods to reconstruct and analyze interacting hydrometeorological elements were used to verify the methods and models (wind components and surface currents in particular);

estimation for ten-day scenarios based on typical hydrometeorological situations, accounting for reoccurrence and duration characteristics. The succession of events was determined with the help of the generator of random numbers and weighting coefficients from the transit correlation matrix.

Trajectory evolution model of oil spill dynamics

An oil spill is assumed to consist of a number of independent little oil spills. A little oil spill is made up of a finite number of markers representing the shape and distribution of oil within this spill. The behavior of an oil spill is divided into four phases: time lag; gravitational-viscous; phase of surface tension; migration and spreading due to the influence of wind and advective-turbulent processes.

The basic equations describing the trajectories of marker motion are represented as follows:

$$\frac{dx}{dt} = u(x_i, y_i, t) + u'(x_i, y_i, t) + w_u(x_i, y_i, t), \quad (1)$$

$$\frac{dy}{dt} = v(x_i, y_i, t) + v'(x_i, y_i, t) + w_v(x_i, y_i, t),$$

where,

x_i, y_i – current coordinates of the i -marker;
 u, v – liquid (currents) velocity components;
 u', v' – turbulent pulsation rate components;
 w_u, w_v – wind components.

$$\begin{aligned} w_u(x, y, t) &= k \times W_u(x, y, t), \\ w_v(x, y, t) &= k \times W_v(x, y, t), \end{aligned} \quad (2)$$

where,

W_u, W_v – zonal and meridional components of the near water coefficient;
 k – wind transport coefficient (in this particular case it is assumed equal to 0.017).

The given equations below were developed from the assumption that the basic dispersion value is conditioned by the current, with wind correction added:

$$\begin{aligned} s_x &= (\sqrt{2 + 0.196v_x^2 + 0.076v_y^2}) * K \\ s_y &= (\sqrt{2 + 0.196v_y^2 + 0.076v_x^2}) * K, \end{aligned} \quad (3)$$

where,

v_x, v_y – liquid current velocity in cm/s,
 K – wind addition parameter.

Equations of oil spreading:

$$\begin{aligned} \frac{d^2R}{dt^2} &= -\frac{3\ddot{A}V_0g}{2\ddot{\partial}R^3} + \frac{3\ddot{\partial}\ddot{\partial}R^t}{\ddot{n}_0^tV_t} + \frac{1}{R}\left(\frac{dR}{dt}\right)^2 \\ &\quad - \frac{2.17\ddot{n}_w\dot{1}^{1/2}R^{3/2}}{\ddot{n}_0^tV_t}\left(\frac{dR}{dt}\right)^{3/2} \\ &\quad - \frac{3\dot{1}_0^t dR}{2R^2 dt} \end{aligned} \quad (4)$$

$$\frac{dR}{dt} = U = \int_0^t \left(\frac{d^2R}{dt^2} \right) dt \quad (5)$$

$$R = \int_0^t \left(\frac{dR}{dt} \right) dt \quad (6)$$

$$R_{max} = \left(\frac{V_0 * 10^5}{P} \right)^{1/2} \quad (7)$$

where,

t – time passed from the moment oil began to spread [s];
 R – spill radius at time t [m];
 $D = (r_w - r_0) / r_w$
 V_0, V_t – initial oil volume and volume of oil spread on the sea surface at time t ;
 $g = 9.8$ [m/s²];
 s^t, r_o^t, n^t – pressure of the spreading oil [n/m], density [kg/m³], kinematic viscosity [m²/s] of oil at moment t ;
 r_w, n_w – density [kg/m³] and kinematic viscosity [m²/s] of water;
 R_{max} – maximal radius of oil spill [m].

The time lag phase is characterized by sufficiently intensive spreading of oil over the sea surface under gravity. For the round oil spill with radius R and thickness h , we can write the following equation:

$$R \approx k_1 \cdot (\ddot{A} \cdot g \cdot V_t)^{\frac{1}{4}} \cdot t^{\frac{1}{2}}, \quad (8)$$

where, k_1 - unity order constant;

In the gravitational-viscous phase of oil spreading one shall account viscous friction in an oil film.

$$R \approx k_2 \left(\ddot{A} \cdot g \cdot V_t \cdot \dot{i}_w^{-\frac{-1}{2}} \right)^{\frac{1}{6}} \cdot t^{\frac{1}{4}}, \quad (9)$$

where, k_2 – unity order constant.

The equation of oil spreading at the phase of surface tension is as follows:

$$R \approx k_3 \cdot \left(\frac{\dot{\sigma}_w^2 \cdot t^3}{\tilde{n}_w^2 \cdot \dot{t}_w} \right)^{\frac{1}{4}}, \quad (10)$$

where, k_3 – unity order coefficient.

The total volume of the oil evaporated from an oil spill is proportional to the spill square area. The expression for calculations is

$$\frac{d m_i}{dt} = \frac{U_*}{15.2} \left(\frac{D_i}{n_a} \right)^{0,61} \frac{x_i P_i}{R_a T_w} \left(p R^2 \right) \left(\frac{V_n}{V_s} \right) \quad (11)$$

$$U_* = 0.04 U_{10} \quad (12)$$

where, for i -group or an individual compound,

$m_i, x_i, P_i, D_i, r_i, M_i$ – number of moles, mole share, vapor pressure [Pa], coefficient of molecular diffusion in the atmosphere [m^2/s], density [kg/m^3], molecular weight [kg/mole] at water temperature (T_w , [K]) by atmospheric pressure;

n_a – kinematic air viscosity, [m^2/s];

R_a – gas constant;

U_*, U_{10} – dynamic wind velocity [m/s] and wind velocity 10 m above the surface [m/s].

The total oil volume evaporated is calculated by the following equation:

$$V_{ev} = - \sum_{i=1}^n \frac{M_i}{r_i} \int_0^t \left(\frac{d m_i}{dt} \right) dt \quad (13)$$

The rate of oil emulsification into water was assumed equal the wave height (H_w , [M]) and the volume of oil in the surface layer.

$$\frac{d V_{em}}{dt} = C_7 V_s H_w \quad (14)$$

where, C_7 – emulsification constant.

For a shallow sea with depth less than 40 m,

$$H_w = 0.07 \frac{U_{10}^2}{g} \left(\frac{g H_s}{U_{10}^2} \right)^{3/5} \quad (15)$$

where, H_s is the depth of the sea.

We assumed the rate of oil dispersion into water to be proportional to the wave height and volume of non-emulsified oil on the sea surface (V_{nem} , [M^3]):

$$\frac{d V_{dis}}{dt} = k_{em} V_{nem} H_w \quad (16)$$

where, k_{em} – emulsification coefficient.

In the course of modeling, we controlled the changes in:

$$V_s = V_0 - V_{ev} - V_{dis} - V_{lost}$$

$$V_{nem} = V_0 - V_{ev} - V_{em} - V_{dis} - V_{lost} \quad (17)$$

$$V_w = C_{wo} V_{em}$$

$$V_t = V_s + V_w$$

where,

V_0 – volume [m^3] of oil discharged;

V_s – volume of oil [m^3] on the sea surface at time t ;

V_{nem} – volume of non-emulsified oil [m^3];

V_w – volume of water [m^3] in water-in-oil emulsion;

V_{lost} – volume of lost oil [m^3] for other reasons;

V_t – total volume of oil and emulsion [m^3];

C_{wo} – coefficient of maximal emulsification of water into oil.

Estimation technique for hydrometeorological scenarios

The estimation technique for hydrometeorological scenarios consists of the following stages:

Development of a table of reoccurring meteorological situations over the data base of on-route ship observations and a corresponding reoccurrence table of the nearest on-land hydrometeorology stations;

selection of typical seasonal meteorological situations from the reoccurrence table;

calculation of spatial fields of near water wind corresponding to the calendar of the selected meteorological situations;

Determination of duration criteria for the selected meteorology and their over the duration factor, construction of correlation matrix;

calculation of generalized harmonic constants for the basic modes of the regional tidal currents supported by instrumental observations and construction of tidal current harmonics at the nodes of a spatial grid (in accordance with shallow water theory);

approximate calculation of wind–wave amplitude at the grid nodes;

construction of climatic density fields and boundary conditions for the model of non-tidal currents;

construction of non-tidal current fields for the selected meteorological situations;

filling the time interval of 15–18 ten-day scenarios for two seasons by typical meteorological situations according to the required statistics of reoccurrence and duration of situations;

construction of ten-day scenarios for selected situations using the transit correlation matrix, optimization of scenarios over the probability criterion;

preparation of the fields of total currents, wind, and waves for hydrometeorological situations and construction of calculated fields

at the nodes of a grid for each 1-h interval of ten-day scenarios, taking into account the condition of smooth transits;

visual control of oil spill migration within the studied scenarios with preliminary modeling over the trajectory model (when necessary, correction of the developed scenarios and/or removal of surplus information);

final preparation of hydrometeorological data for scenarios in the format required for modeling.

Modeling of the worst meteorological situations conditioning the quickest migration of an oil spill to a shoreline was made separately.

Modeling results of oil spills on the Sakhalin shelf

Some examples of modeling for real scenarios are illustrated in Figures 1–6. Figures 1 and 3 demonstrate the calculated trajectories of oil spills for 18 and 15 ten-day scenarios, developed for the northeastern shelf of the Piltun-Astokhskiye oil field and the eastern shelf of Terpeniye Cape. Figures 2 and 4 show the zones of potential impact for the calculated trajectories (Figs. 1 and 3). Figure 5 illustrates the evolution of oil spill characteristics (evaporation, dispersion, emulsification, etc.) 3 days after a “light-oil” spill in the area of the Piltun-Astokhskiye oil field. Figure 6 shows the dynamics of the oil spill square area modeled over 18 ten-day scenarios.

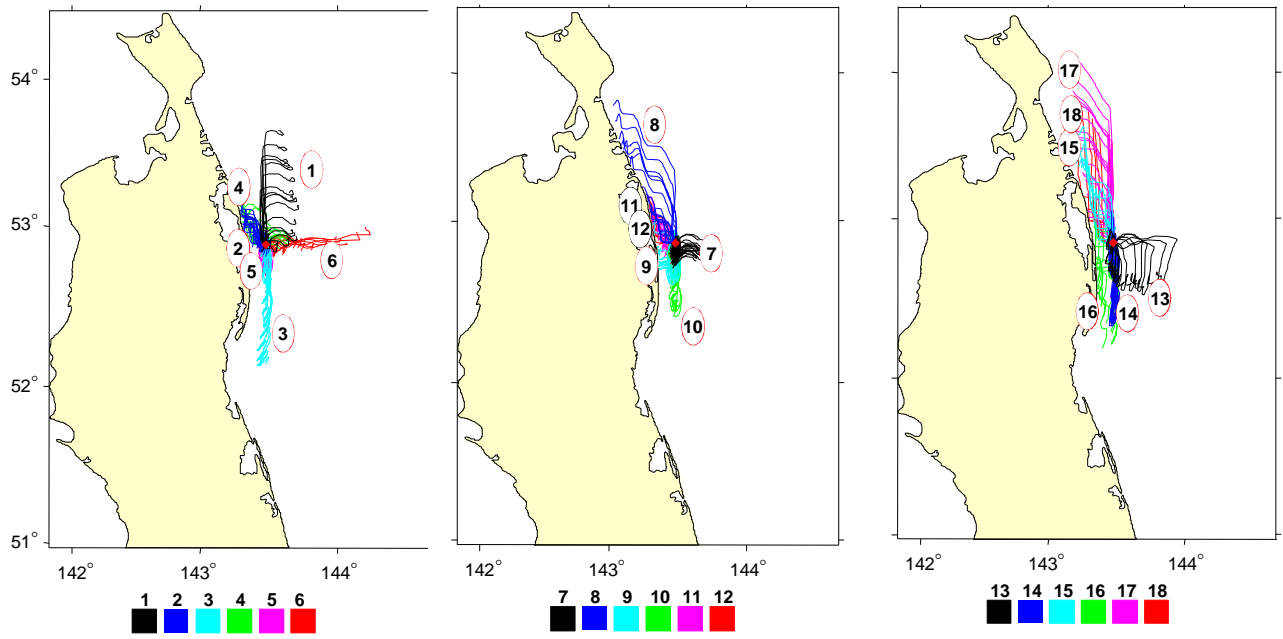


Fig. 1 Oil spill trajectory for 18 hydrometeorological scenarios, summer season, 3 days after the event. The source is in the area of the Piltun-Astokhskoye oil field, Sakhalin shelf.

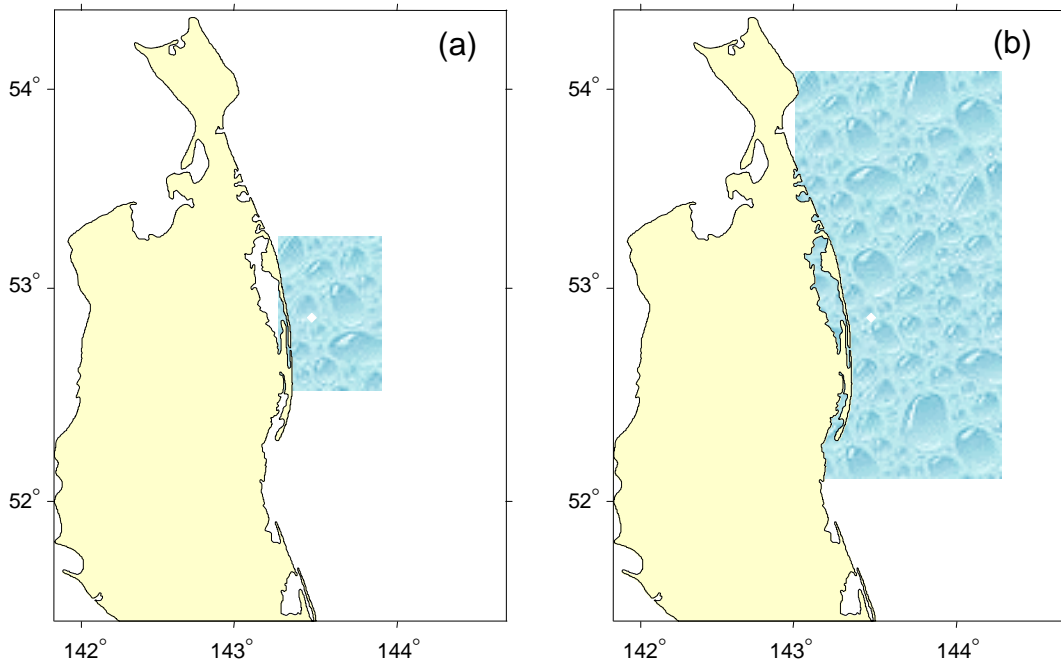


Fig. 2 Zone of potential impact for source located in the area of the Piltun-Astokhskoye oil field, Sakhalin shelf: (a) 1 day after the event and (b) 3 days after the event.

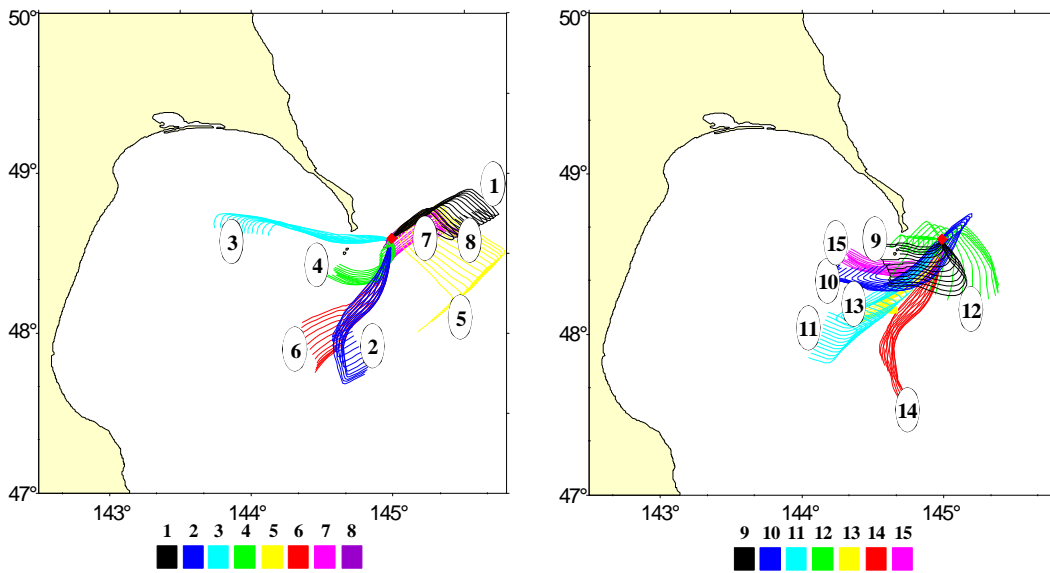


Fig. 3 Migration trajectories of an oil spill for 15 hydrometeorological scenarios, autumn, 3 days after the event. Source is in the area of Terpeniye Cape, eastern Sakhalin shelf.

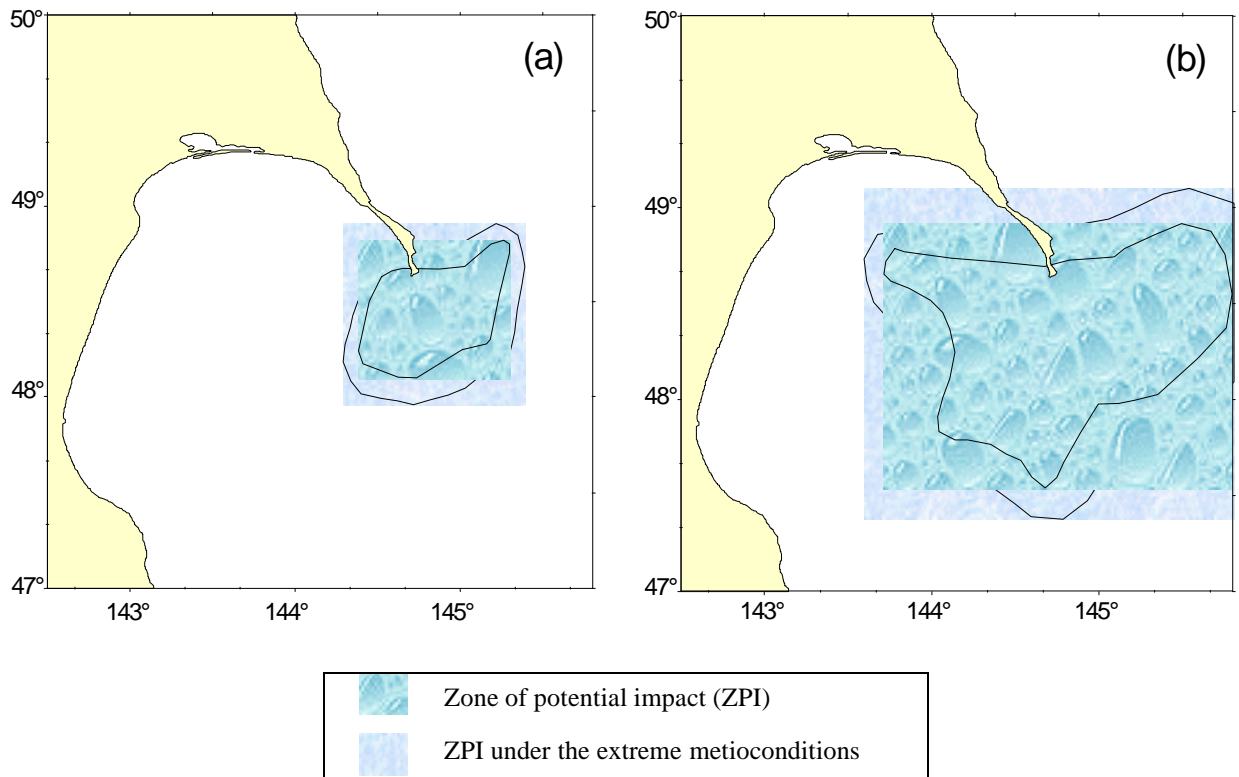


Fig. 4 Zone of potential impact of an oil spill (a) 1 day and (b) 3 days after the event. Source is in the area of the Terpeniye Cape, eastern Sakhalin shelf in the autumn.

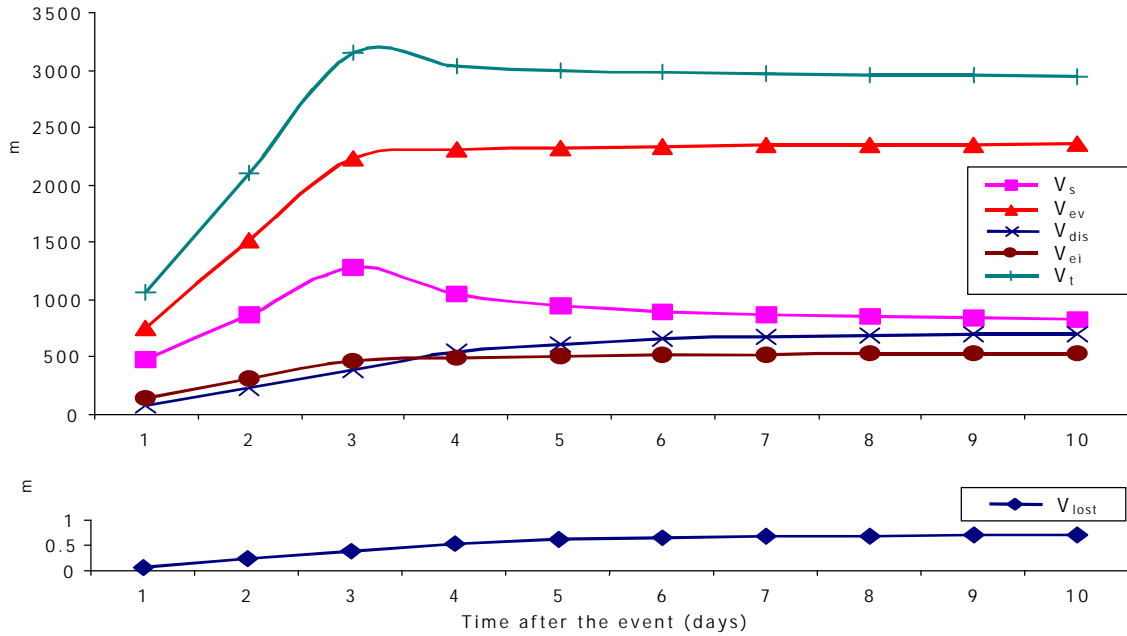


Fig. 5 Changing oil volumes 10 days after the event. Source is in the area of the Piltun-Astokhskoye oil field, Sakhalin shelf. Three days after the event, typical summer conditions: V_s is the oil volume on the sea surface, V_{ev} is the volume of the oil evaporated, V_{dis} is the dispersed oil volume, V_{em} is the emulsified oil volume, V_t is the total oil volume including water-in-oil emulsion, and V_{lost} is the oil volume lost in drops and other ways.

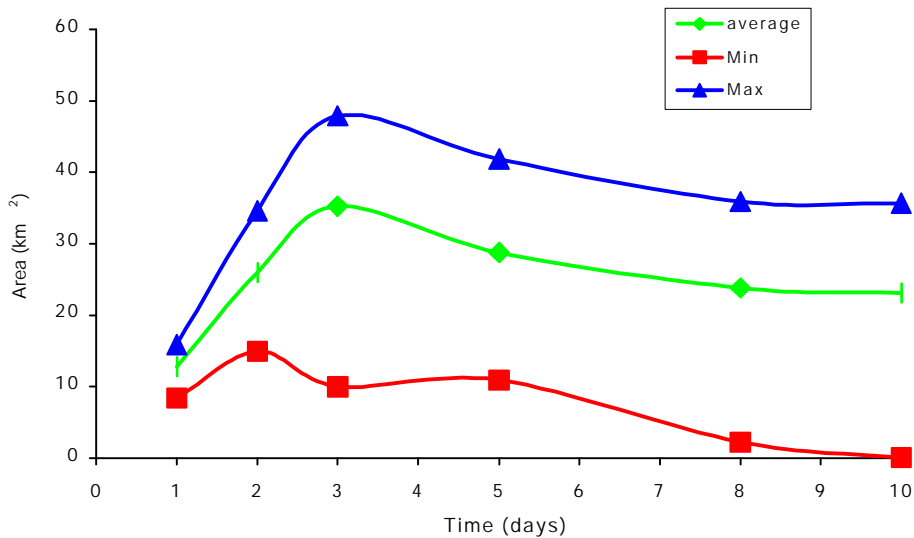


Fig. 6 Changing square area of an oil spill, ten-day evolution of the spill produced by the source located in the area of the Piltun-Astokhskoye oil field (3-day oil spill). Averaged, minimal, and maximal square areas were modeled for 18 ten-day summer scenarios.

Conclusions

1. The shelf of north-eastern Sakhalin is characterized by variable sea water dynamics: in summer oil films tend to migrate to the north, in autumn to the south, and in the area of Terpeniye Cape they mostly migrate to the south-east, south, and southwest.
2. Predominant hydrometeorological situations in the shelf area of northeastern Sakhalin for the sources are located closer to the shoreline (10–20 km) with conditions relatively equal for migration to the west and to the east both in summer and autumn, with distance from the shoreline (more than 20 km) where the eastward migration is better pronounced.
3. The probability of a spot spill migration to a shoreline within 10 days, for a source located 10–20 km away from a shoreline, is 35–55%, for a source located 20–30 km away from shore, it is 10–40%. The greatest probability of an oil spill reaching a shoreline in summer and autumn was observed on the third day.
4. In the worst hydrometeorological situations, the period during which an oil spill can reach a shoreline is estimated to be 8 h in summer and 11 h in autumn.
5. In accordance with oil characteristics, about 60% of the discharged oil will evaporate during the first several days; dispersion of oil into water for the modeled situations is not significant.

Acknowledgments

The authors acknowledge the information and financial support provided by Sakhalin Energy Investment Co. Ltd. for the works on oil spill modeling.

References

- Budaeva, V.D., Makarov, V.G. and Gavrilovsky, A.V. 1997. Seasonal Variability of currents in the area of eastern Sakhalin. *PICES Abstracts, Sixth Annual Meeting*, Pusan, Korea.
- Harlow, F.H. 1964. The particle-in-cell Computing Method in fluid dynamics. *Methods Comput. Phys.*, 3, 319–343.
- Kuipers, H.D. 1981. A simulation model for oil slicks at sea. Department of Civil Eng., Delft Univ. Tech., The Netherlands, pp. 1–168.
- Michoukov V. and Abramova, O. 1997. Experimental study of oil degradation in the Sea of Okhotsk. pp. 376–391. In *Proc. Intl. Mar. Sci. Symp. on Biogeochemical Processes in the North Pacific*, Japan Marine Science Foundation, Tokyo.
- Zatsepa, S., Ivchenko, A. and Ovsienko S. 1992. A local operative model for oil drift and dispersion. pp. 189–192. In *Proc. on Combatting Marine Oil Spills in Ice and Cold Conditions*, Helsinki, Finland, 1–3 December, 1992.

A peculiar water regime of currents in the area of the eastern Sakhalin shelf

Valentina D. BUDAeva¹ and Vyacheslav G. Makarov²

¹ Far Eastern Regional Hydrometeorological Research Institute, Vladivostok, Russia

² Pacific Oceanological Institute, Russian Academy of Sciences, Vladivostok, Russia

Introduction

The shelf zone of East Sakhalin is characterized by complex spatial–temporal variability of water circulation and current fields, hydrological characteristics and their vertical distribution. It is conditioned by the combined effect of multiple factors: atmospheric influence, intensive water exchange with open sea areas, inhomogeneous velocity fields of tidal currents promoting eddy formation, and the Amur water influence (Leonov, 1960; Moroshkin, 1964; Moroshkin, 1966). Although the shelf is promising for the regional economy, it is poorly studied. This is true for mostly late autumn and winter; due to severe and long winters, observations were carried out mostly during the warm seasons.

The concept of water circulation in the area has been developed on the basis of the dynamic method (Leonov, 1960; Moroshkin, 1964; Moroshkin, 1966) and numerical modeling carried out for the Okhotsk Sea at large (Kozlov, 1972; Zyryanov, 1977; Luchin, 1987; Martynov and Kuzin, 1995; Kozlov and Makarov, 1996). Except for Martynov and Kuzin (1995) and Kozlov and Makarov (1996), the idea of cyclonic water circulation in warm and cold seasons is promoted. However, it is noteworthy that shallow depths and the considerable meridional extension of the East Sakhalin shelf makes circulation there to be sensitive to relatively strong local monsoons capable, under certain conditions, of transforming the global sea level gradient and, consequently, the structure of coastal currents. Such inter-year variations of current fields are not accounted for by the dynamic method. This work reveals a peculiar regime of the East Sakhalin shelf currents by synthesis of numerical modeling results with data describing seasonal density fields, typical wind situations, and long-term instrumental measurements.

Water circulation and current fields are calculated over the three-dimensional diagnostic model of the Ekman type (Sarkisyan, 1977; Peng and Hsueh,

1974). Its first version for the coastal sea around Sakhalin and experimental results are given by Budaeva et al. (1980). This model has been tested many times, thus its quality and adequacy characteristics are not considered here.

Model description

Ocean hydrodynamics equations written in the Cartesian coordinate system with hydrostatic approximations, the Boussinesq equations, and sea-water incompressibility equations, ignoring horizontal turbulent exchange, are used. The system of initial equations is closed by a continuity equation. Basic equations of the model are as follows:

$$\begin{aligned} A U_{zz} - i WU &= gG + (g / \mathbf{r}_0) F; \\ u_x + v_y + w_z &= 0; \\ z = 0: AU_z &= -T / \mathbf{r}_0, \\ z = H(x, y): U &= 0, \end{aligned} \quad (1)$$

where

$$\begin{aligned} U &= u + iv, G = \mathbf{h}_{x+} i \mathbf{h}_y, T = T^{(x)} + iT^{(y)}, \\ F &= f^{(x)} + f^{(y)} \equiv \int_0^z (\mathbf{r}_x + i \mathbf{r}_y) dz \end{aligned} \quad (2)$$

The origin of the coordinates rests on an undisturbed oceanic surface $z = 0$, the x axis is directed eastward, y axis northward, z axis vertically down, u, v, w are components of current velocity directed along x, y , and z axes, respectively, $T^{(x)}, T^{(y)}$ are components of tangent wind stress on the sea surface, A is the coefficient of vertical turbulent exchange, W is the Coriolis parameter, \mathbf{r} is sea water density (\mathbf{r}_0 is the mean sea water density in the model area), g is free fall acceleration; H is sea depth, and \mathbf{h} is elevation of the given level and subscript means differentiation.

The integral function of a current is determined by the introduction of full flows

$S = \int_0^H U dz = (S(x) + iS(y))$, with the help of the continuity equation:

$$-Y_y = S^{(x)}, Y_x = S^{(y)} \quad (3)$$

The problem is not completely set up without corresponding boundary conditions for Y . Y values, calculated on the basis of quasi-geostrophic relations from the formula of Sarkisyan (1977), which were set on vertical flank boundaries of the open contour of the model area:

$$Y_{boundary} = - \frac{g}{(r_0 l_1)} \int_0^H (z p dz) \quad (4)$$

To make $Y_{boundary}$ values on the contour comply with the ones inside the area, $r\zeta$ anomaly, determined from equation (5), was used in formula (4) instead of r .

$$r\zeta(x, y, z) = r(x, y, z) - \bar{r}(z), \quad (5)$$

where r is the seawater density near bottom and $\bar{r}(z)$ is the arithmetic mean for all points on a horizon.

The values \bar{r} and $Y_{boundary}$ were calculated for each individual season using seasonal climatic temperature and salinity. Then (DY) currents were corrected on the boundaries of the model area for balance.

An elliptic equation for Y is approximated with the help of a monotonic difference scheme of second order precision (Kozlov, 1977) having conditions on the convergence of the iterational Gauss–Zeidel method which solves the system of linear equations for Y values at the nodes of the grid area.

In numerical realization of the model, the key problem is calculating the F function in equation (1). The classical approach involves the use of the whole three-dimensional density field; it is not easy and requires accurate quantitative and qualitative deep-sea hydrology. Additionally, “*bottom straightening*” (replacement of variables of $z\zeta = z/H(x, y)$ type) used in the numerical model helps to fulfill correct numerical differentiation over space, but brings about an additional problem, that is, the interpolation of initial density fields to the

nodes of the grid. This is why, for density parameterization, the authors used the modified Yoshida model (Yoshida, 1965) which was chosen because it demonstrated good ability to reproduce adequate structure of current fields in the surface layer and distinct analytical solution of equation (1) for horizontal velocities. The model also gives way to simplifications for the case of a deep sea. At $d = s_t + (r_{\bar{y}} - l)/d^*$, where s_t is conventional density, d^* is the characteristic scale of density variability, and $r_{\bar{y}}$ are density values for great depths, the vertical structure of density is determined over the following relation:

$$d(x, y, z) = \bar{\delta}(x, y) \times [1 + z/c(x, y)] \times \exp(-z/c(x, y)), \quad (6)$$

where $\bar{\delta}(x, y)$ coincides with real density distribution on a sea surface. The c parameter, indicating the depth of a density jump, is numerically determined for each station from the condition of the model and real “heat content” equality in a

$$\text{water column } f = \int_0^H d dz.$$

Initial data

The structure of water circulation and three-dimensional current field of the sea around East Sakhalin between 43°50′–54°30′N shoreline and 146°00′E have been studied with the help of 1947–1995 deep sea oceanographic observations and wind situations typical for summer and autumn. Typical wind fields were calculated by setting field data at the fixed sites of the related area and their subsequent interpolation. Calculations were made within the grid that approximated the area under study into the cells 20 × 20 minutes in size. The grid had 282 nodes; maximal depth of the investigated area made up 3200 m. Water transport through the La Peruse and Kunashir Straits was set in accordance with Sekine (1990).

Below is a description of dynamic processes on the shelf of East Sakhalin influenced by the winds mostly typical for summer and autumn, that is, by the winds of the greatest reoccurrence (P).

Summer modification of the scheme of surface currents

South-directed winds (P = 40.8%)

These winds occur most often. The dynamic structure of currents typical for summer is shown in Figure 1. It is manifested in the generation of mesoscale anticyclonic eddies (A_1 , A_2) and a north-directed coastal current. This northern current blocks the East Sakhalin Current and pushes its axis eastward, outside the outer edge of the shelf. A zero isoline moves seaward beyond 144°E . Anticyclonic eddies accumulate the transformed Amur River waters and condition the thermal regime of coastal waters in summer. Stable southern winds blowing along North-East Sakhalin intensify the northeastern branch of the Soya Current and anticyclonic system of currents in Aniva and Terpeniya Bays. The described situation contradicts the common view of currents in the area under study. However, it is noteworthy that weak southern winds do not change the general distribution of surface currents along North-East Sakhalin. The only factor they decrease is the velocity of currents directed northward. In time the generation of north-directed currents coincides with spring reconstruction of atmospheric circulation, that is, the period of considerable winter monsoon weakening and changing of northwestern winds for south and southeastern.

Southwestern winds (P = 15.6%)

In the shelf area of North-East Sakhalin this type of summer wind ranks second. Under stable southwestern winds a narrow alongshore current flowing northward at 5–15 cm/s is unchanged only in the area to the north of 50°N . In general, the transport of surface waters for the East Sakhalin coastal area is predominantly northeast- and east-directed. A surge of waters is registered in the eastern parts of Aniva and Terpeniya Bays. (Fig. 1b and e).

Southeastern and eastern winds (P = 14.6%)

These winds are the most water-surge dangerous. The field of currents reveals an intensive current flowing to the north at 10–20 cm/s and the formation of major cyclonic eddies at the southern and northern steep slopes. In La Perouse Strait the east-directed winds cause the Soya Current to sink.

Northern and northeastern winds (P = 7%)

Notable changes in the general summer scheme of surface currents are observed under stable northern and northeastern winds. In the northern part of the area under study deep-sea waters surging over the shelf edge cause the current to diverge: around $53^\circ\text{--}54^\circ\text{N}$ some waters turn to the northeast and block the south-directed transit of diluted Amur water along the Cape Elizabeth beam. The main current turns to the southwest (south) and, flowing along the northeastern coasts of Sakhalin, enters Terpeniya Bay. A notable activation of cyclonic eddies takes place at the southern steep slope. The southwestern mode also prevails on the shelf of South-East Sakhalin influenced by north and northeast winds predominating along the vectors of the surface alongshore currents. Dynamically active zones, where velocity of surface currents exceeds 50 cm/s, are shallow coastal regions of the shelf and areas around the capes.

Autumn modification of the scheme of surface currents

Western and northwestern winds (P = 46%)

The influence of stable west and northwest winds intensifies the East Sakhalin Current (> 50 cm/s) and coastal surface water drive (most intensive under northwest winds). Under this type of wind condition the formation of a vast cyclonic eddy Z_1 in the north of the area and an anticyclonic eddy A_1 at the southern steep slope is distinguished in the integral water circulation field (Fig. 2a and d). The structure of currents in the south of the area is complex and mostly two-layered. Compensating currents are north-directed.

Northern winds (P=18.6%)

In autumn this wind type ranks second. Under northern winds the surface currents of East Sakhalin are characterized by: polarization of southern vectors, intensification of the East Sakhalin Current and especially its western branch, water drive in Terpeniya and Aniva Bays and a surge of water near the northern coast of Hokkaido. A cyclonic eddy Z_1 exists at the northern steep slope. Another cyclonic eddy Z_2 is formed at the southern steep slope (Fig. 2b and e).

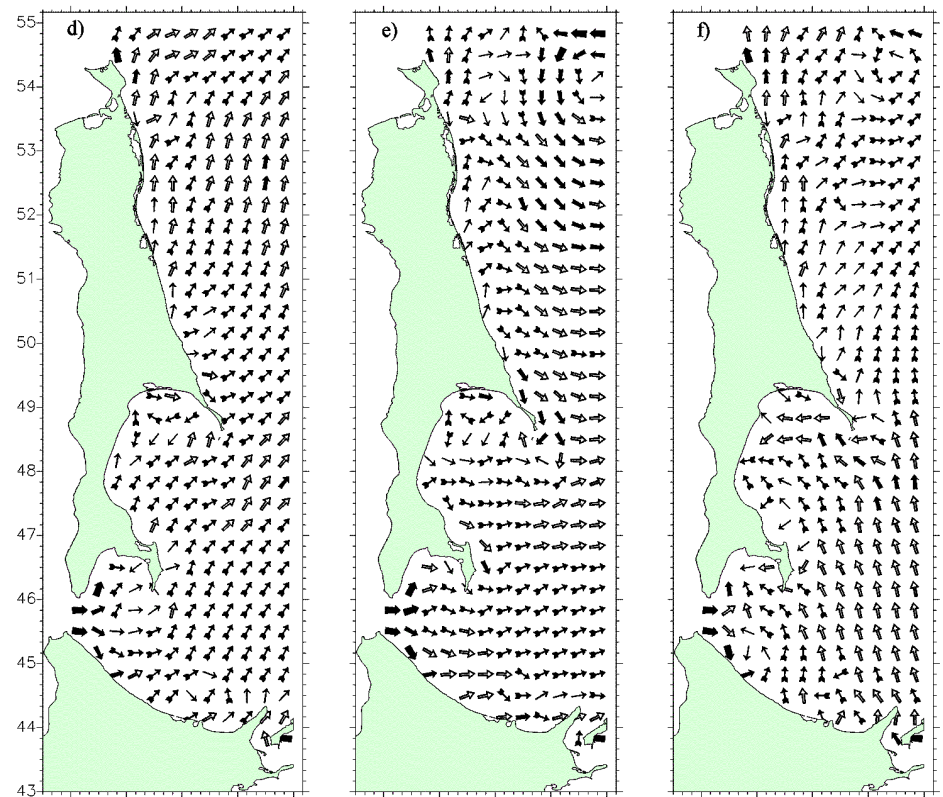
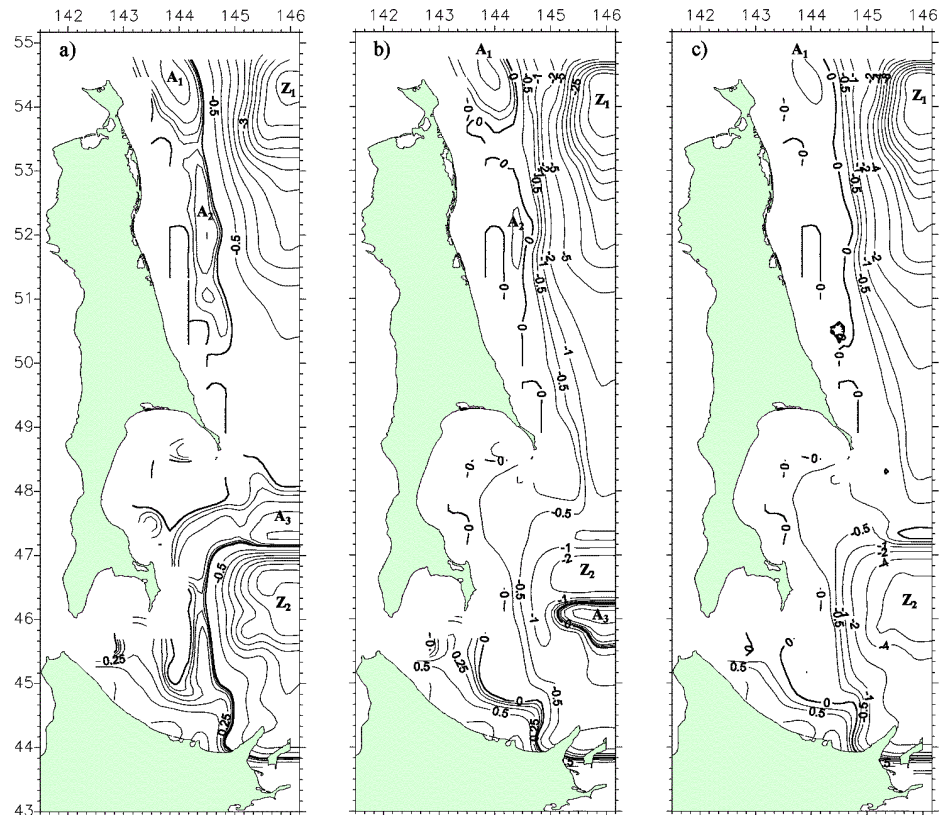


Fig. 1 Typical schemes of integral water circulation (a, b, c; in Sv) and surface currents (d, e, f) in summer: (a, d) southern winds ; (b, e) southwestern winds; (c, f) southeastern and eastern winds (> 4 m/s).

→ → → → → → →
 0 10 25 50 75 and higher, cm/s

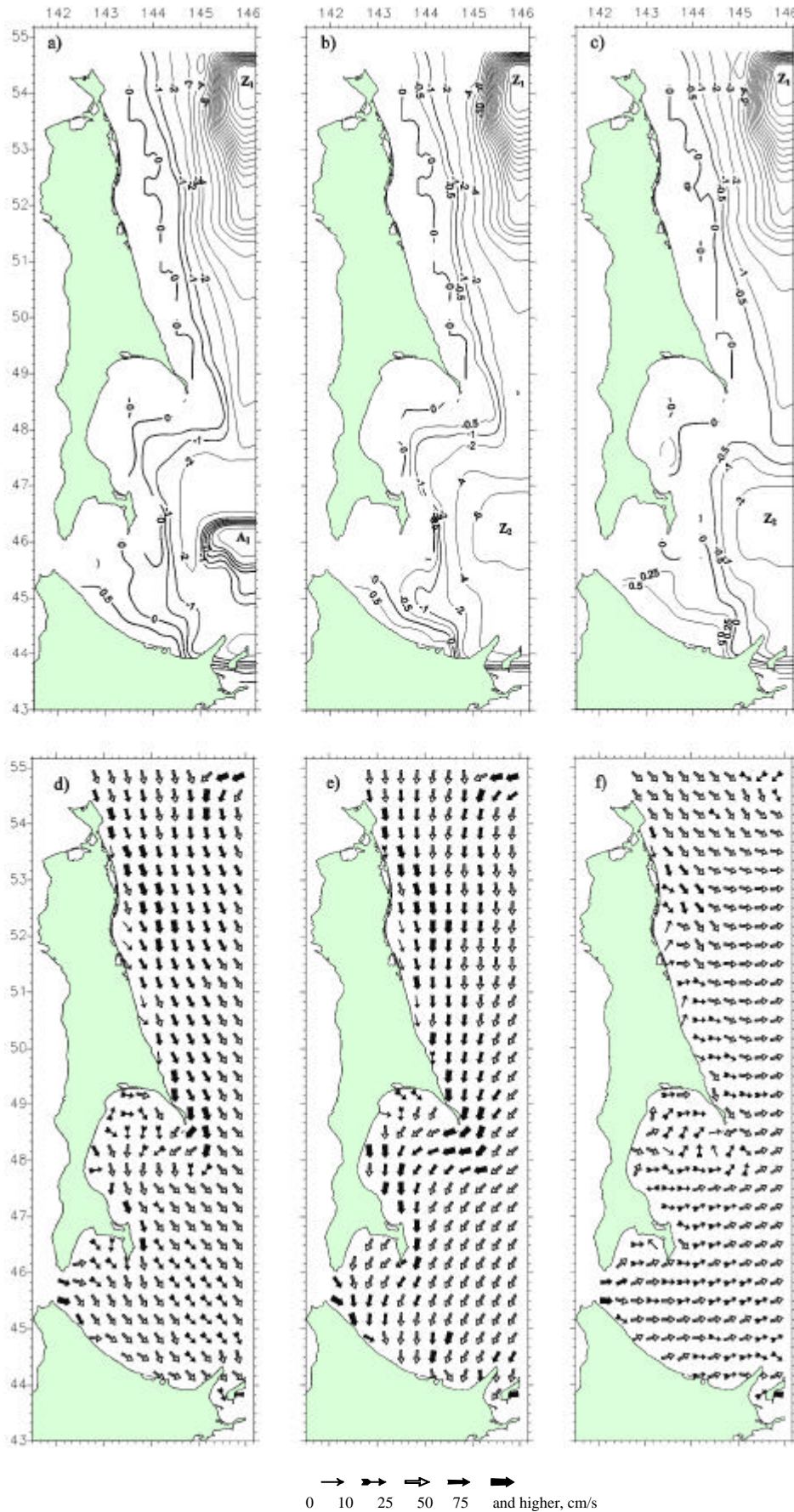


Fig. 2 Typical schemes of integral water circulation (a, b, c; in Sv) and surface currents (d, e, f) in autumn: (a, d) western winds, (b, e) northern winds, (c, f) southern and southwestern winds (> 4m/s).

Southern and southwestern winds (P = 18%)

Under stable southern and southwestern winds the general transport of surface water is northeast-directed, that is, away from the shoreline. The system of currents both on the sea surface and near bottom is predominantly anticyclonic. This situation may result in the shift of the East Sakhalin Current's axis to the shelf edge, the absence of its western branch on the Terpeniya Bay beam, and generation of the vast anticyclonic eddy to the east of Elizabeth Cape. The surge of waters in the eastern part of Terpeniya Bay prevents penetration of seaward waters into the bay. However, in autumn under weak southern winds and calm sea, the seaward waters, namely, the waters of the western branch of the East Sakhalin Current, meet no obstacles and easily enter the eastern part of Terpeniya Bay. Modal velocities of surface currents influenced by stable southern and southwestern winds reach 25–35 cm/s (Fig. 2c and f).

Eastern and northeastern winds (P = 7.8%)

Under these winds the general transport of surface waters is directed mostly to the northwest, that is, to the shoreline. Near the southwestern coasts of Sakhalin and in the western part of the La Perouse Strait the surge of waters takes place; it decreases the Okhotsk/Japan sea-level gradient. The durable influence of northeastern and eastern winds can even change the gradient sign in La Perouse Strait and bring about a west-directed surface current, that is, to block the Soya Current. Under such conditions the vertical structure of currents on the shelf of East Sakhalin has two well-distinguished layers. Maximal velocities of surface currents may reach 50 cm/s and even higher around Aniva and Terpeniya Capes.

Winter regime of currents

Real winter parameters of currents were obtained by the analysis of long-term instrumental measurements carried out by the experts of Sakhalin Energy Investment Co. Ltd. for the Piltun-Astokhskoje oil field in 1996–1997. Station sites were located in the area of the East Sakhalin Current as it is the principal element of water circulation in the area of East Sakhalin. The measurements were made each 60 minutes by integrating instruments (ADCP- (01) 0129 and whilsl-

600072) installed on the moored autonomous buoys.

Total currents

In winter (December–April) the regional surface currents on the shelf of East Sakhalin are characterized by the monomodal regime. The modal sector includes 135°–170°, the general direction of the current is south-southeast, and probability is 25–68% (Fig. 3a). The bimodal regime is characteristic of near-bottom currents. It is manifested in reciprocating motion mostly observed along the NNE–SSW axis. (Fig. 3b). Modal current velocities reach 10–20 cm/s and 20–30 cm/s; maximal velocities are 2–3 times higher. However, probability of maximal velocities is very low.

Two periods (transit and quasi-stationary) with different variability parameters are distinguished in the regime of surface currents in winter (Fig. 3a and c). The transit period is characterized by high variability of current direction (November) and velocity (December–January, 5–140 cm/s). A quasi-stationary period (modal velocities 10–20 cm/s, general direction south-southeast) includes February–April, and in time coincides with relatively stable ice cover over the Okhotsk Sea part of the shelf and notable weakening of tidal currents. It is characterized by relatively low variability of current velocity and direction.

Tidal currents

Regional currents of the East Sakhalin shelf are strongly controlled by tides; their reaction to high-low tides is observed the whole year round. Briefly, tidal currents are characterized as follows: they are of reverse character with modal vectors oriented at a small angle to the general N-S axis; their yearly variability cycle includes well-distinguished periods with asymmetric probability diagrams ($\Delta P \cong 6-8\%$); in January–April (June) the better pronounced are the currents directed northward, in the warm season they are the ones directed southward.

It is noteworthy that for most of the year tidal currents in the surface layers are directed against the predominant monsoon winds. Thus, during the warm season the predominant winds are those directed from the south and southeast, and the vectors directed to the (modal sectors 169°–191° and

146°–169°) in the general tidal current. During the cold season the predominant winds are directed from the north, and modal vectors directed to the north on variability diagrams of tidal currents (349°–11°, 11°–34°, 326°–349°).

Intensification of tidal currents with depth is another peculiarity of winter hydrodynamics. This peculiarity is also manifested in the profile configuration of total current velocity. The increasing velocity modulus of tidal currents in the direction of the seafloor is best pronounced in November–April. The average vertical shift of velocity between surface and near-bottom layers reaches 6–7

cm/s. This phenomenon is not completely understood.

In variability of the tidal current velocity modulus in surface layers the predominant is a yearly harmonic with maximum in August and minimum in March, near bottom it is a half-a-year harmonic with maximum in December, May–June and minimum in March and September. On the shelf of North-East Sakhalin at large, the absolute minimum of tidal currents takes place in March, and in time coincides with the stable ice cover over the Sea of Okhotsk.

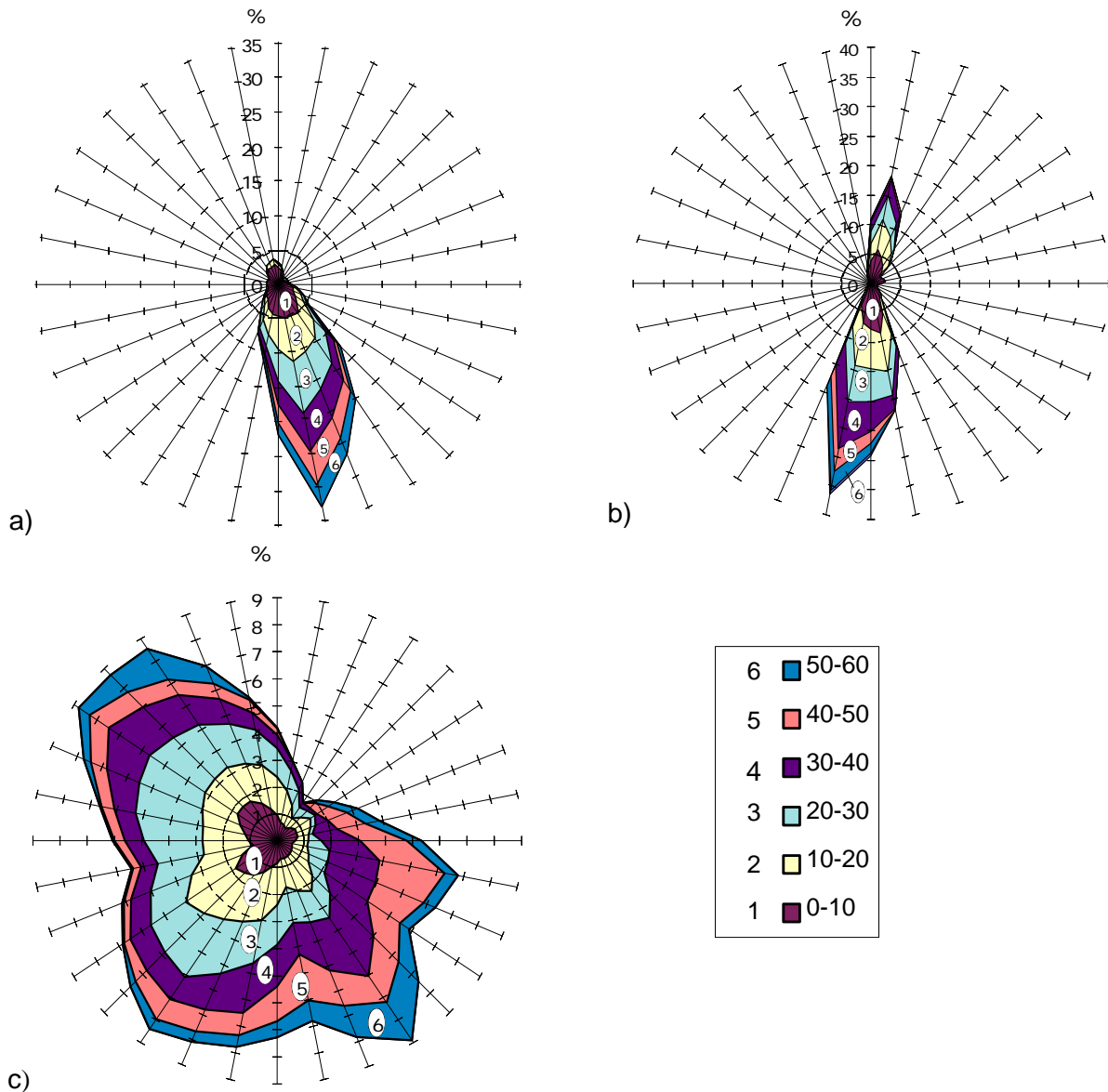


Fig. 3 Diagrams showing distribution of empiric probabilities of vector and velocity of the surface current (%). (a) March, (b) near-bottom horizon, March, and (c) November.

Conclusions

Model calculations made for the shelf of East Sakhalin proved its field to be dynamic and considerably dependent on the characteristics of a wind type situation. In the monsoon regime observed over the eastern Sakhalin shelf, two general types of sea water circulation are conventionally distinguished: summer and autumn (winter). The summer horizontal structure of currents is characterized by the shift of the East Sakhalin Current's axis to the shelf edge and the generation of northern currents with prevailing north-northeastern modes in the surface water. The autumn structure is characterized by southern flow intensification and prevalence of southern and southeastern modes in the vectors of surface currents. The integral transport of waters to the south in this period reaches about 1–2 Sv.

In the winter regime of surface currents two periods are distinguished: transient (November–January) and quasi-stationary (February–April). The vector of the averaged coastal current in surface layers is characterized by a mono-modal type of distribution (S-SE), and the vector of the near-bottom current by a bimodal one (SSE-NNW).

Acknowledgements

The authors express their sincere gratitude to S.M. Varlamov, N.A. Dashko, and A.A. Bogdanovsky for the wind data, to A.V. Gavrilovsky for his assistance in data preparation (all are from FERHRI) and to Sakhalin Energy Investment Co. Ltd for the long-term measurements of Sakhalin shelf currents and financial support of these studies.

References

- Budaeva, V.D., Makarov, V.G. and Melnikova, I.Yu. 1980. Diagnostic calculation of stationary currents of the Aniva Bay and La Perouse Strait. *Proc. FERHRI*, 87, 66–78.
- Kozlov, V.F. 1972. Calculation of level surface in the Sea of Okhotsk. *Proc. FERHRI*, 37, 37–43.
- Kozlov, V.F. 1977. The use of monotonic difference schemes in diagnostic calculation of ocean currents. *Izv. Atmos. Oceanic Phys.*, 13(7), 491–496.
- Kozlov, V.F. and Makarov, V.G. 1996. Background currents in the Sea of Okhotsk. *Meteorol. Hydrol.*, 9, 58–64.
- Leonov, A.K. 1960. *Regional Oceanography. Part 1*. Gidrometeoizdat, Leningrad, 765 pp.
- Luchin, V.A. 1987: Water circulation in the Okhotsk Sea and some features of its inter-annual variability on the diagnostic calculations. pp. 3–13. In *Oceanographic Problems of the Far Eastern Seas*, 36. (in Russian)
- Martynov, A.V. and Kuzin, V.I. 1995. Numerical experiments with 2-D finite-element model of the Okhotsk Sea circulation. pp. 332–336. In *Tenth International Symposium on Okhotsk Sea, Sea Ice and Peoples, Abstracts*, Mombetsu, Hokkaido, Japan.
- Moroshkin, K.B. 1964. A new surface current map in the Okhotsk Sea. *Oceanologia*, 4, 614–643. (in Russian)
- Moroshkin, K.B. 1966. *Water Masses of the Sea of Okhotsk*. Nauka, Moscow. 68 pp.
- Peng, C.Y. and Hsueh, Ya. 1974. Further results from diagnostic modeling of coastal upwelling. *Téthys*, 6(1-2), 1–46.
- Sarkisyan, A.S. 1977. *Numerical Analysis and Forecast of Marine Currents*. Gidrometeoizdat, Leningrad. 182 pp.
- Sekine, Y.A. 1990. Barotropic numerical model for the wind-driven circulation in the Okhotsk Sea. *Bull. Fac. Bio-Resources*, 3, 25–39.
- Yoshida, K.A. 1965. A theoretical model on wind-induced density field in the oceans. I. *J. Oceanogr. Soc. Japan*, 21(4), 154–173.
- Zyryanov, V.N. 1977. Numerical calculation of stationary currents in the Sea of Okhotsk (prognostic model). *Proc. VNIRO*, 119, 24–30.

The oceanographic data bases on the Sakhalin shelf

Nikolay A. RYKOV

Far Eastern Regional Hydrometeorological Research Institute, Vladivostok, Russia

The Regional Oceanographic Data Center (RODC) was established at the Far Eastern Regional Hydrometeorological Research Institute (FERHRI) as a Far Eastern branch of the Russian National Data Center. Its main function is to archive oceanographic data which were obtained by FERHRI research vessels. At the same time, RODC must deal with archived data obtained by other organizations/institutions.

Oceanographic observations by Russia in the Pacific Ocean began in the last century. After the revolution, the archives of the Hydrographic Department, in which the data were stored, were plundered. The oceanographic organizations in Vladivostok were repeatedly created, closed, reconstructed and moved.

There are four oceanographic organizations at the present time in Vladivostok, where oceanographic data sets were made and collected (FERHRI, Pacific Oceanological Institute (POI), Pacific Research Institute of Fisheries and Oceanography (TINRO), and the Hydrographic Service of the Navy). The research vessels of these departments until recently had in common the largest scientific fleet in the world (more than 30 units of large specialized ships). Annually they made about 10,000 hydrographic stations (observations of temperature, salinity, oxygen, chemical elements, currents, meteorological parameters). All of these data were collected in Vladivostok basically as hand-written reports in which copies were sent to the central establishments of departments. Because of the possibility of data loss in Vladivostok, the regional oceanographic data center was organized in the Institute of Automatics and Data Management. However, not being an oceanographic establishment, the center was not able to solve the problems of data set preservation and has stopped this work. Departmental data centers, at the same time, were organized at FERHI, POI, TINRO and the Hydrographic Service of the Navy.

Some of the data in different departments was lost during the transition to new kinds of computer

facilities. So, in FERHRI the data stored as punched tapes and magnetic tapes were lost.

The RODC began work practically from nothing. There were only hand-written reports of cruises since 1959 at its disposal. The material of more than 520 FERHRI cruises have now been collected at RODC (Rykov, 1998a). The routine work of entering, quality control and primary data processing are now carried out from not only the FERHRI archives, but also from other institutes.

The largest problem is international data exchange. For the FERHRI observations to be transferred in an exchange through the Russian National Oceanographic Data Center (NODC) is extremely complicated due to working restrictions. Nevertheless, FERHRI aspires to make available its own numerous (more than 190,000 stations) data sets for the world oceanographic community. About 33,000 stations for the World Ocean are prepared at present for international data exchange.

The total number of oceanographic observations for the Sea of Okhotsk presently include about 70,000 hydrographic stations which were obtained from different countries and organizations. It can be seen that for the cold months oceanographic observations in the Sea of Okhotsk were carried out only in places free from ice cover (Figs. 1–3). Thus the areas of Soya Strait and Tatarskiy Strait are free from ice around the Sakhalin Island, but by May the observations cover most areas of the sea, except the region near the Shantar Islands (where the ice remains almost all summer until August) and the Shelekhova Gulf, where the ice stays until July). The central part of the sea and shelf of Sakhalin Island are least covered with observations in May.

The regional database on the Sakhalin shelf was extracted from the total Okhotsk Sea database. The region of the Sakhalin shelf is covered with a rich network of stations during the warm period (June–October). Such a situation continues until the occurrence of new ice (in late October). Un-

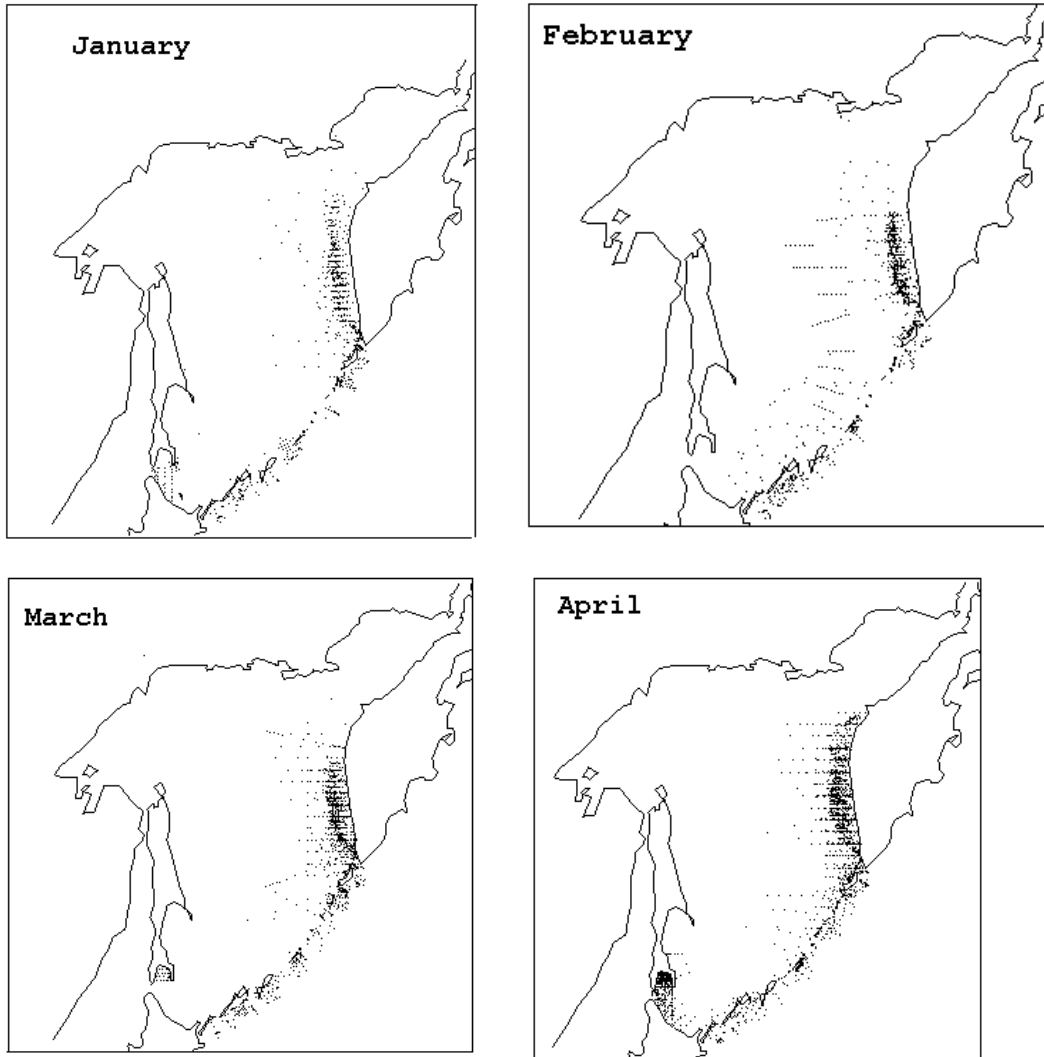


Fig. 1 The data distribution in January–April.

fortunately, the places where coastal polynyas form (including at east coast of Sakhalin) have no oceanographic observations during the cold months of the year. The most valuable data sets are the repeating observations on so-called century sections directed far from Sakhalin Island.

The database includes deep-water observations in the region located from 43° to 56° N and from 142° to 146° E, with a total number of about 13,000 stations. The main measurements were carried out from 1947 to the present and consist of such observations as temperature, salinity, dissolved oxygen, pH, alkalinity and nutrients (see Table 1). However, the composition of observations differs essentially during each cruise.

A large amount of software has been created for data management, processing, visualization and quality control. Part of this software allows the data to be separated into periods, regions, cruises and observed elements.

The system of data quality control allows us to load in the computer memory up to 1,000 stations and to display/print out their locations as well as vertical profiles of measured elements and/or their combinations. A vertical profile of temperature, salinity, oxygen and observation points are shown in Figure 4. This software is used mainly for qualitative data recording.

Another component of the system makes possible

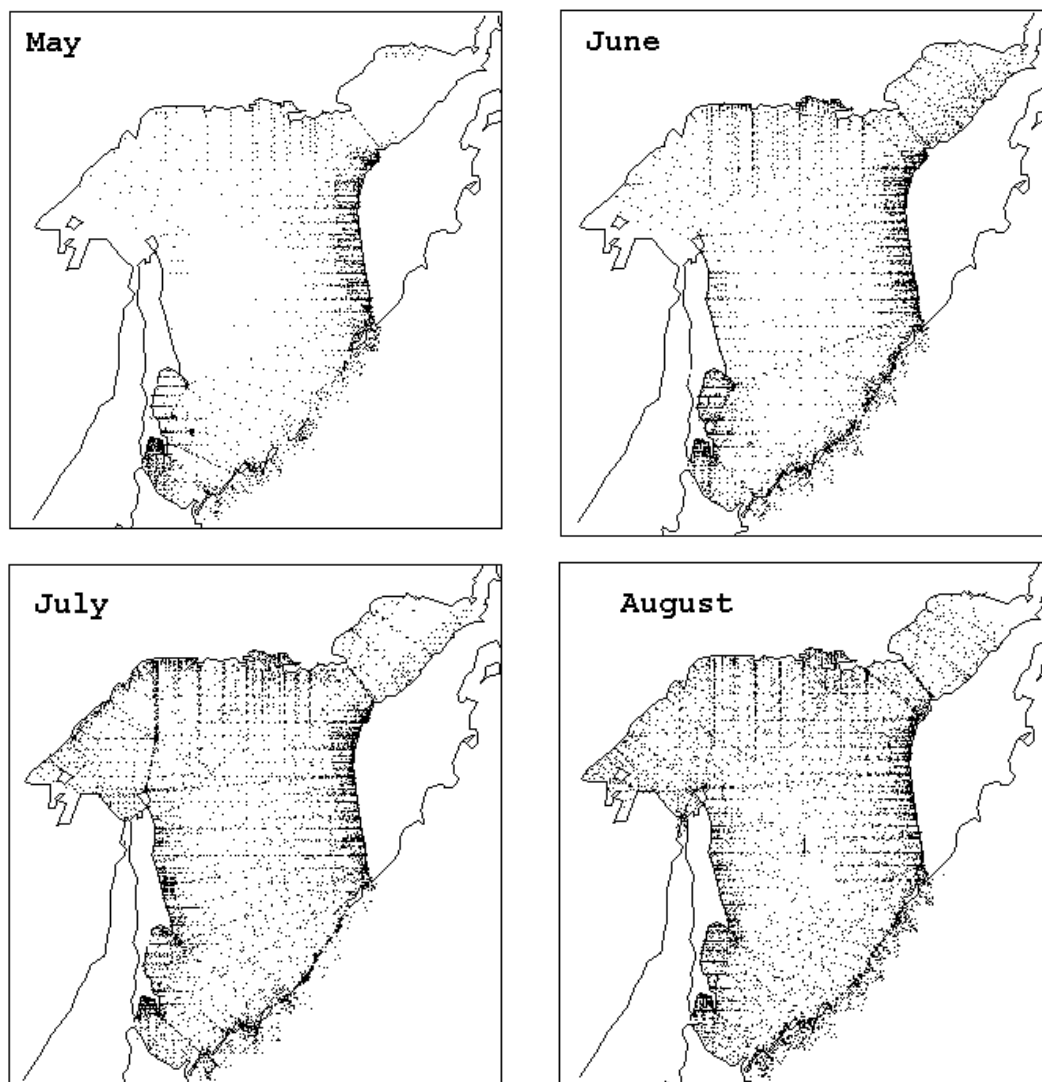


Fig. 2 The data distribution in May–August.

the loading of a random number of stations and the display/printout of vertical profiles of observations for those stations whose measured values differ from the means by more than number of standard deviations set by the operator. It is effective for quality control of historical data in space–time limited sets.

Additionally, the multifunction informational system was created for receiving different references. It allows us to create electronic catalogues of both cruises and stations, to show the points of observations and observed values, to calculate and draw the fields of observed parameters, and so on (see Figure 5).

Processing of sea water density in one degree squares was made in order to estimate whether the number of observations is enough for correct estimation of mean seasonal density fields. The estimates appear to be good over the southern part, but density variability in the northwest part of Sakhalin shelf is too large because of freshwater flowing from the Amur River and elsewhere (Rykov, 1998b).

The data and software tools are used to answer administrative and regional requests in Federal Service of Russia on Hydrometeorology and Environmental Monitoring, for joint scientific studies with specialists from TINRO, POI and other home

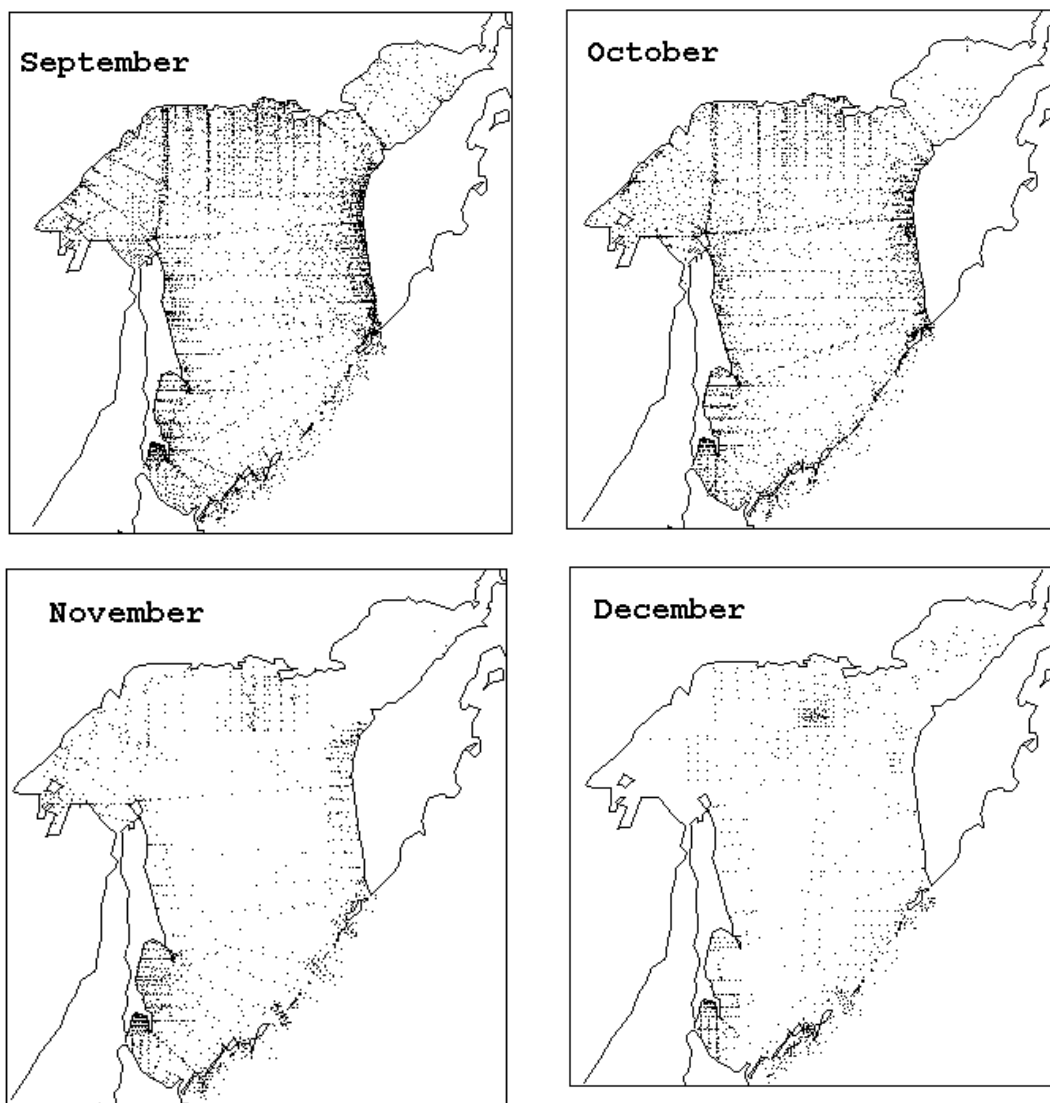


Fig. 3 The data distribution in September–December.

Table 1 Composition of observations on the Sakhalin shelf (43°–56°N, 142°–146°E, 1932–1997).

Month	Temperture	Salinity	Oxygen	pH	Alkalinity	PO ₄	SiO ₃	NO ₂
May	1636	1073	470	315	106	20	34	28
Jun	2203	1555	756	418	140	210	217	216
Jul	2542	1939	917	658	115	167	245	202
Aug	2137	1432	552	355	14	204	217	101
Sep	1583	1301	674	570	93	217	311	191
Oct	1419	1138	627	385	114	188	189	178
Nov	944	710	259	157	88	–	8	15
Dec	410	288	39	6	3	2	2	–
Total:	12874	8836	4294	2864	673	1008	1223	931

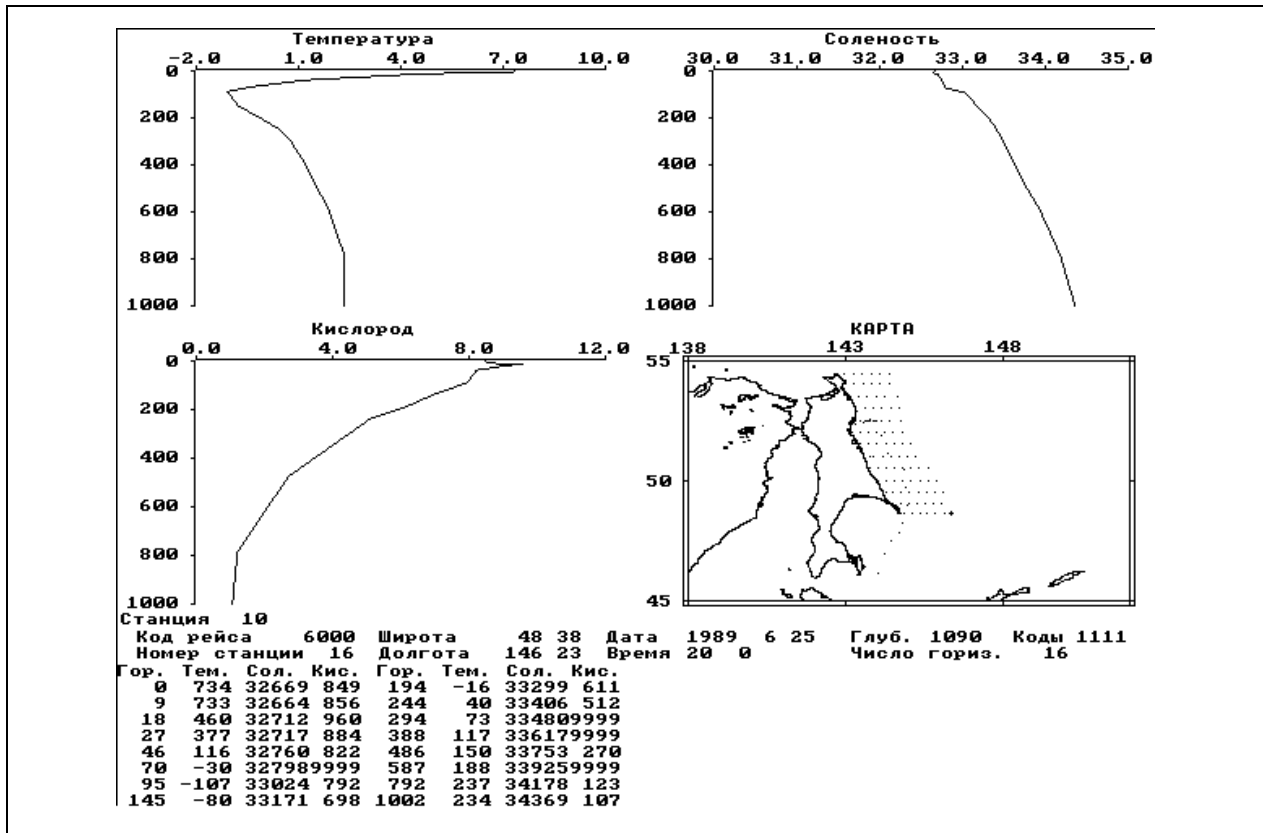


Fig. 4 The working fragment of quality control software.

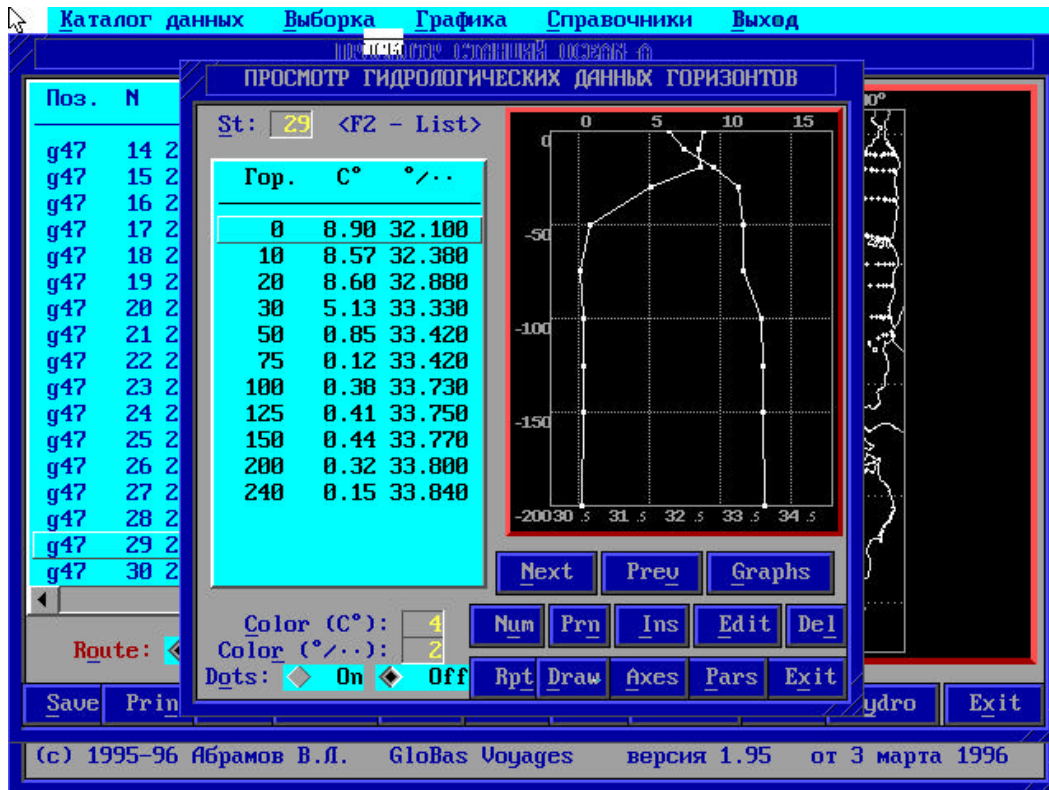


Fig. 5 The working component of the information-reference system.

institutes and agencies, as well as in work on international projects under collaboration in international organizations such as PICES and WESTPAC.

References

Rykov, N.A. 1998a. Oceanographic Databases for Far Eastern Region. pp. 59–60. *Intl. Conf. on*

Expeditionary Research of the World Ocean and Oceanographic Information Resources. October 25–30, Obninsk, Russia,

Rykov, N.A. 1998b. Availability of deep-sea oceanographic data for Okhotsk part of Sakhalin shelf. *Proc. FERHRI, Special Issue*, Vladivostok, pp. 52–61. (in Russian)

Formation of high-density water (over 26.8 sigma-t) near the La Perouse Strait (the Soya Strait)

Akifumi NAKATA¹, Iori Tanaka¹, Hiroki Yagi², Tomomi Watanabe¹, Gennady A. Kantakov³ and Andrew D. Samatov³

¹ Hokkaido Central Fisheries Experimental Station, Yoichi, Japan

² Otaru University of Commerce, Otaru, Japan

³ Sakhalin Research Institute of Fisheries and Oceanography, Yuzhno-Sakhalinsk, Russia

The Soya Warm Current is the only supplier of saline subtropical water to the Okhotsk Sea. The Soya Warm Water obtains high density values comparative to NPIW (North Pacific Intermediate Water) by winter cooling, due to its high salinity value, and may influence the intermediate water in the Okhotsk Sea, which is considered as a source water of NPIW. However, as the northern half of the La Perouse Strait (the Soya Strait) belongs to Russia and the southern half to Japan, no observations across the strait have been made except in the period before the World War II. The vertical resolution and spatial coverage of these old observations are very limited, and the accuracy of the measurement is also very limited due to instruments used in those days. The Joint Oceanographic Observation Program between the Hokkaido Central Fisheries Experimental Station (HCFES) and the Sakhalin Research Institute of Fisheries and Oceanography (SakNIRO) started in August 1995 in order to deduce the detailed structure of the Soya Warm Current in and near the La Perouse Strait and its seasonal and inter-annual variability. By introducing the observational results of the program, the seasonal variability of the Soya Warm Current Water in the La Perouse Strait and the formation of the dense water (heavier than 26.8 sigma-t) is discussed in this paper.

Distributions of temperature, salinity and sigma-t in the section (S1-line) across the La Perouse Strait observed on 12-14 March, 1996 are shown in Figure 1a through Figure 1d, respectively. Low-density water was found in a shallow domain along the coast of Sakhalin, while high-density water was found on the Hokkaido side. Judging from its high salinity characteristics, the

high-density water found on the Hokkaido side seems to be formed by winter cooling of the Tsushima Warm Water. Takizawa (1982) called this water the forerunner of the Soya Warm Water. According to Watanabe and Wakatsuchi (1998), the forerunner of the Soya Warm Water contributes the formation of Kuril Basin Intermediate Water, which would be one of the source waters of NPIW in the Okhotsk Sea. It was shown that the water of the northern part of the La Perouse Strait flows toward the Japan Sea in early spring.

The distributions of temperature, salinity and sigma-t in the section (S1-line) across the La Perouse Strait observed on August 20-21, 1996 are shown in Figures 2a-2d, respectively. In summer, a sharp thermocline was found just below the depth of 10 m. A halocline was found at the same depth, and the corresponding pycnocline is seen in the sigma-t section (Fig. 2c). The oceanic structure in and below the thermocline was very complicated, and the weak density inversion found below 20 m depth is probably the result of limited resolution or accuracy of the observation. A strong horizontal density gradient was also seen (Fig. 2), except just near Sakhalin, but the gradient is opposite to that observed in March (Fig. 1). The denser water is located on the Sakhalin side and the lighter water on the Hokkaido side. The low-density water on the Hokkaido side has high temperature and high salinity values, which are the typical of the Tsushima Warm Water during summer. The water in the surface layer on the Sakhalin side had low temperature and low salinity values, which characterize the Okhotsk

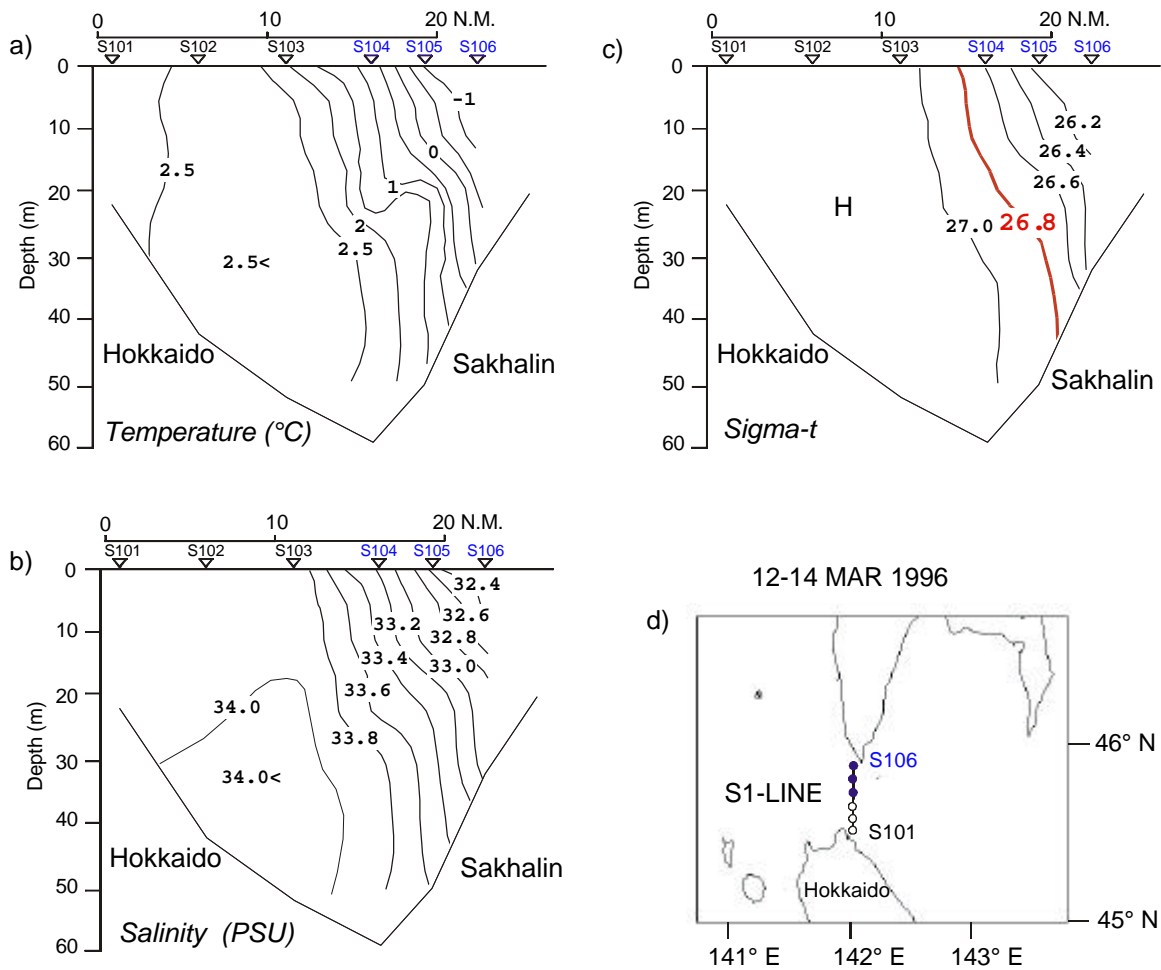


Fig. 1 Distributions of temperature (a), salinity (b) and sigma-t (c) in the section along the S1-line across the La Perouse Strait on 12-14 March 1996. The location of the line and stations are shown in the left-bottom figure (d): solid circles indicate the observation points occupied by Russian vessel, and open circles are those occupied by a Japanese vessel.

Sea Water. The high density water found below the pycnocline on the Sakhalin side has a temperature $< 7^{\circ}\text{C}$ and high salinity, of about 34 psu. The density of this water exceeds 26.8 sigma-t, and is similar to that of the forerunner of the Soya Warm Water found in the March section (Fig. 1). Such high salinity water is difficult to find in the Okhotsk Sea, and probably originated in the Japan Sea. Our observations suggest that this heavy water was brought to the near-surface layer by upwelling along the southwest coast of

Sakhalin. It flows into the Okhotsk Sea through the northern part of the strait, and is one of the sources of the Cold Water Belt Water in the Okhotsk Sea.

It should be noted that high-density water flows into the Okhotsk Sea in summer as well. Flow rates of these dense waters must be determined and it would be desirable to clarify its distribution and seasonal variability in the Okhotsk Sea in future projects.

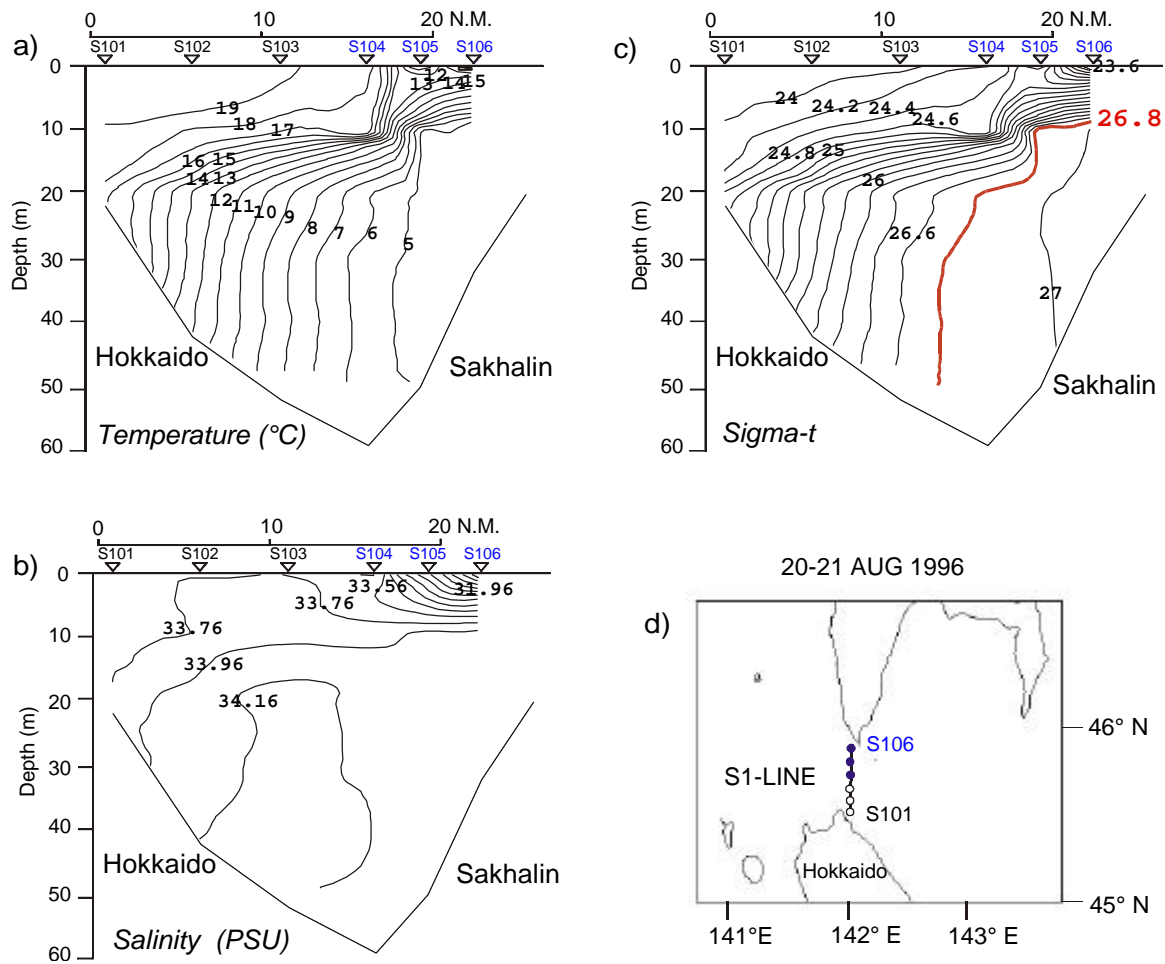


Fig. 2 As in Figure 1 except for 20-21 August 1996.

References

Takizawa, T. 1982. Characteristics of the Soya Warm Current in the Okhotsk Sea. *J. Oceanogr. Soc. Japan*, 38, 281-292.

Watanabe, T. and Wakatsuchi, M. 1998. Formation of 26.8-26.9 σ_t water in the Kuril Basin of the Sea of Okhotsk as a possible origin of North Pacific Intermediate Water. *J. Geophys. Res.*, 103(C2), 2849-2865.

Currents and Tidal Observations by the Hydrographic Department of Maritime Safety Agency, off the Okhotsk Coast of Hokkaido

Minoru ODAMAKI¹ and Kouji Iwamoto²

¹ Hydrographic Department, Maritime Safety Agency of Japan, Tokyo, Japan

² First Regional Maritime Safety Headquarters, Otaru, Japan

Introduction

The Soya Warm Current, originating from the Japan Sea, flows into the Okhotsk Sea through the Soya Strait and along the Okhotsk Coast of Hokkaido. The warm and saline Soya Current Water may influence not only the coastal region along Hokkaido but also the entire Okhotsk Sea. The transport and structure of the Soya Warm Current show considerable seasonal variation. The Soya Warm Current almost disappears in the winter season, but the warm and saline water can be found near the bottom. The Soya Warm Current in the other seasons is strongest in the surface layer and it does reach the bottom. In the region just off the Soya Warm Current, very cold water is found in an intermediate layer, which is called the Okhotsk Intermediate Cold Water. This water originates from the northern Okhotsk Sea. The Soya Current Water may mix with these surrounding waters while flowing along the Hokkaido Coast. The tide of the diurnal K_1 component in the Okhotsk Sea is strong and influences water-mass modifications through mixing processes. The nature of tides and tidal currents just off the Hokkaido Coast is somewhat peculiar, reflecting large differences in tidal amplitude between the Japan Sea and the Okhotsk Sea. In this paper, the current and the tidal observations by the Hydrographic Department of the Maritime Safety Agency of Japan are introduced.

Sea ice and oceanic condition in winter

The Hydrographic Department of the Maritime Safety Agency of Japan and each of the Regional Maritime Safety Headquarters publish bimonthly Prompt reports of the Oceanographic Condition for all of the seas around Japan and for regional seas. The reports are mainly based on ocean

current observations from various ships, satellite images, and other sources. The Hydrographic Department sometimes sends its survey vessels to the Okhotsk Sea, and the First Regional Maritime Safety Headquarters often conducts ocean current observations using its patrol vessels.

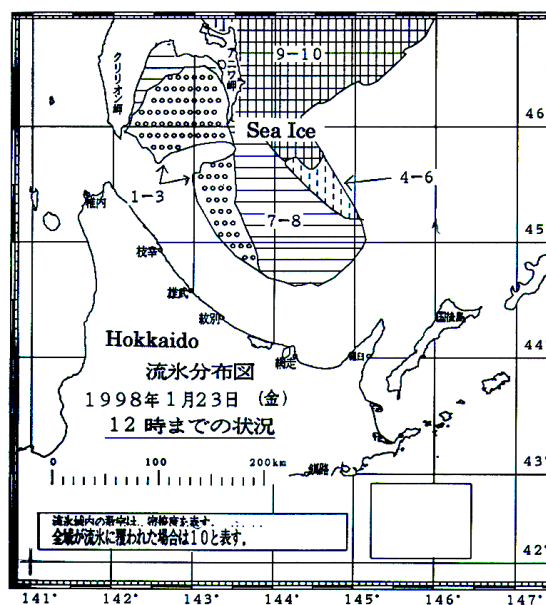


Fig. 1 An example of the Sea Ice Condition Chart published daily by the Sea Ice Information Center of the First Regional Maritime Safety Headquarters. Numerals in the figure indicate sea ice concentration (January 23, 1998). Sea ice area is shaded depending on sea ice concentration. The chart is accessible at <http://www.jhd.go.jp>.

Sea ice appears in coastal regions of Hokkaido usually in late January. Since sea ice severely influences ship navigation, fisheries and other maritime activities off the Okhotsk Coast of Hokkaido, one of the duties of the Hydrographic

Department and the First Maritime Safety Headquarters is to make sea ice surveys and rescue operations in this season. When sea ice is seen off the Hokkaido Coast (usually from late December to April), the Sea Ice Information Center operates in the First Regional Maritime Safety Headquarters. The center collects sea ice information from patrol vessels and air-craft, sea ice radar images (obtained by Sea Ice Research Laboratory of Hokkaido University), available satellite images and so on, and publishes the daily Sea Ice Condition Chart. An example of the chart is shown in Figure 1. The chart is accessible at www.jhd.go.jp.

The First Regional Maritime Safety Headquarters sends its patrol vessel to the area off the Hokkaido Coast almost every December in order to know oceanographic conditions just prior to the sea ice season (First Regional Maritime Safety Headquarters, 1997). Usually, XBT and ADCP observations are carried out on board the patrol vessel. Also, headquarters sends its icebreaker *Soya* at the first appearance of sea ice in the region to carry out sea ice patrol, ship-rescue, and observations of sea ice and oceanographic conditions using CTD and XBT (First Regional Maritime Safety Headquarters, 1998).

An example of the ocean current distribution at 10m depth observed by the patrol vessel *Sorachi* is shown in Figure 2a. The observations were made from 6 to 7 December, 1997. The current field at this time is atypical: the flow in the Soya Strait (observed on December 7) is westward, even in the vicinity of the Hokkaido Coast, where the Soya Warm Current usually flows eastward. The current distribution taken two days later (9 December) is shown in Figure 2b. The weather condition was very severe, and the ADCP records were not clean and included much noise. The observed current might be less accurate especially in its magnitude, but the currents near the Hokkaido Coast in the Soya Strait appear to be northeastward or southeastward as is the usual flow direction of the Soya Warm Current. It is difficult to explain such an atypical Soya Warm Current on December 7, and such a large

variation in current field within two days, but it is plausible that the strong tidal currents in and near the Strait played important role in this curious phenomenon.

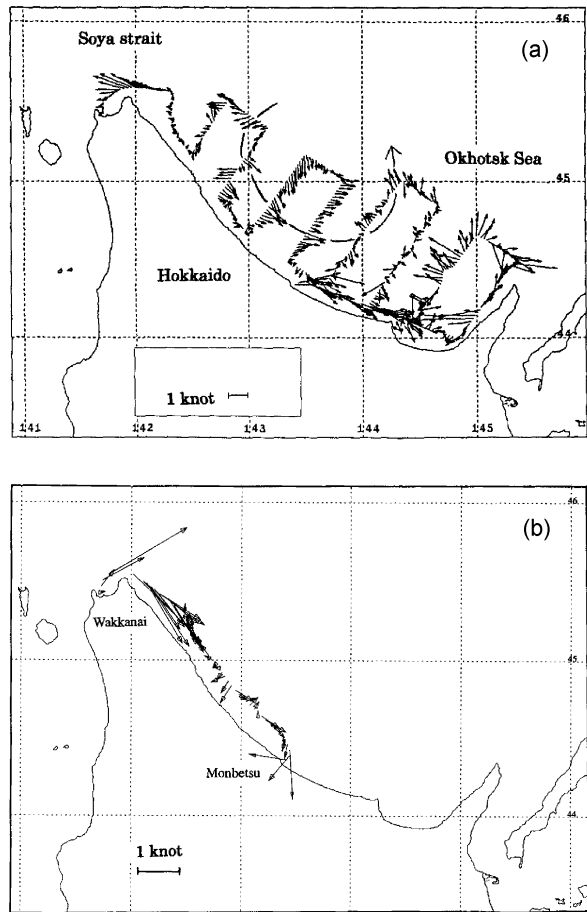
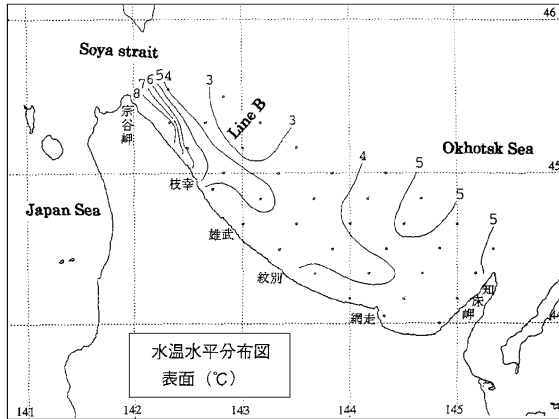


Fig. 2(a) Current distribution (10m depth) observed by ADCP on board the patrol vessel *Sorachi* in the period from December 6-7, 1997. (First Regional Maritime Safety Headquarters, 1997). **2(b)** Current distribution (10m depth) along the course from Wakkanai to Monbetsu observed on December 9, 1997 just after Figure 2a.

The surface temperature distribution in the same period is shown in Figure 3. The warm area extends along the Hokkaido Coast from just off Cape Soya (the southern end of the Soya Strait), indicating that the warm Soya Current Water was flowing into the Okhotsk Sea even though the temporary current field in Figure 2 indicates that the flow was in the opposite direction. The warm

water tongue along the coast disappears before reaching Line B. The temperature cross-section along line B is shown in Figure 4. Warm water is found above the bottom slope of the Hokkaido



Pacific Ocean. Further, the survey project related

Fig. 3 Same as Figure 2(a), except for surface temperature distribution (in °C). Dots indicated XBT observation stations. The temperature cross-section along Line B is shown in Figure 4.

side in this section. The source of this warm but dense (very saline) water cannot be found in the Okhotsk Sea, so the water should be Soya Current Water. The Soya Current Water tends to subside while it is flowing along the Hokkaido Coast due to its high salinity nature.

Tides and tidal currents in the Soya Strait and off the Okhotsk Coast of Hokkaido

The amplitude of tides is generally small in the Japan Sea except near the Tsushima Strait. On the other hand, tides and tidal currents are quite large in the Okhotsk Sea. It is well known that the strong tidal mixing near shoals and in straits plays an important role in water-mass modifications in the Okhotsk Sea. The amplitude of tides is not so large in the Soya Strait, but the current velocity of the diurnal K_1 tide reaches about 1.5 knots, reflecting the large tidal amplitude difference between the Japan Sea and the Okhotsk Sea. It is highly possible that the temporary current measurement by ADCP in and near the Soya Strait would be affected by the tidal current as discussed above.

The Hydrographic Department has responsibility to compile the Basic Maps in the western North

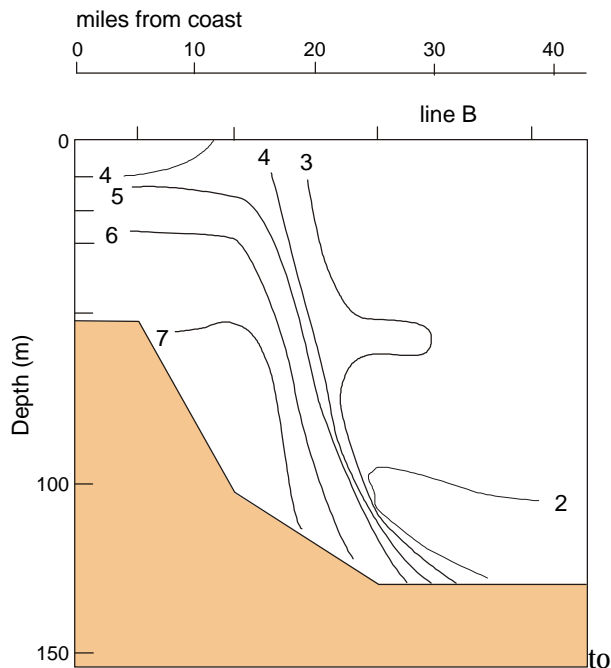


Fig. 4 Temperature cross-section (in °C) along Line B (see Figure 3 for the position of the line). Warm Soya Current water is found above the bottom of Hokkaido side.

to the Basic Maps of the Seas in Coastal Waters has been conducted in the Okhotsk Coast area of Hokkaido from 1988 to 1991, including tide and tidal current observations which were carried out for a period of one month each summer. The results of the observation are shown in Figure 5 for the dominant tidal component, K_1 . An amphidromic point exists just in the Soya Strait. The co-tidal line rotates counterclockwise around the amphidromic point. The co-tidal lines in the offshore area are rather parallel to the Hokkaido Coast, but they are bent in the nearshore area and hit the coast. The tidal phase distribution indicates that the tide travels southeastward along the coast. The interval of the co-tidal lines becomes large in the central part of the Okhotsk Sea, reflecting bottom topography. The tidal amplitude tends to increase away from the Soya Strait.

Though the tidal amplitude tends to increase towards offshore, the prominent tidal current is found only in the nearshore area and diminishes

rapidly to offshore. The phase propagation of the tidal current was much slower than that of tide

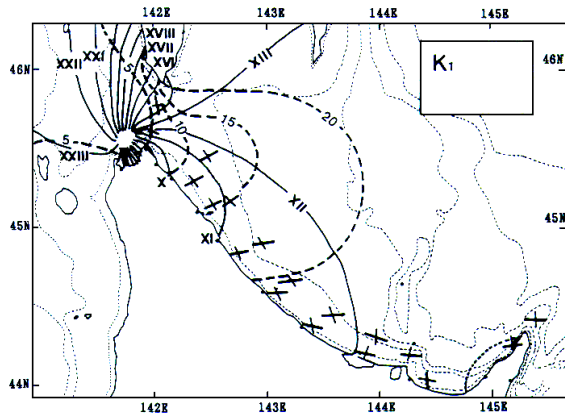


Fig. 5 Co-tidal lines (full lines) and co-amplitude lines (dashed lines) of K_1 tide near the Soya Strait and in the southern Okhotsk Sea. Roman numbers attached to co-tidal line indicate the tidal hour, and numerals attached to co-amplitude line the amplitude (in cm). Crosses indicate the positions of the tidal current observation.

(see Fig. 4a of Odamaki, 1994). Odamaki (1994) explained these characteristics of the tidal current just off the Hokkaido Coast as a shelf wave propagating southeastward along the Hokkaido Coast from the Soya Strait.

Acknowledgment

The authors appreciate the crew of the icebreaker *Soya* and the patrol vessel *Sorachi* for their cooperation during the oceanographic observations, and staff of the First Regional Maritime Safety Headquarters for their support and valuable discussions. They also appreciate Dr. Yutaka Nagata for his kind advice.

References

- First Regional Maritime Safety Headquarters 1997. The southwest area of the Okhotsk Sea, 6th–10th Dec. 1997. *Ocean Current Observation Rep.*, No.6.
- First Regional Maritime Safety Headquarters 1998. The southwest area of the Okhotsk Sea, 3rd–12th Feb. 1998. *Ocean Current Observation Rep.*, No.1.
- Odamaki M. 1994. Tides and tidal currents along the Okhotsk coast of Hokkaido. *J. Oceanogr.*, 50, 265–279.

Oceanographic features of LaPerouse Strait

Mikhail A. DANCHENKOV¹, David Aubrey² and Stephen C. Riser³

¹ Far Eastern Regional Hydrometeorological Research Institute, Vladivostok, Russia

² Woods Hole Oceanographic Institution, Woods Hole, U.S.A.

³ School of Oceanography, University of Washington, Seattle, U.S.A.

Introduction

The Japan and Okhotsk Seas are divided by a shallow area located between Sakhalin Island from the north and Hokkaido Island from the south, and 142.0°E from the west and 143.5°E from the east (Fig. 1). This area, despite the special bottom topography and oceanographic conditions, has no name, but the narrowness between Cape Krilion and Cape Soya has two names: in Russia – Lape-ruza (LaPerouse) Strait, and in Japan – Soya Strait. In this paper the waters of area between the Sakhalin and Hokkaido islands, 142°E and 143.4°E are considered as a whole, therefore, hereafter we will call this region (for convenience of the description) LaPerouse Strait and its western narrowness Soya Strait.

The water structure and currents in the area between Sakhalin and Hokkaido were studied by Aota (1970, 1975, 1984, 1987), Budaeva (1975, 1980) and Takizawa (1982), but the main attention was given to Soya Current. Through LaPerouse Strait warm subtropical water penetrates (as the Soya Warm Current) into the Okhotsk Sea. Re-

sults of a few current measurements (May–June 1933) in the strait indicate that subtropical water in summer enters into Soya Strait over almost all its width (with the exception of its northern part). After Soya Strait, the width of this flow sharply decreases and further warm and salty water exists only in a narrow strip along northern coast of Hokkaido.

The main feature of water structure of this area in summer is a belt of cold water from Krilion Cape to the southeast part of this strait (Fig. 2).

It is usually considered (Tanaka et al., 1996) that cold water inside the belt is formed *outside* the strait – at southwestern coast of Sakhalin as the upwelling of subsurface (deep) waters. It is usually believed that cold water is transported from there into LaPerouse Strait by the so-called “West Sakhalin Current”. Zhabin et al. (1992) wrote, “cold waters through LaPerouse Strait penetrate in the Okhotsk Sea”. We doubt if the cold water in belt is brought in here from the outside (the Japan Sea).

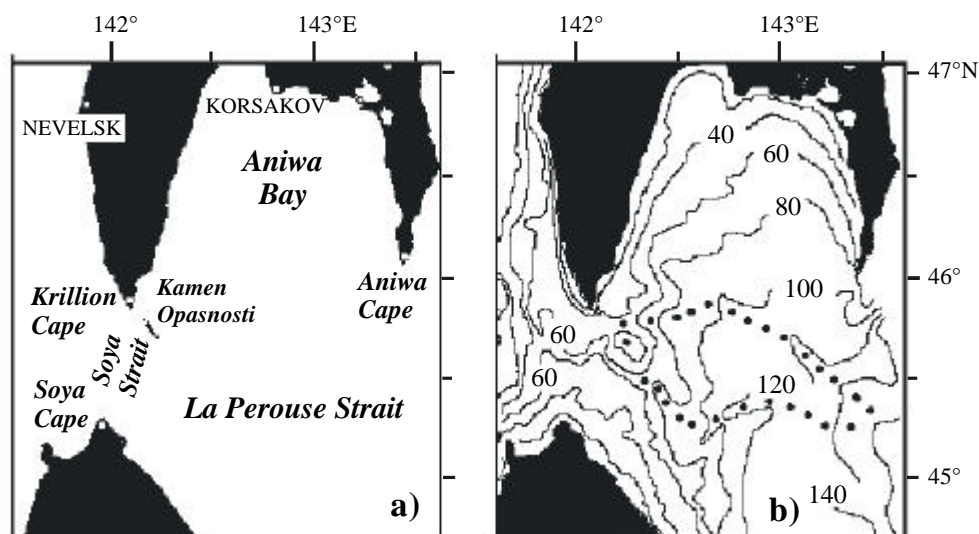


Fig. 1 Schemes of (a) the investigated area and (b) bottom topography. Bottom troughs are indicated by dots. Depth is in meters.

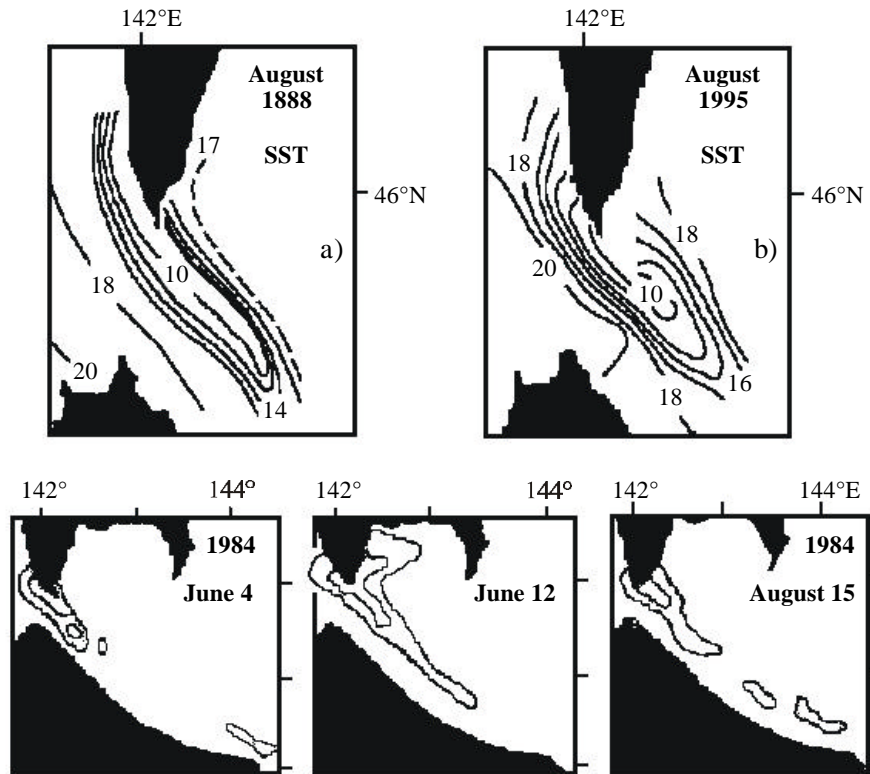


Fig. 2 Surface temperature (a) in summer of 1888 (Makarov, 1894), (b) in summer 1995 (Tanaka et al., 1996) and (lower panels) in summer 1984 (Aota et al., 1985).

Data

In this paper the data of 9 oceanographic expeditions carried out by the Sakhalin Hydrometeorological Administration in April–December, 1962, April–July, 1963 and by the Far Eastern Regional Hydrometeorological Research Institute in September, 1991 are used. Measurements of wind and air temperature (1962–1991) at Sakhalin coastal stations and data from ice surveys in the strait in 1945, 1959, 1961 were also used. All Russian oceanographic measurements in the strait (a total 272 oceanographic stations) were made on 5 meridional sections: 142°E, 142.4°E, 142.9°E, 143.4°E and 46°N. The westernmost section (at 142°E) was situated to the west of Kamen Opasnosti Rock and another (at 142.4°E) was located to the east of it. Thus, the most interesting part of the strait was never investigated in detail.

Bottom topography of LaPerouse Strait

One peculiar feature of the bottom relief of LaPerouse Strait is a small island or rock, named Kamen Opasnosti (Rock of Danger) that divides Soya Strait in two unequal parts. It is located (45.8°N, 142.2°E) 8 miles to the southeast of Cape Krilion.

The rock is relatively small (150 × 50 m); however, an extensive stony area of about 3 miles in length is located around the rock (Fig. 1). Shallow areas between Krilion Cape and Kamen Opasnosti Rock, and to the east of them, creates conditions for vertical mixing and homogenization of the oceanographic characteristics in the area southeast of Krilion Cape.

The depth in LaPerouse Strait is less than 200 m and, in general, decreases from east to the west. In two underwater troughs (Fig. 1b) the depth also decreases (to 100 m), from east to west. By these troughs cold bottom water rises to the surface (Makarov, 1894). A deep-water pass (deeper than 60 m) at the center of Soya Strait allows the transfer of bottom water in the opposite direction.

The distribution of sediments at the bottom of LaPerouse Strait (Dyakova-Savelieva and Djakonov, 1954) gives an indirect description of currents in a strait. Thus, in the area between Cape Krilion and Kamen Opasnosti Rock, and to the southeast of it (and the same – near Aniwa Cape) is located a zone of washed up sediments, which indirectly

testifies to the existence of a strong current between Cape Krilion and Kamen Opasnosti Rock. On the other hand, in most of the strait a silty bottom prevails testifying to the absence of strong flows.

Air temperature, wind and tides

The annual mean air temperature in the area of Cape Krilion (4°C) is lower than at the locations to the north of it at Nevelsk (5°C), Korsakov (3°C) and Moneron Island (4.5°C). This can be explained not only by an influence of warm Tsushima Current in Tartar Strait (Moneron and Nevelsk) but also by an existence of cold water in the area of Cape Krilion. In winter (November–March) the relation between the stations is opposite.

Western and northwestern winds prevail both in summer and in winter in the Cape Krilion area and to the east of it (west of Cape Krilion the wind is opposite). At Moneron Island there is northeastward wind. At the southwestern coast of Sakhalin the southward and southeastward winds prevail. Therefore, such winds cannot cause an upwelling of subsurface water southwest of Sakhalin, but they can cause an upwelling to a southeast off Cape Krilion.

Tides and tidal currents play an important role in the distribution of oceanographic characteristics in LaPerouse Strait. Average sea level of the Japan Sea is about 20 cm higher than sea level of the Okhotsk Sea. Thus the mean flow of the surface water should be directed out of the Japan Sea through LaPerouse Strait into the Okhotsk Sea.

Actual currents between Krilion Cape and Kamen Opasnosti Rock differ from the mean currents. This is caused by daily changes in sea level of the Japan Sea (the sea level at Krilion Cape changes within a day by 120 cm) and by strong tidal currents. The greatest speed of tidal currents is observed in the narrows between Krilion Cape and Kamen Opasnosti where it exceeds 400 cm/s (Veselova, 1963). By means of such tidal currents cold water from LaPerouse Strait penetrates to the southwest coast of Sakhalin (but usually not too far). Cold and low saline water exists in LaPerouse Strait all year below depths of 20 m. It is renewed each winter when ice appears in LaPerouse Strait.

Sea ice

Let us consider typical features of sea ice distribution using as an example the winter of 1945 (when detailed information on ice cover was collected by the USSR Hydrometeorological Service) (Fig. 3.) Sea ice in LaPerouse Strait occurs for the first time in the beginning of January when most of Tartar Strait is already covered with ice.

Ice is formed in Aniwa Bay during the entire winter and during the entire winter cold water is formed there too. In the beginning, the ice, formed in Aniwa Bay, is moved from the coast by offshore winds to the south and thaws there. Therefore, ice cover in LaPerouse Strait becomes significant only with an appearance of ice from the Okhotsk Sea. After the ice appears in Aniwa Bay, a coastal polynya appears (January 22; February 2; February 15; March 4).

By January 20 the ice completely covers the Strait and stays up to the middle of April. From January until April the ice conditions change many times, but ice drift is mainly directed toward the Japan Sea. Sometimes pressure of the ice from the Okhotsk Sea weakens so that along Hokkaido and Sakhalin strips of open water appear (January 27). Sometimes the pressure of ice grows so that the ice penetrates into the Japan Sea (January 15, February 15).

The maximal distribution of ice in LaPerouse Strait occurs one month later than in Tartar Strait. The clearing of ice from LaPerouse Strait occurs later, too. In winter the main direction of flow of subtropical water changes. At the start of winter warm water passes mainly into LaPerouse Strait, and Tartar Strait quickly becomes covered by ice, but when the ice of the Okhotsk Sea closes LaPerouse Strait, all the warm water penetrates into Tartar Strait and a fast clearing of the strait occurs. Hence, ice cover in Tartar Strait is connected with ice cover in LaPerouse Strait: when ice cover of Tartar Strait is maximal, ice cover of LaPerouse Strait is minimal and vice versa.

When LaPerouse Strait is closed by ice warm subtropical water cannot to penetrate into LaPerouse Strait. Only sometimes (when ice pressure from the Okhotsk Sea weakens) can warm water penetrate in small volumes into the strait near the bottom. The vertical water structure of the water column of the strait is different in the beginning of winter and at the end of winter.

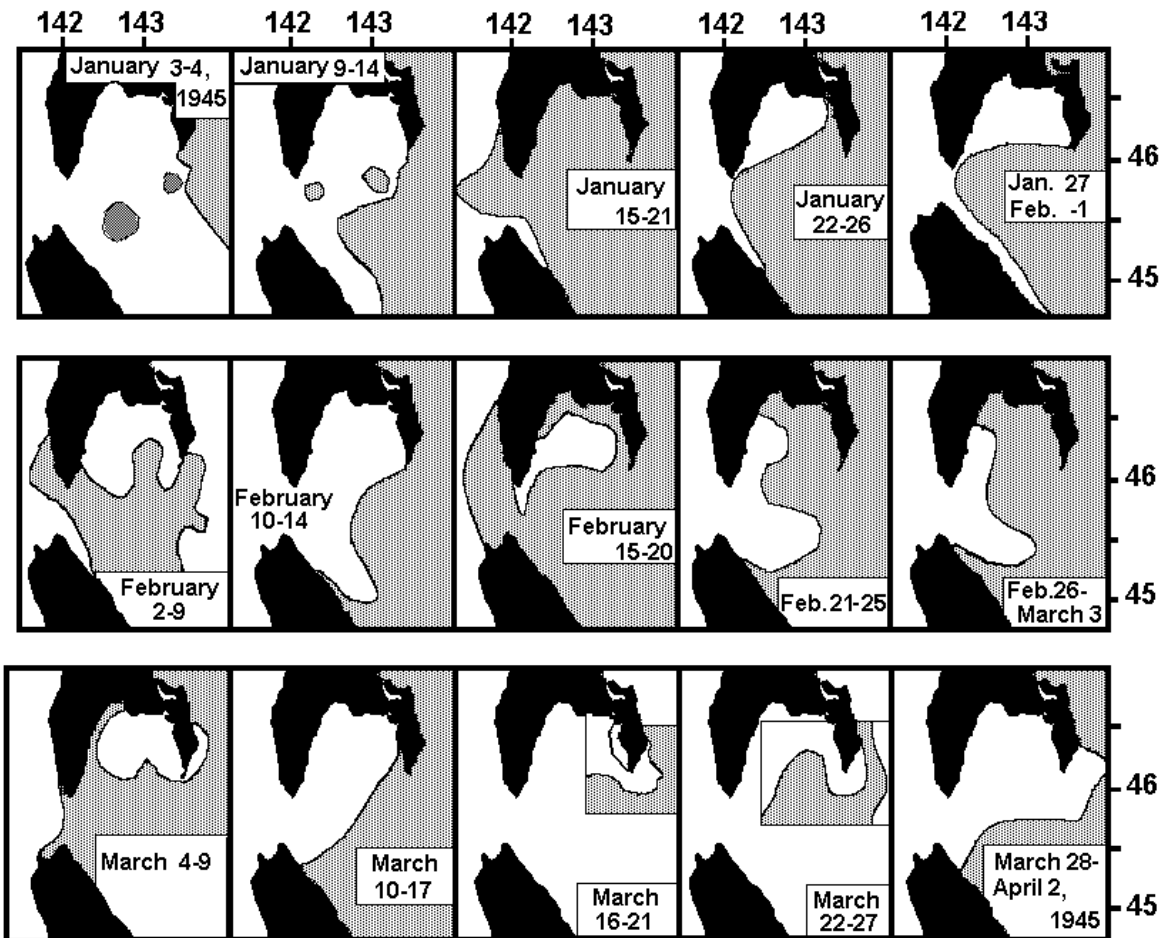


Fig. 3 Distribution of sea ice in LaPerouse Strait. Areas covered with ice are shaded.

Water masses in LaPerouse Strait

The vertical water mass structure of LaPerouse Strait consists of three layers (Aota, 1970, Bobkov, 1995, Pischalnik and Arkhipkin, 1998): a warm intermediate layer, a cold subsurface layer and the surface layer (see Table 1).

However, the data of summer 1991 (Fig. 4) allow us to allocate not three, but four water masses (two different water masses may be identified in the surface layer):

- A – Surface Water Mass of low salinity;
- B – Surface Water Mass of high salinity;
- C – Cold Subsurface Water Mass;
- D – Intermediate Warm Water Mass of high salinity.

Of course, the number of water masses is different in different seasons (two water masses are typical for winter and four for summer) and at different sections (two water masses are typical for the section along 142°E, and four water masses for 143.4°E). In general, four water masses are found in LaPerouse Strait more often than three.

Typical stations (September 1991) can be divided into 4 groups, in which the water structure is different: A+D (stations 34, 37, 43); A+C (stations 22, 24, 29); B+D (station 45); D (station 47). It is necessary to note that there is no combination of B+C (salty surface water and cold subsurface water). This implies that core of salty water is situated not at the surface, but near the bottom only. The typical characteristics of water masses are presented in Table 2.

Table 1 Known water mass characteristics (water temperature T (°C), salinity S (‰)) in LaPerouse Strait.

Source	Warm Water Mass		Cold Water Mass		Surface Water Mass	
	T	S	T	S	T	S
Aota (1970)	3–17,	33.6–34.0	-1.0-3.0	32.5-33.2	-1-14	31.2-32.5
Bobkov (1995)	12–18	33.5–33.9	-1.2-0.5	33.0-33.2	8-15	32.4-32.7
Pischalnik and Arkhipkin (1998)	2–11,	33.1–34.0	-1.5-2.5,	32.6-33.6	2-18	31.2-32.6
Pischalnik (1998)	2–20 5.8 9.0 6.8	33.1–34.0 mean 33.7 spring 33.6 summer 33.5 autumn	-1.5-2.0 0.4 0.2 0.2	32.4-33.4 33.0 spring 33.0 summer 32.8 autumn	2-18 6.7 11.4 7.6	31.2-33.0, 32.2 spring 32.2 summer 32.0 autumn

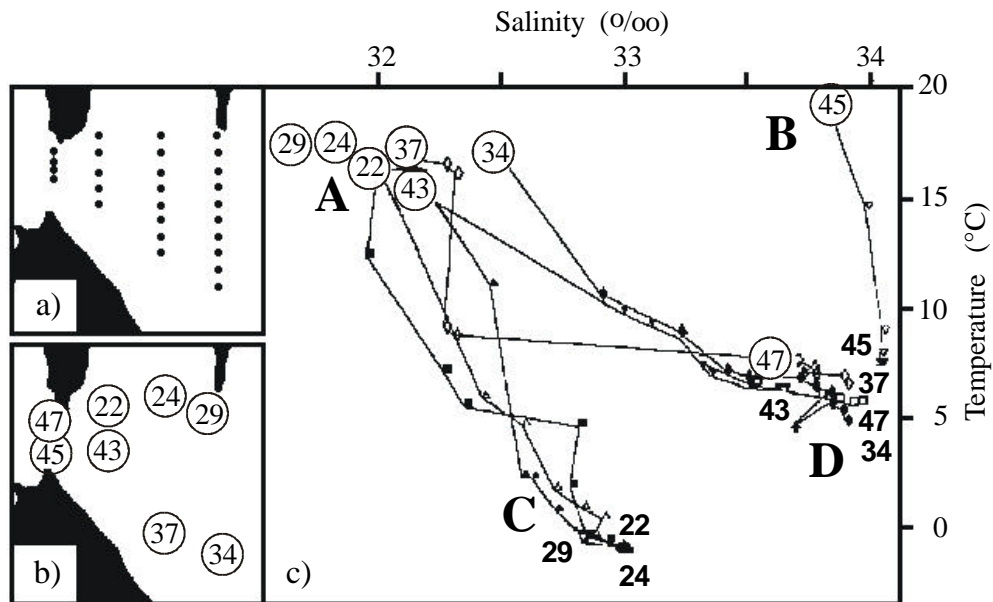


Fig. 4 (a) Position of standard oceanographic stations in LaPerouse Strait and T(S)-curves (c) of (b) some stations in September 1991.

Table 2 Temperature (°C), salinity (‰), density and dissolved oxygen (ml/l) in the core of basic water masses in LaPerouse Strait in summer of 1991.

Section/ Water Mass	A-Surface Fresh (0–10 m)	B-Surface Salty (0–10m)	C-Subsurface Cold (30–100m)	D-Intermediate Warm (20–100m)
142.0°E	–	19, 33.8, 24.2, 5.3	–	8, 34.1, 26.6, 6.4
142.4°E	17, 32.0, 23.3, 5.2	16, 33.8, 24.9, 5.6	–0.7, 32.9, 26.5, 5.1	8, 34.0, 26.5, 6.4
142.9°E	17, 31.8, 23.1, 5.1	15, 32.7, 24.2, 6.0	–1.0, 32.8, 26.4, 5.3	7, 33.6, 26.4, 5.3
143.4°E	17, 32.0, 23.3, 5.9	14, 33.2, 24.8, 5.9	–1.1, 32.9, 26.5, 6.1	8, 33.9, 26.4, 6.3

Surface Salty Water differs from Surface Fresh Water by up to 2‰ in salinity. Surface Fresh Water occupies almost all of LaPerouse Strait, except for a narrow strip along Hokkaido. A typical feature of this water is low salinity (less than 33.0‰). Surface Salty Water occupies a narrow strip along Hokkaido. A typical feature of this water is high salinity (more than 33.8‰). The water temperature of surface water both from the Japan Sea (salty), and from the Okhotsk Sea (low salinity) in summer is almost identical (15°–17°C).

A sharp thermal front divides these water masses. Waters to the south of the front have temperature more than 4°C in April and 8°C in May, while to the north of the front the temperature is less than 2°C in April and less than 5°C in May. The warm and salty surface water disappears in November (Aota et al., 1970) or in August (Pischalnik and Arkhipkin, 1998), but even in December (1962) we found this water (warm and salty) on the surface near Hokkaido.

The Intermediate Water Mass of high salinity (and high temperature) differs from surface salty water, first of all, in temperature. For example, in September 1991 the difference in temperature is 15°C. On the 142°E section Intermediate Water Mass exists at all stations, but on other sections – only at southern stations. On a section at 142°E a core of high salinity was located near the bottom in the winter (50 m, December 1962) and in the spring (60 m, April 1962; May 1963), and in summer (June 1963; September 1991). The greatest salinity on a section at 142°E was found in September 1962 (10 m, 34.63‰). However, usually the salinity in a core is a little lower: in May 1962 at 50 m (34.31‰), in December 1962 (34.23‰), in April 1963 (34.27‰). The position of highest salinity does not coincide with the position of highest temperature. Highest temperature in summer is typical for the surface layer.

Subsurface Cold Water is situated in LaPerouse Strait below Surface Waters and down to the bottom. Its typical feature is low temperature (but also rather low salinity). The depth of the core of this water mass grows from the eastern border of the strait (143.4°E) up to western (142°E) border. Water of lowest temperature and Water of lowest salinity do not coincide with each other spatially. For example, in May 1962 at 142.9°E temperature less than 2°C was below 20 m, but salinity less

than 32.5‰ was just above it). The temperature of Subsurface Cold Water depends on the season. Just after winter (in April and May) the water temperature in its core is close to the temperature of freezing (–1.7°C to –1.0°C). In summer (June, September) the area with a negative water temperature decreases; in December water of this layer already has positive temperature everywhere (but, nevertheless, below 2°C).

We have named the subtropical (high salinity) water as “intermediate” and the subarctic (cold) water as “subsurface”, because in their collision (although the border between them usually is almost vertical), subtropical water is situated below than subarctic water.

Spatial distribution of temperature and salinity

In general, isotherms in LaPerouse Strait are situated along a line NW-SE (parallel to the northern coast of Hokkaido). The main feature of the surface temperature field is a thermal front which divides warm and cold waters. The front represents an outcropping on the surface of the basic thermocline. If at the surface there is a belt of cold water, then instead of one front, two appear. In this case the belt of cold water is situated between fronts (frontal lines). The gradient of water temperature can reach 3°C at 10 miles, but even in case of the absence of the belt at the surface, the belt exists at levels below the surface. Thus, the belt of cold water is a typical feature of oceanographic structure of LaPerouse Strait. In June 1963 (Fig. 5) the belt was typical (lowest temperature in the belt was near Cape Krilion); in April 1962 the belt was unusual (lowest temperature was in the southeastern part of the strait), but typical for other (subsurface) levels; in October 1958 the situation was unusual: there were two belts (one from Cape Krilion, another from Cape Aniwa).

In April (1962) the belt was directed to Cape Krilion. Temperature inside the belt rose from 1.8°C (in the southeastern part of the strait) to 2.8°C (near Cape Krilion). The highest temperatures at the surface were near Hokkaido (more than 5°C) and in Aniwa Bay (more than 4°C). In April 1963 the belt was absent at the surface. In Soya Strait water temperature rose from 2°C (near Cape Krilion) to 7°C (near Cape Soya). In May (1962) the belt was very small (just between Cape Krilion and Kamen Opasnosti Rock). Inside the belt the

lowest temperature was less than 3°C. In May 1963 the size of the belt at the surface was also small and the lowest temperature was about the same (about 3°C). In June (1963) at the surface the belt was weak. Lowest temperature inside the belt was less than 5°C. In October (1958), in addition to a belt from Cape Krilion (lowest temperature was less than 8°C), there was a belt from Cape Aniwa (lowest temperature was the same). Both areas of cold water appear at the surface as the result of an upwelling of subsurface water. The direction of cold water distribution at the surface coincides with the direction of prevailing currents: southeastward from Cape Krilion (due to the Soya Current); southward and northwestward from Cape Aniwa (due to the East Sakhalin Current and LaPerouse Current).

Below the surface (Fig. 6) the distribution of cold water was usually the same in different surveys: the cold belt was directed from the southeastern

part of the Strait to Cape Krilion. The lowest temperature was usually at the southeastern side of the belt. This means that cold water can penetrate the Cape Krilion area from southeastern part of the Strait.

The cold water temperature in the belt decreased with increasing depth (the core of Subsurface Cold Water is located near the bottom). Water with negative temperature was situated just below 30 m. In all surveys (even if the belt at the surface is absent) the cold belt was seen at levels below 20 m. For example, in September 1991 the lowest temperature (below 6°C) was noted near Krilion Cape (at 20 m) and below than 5°C (at 30 m). The salinity distribution has some related features too: the salinity front coincides with the thermal front, and areas for which low water temperature values are characteristic, also differ by low salinity (Fig. 7.)

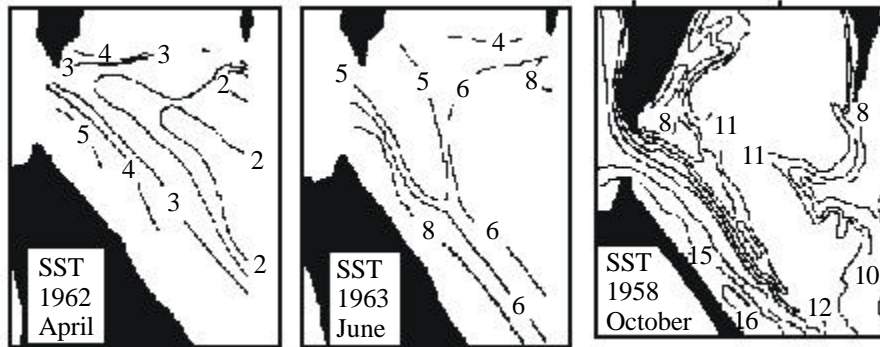


Fig. 5 SST distribution in LaPerouse Strait. Scheme of October 4–10, 1958 is taken from paper of K. Furuya (1994).

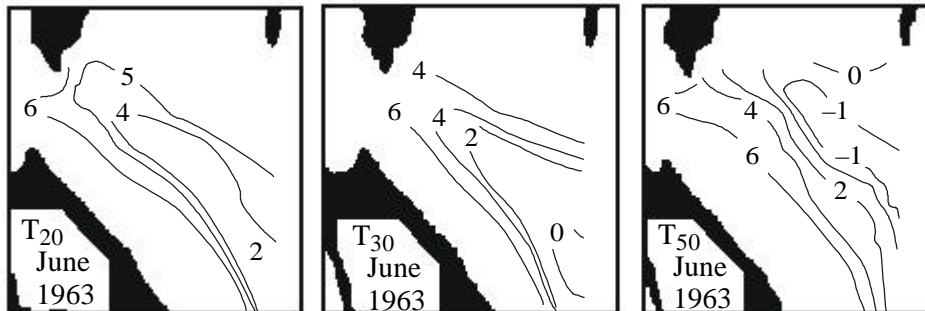


Fig. 6 Distribution of water temperature in summer of 1963 at different levels.

The distribution of water temperature at the main sections (142.4°E, 142.9°E, 143.4°E) for summer (when the belt was seen most frequently) – June 1963 and September 1991, is presented in Figure 8. West of the entrance to the strait (142°E) water temperature from April to December did not fall below 0.6°C. The border of the water masses on this section usually pass a distance of about 8 miles from Cape Krilion, to the north of 45.8°N. Inside this narrow strip, water with salinity less than 33‰ exists only sometimes.

Cold Subsurface Water was found at all sections. On the 142°E section (west of Cape Krilion) it was sometimes found at the most northern station only). For example, in September 1991 Cold Water was not farther than 3 miles from Cape Krilion. On the 142.4°E section (east of Kamen Opanosti

Rock) Subsurface Water was always found. On this section the Cold Water was located closer to the surface compared to other sections. On the third section (142.9°E) Cold Water was always located to the north of 45.3°N, and on the 143.4°E section it occupied almost all the strait. The core of this water and its top border rise from east on west in accordance with the change of a bottom relief, while the core of Warm Intermediate Water on all sections is near the bottom. For example, in April 1963 the depth of the top border rose from 35 m at 143.4°E up to 5 m at 142°E. Water temperature of a layer in the summer rose from 2°C at 143.4°E up to 7°C at 142°E, and salinity grew from 32.8‰ to 33.5‰. As the density of these waters in the summer is 26.4–26.5, and density of subtropical waters is 26.8–27.0, subtropical waters occupy the lower position in the water column.

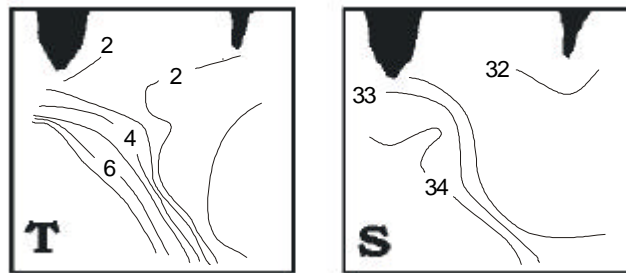


Fig. 7 Distribution of temperature (left) and salinity (right) at the surface for April 26–29, 1963.

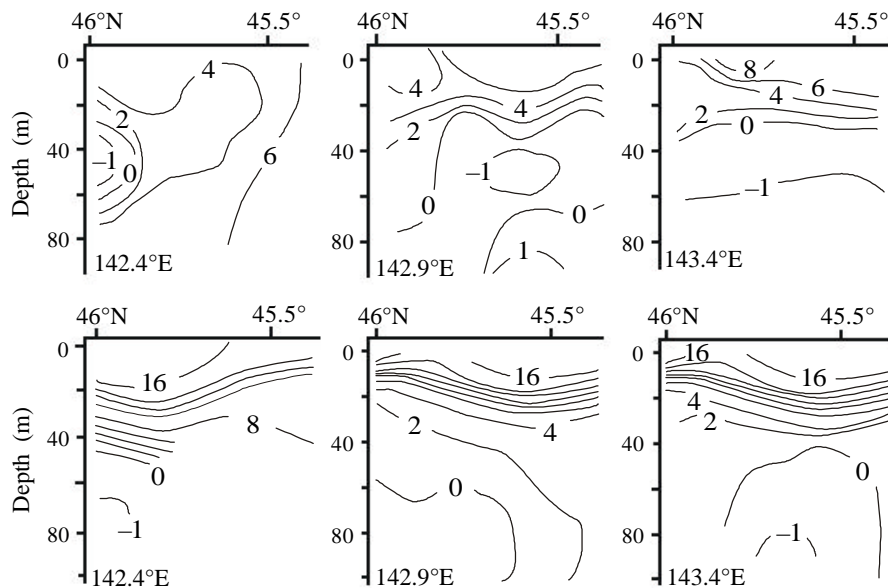


Fig. 8 Distribution of temperature along 142.4°E, 142.9°E and 143.4°E sections in September 1991 (top) and in June 1963 (bottom).

Discussion of the belt of cold fresh water

The belt of cold water near Cape Krilion was traced during most of the year (April, May, June, August, September, October) and in different years (1888, 1958, 1962, 1963, 1991). The existence of the cold water belt (from Krilion Cape to the southeast) is usually explained (Tanaka et al., 1996; Zhabin et al., 1992) by an upwelling along the west coast of Sakhalin and transport into LaPerouse Strait by the so-called (West) Sakhalin Current (Yurasov and Yarichin, 1991). However, characteristics of deep surface and subsurface waters near the Sakhalin coast are usually distinct from characteristics of waters in the belt (with the exception of the inflow of cold waters from LaPerouse Strait).

Water temperature in the belt is 3–5°C (in April–June) and 8–14°C (in September–October) while salinity is within 32.0–32.6‰. Salinity of waters west of Sakhalin is higher (salinity of surface water 33.9–34.2‰ and salinity of deep water about 34.0‰). Local formation of cold water at the surface is seen, for example, from the temperature distribution in October 1958 (Fig. 5) – lowest temperature is seen to the east of Cape Krilion. Therefore, cold and fresh water in the belt is not brought from the Japan Sea – it is formed here – in LaPerouse Strait. In contrast, cold water near southwestern Sakhalin is brought from LaPerouse Strait. At Cape Krilion prevailing offshore winds cause the upwelling of subsurface waters and characteristics of subsurface water here coincide with the characteristics of surface water in belt (Fig. 9).

Local cold waters are formed during winter ice formation in Aniwa Bay. Together with cold waters constantly penetrating from the Okhotsk Sea, they form a layer of cold water existing during year. Cold waters from the Okhotsk Sea move to

Soya Strait as a subsurface current. Because of the special bottom topography of LaPerouse Strait, the direction of this water transport is northwest. The upper border of this layer rises from the east to the west. Near Kamen Opasnosti Rock there is a long stony area. There, during conditions of offshore winds and strong tidal currents, active processes of upwelling and tidal mixing occur. Cold mixed waters from the Kamen Opasnosti area are distributed along the Soya Current, and their width decreases.

Due to a strong tidal current typical for area between Kamen Opasnosti and Cape Krilion, cold water penetrates into the Japan Sea and, under the influence of the Coriolis force, moves to the north along the coast of Sakhalin. Usually surface cold water is distributed not far to the north from Cape Krilion, but sometimes under the influence of storm winds it reaches to Nevelsk. The direction of the wind is very important for this phenomenon. In the case of winds of unusual direction, this belt disappears.

Makarov (1894) is usually considered (Veselova, 1963) to be the first person who described the belt of cold water. We found this not to be correct. Actually the first person to write about this phenomenon was the Russian hydrographer, E. Maidel (1877, 1878, 1879). He described numerous cases of current measurements from the Okhotsk Sea and in the Japan Sea between Krilion Cape and Kamen Opasnosti. He also noted that the water salinity penetrating into the northern part of the strait is essentially lower than salinity of water penetrating in the strait from the Japan Sea. Another little-known paper of Dr. Zuev (1887) noted that the width of the cold strip along Sakhalin decreases to the north (from 8 miles at Cape Krilion to 4 miles at 46.8°N) and is connected with cold flow from LaPerouse Strait and tidal currents.

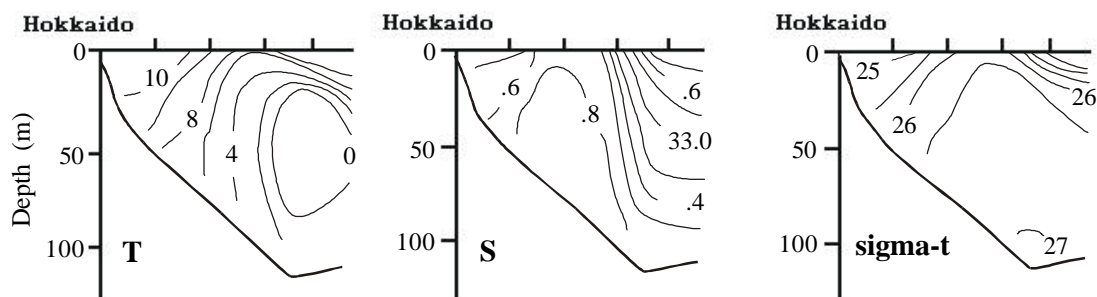


Fig. 9 Distribution of water temperature, salinity and density at section crossing the belt in July 1984 (Aota, et al., 1985).

Cold Krilion Current and cold West Sakhalin Current

Makarov's (1894) map of SST (Fig. 2a) is identical to the map (Fig. 2b) of Tanaka et al. (1996), but their explanations for this phenomenon are contrary. Admiral S.O. Makarov wrote, "the water of the Okhotsk Sea penetrates into the Japan Sea and, due to Earth rotation turns to the right"—the along southwestern coast of Sakhalin and "because of constant water transport from LaPerouse Strait the cold water at the southwestern coast of Sakhalin does not disappear." Tanaka et al. (1996) wrote, "the West Sakhalin Current flows southward along the west coast of Sakhalin ... and directly flows into La Perouse Strait."

The "(West) Sakhalin Current" (probably, for the first time) was cited by Yarichin (1980) with reference to some other works, but the citation was incorrect: information from papers (references) was not given (perhaps they were confidential or unpublished, e.g. Istoshin (1950), Biryulin (1954), Shelegova (1960)). We now consider the views on currents from some of these authors. The most popular scheme of surface circulation (Uda, 1934) shows a *northward* current along southwestern Sakhalin (*from* Laperouse Strait). On schemes from Leonov's papers (1948, 1958a,b) and from his book (1960), based on pre-war Russian investigations, a current *from* LaPerouse Strait into the Japan Sea and a *northward* current along southwestern Sakhalin was shown. Biryulin (1954) wrote, "At a station located to the west of Soya Strait (45.8°N, 141.5°E) is well noticed the freshening action of waters, penetrating into the Japan Sea *from* the Okhotsk Sea." The research of Istoshin (1950) gives the opposite description of currents than is attributed in the review of Yarichin (1980). Yarichin wrote "By way of research of circulation of waters in the northern part of the sea, Yu.V. Istoshin for the first time has established the fact that, instead of a cold current which penetrated in the sea from Aniwa Bay, bending around Cape Krilion and going in a northern direction along the southwest coast of Sakhalin island, in this area there is a steady flow of waters on the south with velocity exceeding 50 cm/s." (Yurasov and Yarichin, 1991). Istoshin (1950) actually wrote something different: "In April 1949 the fields of broken ice from LaPerouse Strait were distributed to the north under action of a southwest wind and current directed *on north*" (page 57), "in April–May 1949 was an output of ice *from* LaPerouse Strait to the southwest coast of Sakha-

lin" (page 61), "at Sakhalin coast all bottles which have been thrown out to the north of Gornozavodsk (46.5°N) were directed *to the north*" (page 63). No evidence of the proposed "West Sakhalin Current" and enough evidence of current from LaPerouse Strait and northward current along southwestern Sakhalin were given. Papers of Shelegova (1960) also give only evidence of the penetration of cold waters to coast of the southwestern Sakhalin by northward current *from* LaPerouse Strait. In a figure from an unknown paper of E.K. Shelegova given in Yurasov and Yarichin, 1991) there is northward current *from* LaPerouse Strait in summer as in winter. Besides the usual penetration of cold waters in area of southwest Sakhalin, Shelegova described typical cases of especially strong transport of cold waters (Shelegova, 1960). In such cases a sharp decrease of water and air temperature, together with a northward current, were described in an area up to Nevelsk.

Thus, only published papers of Yarichin (1980, 1982), Yarichin and Pokudov (1982) and Yurasov and Yarichin (1991) showed the so-called (West) Sakhalin Current as a southward flow of cold fresh water. Notice that there are declared features of the "West Sakhalin Current": it not a branch of the Tsushima Current. It is flow of cold waters to the south; the stability of its direction is more than 90% and water transport is 2 Sv (mean water transport of the Tsushima Current is the same). In one paper (Yarichin and Pokudov, 1982) waters of this current were directed in two directions at once: to the north from 47°N and to the south from 47°N. Such results were obtained from unusual analysis of current measurements. Short-duration data of current measurements made in different years at 46°N and 48°N (Fig.10a) were interpolated so that between points of measurements the currents of different (opposite) directions have appeared (Fig. 10b).

To summarize, we conclude that references to papers were made incorrectly and the existence of the Cold West Sakhalin Current was not accurately shown.

Southwest of Sakhalin there is comparatively strong current, but it is the branch of the Tsushima Current (as directed to the north as directed into Soya Strait). Sometimes at the southwestern Sakhalin coast strong cold currents occur, but *from*

LaPerouse Strait as the result of cooperative action of strong winds and strong tidal currents.

The distribution of density (one example of June 1963, Fig. 11) shows that besides the Soya Warm Current (along the coast of Hokkaido) one can identify in the strait a flow in the opposite direction. This current was named by S.O. Makarov and Dr. Zuev as the “Cold current of LaPerouse Strait” and by E. Maidel as the “Krilon Current”. It is traced at subsurface levels north of the ther-

mal front. Because of shallow depths any geostrophic calculations are impossible, but it is possible to get some information about currents from the density distribution. For example, the famous and widely cited map of surface currents of the Japan Sea (Uda, 1934) was derived from the density distribution. From the density distribution, the northwestward Krilon Current in the strait was seen in different months usually as subsurface flow. We think that the Krilon Current is an essential feature of LaPerouse Strait oceanography.

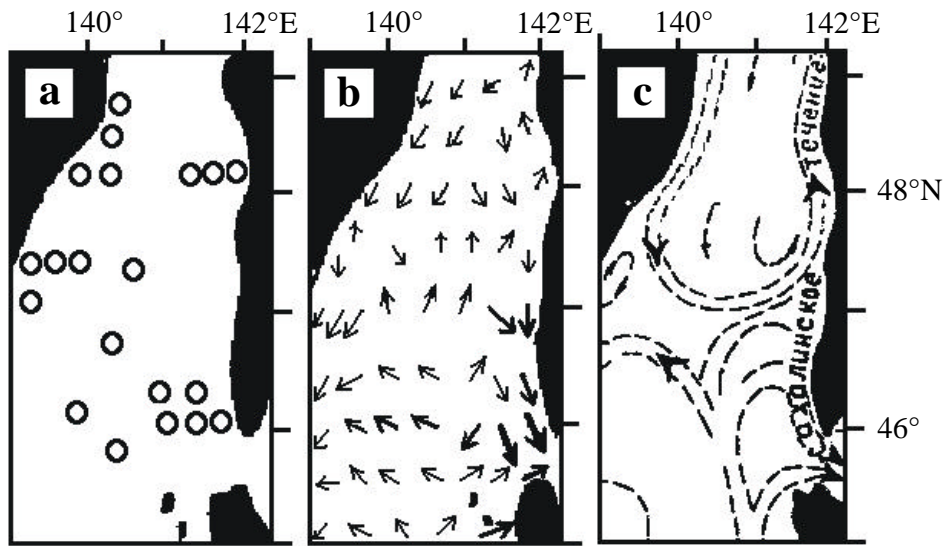


Fig. 10 Distributions of stations with (a) currents measurements, (b) surface currents by currents measurements and (c) a generalized scheme of surface water circulation (Yarichin, 1980; Yurasov and Yarichin, 1982). Notice that currents of different directions were obtained in the area where measurements were not ever conducted. The so-called Sakhalin Current is shown in (c) at the same time in two different directions: to the north and to the south (Yarichin and Pokudov, 1982).

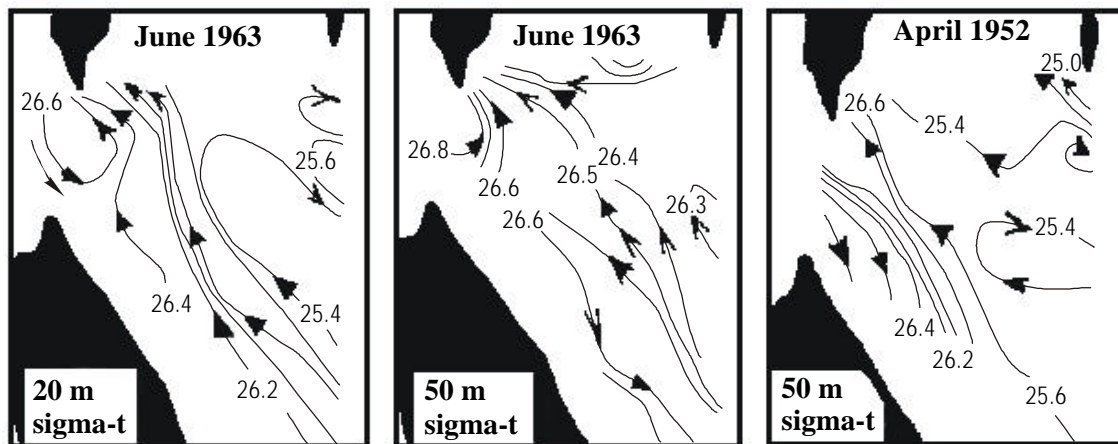


Fig. 11 Examples of currents taken from the density distribution.

Conclusions

1. Over the whole year there are four water masses in LaPerouse Strait. The Subsurface Cold Water Mass exists in the strait during the whole year. This water rises to the surface from the eastern to the part of the strait.
2. A belt of cold water existing near Krilion Cape is a result of local winds, bottom topography and tidal currents
3. The northwestward Cold Krilion Current exists in the strait below 20 m. The existence of the so-called West Sakhalin Cold Current is not proved.

Acknowledgment

The authors are much obliged to Dr. V.B. Lobanov (Pacific Oceanological Institute) for very useful remarks and help.

References

- Aota, M. 1970. Study of the variation of oceanographic condition north-east of Hokkaido in the Sea of Okhotsk. *Low Temp. Sci., Ser. A*, 28, 261–279. (in Japanese)
- Aota, M. 1975. Studies on the Soya Warm Current. *Low Temp. Sci., Ser. A*, 33, 151–172. (in Japanese)
- Aota, M. 1984. Oceanographic structure of the Soya warm current. B. *Coastal Oceanography*, 22, 30–39. (in Japanese)
- Aota, M. and Matsuyama, M. 1987. Tidal current fluctuations in the Soya Current. *J. Oceanogr. Soc. Japan*, 43(3), 276–282.
- Aota, M., Nagata, Y., Inaba, H., Matsuyama, Y., Ono, N., and Kanan, S. 1985. The Soya Warm Current. A typical oceanic current flowing over shelf region. pp.164–187. In: *Ocean Characteristics and their Changes*. Kajiura, K. (ed.), Tokyo, Koseisyu-Koseikaku. (in Japanese)
- Biryulin, G.M. 1954. Hydrometeorological characteristics of fishery areas of Southern Sakhalin. pp.167–303. In *Works of Kuril-Sakhalin Cooperative Expedition of Zin-TINRO in 1947–1949, Vol 1*, USSR Academy of Sciences, Moscow. (in Russian)
- Bobkov, A.A. 1995. Thermohalinic background of the southern part of the Okhotsk Sea. pp .311–316. *Proc. Mombetsu Workshop on Sea Ice and the Okhotsk Sea*, 10.
- Budaeva, V.D. 1975. To the problem of variability of thermal conditions by the south-western coast of Sakhalin Island, in Aniva Bay and in South- Kuril Strait. *Proc. TINRO*, 95, 9–16. (in Russian)
- Budaeva, V.D. and Kharitonova, G.Yu. 1980. Application of Yoshida model for the calculation of vertical circulation of water in some areas of the shelf of Sakhalin Island. *Trudy DVNIGMI*, 86, 119–126. (in Russian)
- Budaeva, V.D., Makarov V.G. and Bulgakov, S.N. 1981. Water circulation in Tartar Strait and it's seasonal variation. *Trudy DVNIGMI*, 83, 35–43. (in Russian)
- Budaeva, V.D., Makarov, V.G. and Mel'nikova I.Yu. 1980. Diagnostic calculations of constant currents in Aniva Bay and in Laperuza Strait. *Trudy DVNIGMI*, 87, 66–78. (in Russian)
- Dyakova-Savelieva, E.N. and Dyakonov, A.M. 1954. Soils of coastal waters of southern Sakhalin and southern Kuril islands. pp. 127–157. In *Works of Kuril-Sakhalin Cooperative Expedition of Zin-TINRO in 1947–1949, Vol. 1*, USSR Academy of Sciences, Moscow. (in Russian)
- Furuya, K. 1994. Sea ice and weed fishing in the coast of Mombetsu. *Proc. Mombetsu Workshop on Sea Ice and the Okhotsk Sea*, 9, 129–133. (in Japanese)
- Istoshin, Yu.V. 1950. Hydrological conditions during the 1949 spring fishing season at southwest Sakhalin coast. *Works of Central Institute for Weather Forecast*, 21, 53–64. (in Russian)
- Leonov, A.K. 1948. Water masses of the Japan Sea. *Meteorologiya i Gidrologiya*, 6, 61–78. (in Russian)
- Leonov, A.K. 1958a. On the peculiarities of thermal structure and the currents of the Japan Sea. *Works of USSR Geographical Society*, 90(3), 244–264. (in Russian)
- Leonov, A.K. 1958b. On currents in the Japan Sea in summer. *Herald of Leningrad State University*, N 18, 125–142. (in Russian)
- Maidel, E.R. 1877. Magnetic and hydrological works in the Eastern Ocean. *Navy Collection*, N 10, 24 pp. (in Russian)
- Maidel, E.R. 1878. Hydrographic works in Amur Bay, at the coasts of the Japan Sea, Tartar Strait and the investigation of the currents in La Perouz Strait. *Navy Collection*, N 1, 10 pp. (in Russian)

- Maidel, E.R. 1879. Extra notes on the cold current in LaPerouse Strait. *Navy Collection*, 171(4), 47–53. (in Russian)
- Makarov, S.O. 1894. “Vityaz” and the Pacific Ocean. Vol. 1. 337 pp., Vol. 2. 511 pp. Saint-Petersburg. (in Russian)
- Pischalnik, V.M. 1998. Water masses of LaPerouse Strait. pp.110–117. In *Ways of Creation of a System of Monitoring the Shelf of the Sakhalin Area*. Sakhalin Publ. Co., Yuzhno-Sakhalinsk. (in Russian)
- Pischalnik, V. and Arkhipkin, V. 1998. The LaPerouse Strait water masses. *Proc. Intl. Symp. on the Okhotsk Sea and Sea Ice*, 13, 292–293.
- Shelegova, E.K. 1960. The case of abrupt cooling in a summer at the South-Western Sakhalin coast. *Proc. TINRO*, 46, 249–251. (in Russian)
- Takizawa, T. 1982. Characteristics of the Soya Warm Current in the Okhotsk Sea. *J. Oceanogr. Soc. Japan*, 38, 281–292.
- Tanaka I., Nakata A., Yagi H., Samatov A.D. and Kantakov, G.A. 1996. Result of direct current measurements in La Perouse Strait (the Soya Strait), 1993–1996. Manuscript, 13 pp.
- Uda, M. 1934. Hydrographical studies based on simultaneous oceanographical survey made in the Japan Sea and its adjacent waters during May–June 1932. *Rec. Oceanogr. Works in Japan*, 6(1), 19–107.
- Veselova, L.E. 1963. Some peculiarities of water thermal conditions at south-western coast of Sakhalin. *Trudy DVNIGMI*, 13, 42–63. (in Russian)
- Veselova, L.E. 1972. Spatial distribution of surface water temperature of the Okhotsk Sea. *Trudy DVNIGMI*, 37, 13–28. (in Russian)
- Yarichin, V.G. 1980. Condition of the study of the Japan Sea water circulation. *Trudy DVNIGMI*, 80, 46–61. (in Russian)
- Yarichin, V.G. 1982. Some peculiarities of horizontal movement of water of the Japan Sea northward of 40°N. *Trudy DVNIGMI*, 96, 111–120, (in Russian)
- Yarichin, V.G. and Pokudov, V.V. 1982. A formation of structure peculiarities of hydrophysical fields in the northern deep-water part of the Japan Sea. *Trudy DVNIGMI*, 96, 86–95. (in Russian)
- Yurasov, G.I. and Yarichin, V.G. 1991. *Currents of the Japan Sea*. Vladivostok, 176 pp. (in Russian)
- Zhabin, I.A., Zuenko, Yu.I., Demina, T.V. 1992. Surface thermal fronts in the northern part of the Japan Sea: Nature, variability, influence on the fishery. In: *Oceanographical Basis of Biological Productivity of the Northwestern Pacific*. pp. 157–167. Moroz, I.F. (ed.), Vladivostok. (in Russian)
- Zuev. 1887. Observations on water temperature in the northern Japan Sea. *Notes on Hydrography*, 2, 53–59. (in Russian)

Results of direct current measurements in the La Perouse Strait (the Soya Strait), 1995-1998

Iori TANAKA and Akifumi Nakata

Hokkaido Central Fisheries Experimental Station, Yoichi, Japan

The La Perouse Strait (the Soya Strait) and its adjacent waters are good fishing grounds, but understanding of the physical, chemical, and biological environment has been very limited as the border between Japan and Russia runs along the center of the strait and a comprehensive survey has not been conducted. As an example, no direct estimates of the transport through the strait have been made.

The Hokkaido Central Fisheries Experimental Station (HCFES) and the Sakhalin Research Institute of Fisheries and Oceanography (SakNIRO) designed a cooperative observation project in the La Perouse Strait and its adjacent waters. This project is called the La Perouse Project, and it started in August 1995. Preliminary results of the project were presented by Yagi et al. (1996), Tanaka et al. (1996) and Nakata et al. (1996) at the 5th PICES Annual Meeting in Nanaimo.

Simultaneous direct current measurements in the La Perouse Strait were conducted by both institutions during the period from August 8 to 9, 1995. HCFES measured horizontal current structure by using a ship mounted ADCP (Acoustic Doppler Current Profiler), and SakNIRO applied two mooring systems along 142°E (Tanaka et al., 1996). Each of the mooring systems were set in the northern half of the strait, and were equipped with two current meters. The measurements were successful and the data series long enough to get residual currents by eliminating tidal current components. The observations of our joint project conducted in August 1995 were an historical first attempt to obtain the total volume transport passing through the whole section of the La Perouse Strait. However, the observation in August 1995 is the only direct current measurement in the northern half of the strait until now.

In this paper, we report the results of the ADCP observations conducted regularly in the southern half of the strait after 1995, by focusing on the long-term variability of the transport of the Soya Warm Current through the strait. Two kinds of ADCP were used on the R/V *Hokuyo Maru* (Wakkanai Fisheries Experimental Station): RD-VM150 (RD Instruments) was used in August 1995 and March 1997. The maximum number of levels measured was 20 and 5, respectively, and a FURUNO CI-30 (Furuno Electric. Co.) for the other observations (the maximum number of levels was 3).

As discussed by Odamaki and Iwamoto (1999), the magnitude of the tidal current may sometimes exceed that of the Soya Current. The ADCP observation in August 1995 were repeated eight times within the period of 25 hours (more exactly 24 hours and 50 minutes), in order to eliminate the diurnal- and semi-diurnal tidal components. After 1996, ADCP measurements were repeated four times within 25 hours. We used a method developed by Katoh (1988) to eliminate tidal components. The original version of his method was based on data repeated four times. The method was extended to accommodate data repeated eight times in the case of 1995. Katoh (1988) applied his method to the data repeatedly observed along a line but in 1995 many fishing boats were operating and many cargo ships navigating in the strait at the time of the observation. Our research vessel could not navigate along a straight line, and was often forced to change speed and direction. Thus, we selected three points, S101, S102 and S103 (Fig. 1) and the vessel came back to each of these stations exactly at the prescribed times so that Katoh's method could be applied. The vertical current shear in the Soya Warm Current is generally weak and the current is almost

barotropic (Aota 1975, Kanari et al., 1984, Tanaka et al., 1996), although the magnitude tends to decrease a little with depth. Here, the vertically averaged velocity is used for the estimation of the transport.

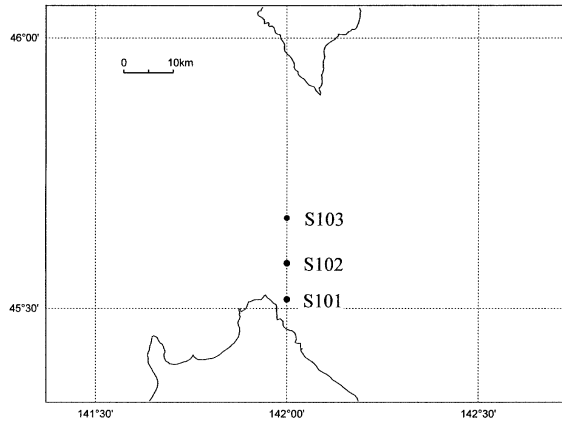


Fig. 1 Selected observation points, S101, S102 and S103, where the ADCP observations were repeated in each cruise, and where the residual current components (oceanic current velocities) were obtained.

HCFES oceanographic observations in the southern half of La Perouse Strait (the Soya Strait) were generally carried out four times per year: March (before 1998) or April (the observation was made both in March and April in 1998), June, August, and December. The ADCP observations repeated over 25 hours are similar to those taken in August 1995, and it was planned to continue these routine observations after 1996 until present. All of the repeated ADCP observations in December could not be conducted due to severe weather conditions so the measurements have been conducted 10 times until now.

The eastward component of the vertically averaged velocity at each station is multiplied by the water depth and by the representative horizontal scale, and integrated from the Hokkaido coast to the central part of the strait (S103). The resulting eastward transport of the Soya Warm Current crossing the southern half of the strait at each observation time is plotted in Figure 2 against the time. The transport of the

Soya Warm Current is between 0.15 and 0.50 Sverdrup except in March 1997, when a negative (westward) transport was found.

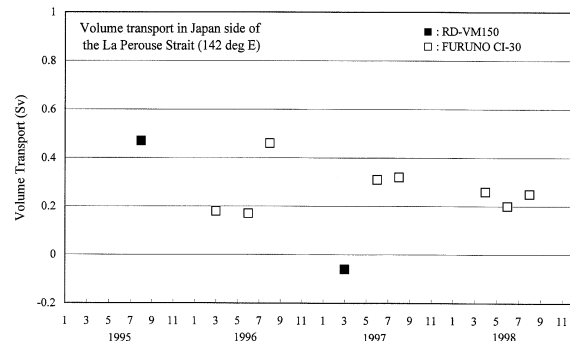


Fig. 2 Temporal variation of the volume transport (in Sverdrup) of the Soya Warm Current crossing the longitude of 142°E of the southern half of the La Perouse Strait (the Soya Strait). The black square indicates ADCP measurements by the RD-VM150 (RD Instruments) and the white square by the FURUNO CI-30 (Furuno Electric. Co.).

The transport of the Soya Warm Current tends to have a maximum in August in each year. The current velocity of the Soya Warm Current is well correlated with the sea level difference between Wakkanai and Abashiri tide gauge stations (Aota et al., 1988, Aota et al., 1985, Aota et al., 1990). By assuming that the Soya Warm Current is driven by the sea level difference between the Sea of Japan and the Sea of Okhotsk and by assuming barotropic flow (Aota 1975, Kanari et al., 1984, Tanaka et al., 1996), Aota (1975), Aota et al. (1985) and Ohshima (1994) were able to derive simple models to explain the basic characteristics of seasonal variation of the Soya Warm Current. Our result is generally consistent with the seasonal variations derived from sea level difference.

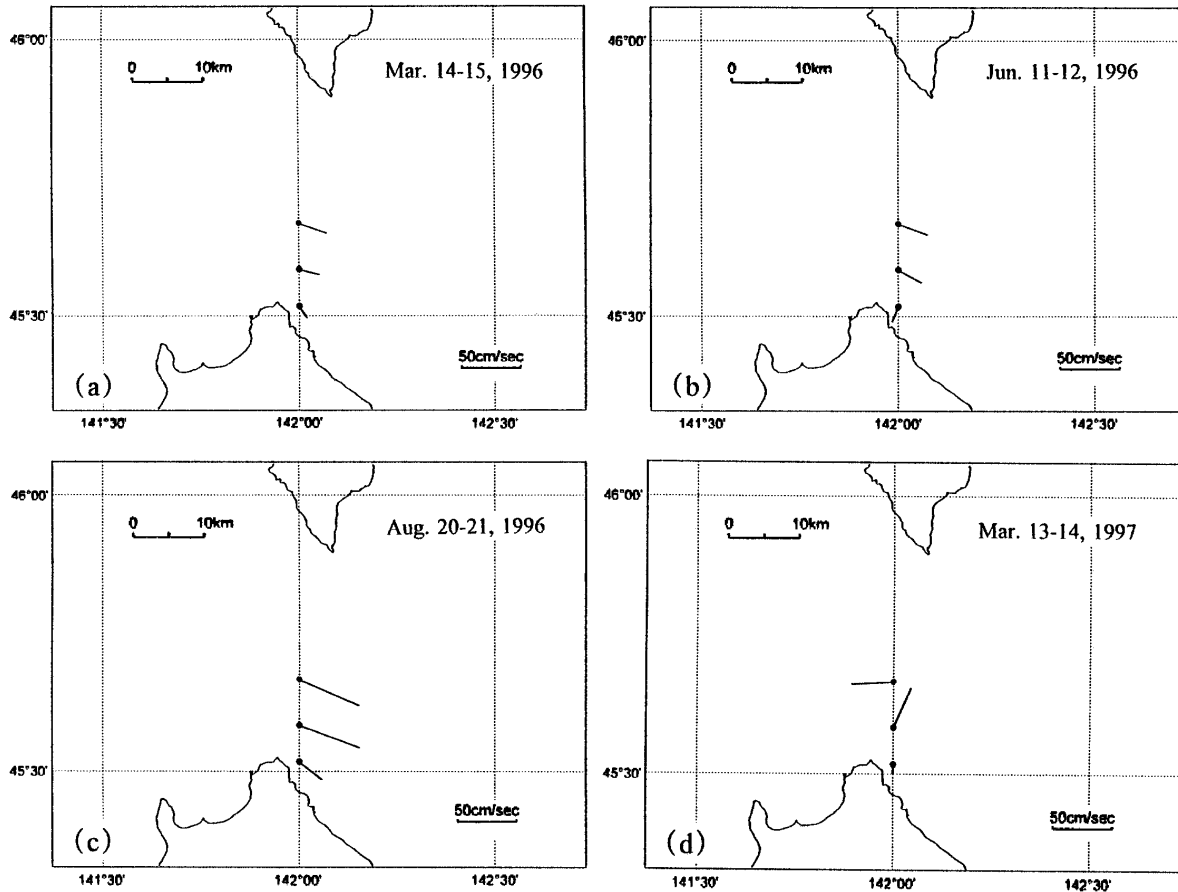


Fig. 3 Examples of the distribution of the vertically averaged residual current velocities: (a) March 14-15, 1996, (b) June 11-12, 1996, (c) August 20-21, 1996, and (d) March 13-14, 1997.

The transport of the Soya Warm Current in summer (the season of the maximum transport) appears to have decreased since 1996. However, the estimation of the transport might be influenced by shorter time scale variations, and further long time series of the observation would be needed to clarify this trend. Also, the detailed analysis of the sea level difference between Wakkanai and Abashiri should be carried out for this purpose.

It is necessary to discuss the negative transport found in March 1997, since the Soya Warm Current is usually found in March every year. Examples of the distribution of the vertically averaged current velocities are shown in Figure 3 for the four observations in the period from March 1996 to March 1997: (a) March 14-15, 1996, (b) June 11-12, 1996, (c) August 20-21,

1996, and (d) March 13-14, 1997. The current profile in March 1996 (Fig. 3a) shows the ordinary pattern of the Soya Warm Current although the magnitude of the currents are considerably smaller than those in summer (Fig. 3c: August 1996). On the other hand, the current distribution in March 1997 (Fig. 3d) is rather confused, and a strong westward flow was observed at Station S103. This westward flow found at Station S103 largely contributes to the negative transport in March 1997. A low density, less saline water with a negative temperature was observed in the surface layer in the northern half of the strait in March 1996 (Yagi et al., 1996; Nakata et al., 1999). Judging from the density structure and the horizontal temperature and salinity distributions, the less saline water seems to originate from the Okhotsk Sea and was carried westward. The current

distribution in Figure 3d might be understood by the extension of the less saline water to the south. The associated westward flow region might cover the Station S103. The complexity of the current distribution in Figure 3d suggests that such a phenomenon occurs sporadically and that short-period disturbances like eddies may appear (Kanari et al., 1984). The model derived by Aota et al. (1990) predicts that the direction of the total volume transport through the La Perouse Strait (the Soya Strait) should be reversed when the mean sea level difference between Wakkanai and Abashiri is very small. Thus, it is plausible that the reversed flow occurs in winter when the sea level difference is relatively small. It might be emphasized that the observation in March 1997 is the first example of a reversal in total volume transport through La Perouse Strait (the Soya Strait) to be confirmed by direct current measurements.

References

- Aota, M. 1975. Studies on the Soya Warm Current. *Low Temp. Sci., Ser. A*, 33, 151–172. (in Japanese with English summary)
- Aota, M., Nagata, Y., Inaba, A., Matsuyama, M., Ono, N. and Kanari, S. 1985. The Soya Warm Current – A typical ocean current on the continental shelf. pp. 164–187. *In Ocean Characteristics and Their Changes*, K. Kajiura, Kouseisya Kouseikaku (eds.), Tokyo. (in Japanese)
- Aota, M., Ishikawa, M. and Yamada, T. 1988. Dynamics of flow in the Soya Strait. *Low Temp. Sci., Ser. A*, 47, 147–160. (in Japanese with English summary)
- Aota, M., Matsuyama, M., Nagata, Y. and Yamada, T. 1990. Long-term variation of the transport of the Soya Warm Current. *Gekkan Kaiyou*, 22, 211–215. (in Japanese)
- Kanari, S., Aota, M. and Koga, M. 1984. Current profile of the Soya Warm Current and structures of eddies found near the front based on the measurements by a shallow water electromagnetic current profiler of free-falling type. *Geophys. Rep. Hokkaido Univ.*, 42, 67–76. (in Japanese)
- Katoh, O. 1988. Measurement of residual current using the Doppler sonar. *Bull. Seikai Fish. Res. Lab.*, 66, 59–67. (in Japanese with English abstract)
- Nakata, A., Tanaka, I., Yagi, H., Kantakov, G.A. and Samatov, A.D. 1996. Origin of water in the Cold Water Belt appearing offshore side of the Soya Warm Current near La Perouse Strait (the Soya Strait). p. 13. *In Extended Abstracts of the Fifth PICES Annual Meeting*, Nanaimo, B.C., Canada.
- Nakata, A., Tanaka, I., Yagi, H., Watanabe, T., Kantakov, G.A., and Samatov, A.D. 1999. Formation of high-density water (over 26.8 sigma-t) near the La Perouse Strait (the Soya Strait). *In Proceedings of the Second PICES Workshop on The Okhotsk Sea and Adjacent Areas*, Lobanov, V.B., Nagata, Y., and Riser, S.C., (eds.), Sidney, B.C., Canada.
- Odamaki, M. and Iwamoto, K. 1999. Currents and tidal observations by Hydrographic Department, Maritime Safety Agency, off the Okhotsk Coast of Hokkaido. *In Proceedings of the Second PICES Workshop on The Okhotsk Sea and Adjacent Areas*, Lobanov, V.B., Nagata, Y., and Riser, S.C., (eds.), Sidney, B.C., Canada.
- Ohshima, K.I. 1994. The flow system in the Japan Sea caused by a sea level difference through shallow straits. *J. Geophys. Res.*, 99, 9925–9940.
- Tanaka, I., Nakata, A., Yagi, H., Samatov, A.D. and Kantakov, G.A. 1996. Result of direct current measurements in the La Perouse Strait (the Soya Strait), 1995–1996. p. 12. *In Extended Abstracts of the Fifth PICES Annual Meeting*, Nanaimo, B.C., Canada.
- Yagi, H., Tanaka, I., Kantakov, G.A., Samatov, A.D., Nakata, A. Watanabe, T. 1996. Seasonal changes of the Cold Water Belt in the Soya Straits and adjacent areas and its chemical and biological properties. p. 10. *In Extended Abstracts of the Fifth PICES Annual Meeting*, Nanaimo, B.C., Canada.

***In situ* observations of Tsushima and West Sakhalin currents near La Perouse (Soya) Strait**

Gennady A. KANTAKOV¹ and George V. Shevchenko²

¹Sakhalin Research Institute of Fisheries and Oceanography, Yuzhno-Sakhalinsk, Russia

²Institute of Marine Geology and Geophysics, Russian Academy of Sciences, Yuzhno-Sakhalinsk, Russia

Abstract

Several current meters were deployed in 1996–1998 in the vicinity of La Perouse (Soya) Strait aiming to provide *in situ* observations of the Tsushima and West Sakhalin currents. Simultaneous moorings at two stations, Tetany 106 and Tetany 202+, clearly demonstrated convergence of these currents in the summer period on the southwestern shelf of Sakhalin Island. For both moorings more than 70% of the total energy was related to diurnal tides. Non-tidal currents were mainly barotropic and had significant seasonal and fortnightly components. The West Sakhalin current was found to play a key role in water exchange between the Sea of Okhotsk and the Sea of Japan.

Introduction

Oceanographic conditions on the southwestern slope and shelf of Sakhalin Island in the Sea of Japan in the vicinity of La Perouse (Soya) Strait are mainly determined by the Tsushima and West Sakhalin currents. The oceanographic features in this region have been investigated by oceanographers beginning in the last century and included a wide range of observations, descriptions, and modeling (Maidel, 1879 (see Veselova (1972) for a review); Makarov, 1895, Matsudaira, and Yasui, 1935, Derugin, 1940 (see Samarin (1996) for a review); Biryulin, 1954; Leonov, 1960; Budaeva et al., 1981; Klimov, 1984; Aota and Matsuyama, 1988; Oshima and Wakatsuchi, 1990; Yurasov and Yarichin, 1991; Bobkov and Foux, 1997; Tanaka and Nakata, 1998; Watanabe et al., 1998). The Tsushima Current transports the subtropical water mass from the south to the northern part of the Sea of Japan, the seasonal flow peak (up to 2 Sv) is normally observed in the early fall. The details of the West Sakhalin Current are poorly known because of lack of data. Calculations of geostrophic currents and some unpublished observational data near the Krilion Peninsula showed that the flow intensity in this area is about 2 Sv (Yurasov and Yarichin, 1991) and that this flow is directed to the south with residual currents up to 0.53 m/s (Zhuikov, 1992). Thus, the Tsushima and West Sakhalin currents flow in opposite directions forming the ‘convergence zone’ (CZ) in the area of the southwestern slope and shelf of Sakhalin Island. However, the interaction of the Tsushima and West

Sakhalin currents has never been carefully investigated.

The digital CTD archives for this region were created by Pishchalnik and Bobkov (1993). Kantakov and Samatov (1996) used these archives for preliminary estimation of the CZ duration and found that it is present primarily during the period April to November. The recent discovery of the La Perouse (Soya) Upwelling (or Cold Water Belt) in the northeastern part of the Sea of Japan off the Krilion Peninsula (Yagi et al., 1996; Nakata et al., 1998) modified previous understanding of water exchange between the Sea of Japan and Sea of Okhotsk. The former existing “clear” and “simple” perception about water exchange turned out to be much more complicated. The data collected during the La Perouse Project showed that the exchange through the strait depends on the Soya Current (Tsushima Branch), West Sakhalin Current (WSC) and the Okhotsk Sea water. The significance of the latter component in the water exchange through La Perouse (Soya) Strait is still overestimated (Danchenkov and Aubrey, 1998).

As part of the cooperative Russian-Japanese La Perouse Project, the oceanographic team of the Sakhalin Research Institute of Fisheries and Oceanography (SakhNIRO) in 1996–1998 made several *in situ* experiments to measure parameters of the Tsushima and West Sakhalin currents. The results of these experiments are presented below.

Data

For the present analysis we used observations of currents made using Aanderaa RCM4 and RCM7 current meters at 2 moorings, Tetany 106 and Tetany 202+ (Fig. 1), as well as some archive data on current in this region (Table 1). The sampling in-

tervals of current records were from 15 to 60 min, the mooring horizons were from 10 to 100 m (see Table 1). We estimated the spectral characteristics of currents in this region, and examined tidal and non-tidal components of the Tsushima and West Sakhalin currents.

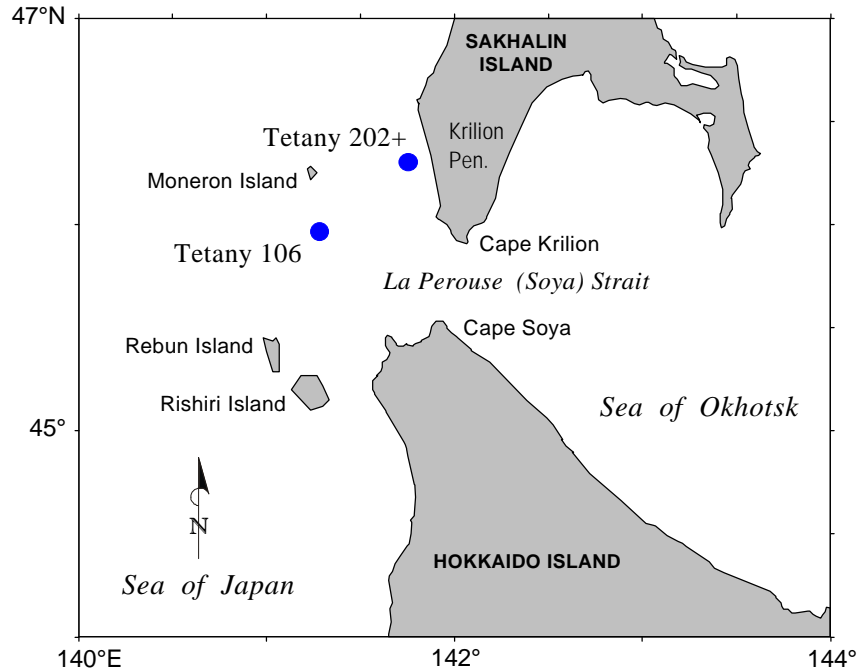


Fig. 1 Location of stations Tetany 106 and Tetany 202+ made during the 1996–1998 La Perouse Project.

Table 1 Submooring log features.

Project	Year	Site	Observation period	Hor	Tem	Con	Dir	Vel	Meter	DT
LP+	1996	Tetany 202+	11.08.96/ 22.08.96	40	+	+	+	+	RCM4 4079	15
LP	1996	Tetany 106	02.08.96/ 16.10.96	10	+	-	+	+	RCM7 11927	30
LP	1996	Tetany 106	02.08.96/ 16.10.97	100	+	+	+	+	RCM4 5759	30
LP	1996/97	Tetany 106	07.12.96/ 04.05.97	15	-	-	-	-	RCM4 5759	60
LP	1997	Tetany 106	13.05.97/ 28.08.97	15	+	+	+	+	RCM4 4079	30
LP	1997	Tetany 106	28.08.97/ 18.12.97	15	+	+	-	+	RCM4 4079	60
LP	1997/98	Tetany 106	18.12.97/ 16.03.98	20	+	-	+	+	RCM7 11927	60

Comment: ‘Hor’ is the observation horizon (m), ‘Tem’ is the water temperature, ‘Con’ is the conductivity, ‘Dir’ and ‘Vel’ are the direction and magnitude of currents, ‘Meter’ is the type of the current meter and its number, DT is the sampling interval (min), ‘+’ is the existing data.

Mean currents

To examine low-frequency variability of currents on the southwestern shelf of Sakhalin Island we computed and removed tides from the initial series. The residual currents were used for further analysis. There were only 11.5 days of simultaneous observations in August, 1996 at sites Tetany 106 and Tetany 202+, but these observations show very clear convergence between Tsushima and West Sakhalin currents: The former is relatively weak (about 7.5 cm/s), located over the slope of Sakhalin Island, and directed to NNW; the latter is much stronger (about 44 cm/s), located very close to the shoreline, and directed to SSE (Fig. 2a).

The historical data collected in the late 1970s (during the oil and gas exploration in this area) gave results, which were very similar to those obtained during the La Perouse Project. These results show that the West Sakhalin Current is a narrow shelf flow directed to the South (Fig. 2b). The estimated non-tidal currents were 42 cm/s at site Vindisskaya and 24 cm/s at Kuznetsovskaya. The difference in the current speed at these two sites is apparently related to the fact that Kuznetsovskaya was farther offshore than Vindisskaya, proving that the WSC is a very narrow current bound to the shore.

Seasonal variations of the Tsushima Current (station Tetany 106) are characterized by the decline

to zero of the North transport component in the middle of October (Fig. 3) and by the further abrupt heat loss of the corresponding water (Fig. 4). As was emphasized by Aota and Matsuyama (1988), strong seasonal changes of currents are a remarkable feature of the area of La Perouse (Soya) Strait.

Tidal currents

Diurnal tidal motions strongly prevail in the original of current records measured on the southwestern shelf of Sakhalin Island (Fig. 5). Apparently this is typical for the whole area of La Perouse (Soya) Strait (cf. Aota and Matsuyama (1988); Odamaki (1994)). To examine statistical properties of the velocity field and the relative contribution of various periodic components in the total variance of currents in this area, we used rotary spectral analysis. The velocity records at stations Tetany 106 and Tetany 202+ were Fourier transformed to clockwise u^- and counterclockwise u^+ rotary components (Gonella, 1972) and the corresponding spectral estimates, S^- and S^+ , were then obtained for each component. It was found that more than 70% of the total energy at these stations is in the diurnal tides, in agreement with the results of previous analysis of some historical data in this region (Kantakov and Gustoev, 1998).

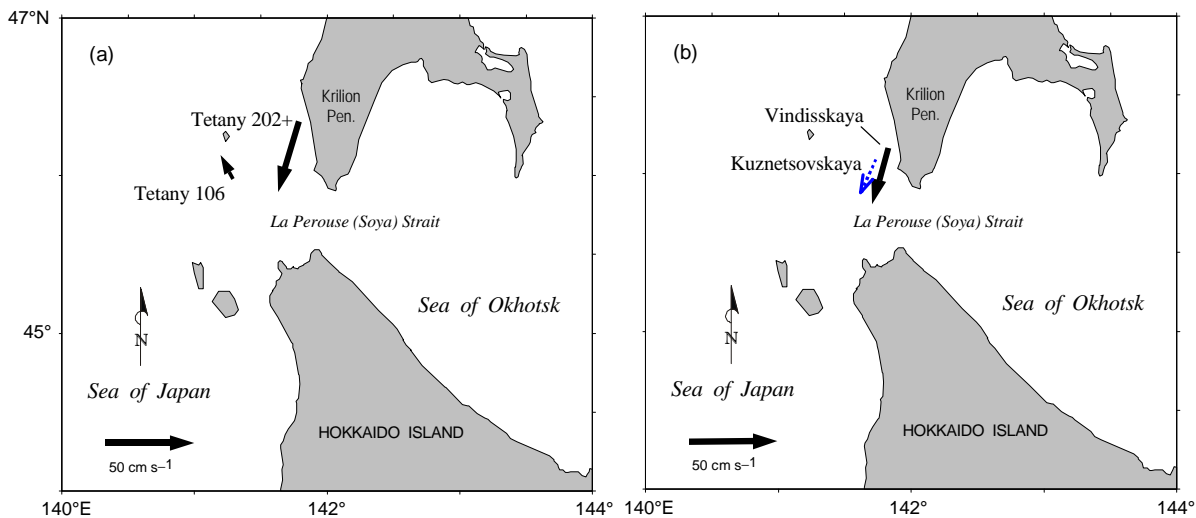


Fig. 2 (a) Mean currents in the convergence zone off the Krilion Peninsula recorded at stations Tetany 106 and Tetany 202+ (August 1996, SakhNIRO). (b) Mean currents at Kuznetsovskaya (dashed line, May-June 1978) and Vindisskaya (solid line, June 1979) during oil and gas exploration (with permission of the Ecological Company of Sakhalin).

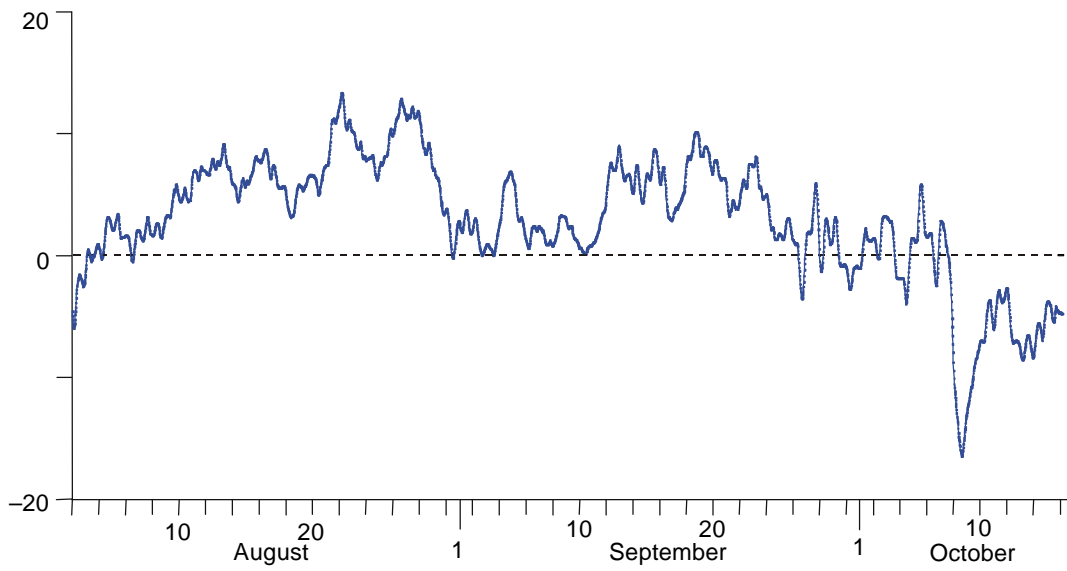


Fig. 3 Variations of the meridional (north-directed) component of non-tidal currents at station Tetany 106 (10 m) for the period August–October, 1996 (after smoothing by the 25-h sliding window).

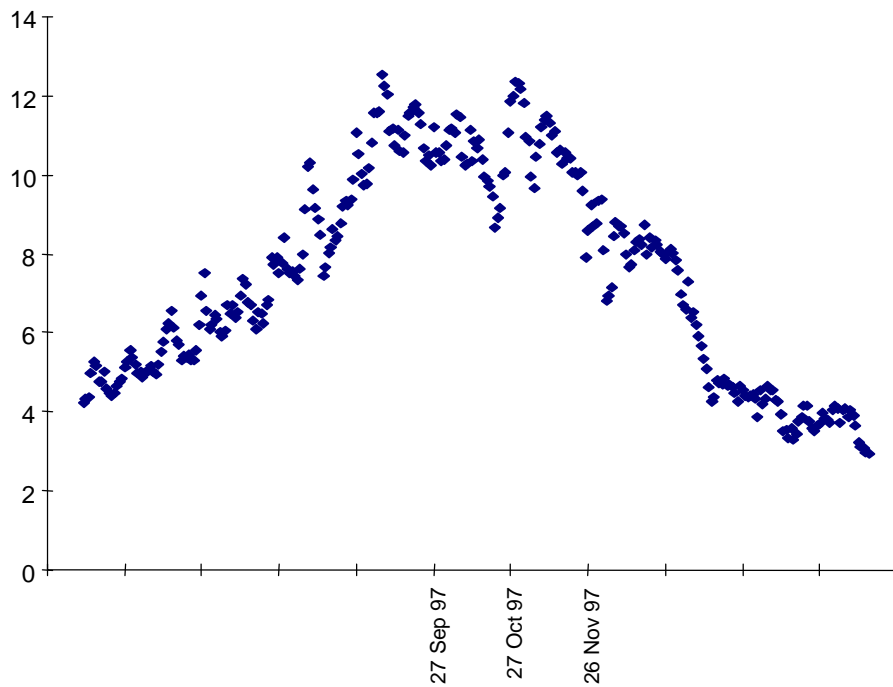


Fig. 4 Variations of daily temperatures at station Tetany 106 in 1997–1998 at 15 m depth.

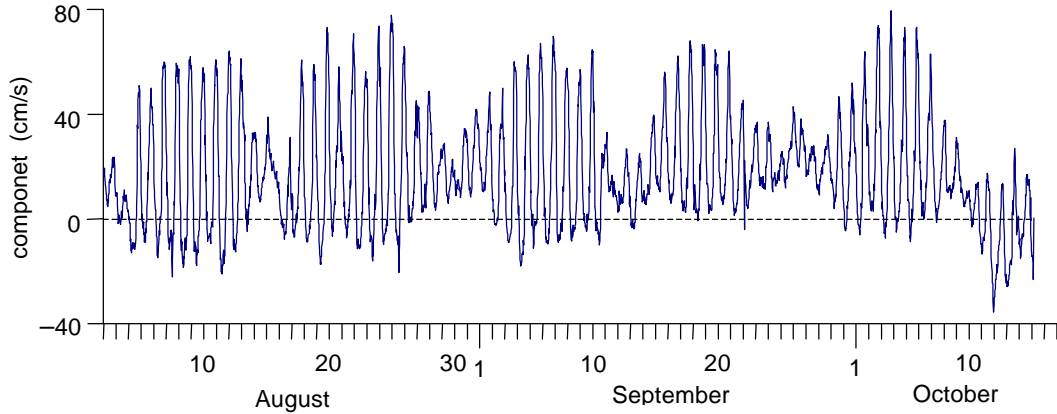


Fig. 5 Variations of the meridional (north-directed) component of currents at station Tetany 106 (depth 100 m) from August to October 1996.

The results of rotary spectral analysis of current velocities measured at station Tetany 106 (depths 10 and 100 m) are presented in Figure 6. For both depths the general character of the spectra is similar, clockwise (anticyclonic) motions dominate at all frequencies higher than 3 cpd (i.e. on periods more than 8 h). The diurnal tidal peak is the main feature of the spectra. The semidiurnal currents are surprisingly weak: The M_2 peak at the upper (10 m) layer is not seen at all, and at 100 m it is approximately two orders of magnitude lower than the diurnal peak. The energy of diurnal tides in the near-bottom layer is 5 times greater than in the upper layer. The remarkable feature of the near-bottom and especially upper currents is the existence of inertial oscillations with a period of 16.7 h, which is very close to the inertial period $T = 2\pi / f$, where $f = 2\Omega \sin j$, Ω is the frequency of the Earth's rotation, j is the latitude. Fortnightly oscillations, found in the northern part of the Sea of Japan by Isoda et al. (1996), are not seen in the spectra of Tetany 106 (Fig. 6), probably because of insufficient spectral resolution at low frequencies. However, they were evident at depth 15 m in summer 1997 (Figure 4 indicates similar oscillations of water temperature). Probably, these currents are associated with an anticyclonic eddy occurring in the area of the Tsushima Current. Additional information (atmospheric pressure, wind and satellite images) will be useful to examine fortnightly oscillations more carefully.

We used least square method to estimate the amplitudes and phases of tidal constituents both for zonal, u , and meridional, v , components of cur-

rents (A_u , G_u , and A_v , G_v , respectively). The results of tidal analysis of currents measured at station Tetany 106 (Table 2) are in good agreement with the results of similar analyses of historical data from the same area (Table 3). Amplitudes of diurnal constituents K_1 and O_1 were about 15–20 cm/s while the major semidiurnal constituent M_2 was only 3–5 cm/s. Ellipses of the diurnal tidal currents are extended in the northwest direction, approximately along the coastline of the Krilion Peninsula, southern Sakhalin (Fig. 7).

The reason for such strong diurnal currents (in comparison with semidiurnal) is not clear. As was shown by Aota and Matsuyama (1988) and Odamaki (1989), diurnal tides in the northeastern part of the Sea of Japan are formed mainly by the tidal waves incoming through La Perouse (Soya) Strait from the Sea of Okhotsk. Several scientists (cf. Ogura (1933); Aota and Matsuyama (1988); and Odamaki (1989)) noted two specific features of the area of La Perouse Strait: (1) Sea level tidal oscillations in the Sea of Japan are much weaker than in the Sea of Okhotsk resulting in a significant gradient and strong tidal currents in the strait (40–80 cm/s); (2) Amphidromic points both for K_1 and O_1 diurnal harmonics are located just at the entrance of La Perouse Strait. The strength of diurnal currents, in comparison with semidiurnal, and the evident difference between the corresponding current ellipses clearly demonstrates that diurnal and semidiurnal tidal currents have different generation mechanisms. Rabinovich and Zhukov (1984) explained similar effects on the northeastern shelf of Sakhalin Island by the influence of barotropic trapped shelf waves

on diurnal tides (quasi-geostrophic subinertial shelf waves produce much stronger currents than ordinary gravity waves forming semidiurnal tides). Odamaki (1994) showed that such diurnal shelf waves exist also on the Okhotsk Sea shelf of Hokkaido Island causing strong diurnal tidal currents in this area. Probably the same mechanism is responsible for the formation of diurnal tides on southwestern shelf of Sakhalin Island, i.e. in the area of present study.

The parameters of tidal ellipses (major and minor axes, phase, orientation, etc.) measured at station Tetany 106 at depth 100 m in August-October,

1996 and at depth 15 m in May–August 1997 were stable and in a good agreement, the differences between currents recorded at different years and at different depths were negligible (Fig. 7). Such character of diurnal tidal currents supports an assumption that these currents have been produced by a barotropic tidal flow. However, tidal currents measured in August-October, 1996 at 10 m depth were unstable and much smaller than at 100 m (see Figure 6). Apparently the upper mixed layer at that time was strongly influenced by baroclinic processes.

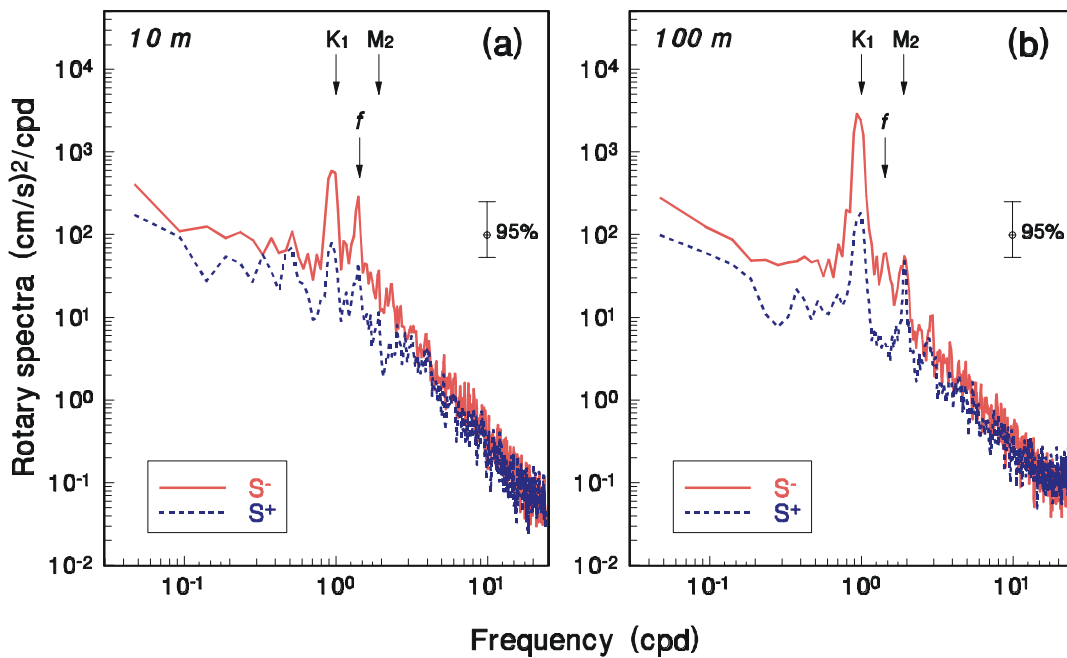


Fig. 6 Rotary spectra of currents measured at station Tetany 106 at depths (a) 10 m and (b) 100 m.

Table 2 Computed amplitudes and phases of u (eastward) and v (northward) tidal components at station Tetany 106, depth 100 m (August–October, 1996).

Tidal constituent	u -component		v -component	
	A_u (cm/s)	G_u (deg)	A_v (cm/s)	G_v (deg)
Q_1	1.9	29	2.6	245
O_1	14.5	12	19.4	256
K_1	12.8	54	17.5	298
P_1	4.2	54	5.8	298
N_2	0.7	11	1.3	200
M_2	3.1	7	5.0	213
S_2	1.8	41	2.0	239

Table 3 Computed amplitudes and phases of u (eastward) and v (northward) tidal components at station Kuznetsovskaya, depth 3 m (May–June 1978)

Tidal constituent	u -component		v -component	
	A_u (cm/s)	G_u (deg)	A_v (cm/s)	G_v (deg)
Q_1	3.5	300	1.2	114
O_1	7.5	337	16.2	251
K_1	0.7	264	29.6	232
M_2	3.2	292	8.5	220
S_2	7.4	35	10.1	8

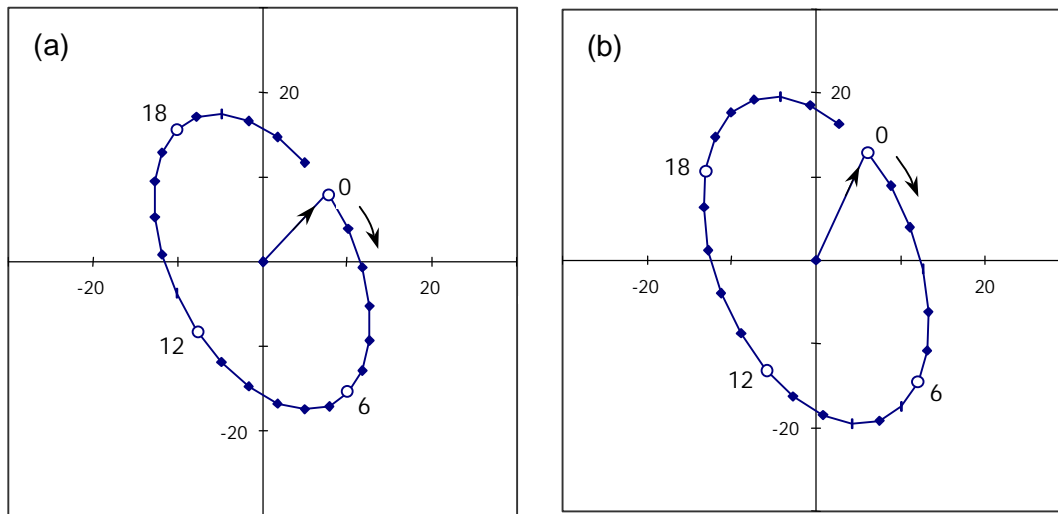


Fig. 7 Tidal ellipses for K_1 constituent at station Tetany 106. (a) depth 15 m, May–August 1997; (b) depth 100 m, August–October 1996.

Conclusions

Based on the results of current measurements made in 1996–1997 on the southwestern shelf of Sakhalin Island in the vicinity of La Perouse (Soya) Strait, as well as on some historical data obtained in the same area, we can make the following conclusions:

1. Simultaneous measurements of currents at stations Tetany 106 and Tetany 202+ in August, 1996 demonstrate existence of the convergence zone in this area formed by the Tsushima and West Sakhalin currents. Historical data show that the West Sakhalin

Current is a narrow along-shelf stream directed to the south.

2. According to the Tetany 202+ data the minimum intensity of the West Sakhalin Current in August 1996 was about 1 Sv. The West Sakhalin Current together with the Soya Current play an important role in heat and salinity exchange between the Sea of Japan and the Sea of Okhotsk.
3. Strong seasonal variability is a typical feature of the Tsushima Current. The cessation of the northward transport by the Tsushima Current occurring in October does not produce immediate heat losses. These losses in

the upper layer of the Tsushima Current are normally observed later (in November–December).

4. More than 70% of the total spectral energy of currents in the vicinity of La Perouse (Soya) Strait are related to diurnal tidal constituents K_1 and O_1 . Semidiurnal tidal currents are negligible in comparison with diurnal currents. Diurnal tidal currents at depths 15–100 m are mostly barotropic. A noticeable influence of baroclinity on tidal currents is observed only in summer time and only in the upper mixed layer (0–10 m).
5. There are two important peaks in spectra of non-tidal currents: (1) *inertial* with a period of about 16.7 h, which is evident in the upper layer, and (2) *fortnightly*, which is better seen in the lower layer. The fortnightly oscillations are apparently a common feature of the eastern Sea of Japan (there are numerous observations of these oscillations in the vicinity of Tsugaru Strait), but were not recorded on the southwestern shelf of Sakhalin Island, probably because of the short observational time.

Acknowledgments

We would like to thank our Japanese colleagues, Akifumi Nakata and Iori Tanaka from the Oceanographic Division of the Hokkaido Central Fisheries Experimental Station, for many fruitful discussion of the results of the paper. The deployment of stations Tetany 106 and Tetany 202+ were made with help of crewmembers of research vessels *Dmitry Peskov* and *Vladimir Girenko*. Our special gratitude goes to the unknown fisherman from Sarofutu Village, Japan, for his invaluable help during the last Tetany 106 recovery operation. We also would like to thank Drs. Alexander Rabinovich, Shirshov Institute of Oceanology, Moscow, Russia and Howard Freeland, Institute of Ocean Sciences, Sidney, Canada, for constructive comments and careful editing of the text.

References

Aota, M. and Matsuyama Y. 1988. Tidal current fluctuations in the Soya current, *J. Oceanogr. Soc. Japan*, 43, 276–282.

Biryulin, G.M. 1954. Hydrometeorological characteristics of the fishery sites at the Sakhalin South-West. pp. 167–303. In *Proc. Kuril-Sakhalin Marine Complex Expedition ZIN-TINRO, 1947-1949*. (in Russian)

Bobkov, A. and Foux, V.R. 1997. Tidal origin of thermohaline anomaly in La Perouse Strait. pp. 242–247. In *Twelfth Intl. Symp. on the Sea of Okhotsk and Sea Ice*, Mombetsu, Japan.

Budaeva, V.D., Makarov, V.G. and Bulgakov, S.N. 1981. Water circulation in Tatar Strait and its seasonal variability. *Proc. FEHRI*, 83, 35–43. (in Russian)

Danchenkov, M.A., and Aubrey, D. 1998. Oceanographic peculiarities of La Perouse Strait. p. 9. In *Second PICES Workshop on the Okhotsk Sea and Adjacent Areas, Abstracts*, Nemuro, Japan.

Derugin, K. 1940. Japanese hydrological research in the Sea of Japan and Sea of Okhotsk. *Marine Collection*, 6. (in Russian)

Gonella, J. 1972. A rotary-component method for analysing meteorological and oceanographic vector time series. *Deep-Sea Res.*, 19, 833–846.

Isoda, M. and Nakayama, O. 1996. Moored instrument observation in the Tsushima Current west of Tsugaru Strait. pp. 119–121. In *Proc. Fourth CREAMS Workshop*, Vladivostok.

Kantakov, G.A. and Samatov, A.D. 1996. Upwelling in La Perouse Strait: Oceanographical and hydrobiological properties. pp. 63–75. In *Proc. Intl. Workshop on the Okhotsk Sea and Arctic*, Tokyo, Japan.

Kantakov, G.A. and Gustoev, D.V. 1998. Tsushima and West Sakhalin currents interaction. In *Thirteenth Intl. Symp. on the Sea of Okhotsk and Sea Ice*, Poster, Mombetsu, Japan.

Klimov, S.M. 1984. *Estimation of Characteristics of the Upper Layer and Hydrothermic Conditions in Tatar Strait during Warm Period*, Ph.D. Thesis, Yuzhno-Sakhalinsk. (in Russian)

Leonov, A.K. 1960. *Regional Oceanography, Part 1*. Gidrometeoizdat, Leningrad, 765 pp. (in Russian)

Maidel, A. 1879. Additional notes about the cold current in the La Perouse Strait. *Marine Collection*, 171(4), 47–53. (in Russian)

Makarov, S.O. 1894. “Vityaz” and Pacific Ocean. Saint-Petersburg, 511 pp. (in Russian)

Matsudaira, Y. and Yasui, Z. 1935. Results of the surface observation in the Soya-Kaikio and Aniwa-Wan. *J. Oceanogr.*, 7(2).

Nakata, A., Tanaka I., Yagi, H., Watanabe, T., Kantakov, G.A. and Samatov, A.D. 1998.

- Formation of high-density water (over 26.8 sig-t) near La Perouse Strait (the Soya Strait). p. 19. In *Second PICES Workshop on the Okhotsk Sea and Adjacent Areas, Abstracts*. Nemuro, Japan.
- Odamaki, M. 1989. Co-oscillating and independent tides of the Japan Sea. *J. Oceanogr. Soc. Japan*, 45, 217–232.
- Odamaki, M. 1994. Tides and tidal currents along the Okhotsk coast of Hokkaido. *J. Oceanogr.*, 50, 265–279.
- Ogura, S. 1933. The tides in the seas adjacent to Japan, *Bull. Hydrogr. Dept.*, 7, 1–189.
- Oshima, K.I. and Wakatsuchi, M. 1990. A numerical study of barotropic instability associated with the Soya Warm Current in the Sea of Okhotsk, *J. Phys. Oceanogr.*, 20(4), 570–584.
- Pishchalnik, V.M. and Bobkov, A.O. 1993. Author's certificate for software application "ATLAS", RosAPO, No. 930078, Moscow.
- Rabinovich, A.B. and Zhukov, A.Ye. 1984. Tidal oscillations on the shelf of Sakhalin Island. *Oceanology*, 24, 184–189.
- Samarin, I.A. 1996. *History of Moneron Island*. Sakhalin Publ. House, Yuzhno-Sakhalinsk, 141 pp. (in Russian)
- Tanaka, I. and Nakata, A. 1998. Result of direct current measurement in La Perouse (Soya) Strait, 1996–1998. pp. 28–29. In *Second PICES Workshop on the Okhotsk Sea and Adjacent Areas, Abstracts*, Nemuro, Japan.
- Veselova, L.E. 1972. Spatial distribution of the upper layer temperature in the Sea of Okhotsk. *Proc. FEHRI*, 37, 13–28. (in Russian)
- Watanabe, T., Yagi, H., Nakata, A., Miyazono, A., Tanaka, I., Kantakov, G. and Samatov, A. 1998. Seasonal and annual changes of the distributions of the dissolved oxygen, nutrients and chlorophyll-*a* in the Soya Strait and adjacent seas. pp. 29–30. In *Second PICES Workshop on the Okhotsk Sea and Adjacent Areas, Abstracts*, Nemuro, Japan.
- Yagi, H., Tanaka, I., Kantakov, G., Samatov, A., Nakata, A., Watanabe, T. 1996. Oceanographic observations of the Cold Water Belt in summer in Soya Strait and adjacent sea areas and its origin estimated from nutrient, DO and T–S analyses. pp. 58–61. In *Proc. Intl. Workshop on the Okhotsk Sea and Arctic*, Tokyo, Japan.
- Yurasov, G.I. and Yarichin, V.G. 1991. *Currents of the Sea of Japan*. USSR Acad. Sci., Far-Eastern Branch, Vladivostok, 176 pp. (in Russian)
- Zhukov, A.Ye. 1992. Dynamical Characteristics on the Sakhalin Shelf (Instrumental Observations). *SakhNIRO Sci. Rep.*, Yuzhno-Sakhalinsk, 78 pp. (in Russian)

Geographical and biological characteristics of the net zooplankton in the southwestern part of the Sea of Okhotsk during 1987–1996

Irina Y. BRAGINA

Sakhalin Research Institute of Fisheries and Oceanography, Yuzhno-Sakhalinsk, Russia

Abstract

During 1987–1996 zooplankton studies were conducted by standard stations in the neritic, shelf and continental slope zones in the southwestern part of the Okhotsk Sea. Zooplankton species were collected by Juday net by total catch from 100 m up to the surface. The comparative zooplankton species analysis included 88 forms from 5 subareas and one transect that covered different geographical conditions. Defined: (1) species determination, biomass dynamics, distribution and possible driving environmental factors of the net zooplankton biomass, (2) zooplankton ecological characteristics, (3) taxonomic group predominance in biomass (*Chaetognatha*, *Euphausiidae*, *Copepoda*) and (4) proportion of the predator/prey ratio. Regions were determined where conditions for the fish feeding was estimated as the richest. Level biomass range varied from 203–2055 mg/m³. The most productive area has been estimated to be east off Terpenia Peninsula. The role of *Chaetognatha* predominance (up to 75% in plankton biomass) was determined as negative in feeding accessibility as well for the fish juvenile survival. The high zooplankton biomass level corresponded to low-temperature years.

Introduction

Structure and zooplankton community dynamics are the factors influencing fish concentrations such as herring, walleye pollock, atka mackerel, and juvenile salmon, which are critically important for the Sakhalin fishery industry. Relations between zooplankton community conditions and reproduction, quantity and distribution of pelagic fishes that inhabit the southwestern part of the Sea of Okhotsk are well investigated (Kun 1951, 1975, 1985; Mikulich, 1957; Lubny-Gercik, 1962; Guryeva, 1973; Shvetsova and Budaeva 1975; Fedotova, 1978a, 1978b, 1980, 1992; Chuchukalo, 1988; Bragina and Fedotova 1990, 1991; Bragina 1989, 1992, 1994, 1997; Gorbatenko, 1990; Volkov et al., 1990; Seki et al., 1995; Fedotova and Hudya 1995; Afanasyev, 1981; Shuntov and Dulepova 1996; Samatov 1994, 1995).

During the last decade, climatic fluctuations in the Northern Pacific had an impact, particularly on the Sea of Okhotsk oceanographic regime. Principally, the investigation of marine ecosystem response to that impact is the prime goal of numerous studies conducted here by national and international institutes and organizations, including PICES. Net zooplankton were collected by the Sakhalin Research Institute of Fisheries and Oceanography (SakhNIRO) around Sakhalin on standard grid stations from 1987 to 1996. The

goal of this paper is to describe the seasonal and interannual changes in the zooplankton community from the southwestern part of the Sea of Okhotsk during this period.

Data and Methods

Zooplankton grid stations are shown in Figure 1. Zooplankton were sampled by Juday net (net mouth area 0.1 m², mesh size 0.112 mm) from 100 m depth or from bottom to the surface. Plankters were fixed by 4% formalin on board ship and analyzed in the laboratory on land (Volkov et al., 1980; Volkov, 1984). Analysis consisted of two steps: species determination (Brodsky, 1950; Lomakina, 1978; Kasatkina, 1982; Gurjanova, 1951; Zevina, 1981; Stepanyants, 1967; Naumov, 1960, 1961; Kryuchkova, 1987) and biomass calculations (Lubny-Gercic, 1953; Chislenko, 1968). Total number of samples analyzed were 1480.

Geographical division of the southwestern part of the Sea of Okhotsk is based on bay borders (Aniva, Terpeniya), the deepest part of the Sea of Okhotsk, the wide northeastern shelf and slope off Sakhalin, south of 50°30'N latitude. Hence, 5 regions in the southwestern part of the Sea of Okhotsk with different geographical conditions are presented for the net zooplankton dynamics investigation. The line between Sakhalin and Kunashir

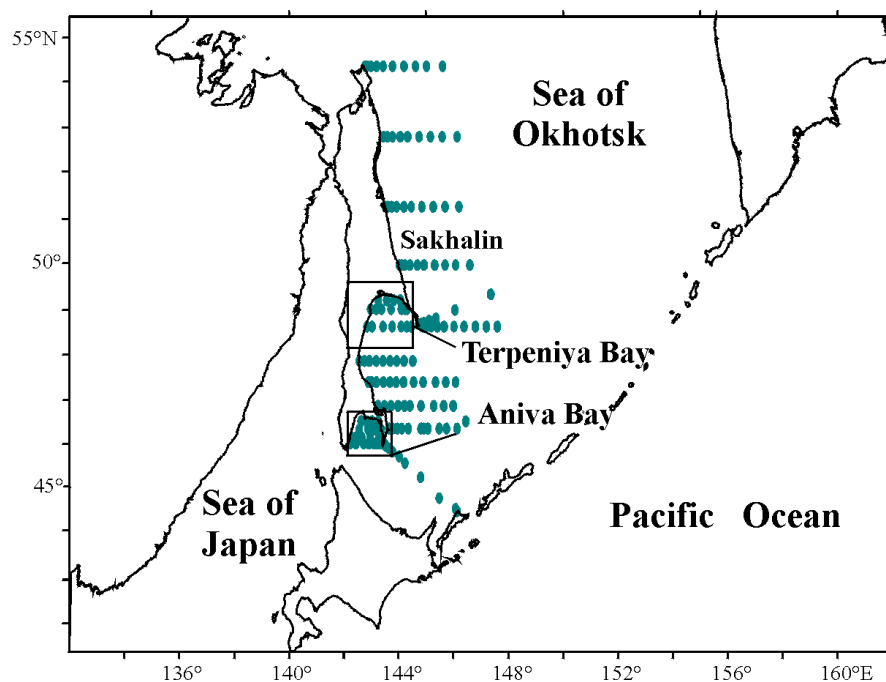


Fig. 1 Standard SakhNIRO grid sampling stations in the southwestern part of the Sea of Okhotsk, including Terpeniya and Aniva bays.

islands had a specific zooplankton composition and showed independence from other regions due to the influence of warm and saline waters of the Soya and West Sakhalin currents (Kantakov and Shevchenko, 1999).

In each region three biological parameters of the net zooplankton community were examined seasonally and interannually: total biomass (mg/m^3), ecological zooplankton group (i.e. species with similar temperature optimums) compositions, having main contributions in the net biomass (Kun, 1975). The third parameter was chosen as a ratio carnivore/omnivore (Omori and Ikeda, 1984) species of the net zooplankton.

Results

Species determination, biomass dynamics, distribution and possible environmental driving factors

Net zooplankton fauna were represented by a total of 88 forms belonging to the 9 types and 15 classes. More diversity was obtained for the *Copepoda* and *Euphausiacea* taxons. In biomass three plankton groups predominated: *Copepoda*, *Euphausiacea*, and *Chaetognatha*. A short species list is given in Appendix I.

In the spring macroplankton (2–20 mm) cold water species *Thysanoessa raschii*, *Parasagitta ele-*

gans, and *Metridia okhotensis* formed most (68–86%) of the net zooplankton biomass (just biomass in following). In the fall period mezoplankton increased due to growth in biomass of *Pseudocalanus minutus*, *Centropages abdominalis*, the early stages of copepod coarse forms such as Fam. *Calanidae*, as well as the plankton stages of the benthos. The maximum (54–74%) of the mezoplankton part in biomass was found in the bays. The microplankton fraction (*Oithona similis*, copepods, eggs and nauplius of Copepoda, and larvae of benthic animals) composed both in spring and fall from 3 to 20 % of the biomass, but prevailed in quantity.

Biomass dynamics seasonally and interannually are shown in Figure 2. A remarkable feature of the biomass dynamics was minimum expression in the 1991 in all detached regions. The ranges of seasonal and interannual variabilities were close to each other (see Figure 2).

In spring biomass by regions varied from 216 to 2055 mg/m^3 . The highest biomass was obtained in the bays and for region located south of 50°30'N. (See Figure 2A, D, and E and, as an example of the net zooplankton distribution, Figure 3) The poorest biomass measurement was for the north-eastern offshore (north of 50°30'N; see Figure 2F).

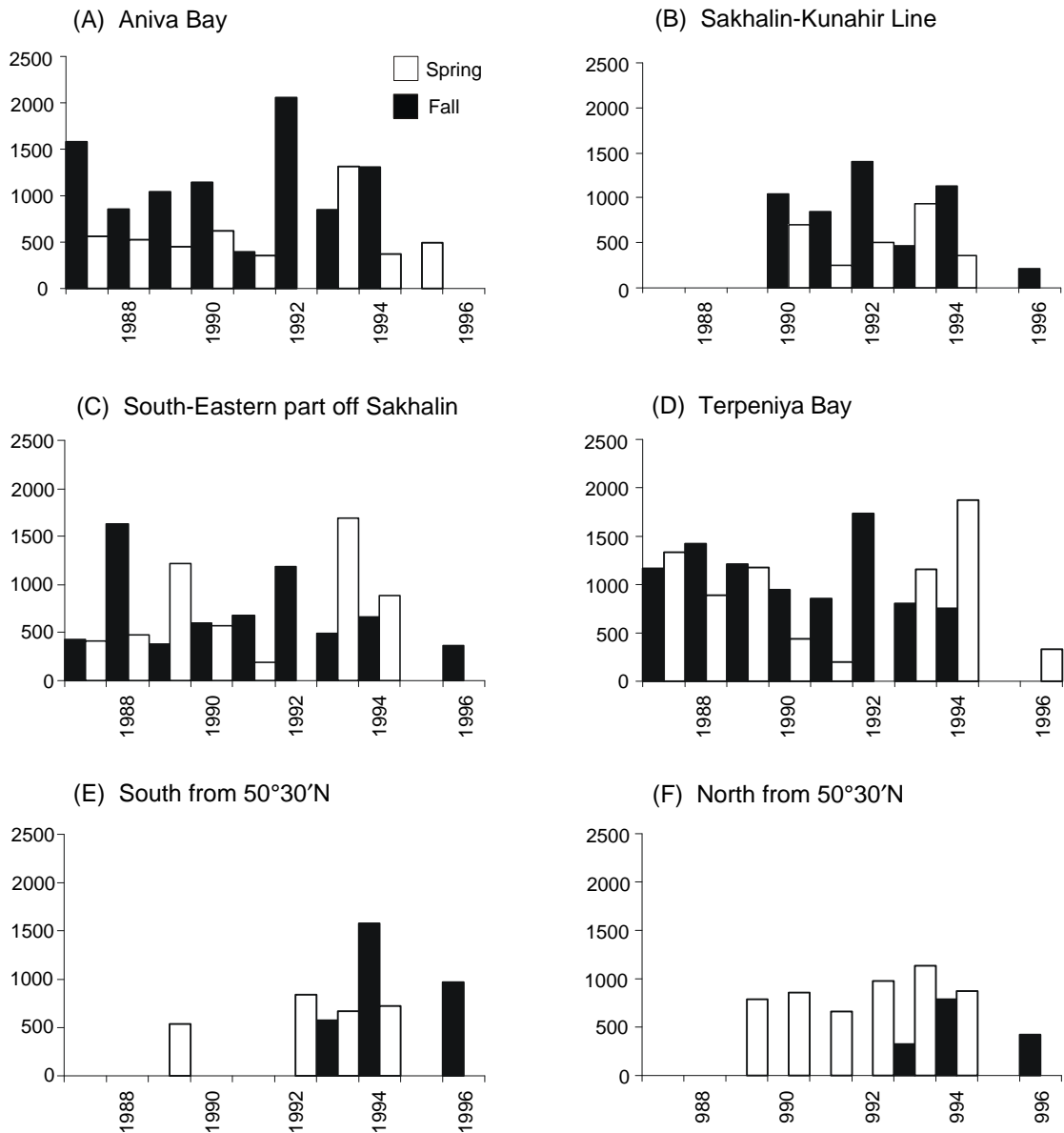


Fig. 2 Biomass (mg/m³) dynamics by region and the Sakhalin–Kunashir line during the 1987–1996 period.

In the fall biomass ranged from 203–1871 mg/m³. Meanwhile, in the deepest region southeast of Sakhalin and on the northeastern shelf, the biomass reached values higher than that for spring (Fig. 2 C and F).

In the Aniva and Terpeniya bays, biomass maximums registered in 1992 when environmental conditions were characterized by the smallest area of the Sea of Okhotsk ice cover, the East Sakhalin current relaxation and poor solar heating (Kanta-

kov, 1993). The environmental factors indicate a possible impact (Kantakov, personal communication) of the numerous oceanological parameters on the zooplankton biomass as well species structure (see Table 1).

Ecology

Cold water species (CWS) were determined to be less than 50% of the forms from total species list, but they prevailed in biomass in the spring and

Table 1 Correlation between environmental and net zooplankton factors in spring time for Aniva Bay (data raw 1988–1994).

	BM	Cop	Efz	Chaet	Amph	Pred	Prey
BM	1.00						
Cop		1.00					
Efz	0.73		1.00				
Chaet	-0.60	-0.76	-0.34	1.00			
Amph	0.59		0.50		1.00		
Pred	-0.58	-0.87		0.96		1.00	
Prey	0.59	0.87		-0.97		-1.00	1.00
T50					-0.61		
T50_100	-0.98		-0.56		-0.81	0.51	-0.52
A50							
A50_100	-0.75				-0.86		
< 32	-0.63		-0.63	0.84		0.65	-0.69
32–33	0.90		0.69	-0.75		-0.62	0.66
33–34				-0.53	-0.51		
> 2			-0.92				
0–2	0.94		0.81	-0.67		-0.66	0.66
-2–0		-0.52	0.79				
N	-0.94		-0.80	0.56	-0.68		
S			0.74				
T	-0.77				-0.67		

Remarks: BM – biomass (mg/m^3), Cop – copepod biomass, Efz – *Euphausiidae* biomass, Chaet – *Chaetognatha* biomass, Amph – *Amphipoda* biomass; Pred – predators, Prey – prey zooplankton, T50 – temperature in the upper 50-m layer, T50_100 – temperature in the 50–100 m layer, A50 – temperature anomaly in the upper 50-m layer, A50_100 – temperature anomaly in the 50–100 m layer; <32, 32–33, 33–34 – salinity classes; >2, 0–2, -2–0 – temperature classes; N, S, T – water mass transit to the north, south and total (respectively).

fall periods (Figs. 3 and 4). The exception was in the Aniva and Terpeniya bays in the fall of 1994 when the share of the CWS biomass was 39–43% (Fig. 4A and D). The CWS part of the biomass reached a maximum on slope and deep-water regions in the southeast off Sakhalin and in the south of 50°30'N (92–95% of the biomass). The main species of CWS group were composed of: *Thysanoessa raschii*, *Parasagitta elegans*, *Metridia okhotensis*, and *Pseudocalanus minutus*.

The major species of the zooplankton fauna were the moderate cold water species (MCW): *Calanus plumchrus*, *Metridia pacifica*, *Scolecithricella minor*, *Centropages abdominalis*, *Oithona similis*, etc., but they played less of a role in biomass formation compared with the

cold water species (Fig. 5): 11–23% in spring, 12–35 % in fall with maximums found in Aniva and Terpeniya bays: 60 and 52%, respectively.

Warm water species (WWS) from south-boreal and subtropical biogeographic groups (*Calanus pacificus*, *Candacia bipinnata*, *Corycaeus sp.*, and *Sapphirina sp.*) were found in Aniva Bay and at the Sakhalin–Kunashir Line. Their share does not exceed the 2% level of the biomass. Other WWS representatives with a wider propagation: *Neocalanus tenuicornis*, *Microsetella rosea*, *Oithona plumifera*, *Acartia clausi*, *Paracalanus parvus* were determined to make up to 10% of biomass in the fall (Fig. 5, for example, Aniva Bay, 1990).

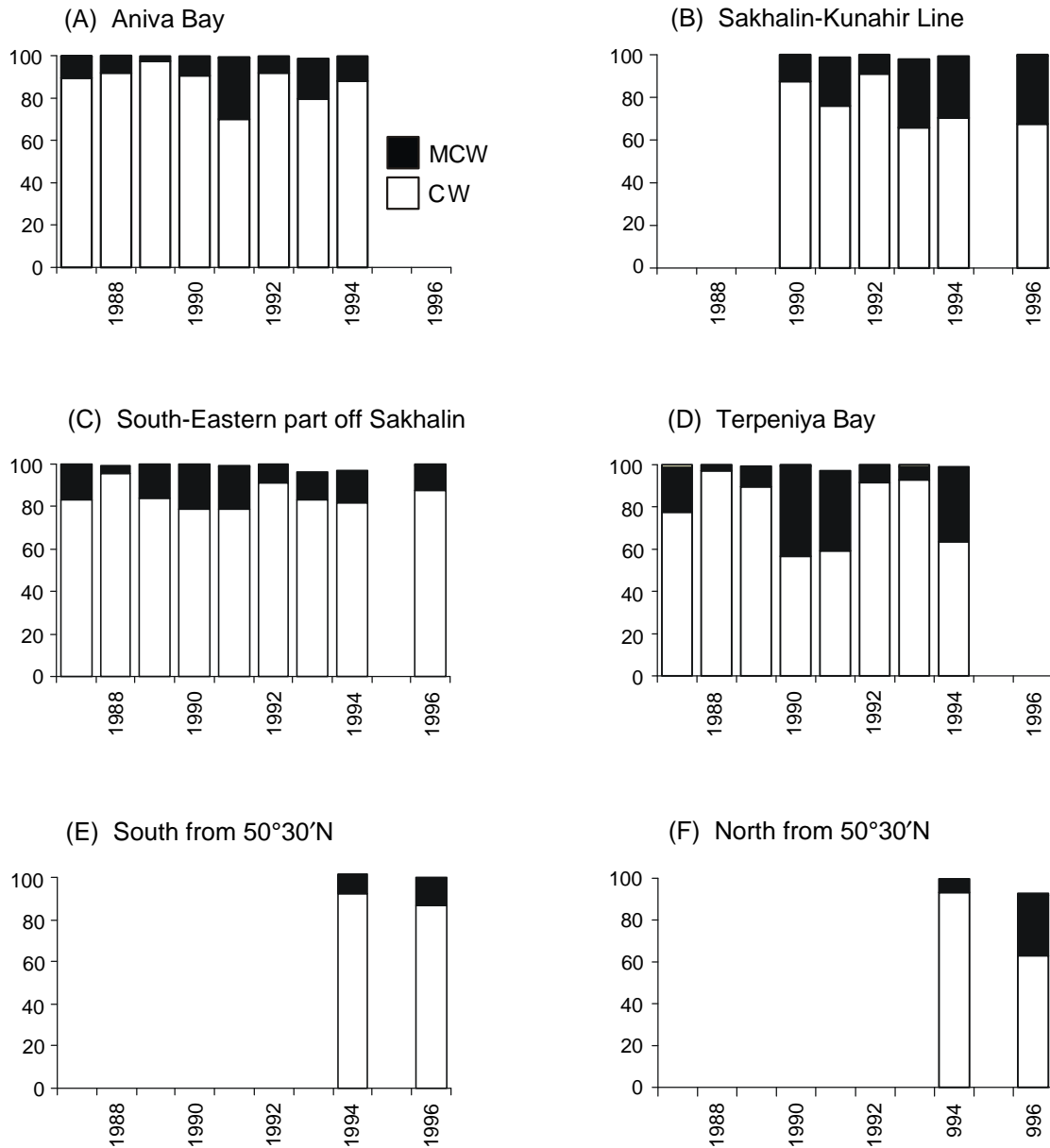


Fig. 4 Ecological group dynamics in the spring period (CW – cold water species, MCW – moderate cold water species; WWS – warm water species) by region and by the Sakhalin–Kunashir Line (lack of data for the northern shelf and slope is explained the presence of ice floes in post-spring and early summertime).

During the seasonal peak of warming period of the upper layer (early fall), the neritic complex actively grew: *Centropages abdominalis*, *Eurytemora herdmanni*, *Tortanus discaudatus*, *Decapoda larvae*, *Gastropoda larvae*, *Bivalvia larvae*, etc., This phenomena especially characterized the bay regions where the biomass of the neritic share grew to 17–25% compared to spring time.

Carnivorous/Omnivorous Ratio

The predator fraction, having a predominance of *Parasagitta elegans*, had a wide range, from 2 to 75% of the biomass. The highest presence of predators was found in Aniva Bay (75%) and Terpeniya Bay (73%), but in different years (spring time). Peak of the carnivorous zooplankton can be noted in the appointed bays (Fig. 6).

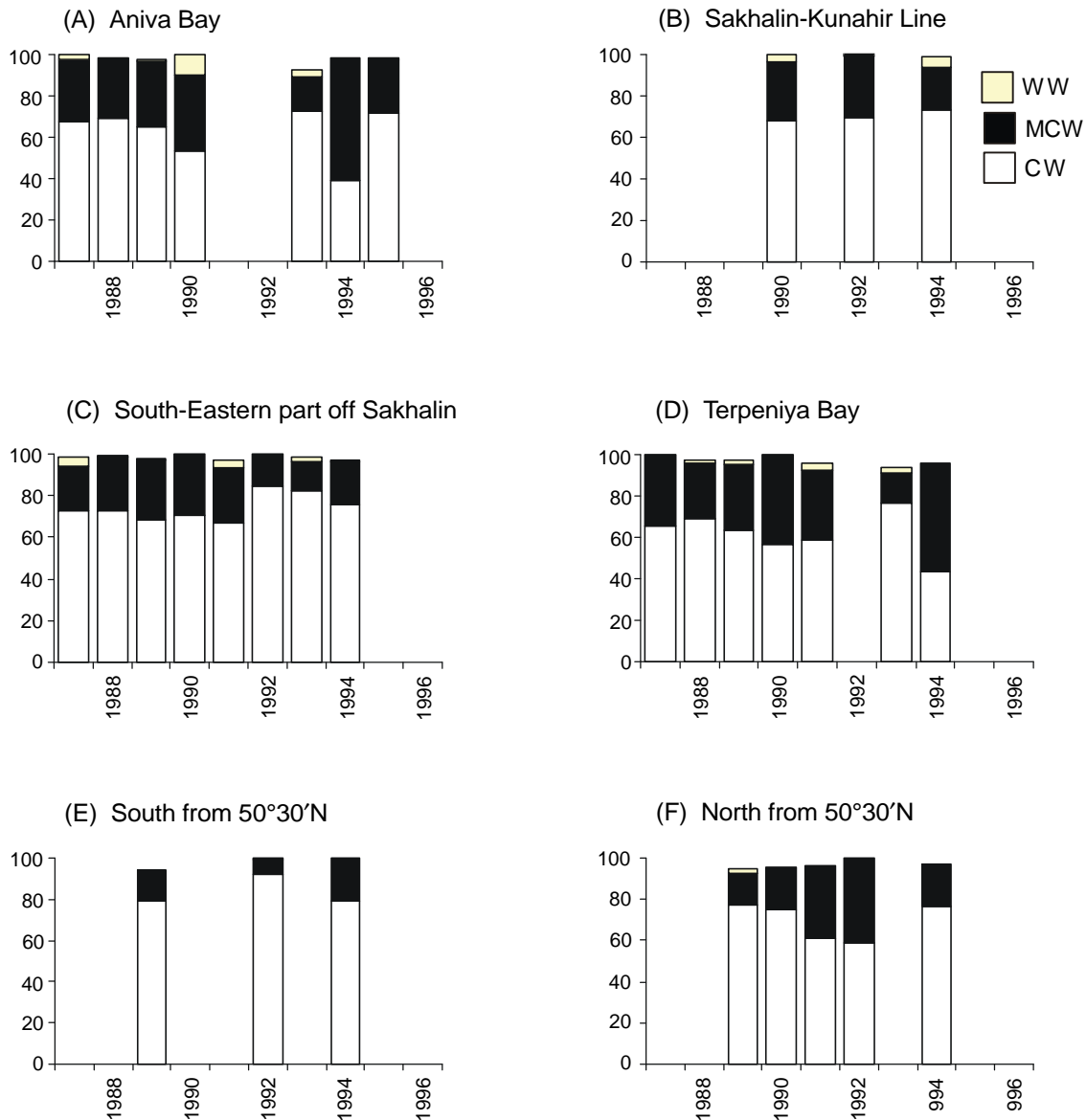


Fig. 5 Ecological group dynamics in the all period (CW – cold water species, MCW – moderate cold water species; WW – warm water species) by region and the Sakhalin–Kunashir Line.

Compared with springtime, predators in the fall season were obtained less often, except in the northeastern shelf of Sakhalin and the Sakhalin–Kunashir Line (Fig. 6 B, E and F). Nevertheless, the predator biomass absolute value varied from 102 to 140 mg/m³ (averaged by regions) in the fall.

Conclusions

- 1) The seasonal and interannual variability magnitudes of the net zooplankton biomass were similar to each other. Independent from

widely separated regions, biomass had an absolute minimum in the 1991. Preliminary investigation has shown a possible strong impact of the environment on the biomass, species structure and distribution of net zooplankton during last decade in the southwestern part of the Sea of Okhotsk. Biomass corresponded with layer temperature with negative correlation. Hence, in the cold years zooplankton biomass was greater than in warm years.

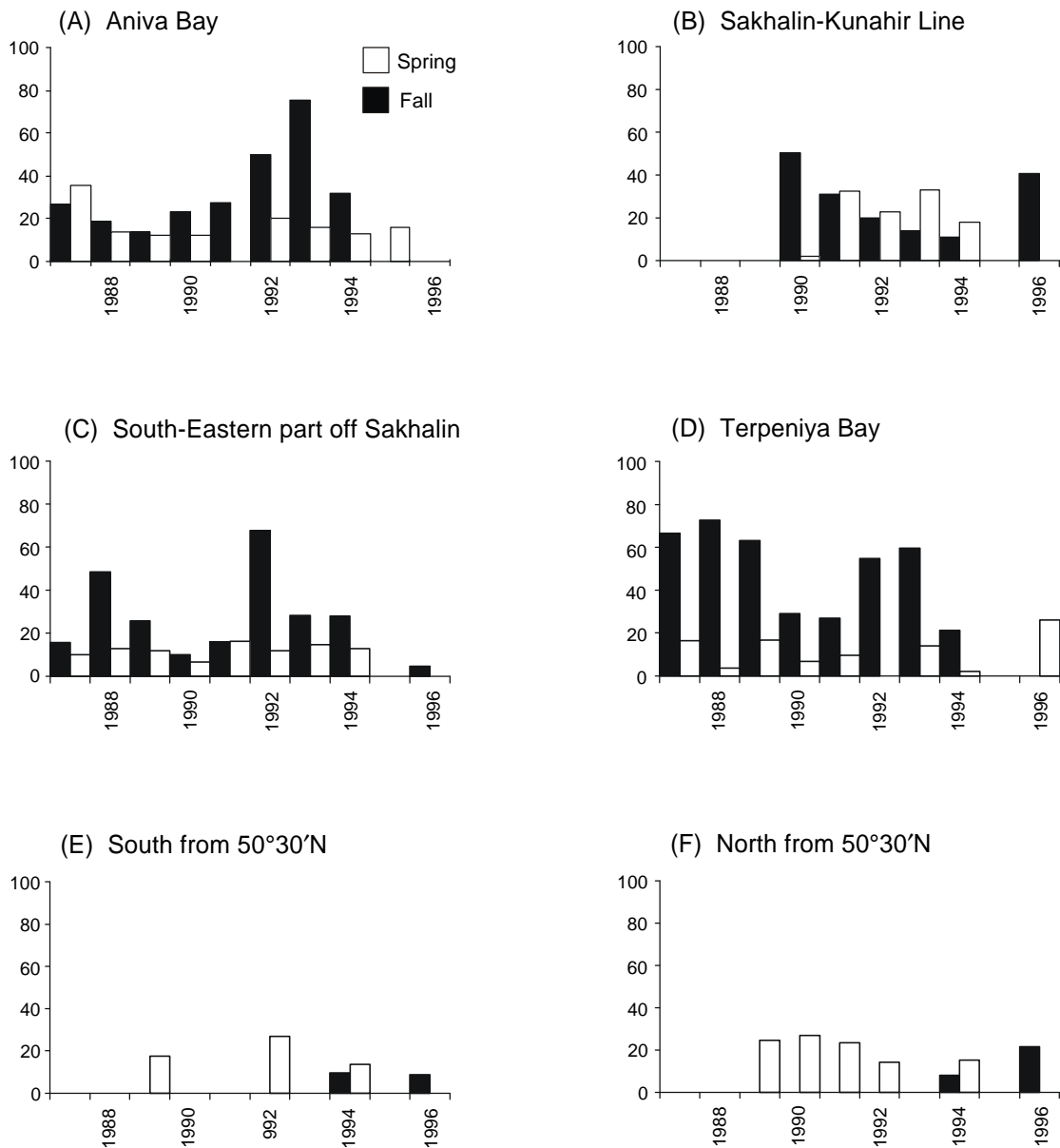


Fig. 6 Part of carnivorous zooplankton species (%) in biomass net zooplankton dynamics by region and the Sakhalin–Kunashir Line from 1987–1996.

- 2) Zooplankton fauna represented by a total of 88 forms belonging to 9 types and 15 classes. More diversity was obtained for the *Copepoda* and *Euphausiacea* taxons. Three plankter groups predominated in terms of biomass: *Copepoda*, *Euphausiacea*, and *Chaetognatha*.
- 3) The general ecological feature of the southwestern part of the Sea of Okhotsk zooplankton was the predominance of the cold water species: *Thysanoessa raschii*, *Parasagitta elegans*, *Metridia okhotensis*, and *Pseudoclanus*

minutus. Meanwhile, in the 1994 (Aniva and Terpeniya bays) cold water species were displaced by another group – moderate cold water species: *Centropages abdominalis*, *Calanus plumchrus*, and *Tortanus discaudatus*.

Appendix I

(Supplement to the paper *Geographical and Biological Characteristics of the Net Zooplankton in the South-Western Part Sea of Okhotsk during 1987-1996* by Irina Y. Bragina)

Species list of the net zooplankton in the south-western part of the Sea of Okhotsk according to an analysis of 1480 samples (1987–1996 SakhNIRO collection).

Phylum Protozoa
Class Sarcordina
Subclass Rhizopoda
Order Foraminifera
Family Globigerinidae
Genus *Globigerina*
Globigerina bulloides

Phylum Coelenterata
Subphylum Cnidaria
Class Hydrozoa
Subclass Hydroidea
Order Leptolida
Suborder Athecata
Family Tubulariidae
Genus *Corymorpha*
Corymorpha sp.
Family Eudendriidae
Genus Eudendrium
Eudendrium ramosum
Suborder Thecaphora
Family Campanulariidae
Genus Obelia
Obelia longissima
Order Trachylida
Suborder Trachymedusa
Family Trachynemidae
Genus *Aglantha*
Aglantha digitale
Medusae sp.
Subclass Siphonophora
Order Calyphorida
Family Dimophidae
Genus *Dymophyes*
Dymophyes arctica

Subphylum Acnidaria
Class Ctenophora
Subclass Atentaculata
Family Beroidea
Genus *Beroe*
Beroe cucumis

Phylum Nemertini
Nemertini, larvae

Phylum Annelida
Class Rotatoria
Rotatoria sp.
Class Polychaeta
Polychaeta, larvae

Phylum Arthropoda
Class Crustacea
Subclass Entomostraca
Order Branchiopoda
Suborder Cladocera
Family Polyphemidae
Genus *Evadne*
Evadne nordmanni
Genus *Podon*
Podon leuckarti
Order Ostracoda
Suborder Myodocopa
Family Conchoeciidae
Genus *Conchoecia*
Pseudoconchoecia borealis
Conchoecia sp.
Order Copepoda
Suborder Calanoida
Family Calanidae
Genus *Calanus*
Calanus plumchrus
C. glacialis pacificus
C. cristatus
Neocalanus tenuicornis
Family Eucalanidae
Genus *Eucalanus*
Eucalanus bungii
Family Paracalanidae
Genus *Paracalanus*
Paracalanus parvus
Family Pseudocalanidae
Genus *Pseudocalanus*
Pseudocalanus minutus
Ps. gracilis
Genus *Microcalanus*
Microcalanus pygmaeus
Genus *Clausocalanus*
Clausocalanus arcuicornis
Family Aetideidae
Genus *Undinopsis*
Undinopsis pacificus
Genus *Gaidius*
Gaidius brevispinus
Genus *Gaetanus*
Gaetanus simplex
Family Euchaetidae
Genus *E.marina*
Genus *Pareuchaeta*
Pareuchaeta japonica
Family Scolecithricidae
Genus *Scolecithricella*
S.minor
Family Themoridae
Genus *Eurytemora*

	<i>Eurytemora herdmani</i>	Genus	<i>Parathemisto</i>
	<i>Eurytemora pacifica</i>		<i>Parathemisto japonica</i>
Family	Metridiidae		<i>P. libellula</i>
Genus	<i>Metridia</i>	Order	Euphausiacea
	<i>Metridia pacifica</i>	Family	Euphausiidae
	<i>M. okhotensis</i>	Genus	<i>Euphausia</i>
Family	Centropagidae		<i>E. pacifica</i>
Genus	<i>Centropages</i>	Genus	<i>Thysanoessa</i>
	<i>Centropages abdominalis</i>		<i>Th. raschii</i>
Family	Candaciidae		<i>Th. longipes</i>
Genus	<i>Candacia</i>		<i>Th. inermis</i>
	<i>Candacia bipinnata</i>		Euphausiidae st. Furcilia
Family	Pontellidae		Euphausiidae st. Caliptopis
Genus	<i>Epilabidocera</i>		Euphausiidae st. Naupl.
	<i>E. amphitrites</i>		Euphausiidae st. Ova
Family	Acartiidae	Order	Decapoda
Genus	<i>Acartia</i>	Suborder	Macrura
	<i>Acartia clausi</i>	Family	Hippolithidae
	<i>A. longiremis</i>	Genus	<i>Spirontocaris</i>
	<i>A. tumida</i>		<i>Spirontocaris</i> ,
Family	Tortanidae	Genus	<i>Eualus</i>
Genus	<i>Tortanus</i>		<i>Eualus</i> , larvae
	<i>Tortanus derjugini</i>	Family	Crangonidae
	<i>T. discaudatus</i>	Genus	<i>Nectocrangon</i>
Suborder	Cyclopoda		<i>Nectocrangon</i> , larvae
Family	Oithonidae	Genus	<i>Sclerocrangon</i>
Genus	<i>Oithona</i>		<i>Sclerocrangon salebrosa</i> , larvae
	<i>Oithona similis</i>	Suborder	Anomura
	<i>Oithona plumifera</i>	Family	Paguridae
Family	Oncaeidae	Genus	<i>Pagurus</i>
Genus	<i>Oncaea</i>		<i>Pagurus</i> sp., larvae
	<i>Oncaea borealis</i>	Family	Lithodidae
	<i>O. conifera</i>	Genus	<i>Paralithodes</i>
Genus	<i>Corycaeus</i>		<i>Paralithodes camtschatica</i> , larvae
	<i>Corycaeus</i> sp.	Genus	<i>Hapalogaster</i>
Suborder	Harpacticoida		<i>Hapalogaster grebnitzkii</i> , larvae
Family	Ectinosomidae	Suborder	Brachyura
Genus	<i>Microsetella</i>	Family	Majidae
	<i>Microsetella rosea</i>	Genus	<i>Hyas</i>
Family	Harpacticidae		<i>Hyas coarctatus</i> , larvae
Genus	<i>Harpacticus</i>	Genus	<i>Chionoecetes</i>
	<i>Harpacticus</i> sp.		<i>Chionoecetes opilio</i> , larvae
Genus	<i>Sapphireella</i>	Genus	<i>Erimacrus</i>
	<i>Sapphireella</i> sp.		<i>Erimacrus isenbeckii</i> , larvae
	Copepoda, Nauplii		
	Copepoda, Ova	Phylum	Mollusca
Order	Cirripedia	Class	Gastropoda
Suborder	Thoracica		Gastropoda larvae
Family	Balanidae	Order	Pterapoda
Genus	<i>Balanus</i>	Suborder	Gymnosomata
	<i>Balanus</i> sp.st.Naupl.	Family	Clionidae
	<i>Balanus</i> sp.st.Cypris	Genus	<i>Clione</i>
Subclass	Malacostraca		<i>Clione limacina</i>
Order	Cumacea	Suborder	Thecosomata
Family	Diastylidae	Family	Limacinidae
Genus	<i>Diastylis</i>	Genus	<i>Limacina</i>
	<i>Diastylis bidentata</i>		<i>Limacina helicina</i>
Order	Amphipoda	Class	Bivalvia
Suborder	Hyperidea		Bivalvia, larvae
Family	Hyperiididae	Class	Cephalopoda

	Cephalopoda, larvae		<i>Strongylocentrotus sp.</i> , larvae
Phylum	Tentaculata	Class	Holothuroidea
Class	Phoronidea	Order	Dendrichirota
	Phoronidea, larvae	Family	Cucumariidae
Class	Chaetognatha	Genus	<i>Cucumaria</i>
Genus	<i>Parasagitta</i>		<i>Cucumaria japonica</i> , larvae
	<i>Parasagitta elegans</i>		
Phylum	Echinodermata	Phylum	Chordata
Class	Asteroidea	Subphylum	Tunicata
	Asteroidea, larvae	Class	Appendicularia
Class	Echinoidea	Genus	<i>Oikopleura</i>
Order	Diadematoidea		<i>Oikopleura labradoriensis</i>
Family	Strongylocentrotidae	Genus	<i>Fritillaria</i>
Genus	<i>Strongylocentrotus</i>		<i>Fritillaria borealis</i>

References

- Afanasyev, N.N. 1981. Macroplankton characteristics of the Sea of Okhotsk as a base of food stock of pelagic fish. *Proc. TINRO*, 105, 56–60. (in Russian)
- Bragina, I.Y. 1989. Specific Composition and Features of Zooplankton Distribution in the Shelf Waters of the Sakhalin during 1986–1987. *Ann. Rep. SakhNIRO*, Yuzhno-Sakhalinsk, 40 pp.
- Bragina, I.Y. 1992. Features of Zooplankton Distribution in the Northern Part of the Japan Sea and South-Western Part of the Okhotsk Sea in 1990. *Ann. Rep. SakhNIRO*, Yuzhno-Sakhalinsk, 56 pp. (in Russian)
- Bragina, I.Y. 1994. Features of Zooplankton Distribution in the Northern Part of the Japan Sea and South-Western Part of the Okhotsk Sea in 1992. *Ann. Rep. SakhNIRO*, Yuzhno-Sakhalinsk, 71 pp. (in Russian)
- Bragina, I.Y. 1997. Features of Zooplankton Distribution in the South-Western Part of the Okhotsk Sea in 1994. *Ann. Rep. SakhNIRO*, Yuzhno-Sakhalinsk, 52 pp. (in Russian)
- Bragina, I.Y. and Fedotova, N.A. 1990. Specific Composition and Features of Zooplankton Distribution in the Northern Part of the Japan Sea and South-Western Part of the Okhotsk Sea in 1988. *Ann. Rep. SakhNIRO*, Yuzhno-Sakhalinsk, 53 pp. (in Russian)
- Bragina, I.Y. and Fedotova, N.A. 1991. Specific Composition and Features of Zooplankton Distribution in the Northern Part of the Japan Sea and South-Western Part of the Okhotsk Sea in 1987–1989. *Ann. Rep. SakhNIRO*, Yuzhno-Sakhalinsk, 62 pp. (in Russian)
- Brodsky, K.A. 1950. *Copepods (Calanoida) of the Far-Eastern Seas and Polar Basin*. USSR Acad. Sci., Moscow–Leningrad, 441 pp. (in Russian)
- Chislenko, L.L. 1968. *Nomograms for the Determination of Hydrobiont Weights by Size and Body Form*. Nauka, Leningrad, 106 pp. (in Russian)
- Chuchukalo, V.I. 1988. Estimation of plankton and benthic community conditions and feeding of fish of the far-eastern seas and north-western part of the Pacific Ocean. *Rep. TINRO*, Vladivostok, 174 pp. (in Russian)
- Fedotova, N.A. 1978a. Peculiarities of Zooplankton Development in the South-Western Part of the Okhotsk Sea. *Ann. Rep. SakhNIRO*, Yuzhno-Sakhalinsk., 39 pp. (in Russian)
- Fedotova, N.A. 1978b. Regularities of Zooplankton Community Formation in the South-Western Part of the Okhotsk Sea. *Ann. Rep. SakhNIRO*, Yuzhno-Sakhalinsk, 27 pp. (in Russian)
- Fedotova, N.A. 1980. Regularities of Zooplankton Community Formation and Employment of Fish in the South-Western Part of the Okhotsk Sea. *Ann. Rep. SakhNIRO*, Yuzhno-Sakhalinsk, 29 pp. (in Russian)

- Fedotova, N.A. 1992. Description of the Zooplankton Community from Regions of Herring Reproduction in Sakhalin Waters and Mainland Coast of the Tatar Strait. *Ann. Rep. SakhNIRO*, Yuzhno-Sakhalinsk, 43 pp. (in Russian)
- Fedotova, N.A. and Hudya, V.N. 1995. Feeding Peculiarities of Pacific Sand Lance, Capelin, and Walleye Pollack Juveniles and other Fish of the Eastern Sakhalin Shelf Waters Coastal Complex in July–August 1994. *Rep. SakhNIRO*, Yuzhno-Sakhalinsk. 46 pp. (in Russian)
- Gorbatenko, K.M. 1990. Structure of plankton communities in the epipelagic layer of the Okhotsk Sea in summer. *Proc. TINRO*, 111, 103–113. (in Russian)
- Gurjanova, E.F. 1951. *Amphipoda of Seas of the USSR*. USSR Acad. Sci., Leningrad, 1129 pp. (in Russian)
- Gurjeva, V.D. 1973. Some data on the feeding of juvenile herring and zooplankton composition in the north-western part of the Okhotsk Sea. *Proc. TINRO*, 86, 34–48, Vladivostok. (in Russian)
- Kantakov, G.A. 1993. Some Features of the Oceanographic Regime in the Sakhalin–Kuril Region in 1992. *SakhNIRO Rep. No. 6493*, Yuzhno-Sakhalinsk, 78 pp. (in Russian)
- Kantakov, G.A. and Shevchenko, G.V. 1999. *In situ* observations of Tsushima and West-Sakhalin currents near La Perouse (Soya) Strait. pp. 177–185. In *Proc. Second Workshop on the Okhotsk Sea and Adjacent Areas*, PICES Sci. Rep. No. 12, Labonov, V.B., Nagata, Y., and Riser, S.C. (eds.), Sidney, B.C., Canada.
- Kasatkina, A.P. 1982. *Chaetognatha of the Seas of the USSR and Adjacent Waters*. Nauka, Leningrad, 135 pp. (in Russian)
- Kryuchkova, G.A. 1987. *A Short Reference Book for the Determination of a Few Kinds of Invertebrate Larvae*. Institute of the Marine Biology, Vladivostok, 56 pp. (in Russian)
- Kun, M.S. 1951. Distribution of zooplankton and the feeding of herring in the northern part of the Okhotsk Sea. *Proc. TINRO*, 35, 87–96, Vladivostok. (in Russian)
- Kun, M.S. 1975. *Zooplankton of the Far-Eastern Seas*. Pishchevaya Prom. 142 pp. (in Russian)
- Kun, M.S. 1985. Food relationship of plankton-eating fish in the Japan Sea and the effect of competition in their feeding upon different populations. pp. 122–123. In *Tez. Allunits Conf. Reports*, Vladivostok, (in Russian)
- Lomakina, N.B. 1978. *Euphausiids (Euphausiacea) of the World Ocean*. Nauka, Leningrad, 222 pp. (in Russian)
- Lubny-Gercic, E.A. 1953. Weight characteristics of major zooplankton specimens of the Okhotsk and Bering Seas. *USSR Acad. Sci.*, 91(4), 949–952. (in Russian)
- Lubny-Gercic, E.A. 1962. Relation of wall-eye pollack food composition and zooplankton distribution. *Proc. Oceanology USSR Acad. Sci.*, 58, 158–162. (in Russian)
- Mikulich, L.V. 1957. *Feeding of Fattening Herring in the Northern Part of the Okhotsk Sea. Part 1*, FEGU, Vladivostok, pp. 191–204. (in Russian)
- Naumov, D.V. 1960. *Systematic Reference Book of Hydrozoa*. Moskow–Leningrad, 626 pp. (in Russian)
- Naumov, D.V. 1961. *Systematic Reference Book of Scyphozoa*. Moskow–Leningrad, 97 pp. (in Russian)
- Omori, M. and Ikeda, T. 1984. *Methods in Marine Zooplankton Ecology*. John Wiley, N.Y., 332 pp.
- Samatov, A.D. 1994. Composition and Distribution of Zooplankton of the Tatar Strait and South-Weastern Part of the Okhotsk Sea in 1991. *Ann. Rep. SakhNIRO*, Yuzhno-Sakhalinsk, 71 pp. (in Russian)
- Samatov, A.D. 1995. Composition and Distribution of Zooplankton of the South-Western Part of the Okhotsk Sea in 1993. *Ann. Rep. SakhNIRO*. Yuzhno-Sakhalinsk, 50 pp. (in Russian)
- Seki, J., Shimizu, I., Ueno, Y., Kawasaki, Y. and Kono, T. 1995. Composition and distribution of the zooplankton in the south Okhotsk Sea and western North Pacific Ocean off the Kuril Islands. *Salmon Rep. Ser., No. 40*, Fisheries Agency of Japan, pp. 45–56.
- Shuntov, V.P. and Dulepova, E.P. 1996. Current status and interannual dynamics of the demersal and pelagic communities in the ecosystem of the Okhotsk

- Sea. *Proc. TINRO*, 119, 3–32. (in Russian)
- Shvetsova, G.M. and Budaeva, V.D. 1975. Distribution and specific composition of macroplankton in south-western part of the Okhotsk Sea. *Proc. TINRO*, 95, 17–25, Vladivostok. (in Russian)
- Stepanyants, S.D. 1967. *Reference Book of the Siphonophora Family*. Nauka, Leningrad, 216 pp. (in Russian)
- Volkov, A.F. 1984. Recommendations on Express-Processing of Net Plankton in the Sea. *Publ. TINRO*, Vladivostok, 30 pp. (in Russian)
- Volkov, A.F., Gorbatenko, K.M. and Efimkin, A.Y. 1990. Strategy of walleye pollack feeding. *Proc. TINRO*, 111, 123–132, Vladivostok. (in Russian)
- Volkov, A.F., Karedin, E.P. and Kun M.S. 1980. Instructions on Collecting and Preliminary Processing of Plankton in the Sea. *Publ. TINRO*, Vladivostok, 45 pp. (in Russian)
- Zevina, G.B. 1981. *Reference Book on the Scalpellidae Family*. Nauka, Leningrad. 406 pp. (in Russian)

List of Corresponding Authors

Masaaki Aota
Sea Ice Research Laboratory
Hokkaido University
6-4-10 Minamigaoka,
Mombetsu, Hokkaido,
Japan. 094
e-mail: aota@pop.lowtem.hokudai.ac.jp

Boris S. Dyakov
Pacific Research Institute of Fisheries and
Oceanography (TINRO-Centre)
4 Shevchenko Alley,
Vladivostok,
Russia. 690600
e-mail: root@tinro.marine.su

Toshiyuki Awaji
Department of Geophysics
Kyoto University
Kyoto,
Japan. 606-8502
e-mail: awaji@stooge.kugi.kyoto-u.ac.jp

Alexander L. Figurkin
Pacific Research Institute of Fisheries and
Oceanography (TINRO-Centre)
4 Shevchenko Alley,
Vladivostok,
Russia. 690600
e-mail: root@tinro.marine.su

Irina Y. Bragina
Sakhalin Research Institute of Fisheries and
Oceanography (SakhNIRO)
196 Komsomolskaya Street,
Yuzhno-Sakhalinsk,
Russia. 693016
e-mail: stab@tinro.sakhalin.ru

Yasushi Fukamachi
Institute of Low Temperature Science
Hokkaido University
Sapporo,
Japan. 060-0819
e-mail: yasuf@soya.lowtem.hokudai.ac.jp

Valentina D. Budaeva
Far Eastern Regional Hydrometeorological
Research Institute (FERHRI)
24 Fontannaya Street,
Vladivostok,
Russia. 690600
e-mail: Vbudaeva@hydromet.com

Hajime Ito
National Polar Region Research Institute
Tokyo,
Japan
e-mail: hajime@nipr.ac.jp

Mikhail A. Danchenkov
Far Eastern Regional Hydrometeorological
Research Institute (FERHRI)
24 Fontannaya Street,
Vladivostok,
Russia. 690600
e-mail: hydromet@online.ru

Gennady A. Kantakov
Sakhalin Research Institute of Fisheries and
Oceanography (SakhNIRO)
196 Komsomolskaya Street,
Yuzhno-Sakhalinsk,
Russia. 693016
e-mail: okhotsk@tinro.sakhalin.ru

Katsuro Katsumata
Tokyo University
Graduate School of Science
Department of Earth and Planetary Physics
7-3-1 Hongo, Bunkyo-ku,
Tokyo,
Japan. 113-0033
e-mail katsu@ocean.geoph.s.u-tokyo.ac.jp

Yasuhiro Kawasaki
Hokkaido National Fisheries Research Institute
116 Katsurakoi,
Kushiro, Hokkaido,
Japan. 085-0802
e-mail: ykawasak@hnf.affrc.go.jp

Igor E. Kochergin
Far Eastern Regional Hydrometeorological
Research Institute (FERHRI)
24 Fontannaya Street,
Vladivostok,
Russia. 690600
e-mail: hydromet@online.ru

Vyacheslav B. Lobanov
Pacific Oceanological Institute
43 Baltiyskaya Street,
Vladivostok,
Russia. 690041
e-mail: pacific@online.marine.su

Vladimir A. Luchin
Far Eastern Regional Hydrometeorological
Research Institute (FERHRI)
24 Fontannaya Street,
Vladivostok,
Russia. 690600
e-mail: hydromet@online.ru

Yutaka Nagata
Japan Hydrographic Association
Marine Information Research Center
Mishima Bldg. 5F
7-15-4 Ginza, Chuo-ku,
Tokyo,
Japan. 104
e-mail: nagata@mirc.jha.or.jp

Tomohiro Nakamura
Department of Geophysics
Kyoto University
Kyoto,
Japan. 606-8502
e-mail: nakamura@stooge.kugi.kyoto-u.ac.jp

Akifumi Nakata
Division of Oceanography
Hokkaido Central Fisheries Experimental
Station
238 Hamanaka-cho, Yoichi-cho,
Hokkaido,
Japan. 046
e-mail: kfc01743@niftyserv.or.jp

Minoru Odamaki
Hydrographic Department
Maritime Safety Agency
Tokyo,
Japan
e-mail: nakataa@fishexp.pref.hokkaido.jp

Aleksandr G. Petrov
Far Eastern Regional Hydrometeorological
Research Institute (FERHRI)
24 Fontannaya Street,
Vladivostok,
Russia. 690600
e-mail: hydromet@online.ru

Vladimir Ponomarev
Pacific Oceanological Institute
43 Baltiyskaya Street,
Vladivostok,
Russia. 690041
e-mail: pacific@online.marine.su

George V. Shevchenko
Institute of Marine Geology and Geophysics
Nauki Street,
Yuzhno-Sakhalinsk,
Russia. 693002
e-mail: tsunami@sakhmail.sakhalin.ru

Stephen C. Riser
School of Oceanography
University of Washington
Seattle, WA 98195-7940,
U.S.A.
e-mail: riser@ocean.washington.edu

Iori Tanaka
Division of Oceanography
Hokkaido Central Fisheries Experimental
Station
238 Hamanaka-cho, Yoichi-cho,
Hokkaido,
Japan. 046
e-mail: tanaka@fishexp.pref.hokkaido.jp

Konstantin A. Rogachev
Pacific Oceanological Institute
43 Baltiyskaya Street,
Vladivostok,
Russia. 690041
e-mail: pacific@online.marine.su

Igor Zhabin
Pacific Oceanological Institute
43 Baltiyskaya Street,
Vladivostok,
Russia. 690041
e-mail: pacific@online.marine.su

Nikolay A. Rykov
Far Eastern Regional Hydrometeorological
Research Institute (FERHRI)
24 Fontannaya Street,
Vladivostok,
Russia. 690600
e-mail: hydromet@online.ru